Spatial modelling of the contributions from surface and subsurface water to river flow in catchments

by

Nina-Marié Snyman

submitted to the

Faculty of Science

in fulfilment of the requirements of the degree of

Doctor of Philosophy

in the **Department of Hydrology** at the **University of Zululand**

Supervisor: Prof. B.E. Kelbe

Date submitted: 28 February 2007

Abstract

The groundwater and surface water resources were historically modelled separately because of laws of the governing bodies. Movement towards equity and sustainable development demands the integration of groundwater and surface water in decision making and modelling of these water resources.

This research attempts to simulate the contributions in river runoff from surface and groundwater resources, by conceptualizing the flow pathways of the different resources present in a river's catchment. It utilizes the spatial information of the catchment, along with the observed flow hydrograph characteristics, to create a model of the flow components in the river runoff sequence.

The model conceptualizes the observed flow hydrograph from a rainfall event as a combination of flow from three different pathways. Excess rainfall (the part of measured rain that causes the storm hydrograph) is separated into the surface runoff; the throughflow (through the unsaturated soil structures and macropores); as well as baseflow (through the deeper saturated soil structures of the catchment): All of these components contribute to the measured flow at the catchment outlet.

Analysis of observed flow hydrographs (i.e., the separation of the observed flow into different flow components); indicates constant recession rates for each flow component present in the hydrograph. Information derived from observed flow hydrograph analysis includes the recession rate of each flow component, the percentage of water that is allocated to each flow component for a particular storm event, and the times to peak and recede. This information is used along

with the spatial information of the catchment, to derive a simulated flow hydrograph for a rainfall event, for each flow path.

The Digital Elevation Model (DEM) of the catchment and geological features are used to determine the pathways and distances that water travels to the outlet. Flow velocities, along these pathways, are influenced by the slopes and the roughness of the medium over/through which the water travels. The flow velocities are estimated from adaptations of recognized hill slope and channels flow velocity equations. The channel geometry, that determines the flow rate through each catchment segment in the DEM, is derived from the contributing area and scaled by the total catchment size.

Cumulative flow times along each pathway are used to derive a flow response function for each flow component. These response functions are unique to each catchment and represent the equivalent of a unit hydrograph for each flow component. These response functions are scaled and superimposed to simulate the observed storm hydrograph of a rain event.

Storm events are divided into four scenarios representing a combination of high and low intensity rainfall events, as well as events of long and short duration.

The model is applied to a rainfall series of five months in the Ntuze research catchments, during which various rain storm types occurred.

Model parameters are applied to the much larger Goedertrouw Dam catchment to evaluate the transferability of the model.

Acknowledgments

Special acknowledgment is extended to the sponsors of this project:

1) the Water Research Commission of South Africa (WRC), and

2) the National Research Foundation (NRF).

Special thanks are extended to the donors of the hydrological data. The development of the model was accomplished with data extracted from the database at the Department of Hydrology, University of Zululand. Testing of the model on the Goedertrouw Dam catchment utilized data from the Department of Water Affairs and Forestry (DWAF) database in Durban, South Africa.

Thank you to Brian Rawlins who agreed to study this *entire* thesis for further enhancement of the work.

A special word of gratitude is extended to the examiners who contributed with positive, constructive criticism toward the standard of this thesis.

Thanks to Prof. Bruce Kelbe who encouraged me to make use of this opportunity to finish this degree, as well as for excellent guidance and patience throughout the whole research project.

Thank you to my Heavenly Father. "But by the grace of God I am what I am." (I Cor. 15:10).

Statement of originality

The author of the dissertation hereby declares that the research done and reported in this dissertation is original work done by herself, and was not copied from any other source, unless referenced clearly.

Table of Contents

****

List of figures

List of tables

****

1 Introduction

Knowledge about water resources and how they interact in the hydrological cycle of a catchment, is essential for best management practice (Arnold and Allen, 1996). For example, knowledge about the quantities of water in different water resources and the contributions from different water resources can influence management decisions about the allocation of limited resources for the most beneficial use of aquatic systems (Figure 1.1). It is therefore important to understand the role, function and magnitude of the different water resources. This broadens our understanding of a catchment's water cycle and contributions from the water resources (Arnold and Allen, 1996).

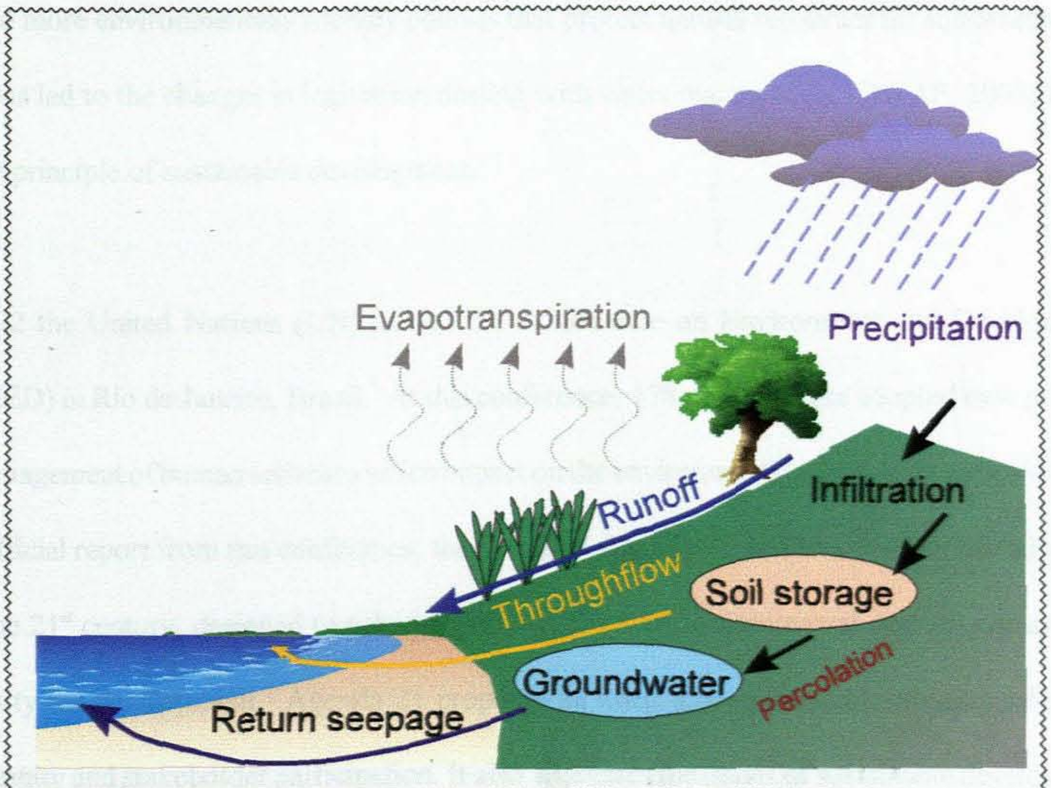

Figure 1.1: The different water resources within the hydrological cycle.

Prior to 1998, the surface water and groundwater resources in South Africa were managed separately in legal and political forums, and therefore also in the hydrological arena (Braune, 2000). Previous South African legislation (Water Act No 54 of 1956) recognized surface water resources as being separate from groundwater resources. Under this legislation, most groundwater was regarded as private water. Consequently, most land owners had sole rights to the groundwater except in demarcated areas. There were very few attempts at integrated water resource management that included all systems in the hydrological cycle (Kelbe and Rawlins, 2004). However, the South African National Water Act, No 36 of 1998, (NWA) states that all water components, described by the hydrological cycle, are to be managed as a single unit.

The recent holistic view of water resource management in South Africa is in line with international trends in resource protection for sustainable development (DWAF, 2003). Globally, there has been a change in attitude toward water management: moving from exploitation of water resources toward more environmentally friendly policies that protect natural resources for sustainable use. This has led to the changes in legislation dealing with water management (DWAF, 2003) based on the principle of sustainable development.

In 1992 the United Nations (UN) hosted the Conference on Environment and Development (UNCED) in Rio de Janeiro, Brazil. At this conference, 178 governments adopted new policies for management of human activities which impact on the environment (including water resources). The official report from this conference, the so-called Agenda 21, is a blueprint for global action into the 21st century, designed to solve the twin problem of environmental degradation and the necessity for development. Agenda 21 proposes an integrated approach to poverty relief, via community and stakeholder participation. It also addresses the issues of sustainable development along with management of all natural resources, including water resource management (DWAF, 2003).

In the year 2000 the UN reaffirmed their support "...for the principles of sustainable development, including those set out in Agenda 21." (United Nations Millennium Declaration, 2000). The UN web pages (http://www.un.org/millenniumgoals/, 2005) states that all 191 member states of the United Nations pledged to meet the eight UN Millennium Development Goals by the year 2015. The seventh goal is to ensure sustainable development of the environment which binds governments (quoted from web page http://www.un.org/millenniumgoals/, 2005):

1) to integrate the principles of sustainable development into country policies and to reverse the loss of environmental resources,
2) to reduce by half the proportion of people without sustainable access to safe drinking water and
3) to achieve significant improvement in the lives of at least 100 million slum dwellers, by 2020.

The South African Bill of Rights embraces the concepts outlined in Agenda 21 towards the development of policies and legislation that are socially enabling, while also ensuring sustainable development (DWAF, 2003). The NWA (1998) provides specific guidelines for the management of water resources, which attempts to bring about this holistic approach to management and to ensure sustainable management. This act specifically encourages movement towards the integrated management of surface and groundwater resources.

The NWA (1998) requires the classification of all water resources. After classification of water resources, the resource quality objectives must be determined. "The purpose of the resource quality objectives is to establish clear goals relating to the relevant water resources." (NWA, 1998.) But before these objectives can be established and before the classification can be determined, "The Reserve" must be established. The Reserve of water resources is defined by the NWA (1998) as "the quantity and quality of water required to satisfy basic human needs ... and to protect aquatic ecosystems in order to secure ecological sustainable development and use of the water resources."

Chapter Three of the NWA (1998) sets out the legal framework for the protection of water resources. This framework has been constructed as a series of management functions implemented as Resource Directed Measures (RDM). The RDM includes:

1) the classification of resources in terms of its past, present and future conditions;
2) The Reserve determination, in terms of the ecological water rights for the resource; and
3) the setting of resource quality objectives that are required to protect the resource.

The NWA (1998) requires that water resources must be managed holistically. This requirement defines a different approach from previous legislation toward the modelling of water resources. The new approach in management requires a reassessment of current knowledge of resource dynamics. It also requires the development of new analytical techniques to assist water resource management in determining The Reserve for the different resources. In some situations one water resource is partially or wholly derived from another resource. In these cases the management of both resources must recognize the contributions from each resource. Where river flow is derived from groundwater (i.e., baseflow), the groundwater management forms part of the surface water management. Research is being done, both in South Africa and abroad, to develop a wide variety of analytical methods to determine the ecological water requirements; as referenced throughout this report. Research areas also focus on the interaction between rivers, estuaries and groundwater. The methodologies for establishing the ecological water requirements of surface water resources are presently not well established, especially where the surface water resources receive some contributions from groundwater.

Hydrological procedures and methods for determining the ecological water requirements for rivers have been developed by Hughes and Munster (2000). Similar procedures and methods for determining the resource quality objectives for groundwater are being developed by Parsons (2003). Hydrological procedures and methods have also been developed to establish the ecological water requirements of estuaries, but their groundwater contributions are still not included in the RDM procedures (Van Niekerk, 2004). However, all these assessments are limited to a single resource and the levels of estimating the contributions from different resources, are limited.

In order to establish The Reserve for a river system, some basic knowledge about the groundwater component (or baseflow) needs to be established. Hughes, Hannart and Watkins (2003) applied a statistical method for continuous baseflow separation from time series of daily and monthly streamflow data. The method determines the quantity component of instream flow requirements needed during implementation of the NWA (1998).

There are numerous methods available in the world for estimating river runoff, but only a few extremely complex models, such as Mike-SHE, can provide the estimates of the various contributions to surface water (from Beven, 2003). This research aims to develop a method for simulating various components of river runoff that can be associated with different pathways, using the spatial information of a catchment.

This study examines the contributions from surface water and groundwater to streamflow, and attempts to develop a method of simulating the main water resource components of river runoff (in particular the groundwater component) using physically measured information (such as slopes, soil types and vegetation). The methodology makes use of the spatial characteristics of the catchment to generate the flow at the catchment outlet. It seeks to adopt and integrate the physically based spatial techniques to simulate river runoff. It utilizes the spatial information to simulate more than one hydrological flow pathway down the catchment slopes; pathways that define the subsurface flow, as well as the surface flow, down the catchment slopes.

1.1. Existing models simulating interaction between surface and groundwater resources

Recent development in modelling of surface water and groundwater interaction uses the combination of a "traditional surface water model" and a "traditional groundwater model" to "work alongside" each other. They include the interaction of the water resources as an added feature to existing models. Each "combined model" covers different aspects of the interaction, like the recharge of groundwater from rainfall (described by Gupta and Paudyal, 1988), or the effects of irrigation on groundwater recharge (for example the work of Criss and Davidson, 1996), or the effects of land use change on groundwater levels (for example the work of Borg, Stoneman and Ward, 1998, as well as Bell, Schofield, Loh and Abri, 1990). The stream function linked to the Modflow groundwater model (Guiguer and Franz, 1996) provides an estimate of the base flow but cannot simulate storm flow events.

1.1.1. Interaction of surface water models and groundwater models

A method of integrating surface water and groundwater modelling has been achieved by Chiew, McMahon and O'Neill (1992). Their study utilizes the surface water model HYDROLOG (a daily rainfall-runoff model) and AQUIFEM-N (a finite-element groundwater model). The integration of the two models was achieved by optimizing the two sets of parameters from the two models: Two objective functions were formulated during the (automated) calibration of the models, to minimize the difference between the simulated and observed flows and potentiometric head. Thus, during the calibration, the two objective functions were optimized together to get the best set of parameters for both the surface and groundwater models. Certain interaction of surface and groundwater resources was incorporated into the calculations of the two models, utilizing input and output from each. Advantages of the integrated model include a higher level of accuracy of the groundwater recharge simulation, especially during months of irrigation. The biggest advantage is the ability to optimize parameters for both models against both streamflow and potentiometric head data (Chiew *et al*, 1992).

Berger and Entekhabi (2001) investigated the long term hydrologic response with an equilibrium surface water/groundwater interaction model. Their model couples the surface water and groundwater by describing the land-surface hydrologic partitioning as a function of water table depth. Upstream areas in the catchment with deep groundwater depths are groundwater recharge areas during heavy rainfall events. River banks with shallow groundwater depths are groundwater discharge areas. For the areas between these recharge and discharge areas, the model assumes that the groundwater energy slopes parallel to the surface slopes (Berger and Entekhabi, 2001).

Their model applies at a catchment scale to long term equilibrium conditions.

1.1.2. Contributions from both surface water and groundwater resources

Some attempts have been made to directly model the contributions from both the surface water and groundwater, where the interaction between water resources is the foundation of the model, instead of an added feature to existing models. However, these models are few and often specific to certain conditions (catchment's characteristics, antecedent storm conditions, etc.).

The work of Wittenberg and Sivapalan (1999) is an example of such an integrated model, but the emphasis of their work is on the determination of groundwater recharge, and not on the amount of water which moves from the groundwater flow component to the river runoff (groundwater discharge).

Ledoux, Girard and de Marsily (1989) jointly model the surface and groundwater resources with a deterministic physically-based model. Their "Modèle Couplé" simulates the available water resources for surface water, river flow, flow in both the saturated and unsaturated zones, as well as the interaction between the different water resources. They also summarise research on integrated surface and groundwater modelling, and acknowledge that some of these models require the estimation of a relative large number of parameters.

1.2. Aims and objectives

The aim of this study is:

To adapt and integrate existing models and methods of spatial analysis of river runoff to simulate the main hydrological components of river runoff in ungauged catchments.

To achieve this aim, several specific **objectives** were set. These include:

1) Reviewing of the main hydrological pathways along which surface and groundwater resources travel.

2) Determining and applying methods for evaluating the contributions of the different hydrological pathways to river runoff in gauged catchments, for model validation and verification.

3) Evaluating methods and techniques that can be used to simulate the hydrological pathways using spatial information.

4) Adapting and combining the methods and techniques to create a model to simulate the main hydrological components of river runoff.

****

2 Conceptualized flow processes

The previous chapter indicated the world wide movement towards integrated water resource management and the necessity to manage and model the contributions from both surface water and groundwater resources on one platform. This chapter will describe conceptual understanding of the contributions from the surface and groundwater resources to the flow in a river system. It will then introduce the conceptualization of the different flow processes within a catchment that are used in the description of the conceptualized model which simulates the flow components, making use of the spatial information, described in Chapter three.

Simulation of water resources are based on conceptual and perceptual models of a catchment's flow response to rainfall. These perceptual models are influenced by the modelers' hydrological perceptions, which again are influenced by their training; networking; hydrological data they have analysed; observations made during field trips to catchments of different environments; etc. The mathematical model is then the simplified description derived from the perceptual model. Despite the oversimplifications implemented in hydrological modelling, some mathematical models still remain sufficient to provide adequate predictions (Beven, 2001).

2.1. Introduction

Wittenberg and Sivapalan (1999) concur with Cey, Rudolph, Parkin and Aravena (1998) who have found that "even in flood periods, discharge from shallow groundwater is the major contributor to streamflow."

It is important to distinguish between deeper lying groundwater and more shallow groundwater. According to Seiler and Lindner (1995), deeper groundwater participates in the hydrological cycle only in intervals of hundreds or even thousands of years. It can be distinguished from shallower groundwater by increases in the measurements of the concentrations of radioactive environmental isotopes in the groundwater for tritium (half life 12 years) and carbon-14 (half life 5730 years). In this study, the deeper and "older" groundwater resources are assumed to make a negligible contribution to the river runoff. In reality it could be a constant and very low flow. Therefor, it is not considered for the model development.

2.2. Conceptualization of the river flow components

Beven (2001) indicated that there can be as much as five to six different flow components contributing to river runoff. Analysis of observed streamflow of headwater catchments by Kelbe and Germishuyse (1999) indicated that the observed hydrograph consists of three distinct flow components that constitute surface, unsaturated subsurface and saturated flow processes. Figure 2.1 depicts the processes that contribute to the pathways as conceptualized for these three flow components.

The quickflow is regarded as the water that flows fairly quickly over the catchment's soil layers into the rivers and runs down to the catchment outlet along a "surface" route, causing the sharp high peak in runoff after a short duration storm. This is often conceived to be the contribution from the various processes shown in Figure 2.1.

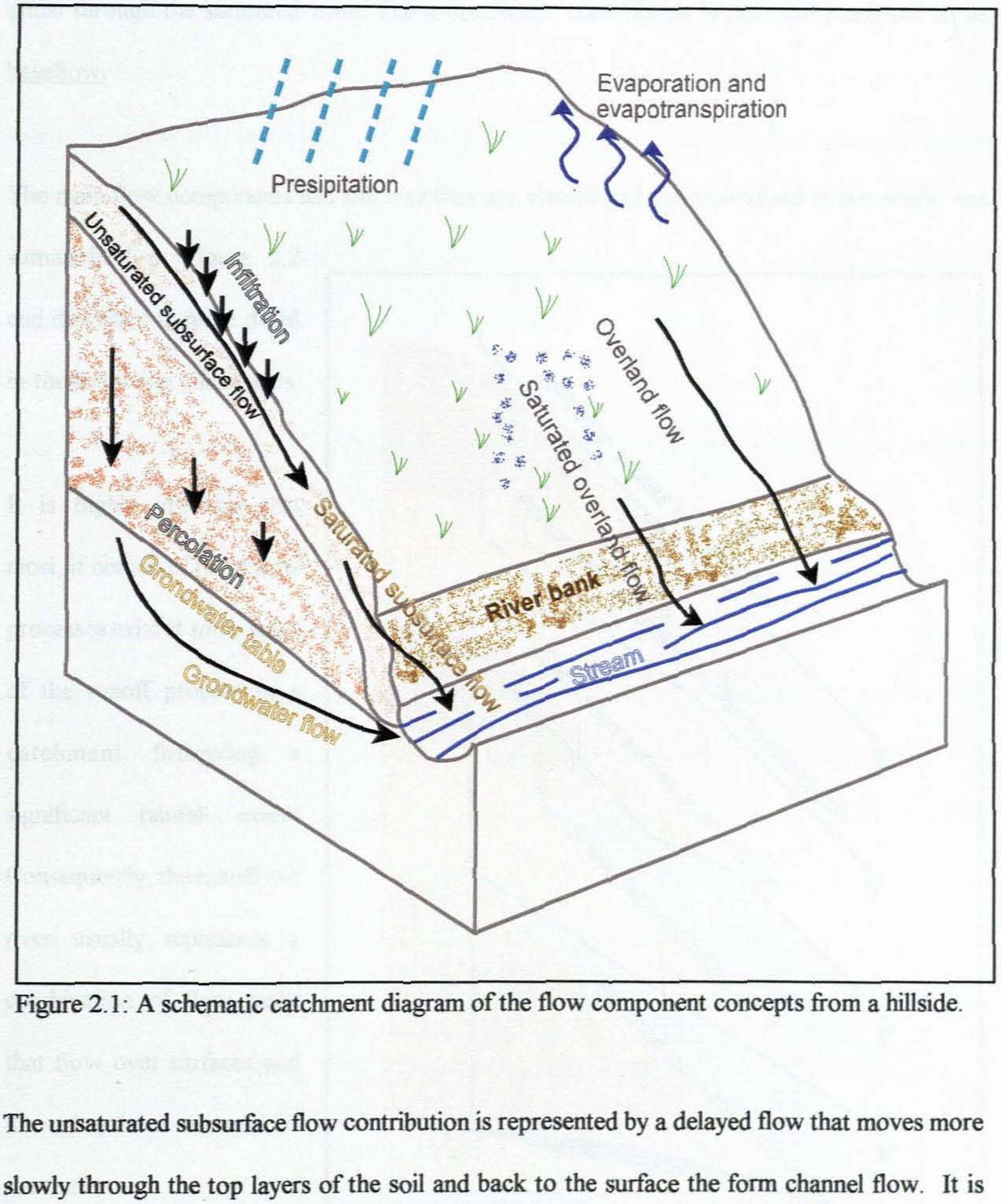

Figure 2.1: A schematic catchment diagram of the flow component concepts from a hillside.

The unsaturated subsurface flow contribution is represented by a delayed flow that moves more slowly through the top layers of the soil and back to the surface the form channel flow. It is usually referred to as <u>throughflow</u>, intermediate flow or macropore flow. It is often associated with flow through preferential channels (or macropores) in the soils in the unsaturated soil structure, or the vadose zone. Some water percolates deeper into the soil to reach the saturated zone. It moves more slowly to reach the catchment outlet, as it follows longer, more arduous paths through the saturated zone. The groundwater contribution is commonly referred to as baseflow.

The main flow components and the way they are viewed and conceptualized in this study, are summarized in Figure 2.2 and described in more detail in the following paragraphs.

It is highly probable that most, if not all, of these flow processes exist at some stage of the runoff process in a catchment following a significant rainfall event. Consequently, the runoff in a river usually represents a combination of flow paths that flow over surfaces and through porous material to the outlet.

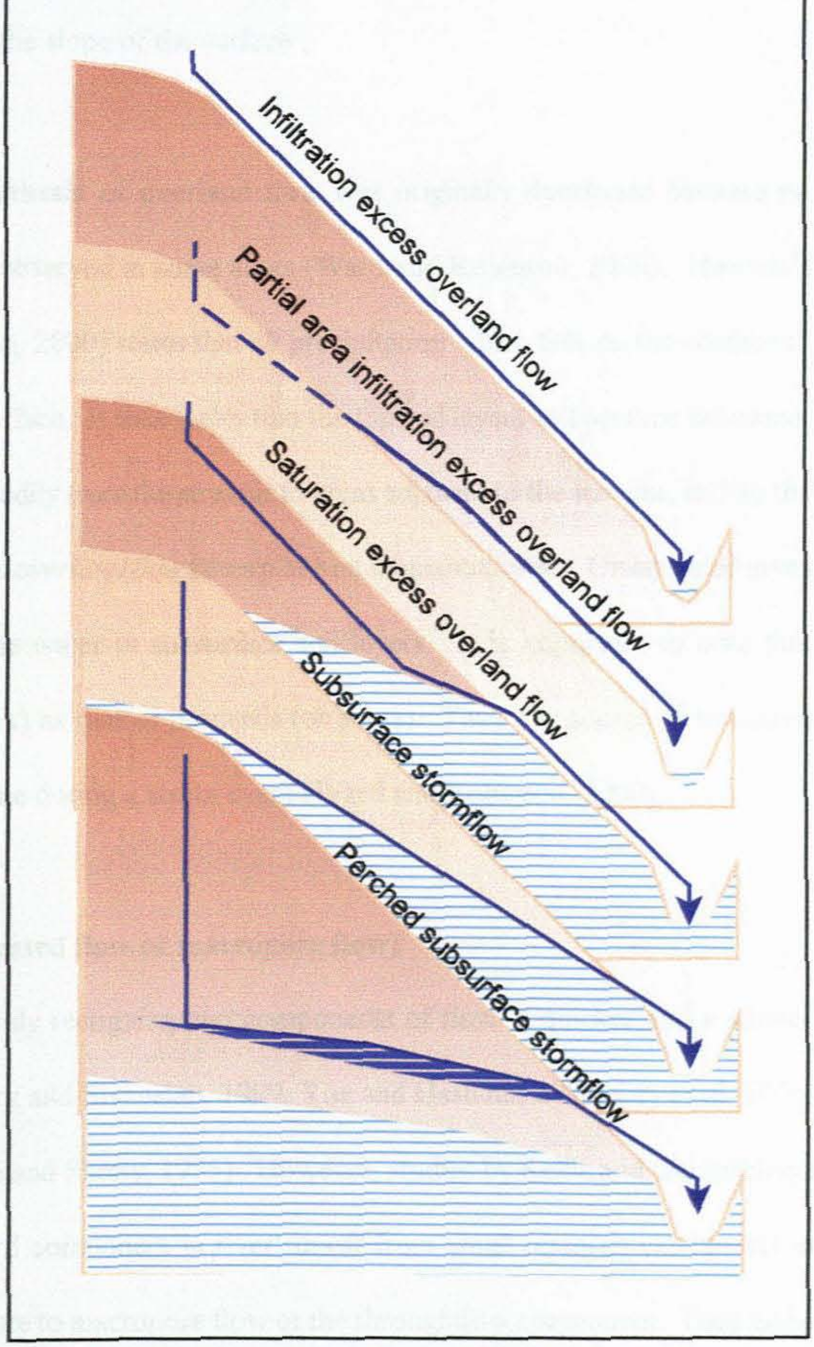

Figure 2.2: Division of measured rainfall into flow components (after Beven, 2001).

2.2.1. Overland flow

The **Hortonian quickflow model** assumes that all rainfall in excess of the infiltration capacity of the soil will flow over the surface to the discharge point in the stream. Hortonian overland flow is then described as the rapid overland flow which does not penetrate the soil (Ward and Robinson, 2000). The main controlling factors are the rainfall intensity and the infiltration capacity of the soil, as well as the slope of the surface.

The **Hewlett quickflow hypothesis** of overland flow was originally developed because no Hortonian overland flow was observed in some areas (Ward and Robinson, 2000). Hewlett's hypothesis (Ward and Robinson, 2000) states that all precipitation which falls on the catchment will initially infiltrate the soil surface. It then states that the top soil layers will become saturated. These saturated areas grow steadily from the streams to areas adjacent to the streams, and up the catchment slope, until *saturated overland flow* takes place on substantial areas. Unsaturated areas will either transfer or store the water in subsurface soil layers. It is important to note that saturated areas grow (or shrink) as rainfall proceeds (or stops). Thus, the source of saturated overland flow changes with time during a storm event (Ward and Robinson, 2000).

2.2.2. Throughflow (unsaturated flow or macropore flow)

Some models of streamflow only recognize two components of flow: a quicker and a slower flowing component (Wittenberg and Sivapalan, 1999, Yue and Hashino, 2000, Cey *et al*, 1998, Arnold and Allen, 1996, Ponce and Shetty, 1995). However, studies by Kelbe and Germishuyse (1999) clearly identified a third component in river runoff from small research catchments in South Africa, which they atribute to macropore flow or the throughflow component. They make use of the sequence of dissolved solids measurements in response to storm events in the river runoff, to support the existence of an intermediate flow component (Figure 2.3).

Water enters the soil layers through infiltration. Once it is in the soil structure, it flows along preferential *pathlines*. (Pathlines are the exact lines along which water particles flow.) Musy, Soutter and Perrochet (1989), acknowledging the complexity of the throughflow drainage systems, suggest that all evaluation of hydrological response of throughflow leads to several oversimplifications at all levels of the throughflow analysis.

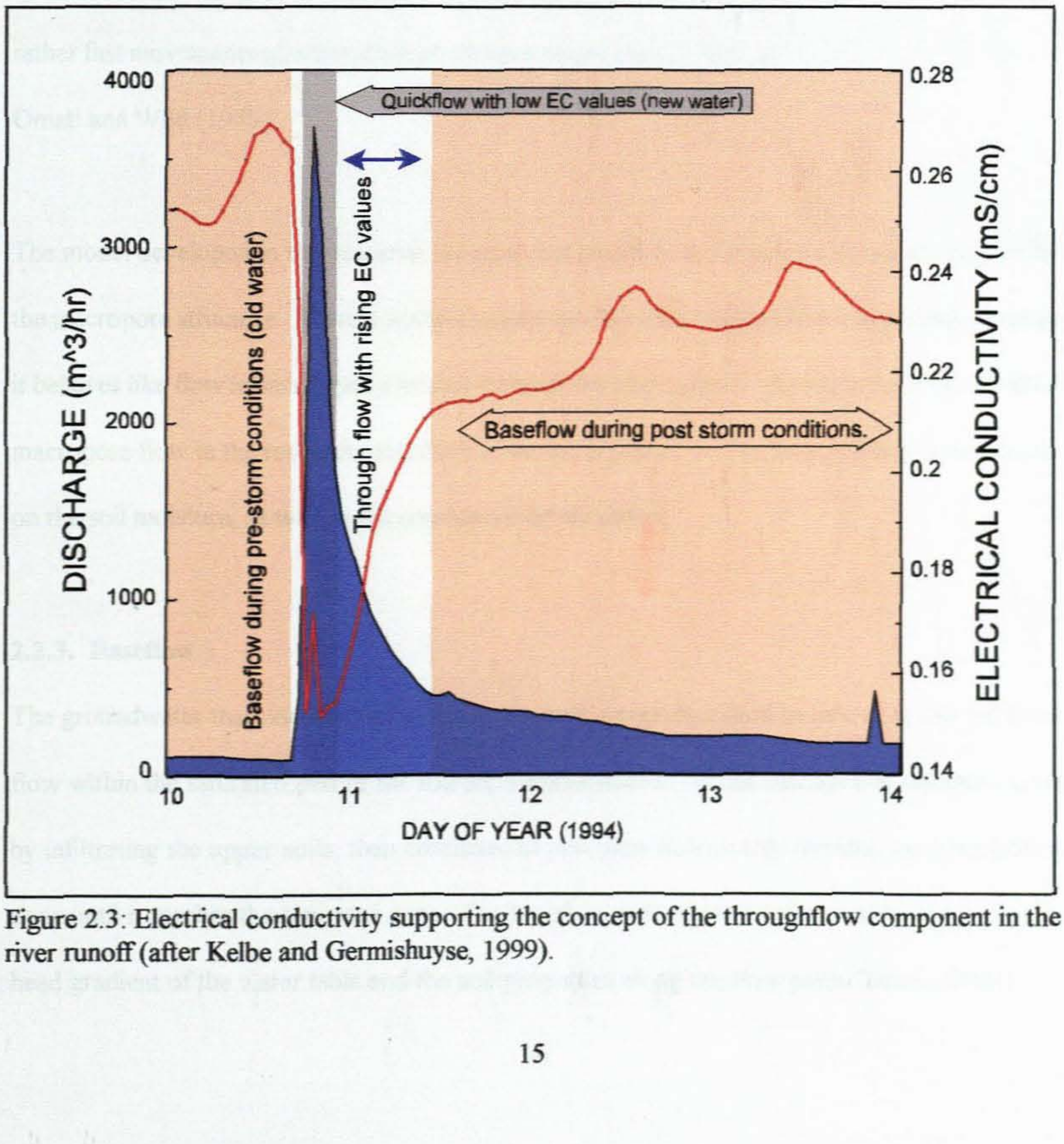

Figure 2.3: Electrical conductivity supporting the concept of the throughflow component in the river runoff (after Kelbe and Germishuyse, 1999).

Throughflow has been described by Hewlett and Hibbert (1967) as flow through the upper soil matrix which causes a displacement response. They propose that the rain (new water) replaces the water in the soil structure (old water) to induce quicker flow response in the rivers, as indicated by increasing electrical conductivity measurements. They indicate that, if a soil column in a laboratory is drained to field capacity, adding another drop of water at the top will result in some water flowing from the bottom almost immediately. Ligon, Wilson, Allen and Singh (1977) used tritium as a tracer to indicate that the flow rate is much faster than predicted by the complete displacement of initial waters. They suggest that, in their research catchment, only about 50% of the initial water storage was displaced, due to some rapid flows through large macropores. These rather fast movements of water through the macropores are confirmed by other tracer studies by Omati and Wild (1979).

The model developed in this research assumes that pathlines in the topsoil layers are created by the macropore structure. There it is able to move quicker than the baseflow component, because it behaves like flow in small open channels through the macropores. An example of unsaturated macropore flow in the research catchment is shown in plate 2.1. The flow velocity is dependent on the soil moisture, as well as the macropore development.

2.2.3. Baseflow

The groundwater that contributes to the river runoff, generally called baseflow, is derived from flow within the saturated part of the soil and rock structure. Water reaches this saturated zone by infiltrating the upper soils, then continues to percolate downwards through the unsaturated zone until it reaches the saturated zone. The baseflow movement is influenced by the hydraulic head gradient of the water table and the soil properties along the flow paths (Beven, 2001).

Plate 2.1: Water flow from the macropores of the channels several days after a rainfall event in the catchment of the Ntuze River. This flow is conceptualized as throughflow (Photo: BE Kelbe).

For the purpose of this study it is assumed that the saturated zone will flow according to groundwater principles and governing equations that are dependent on the hydraulic head gradient or piezometric profile and soil properties.

2.2.4. Fractured rock outflow

The contribution to catchment outflow from fractured rocks and faults will be significant if a continuous fracture network exists in the catchment. The form of the bedrock surfaces will dominate the flow pathlines of water that percolates to the saturated zones. A general assumption of an impermeable bedrock that underlies a study area, is often applied to baseflow simulation for hill slope processes. This is not always a valid assumption. Secondary permeability, in the form of rock joints and fractures, can alter the flow pathlines of groundwater (Beven, 2001).

These fractures, if filled with water, can act like water pipes: If a water pipe is filled with water, it will transmit water immediately from the bottom end as soon as water is pored into the top end, regardless of the size of the pipe and the velocity of water in the pipe (Beven, 2001). Thus, fractures in bedrock (if filled with water) provide a divergent pathway in an otherwise homogeneous soil for groundwater to flow more quickly after rain has infiltrated the saturated zones (Beven, 2001). On the other hand, fractured rocks and joints can also provide storage of subsurface water. If these areas of storage are recharged during a rain storm, it causes a time delay before discharge is released from the groundwater resources. These sources can also maintain flow in the river long after rain events (Beven, 2001).

Thus, fractured rocks can have a diverse effect on the average travel time of water along the baseflow pathlines; depending on the characteristics and extent of the fracture network in the catchment. Like macropores, fractures provide a pathway through the hill slope profile. Fractures have to be modelled carefully, due to the uncertainty that surrounds their positions and the flow processes along these pathways.

2.3. Interaction between the surface and subsurface flow components

In this study it was found, for the small headwater catchments, that only about 20% of the rainfall from a storm event will discharge at the catchment outlet within the first 24 to 48 hours after a storm event. Some water will be lost from the catchment's flow components through evaporation and evapotranspiration. Nonetheless, the small fraction of water that discharges from the catchment straight after rain, indicates that large amounts of water will penetrate the soils during storm flow conditions. It confirms that water moves from the surface to the groundwater resources during storm flow conditions. Water from the subsurface resources moves slowly back to the river, contributing to the river's baseflow long after the rain event.

It is recognized that there is a difference between the geochemical quality of water stored in the catchment before a rain event, and the quality of rainfall(Beven, 2001). The high percentages of storm water contributing to the storm hydrograph, which originates from the catchment storage, is indicated by Cey *et al* (1998). The quality of the pre-event water, which contributes to the observed storm hydrograph (Figure 2.3), indicates that the water in the storage zones of the catchment is displaced quite quickly. However, the velocities of subsurface flow are traditionally estimated to be much slower than those of surface water. The explanation for this contradiction is in the physics of the flow processes in the saturated zone (Beven, 2001). The disturbance in the saturated zone, due to a rainfall event, causes a pressure wave. This pressure wave is "translated" to the rest of the saturated zone very quickly. The theory proposes that very small disturbances will propagate very quickly, and that larger disturbances will have smaller wave velocities. The magnitude of this disturbance is a function of the inverse of the effective storage capacity in the soil. The effective storage capacity is the difference between the soil moisture content in the saturated zone and the soil moisture immediately above the water table. This simply means that, in a wet catchment, the wave velocity may be much faster than the actual flow velocity of water. This then suggests that the water stored in the soil profile close to the streams, will be forced out much faster than the water that travels the full length of the pathway.

For a more explicit explanation, see Beven (2001). It is important to note that the pressure wave (described by Beven, 2001) is assumed to operate in the saturated zone and not in the unsaturated zone; unless an artificial water table (wetting front) is created that traps air in the unsaturated zone.

For the purpose of the model developed in this study, a simple conceptual model of the groundwater flow paths is adopted. The amount of water which emerges at the catchment outlet is comprised of several flow components (Figure 2.2). Water following the quicker pathlines (the paths of least resistance) down the catchment slopes through overland flow or surface flow, is lumped into one component called quickflow. Water infiltrating and percolating through the soil layers into the saturated zone (paths of maximum restrictions), will be classified as groundwater which emerges in the river as baseflow. The throughflow component follows lateral pathlines of less resistance through the upper unsaturated soil structure (macropores).

This simple conceptualization of the flow of water through the soil structure of a catchment is, for most catchments, an oversimplification. More detailed and complex modelling of flow paths along the hill slopes of catchments is suggested by Lorentz, Thornton-Dibb, Pretorius and Goba (2003). They describe sequences of tensiometer responses measured on the hill slope of their research catchment, called the Weatherley catchment (situated in the Eastern Cape province of South Africa). These time series were used to observe a perched water table relatively close to the surface of the catchment. This water table is formed during the rain season when it causes rapid lateral flow in the macropores. Water then seeps out at the toe of the hill slope over a bedrock outcrop. The perched water table dries up during the dry winter season.

Lorentz, Bursey and Idowu (2006) used measurements of subsurface resistivity to show that the river bed in the Weatherley catchment is *not* connected with the regional groundwater table. They concluded that perennial water in the river originates from the fractured sand stone, situated higher up the hill slope, some distance from the river. This source will discharge into the river in a similar manner to the baseflow, from a diverted groundwater source.

2.4. Partitioning of measured rainfall

The resources feeding the various pathways flowing to the river are dependent on the form and duration of the rainfall. Literature often refers to the *excess rainfall* as that part of the measured rainfall that causes the peak in the observed flow hydrograph after a storm event (e.g., Ward and Robinson, 2000; Shaw, 1994; Maidment, Olivera, Calver, Eatherall and Fraczek, 1996). Some use the term *effective rainfall* for the same concept (e.g., Chow, Maidment and Maize,1988; Wilson, 1983; Beven, 2001). However, there is reference in the literature to *effective rainfall* as that part of the measured rainfall that infiltrates into the lower soil structure, and eventually becomes part of the groundwater resources (e.g., Besbes and De Marsily, 1984). In this thesis the term *excess rainfall* is used to refer to that part of the measured rainfall that contributes to the observed hydrograph at the catchment outlet after a storm event.

The conceptualization of the rainfall that falls on a catchment and that causes outflow via various pathways, suggests a partitioning of the rainfall into different resources (Figure 2.4). Some of the measured rainfall will follow the route of evaporation and evapotranspiration, and some will infiltrate deep into the soil where fractured rocks and joints can cause detention of water (also see Shaw, 1994 and Beven, 2001). Some will follow the route of water flowing back to the rivers along the four conceptualized *pathways.* (A pathway is defined as a set of pathlines conceptually grouped together.) These pathways are associated with Hortonian flow, Hewlett flow, throughflow and baseflow. Both the Hortonian and Hewlett flows have been lumped as quickflow runoff responses (Figure 2.4).

The excess rain that falls on the catchment might not be that exact same water flowing from the catchment outlet during the peak flow, but may cause existing water in the soil layers of the catchment to flow out and to be replaced by the rain (Cey *et al*, 1998). Should this happen, some of the measured rainfall will be 'left behind' in the soil structure to add to a follow-up rain event's runoff. The more excess rainfall, the more runoff is measured from a catchment. Similarly, the less excess rainfall, the less runoff is measured. Thus, antecedent catchment conditions (be it wet or dry catchment conditions) play an important role in the estimation of excess rainfall of a storm event.

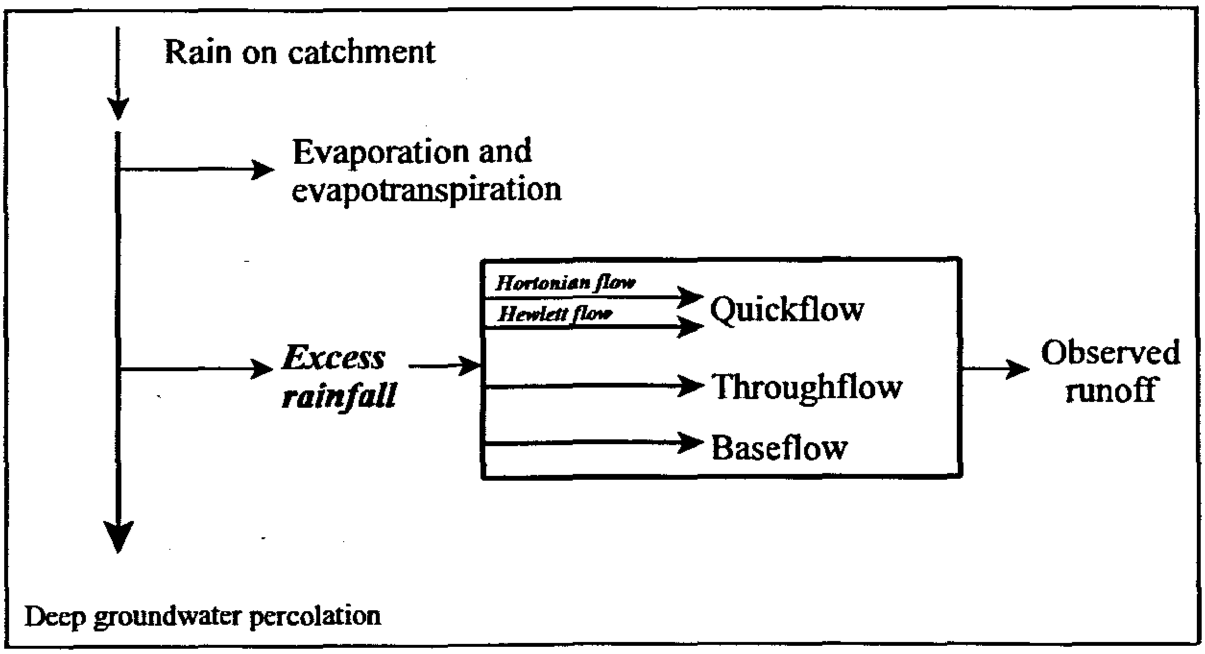

Figure 2.4: Partitioning of rainfall among different conceptualized pathways.

2.5. Conceptualization of water flow velocities down the catchment slopes

The preceding sections have highlighted the various hydrological pathways that water can follow over/through the catchment to the outlet. The rate at which the flow occurs, measured at a point, is defined as a volume per time unit. Consequently, it is necessary to determine the velocity profile along the different pathways in order to derive an estimate of the discharge profile.

The velocity at which water travels through the different paths is dependant on the path length and a time unit:

$$\boxed{\text{Velocity} = \frac{\text{Distance}}{\text{Time unit}}}$$

While the pathway (or streamline) is a vector that reflects the physical characteristics of the catchment profile (slope, slope length, etc.); the velocity profile is likely to differ among the flow components' pathways. These velocity profiles vary along each pathway and will determine the time that water takes to reach the outlet. The three different flow components, as described earlier, are distinguished mainly by the different travel velocities along their respective pathways.

2.5.1. Surface flow

Surface flow is usually the fastest moving flow component and will reach the catchment outlet first. Surface flow travels along the pathways determined by the slopes and aspects of the catchment's surface. It's travel velocity is a function of the surface roughness, the surface slope and the hydraulic depth of flow. These travel velocities can be estimated from Manning's equation. Kelbe, Snyman and Mulder (1996) used this method to estimate the flow rates for a rainfall event on a small catchment in the Ngoye hills. They assume:

1. that the land use indicates the surface roughness (indicated by Manning's n),
2. that there is a constant hydraulic depth for a unit of rainfall for each unit area, and
3. that the slope of the catchment indicates the slope of the surface flow.

Manning's equation has also been used to determine the velocity of channel flow (V, in m/s) (Chow *et al*, 1988):

$$V = \frac{R^{2/3} S^{1/2}}{n}$$

where R = the cross sectional radius of the channel flow (in metres)

S = slopes of the channel

n = Manning's coefficient (a roughness coefficient).

The Manning's equation is derived for the concept of flow in a circular pipe of hydraulic radius R where (Chow *et al*, 1988):

$$R = \frac{A}{P} = \frac{\pi D^2 / 4}{\pi D} = \frac{D}{4}$$

where

A = the cross sectional area of the pipe,

P = the wetted perimeter of the cross section of the pipe,

D = diameter of the pipe.

Kelbe *et al* (1996) adapted Manning's equation to determine flow velocity of saturated surface flow by replacing the hydraulic radius R with the hydraulic depth of the flow. Chow *et al* (1988) explains this assumption for turbulent flow, where the friction against flow in a pipe depends on the surface roughness.

2.5.2. Baseflow

Baseflow travels through the soil structure until it reaches the saturated zone, from where it follows the paths of least resistance along the hydraulic gradient. The travel velocity is dependent on the the soil permeability and the hydraulic gradient of the groundwater along the flow path through the soil matrix or fractured zone.

The flow rate is determined by the hydraulic properties of the saturated zone that can be described by Darcy's Law (Todd, 1980). The Darcy velocity (specific discharge) is directly proportional to the hydraulic gradient (∂h/∂L) of the drainage surface and the hydraulic properties of the porous material (the hydraulic conductivity K).

$$Q = AK\frac{\partial h}{\partial L}$$

Where Q = the specific discharge

A = cross sectional area (m^2)

K = hydraulic conductivity (in metres per day)

∂h = difference in vertical height

∂L = difference in horizontal length

The hydraulic gradient is generally described by the slope of the water table (Figure 2.5).

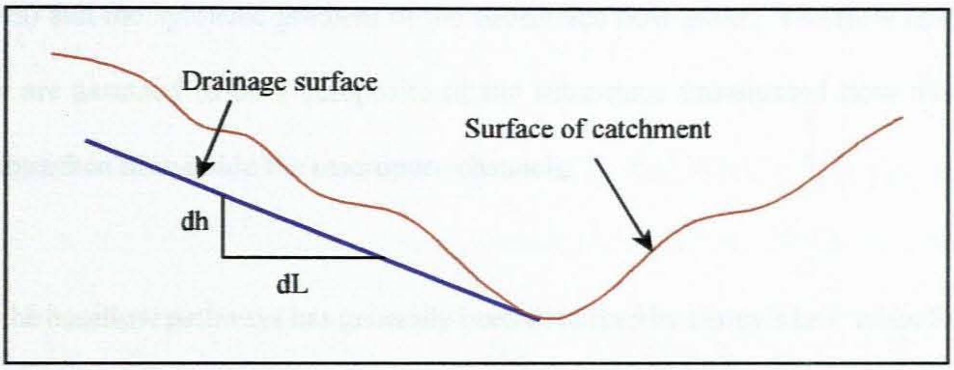

Figure 2.5: Groundwater slope and surface of the catchment.

The hydraulic conductivity strongly depends on the nature of the soils. Typical values of the hydraulic conductivity are available in most groundwater text (e.g., Table 2.1 from Todd, 1980).

The flow path through fractured rock and joints and their travel times are not easily defined, although the geochemistry of the water can indicate the nature of these pathways, especially in the case of long residence times (Beven, 2001). The necessity to determine these pathways has been motivated by a concern of water quality (Eagleson, 1986). Estimation of travel times along these pathways in fractured rock is still an open field for research (Beven, 2001).

2.5.3. Throughflow

Throughflow is a slightly delayed flow through the unsaturated soils. It has been described (Paragraph 2.2.2) as a mixture of water flowing through the soil matrix and macropore openings in the soil structure. The macropore flow would function like surface flow, while the soil flow would be equivalent to Darcy's flow. Flow along the throughflow pathways is dependent on the soil properties and the level of macropore development. Velocity of the throughflow is dependent on the soil moisture and resistance against flow. Throughflow will firstly infiltrate the soil structure and then follow the way of least resistance through the macropore structures. Flow velocities are influenced by the macropore development (which could be influenced by land use and soil types) and the hydraulic gradient of the subsurface flow paths. The flow rates of the throughflow are assumed to be a composite of the subsurface unsaturated flow matrix and saturated subsurface flow inside the macropore channels.

Flow along the baseflow pathways has generally been described by Darcy's law, while Richards' equation was developed as a generalization of baseflow to include unsaturated flow (De Backer, 1989; Richards, 1931). Richards (1931) viewed baseflow (flow in the saturated zone) as a special case of unsaturated flow. It applies the same linear relation between the flow velocity and hydraulic gradient (Paragraph 2.5.2), but allows the hydraulic conductivity to vary with soil moisture content. In order to apply the principles suggested by Richards, a full mass balance of soil moisture content in the catchment must be considered.

Beven (1989) gives a full description of the processes involved in the modelling of flow along macropores on the hill slope scale. He lists the variables that play a role in a water movement matrix for unsaturated conditions, where water flows in both vertical and horizontal directions: The compactness of the soil surface, the change in water content, the wetting front velocity, the depth to the water table, the saturated zone wave velocity, the distance to the river and time to reach the river, as well as the time to reach the water table. Some of these variables changes over time according to some function and need one or more parameters to describe the flow (Beven, 1989).

A more simplistic approach is adopted in this research. Throughflow is conceptualized as flow in the unsaturated soil matrix along a surface profile corresponding to the upper surface gradient, along parallel macropores of similar (average) size and lengths. Flow velocities in these macropores are restricted by surface roughness related to the soil structure, soil moisture and land use. The model considers *flow velocities* along the throughflow pathways. The model conceptualizes the flow along throughflow pathways to be dominated by macropore flow. It utilizes the fast movement of water along the macropores in the soil structure to simulate the flow with an adaption of Manning's equation (where Manning's equation is described in Chow *et al* (1988)).

2.6. Influence of catchment morphology on the flow times

The flow velocity in each segment of the catchment is influenced by the upstream area (or the contributing area) of that catchment segment. The larger the upstream area, the more water will be flowing in the stream (pathways) which channels the water through the segment. Also, for a smaller contributing area of a catchment segment (like areas on the catchment boundaries, with no contributing catchment area), it is unlikely to have any stream that channels the water through the segment. In this case the flow times along the segment of the pathway will be much longer than those of water in a river channel close to the catchment outlet.

This brings forth the necessity to add the catchment characteristics, in the form of the contributing area of each point in the catchment, when considering the estimation of the resistance against flow over segments of the flow paths.

2.7. Partitioning of flow along pathways

Conceptually, the excess rainfall will be divided among the different flow paths in the catchment: quickflow, throughflow and baseflow. The amount of excess rainfall partitioned as quickflow is dependent on the interception, infiltration and evaporation rates. The amount of excess rain partitioned to the throughflow and groundwater components depends on the infiltration and percolation rates. Both infiltration and percolation are dependent on the antecedent conditions, the soil properties and the amount of fractured rock in the soil structure.

The kind of rainfall event determines how quickly the soil structure gets saturated during the rainfall event, and thus determines the partitioning of the excess rainfall among the different flow pathways. Soil infiltration rates play a major role in this case. A rain event of low intensity and long duration will allow enough time for a high percentage of the rain to infiltrate the soils (even through crusts on the surface) and percolate down to the saturated zone.

On the other hand, a rain event of high intensity and short duration may exceed the infiltration rate of the soil, limiting the amount of infiltration and percolation. This depends on the antecedent catchment conditions. In the case of a wet catchment, the wetter soils will saturate faster and allow a higher percentage of rain to flow through the surface routes and to reach the river runoff as quickflow. When a dry catchment receives a high intensity storm of short duration, the infiltration of water into the soils might be delayed due to hard crusts on the land surface (depending on the soil type and land use of the catchment). This will also cause a high percentage of surface flow to the rivers.

The rainfall properties, which determine the proportions of flow along each pathway, have been characterized on the basis of duration and intensity. Four basic classes have been arbitrarily defined at this stage of model development: High and low rainfall intensities, both combined with longer and shorter durations of the rain events.

2.8. Mixing of flow components in larger catchments

The three different flow components of river flow are distinguished by their different flow characteristics, derived from the travel paths and the different travel velocities. However, a certain amount of mixing of the three components takes place during and even while the water flows down the river course. These conceptualised flow routes are extreme simplifications of reality where the actual flow is represented by an infinite large number of pathways. Each conceptualized flow pathway is expected to represent the average conditions for a range of paths that exhibit similar characteristic (mean) travel lengths and time scales. The distribution of the travel lengths for the three conceptualized flow components is represented schematically by the diagram in Figure 2.6. The quickflow component is expected to occur over smaller time scales than the throughflow component, while the baseflow component is expected to have the slower pathways, peaking at a point in time much later than the other flow components.

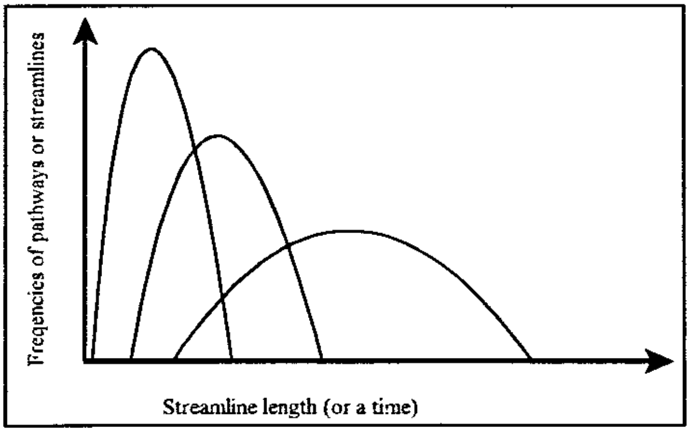

Figure 2.6: Streamline frequencies in the flow net of a catchment.

This concept applies to the physically defined processes in the hill slopes when the flow reaches the nearest channel. The three flow components are immediately mixed in the stream channel.

The mixture of water belonging to the different flow components becomes more evident in larger catchments than smaller catchments, so that the different flow components may not be analytically detectable in the river's hydrograph for large catchments. Not only does the water from different flow components mix, but also water from different subcatchments that is routed along different channel lengths.

This study develops a method for separating the amount of water belonging to each flow component that is validated for small headwater catchments. The transfer process to larger catchments must be done with great caution, because it is not possible to detect these individual flow components for the larger catchments in the same analytical way as headwater catchments.

Despite the mixing of water components in the channels, assumptions of the method only relate to the relative time span that a flow component flows along the hill slopes. Thus the method described in this chapter should theoretically be applicable to larger catchments, making use of spatial information at an appropriate scale.

2.9. Conclusions

This chapter described the conceptualized flow processes of the model. The concepts will be utilized in the determination of a unit hydrograph (defined as a response function) from a rainfall event, using spatial information of the catchment.

The next chapter describes the concepts around the unit hydrograph and response function theory, as well as the separation of flow components in an observed flow hydrograph. It goes on to indicate how these concepts (along with the spatial information of the catchment) can be used to determine a response function for each flow component.

****

3 Conceptualized model

The previous chapter outlined the conceptualized catchment with its hydrological processes, including some concepts regarding the flow of water from the catchment, through the different pathways. This chapter will provide more detail on the hydrograph observed in the streamflow after a rainfall event and the responses along each of the flow pathways to a rain event that is used to validate the model. These responses, in turn, describe the different characteristic flow components. This chapter details the concepts on which the spatial storm hydrograph model is built.

3.1. Conceptual model of the unit hydrograph

Wilson (1983) describes a hydrograph as follows (Figure 3.1): When a rainfall event starts, most of the initial rain is infiltrated into the top soil layers until the soil becomes saturated. Thereafter, water flows either overland or through the soil layers to the streams, which start filling up, indicating the *rising limb* of the hydrograph. This continues until the rain event ceases. Streamflow will reach a *peak flow* and then starts to decline along the *recession limb*. At the *inflection point*, it is assumed that most of the quickflow has stopped running from the catchment. Meanwhile, water, which percolated to the groundwater resources, will gradually move through the catchment soils toward the streams, creating the extended depletion curve. During this time the river flow conditions are called *baseflow conditions*.

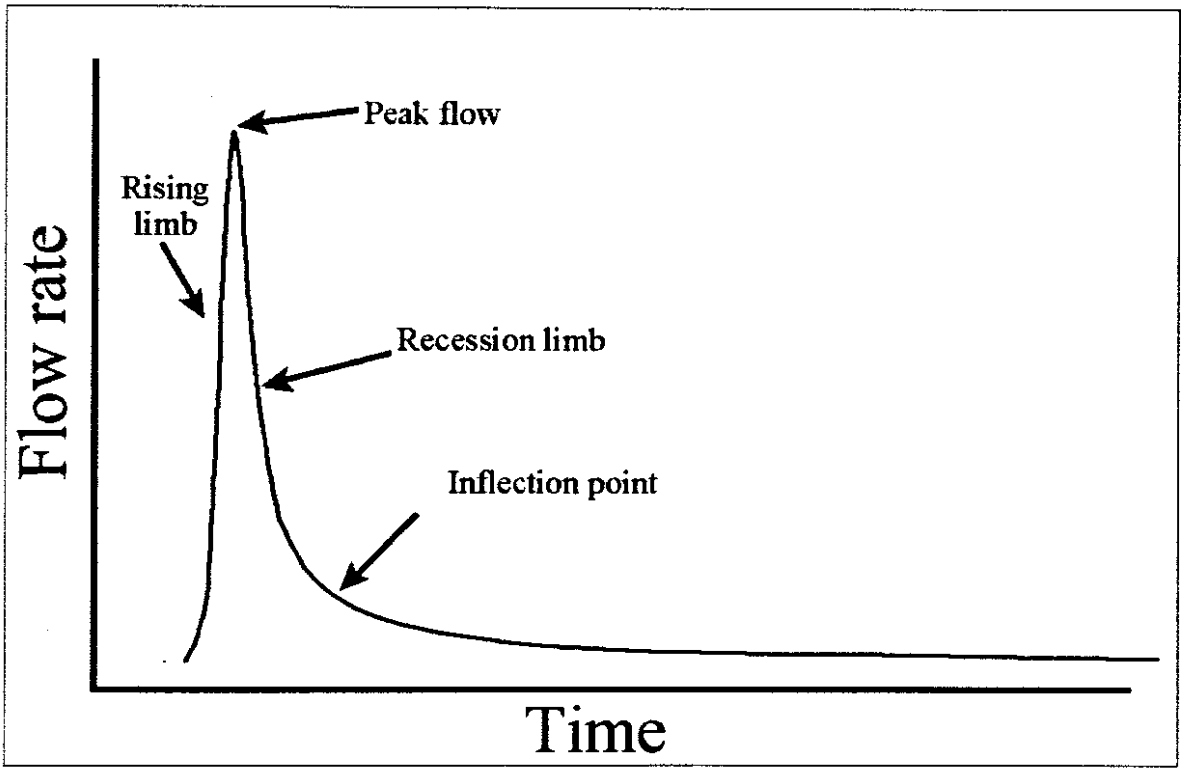

Figure 3.1: Example of a flow hydrograph during and after a rain event.

This model of a hydrograph is a composite of the surface flow hydrograph, the throughflow hydrograph and the baseflow hydrograph.

The **unit hydrograph** [as described by Chow (1988), Shaw (1994), Wilson (1983) and many others] is the streamflow hydrograph produced by only one unit of excess rainfall which falls on the entire catchment as an isolated rain event during one unit of time. The unit hydrograph concept invokes the following assumptions (Shaw, 1994):

1) The <u>excess rainfall is directly proportional to the river runoff</u>. This indicates that a rainfall event of two units of excess rainfall in one unit of time, will produce a hydrograph with ordinates twice as high as the ordinates of the unit hydrograph. For example, a rainfall event of 4 mm excess rainfall will produce a hydrograph which is calculated by multiplying the ordinates of the unit hydrograph (if one unit = 1 mm) by four.

2) The assumption of superposition indicates that two consecutive rainfall events (the second event T hours after the first) will produce a hydrograph which can be calculated by adding the ordinates of the two hydrographs, with the second one being delayed T hours after the first.

3) The assumption of invariance indicates that the direct relationship between the excess rainfall and the runoff does not change over time. This means that the same unit hydrograph applies for different pre-storm catchment conditions. This is the reason for introducing the concept of excess rainfall: The excess rainfall is that part of the measured rainfall that causes the peak in the flow hydrograph after a storm event.

Weaknesses of the unit hydrograph concept stemming from these assumptions, include the following (from Shaw, 1994):

1) Excess rainfall must be estimated for different pre-storm catchment conditions, i.e., wet and dry conditions, as well as the type of rain event.

2) The assumption of superposition implies that the river responses of consecutive rainfall events are independent from each other. In reality, the response of the catchment on the second rain event will very likely depend on the catchment response on the first. However, this weakness is handled by the difference in excess rainfall from one storm event to the next.

3) The assumption of uniform rainfall over the entire catchment is unrealistic in areas where rainfall varies in relation to the size of the catchment.

Cey *et al* (1998) have indicated the importance of pre-storm catchment conditions for the estimation of the storm hydrograph. They conclude (on the issue of storm events) that "antecedent soil moisture conditions may have the largest influence on stream flow response...effecting the magnitude...of stream flow...during a single storm event...In particular, it appears that the riparian zone has a considerable influence on the magnitude and timing of streamflow during a storm event."

The invariant unit hydrograph concept has been adopted in this study and is used as the basis of the spatial model.

3.2. The runoff coefficient from the literature

Peak runoff of a storm event can be calculated from the runoff coefficient of the catchment. Shaw (1994) defines the runoff coefficient as:

$$Q_p = C A I$$

where Q_p = the peak flow of a storm event

C = the runoff coefficient of the catchment

A = catchment area

I = the intensity of rainfall during the time of concentration T_c

The time of concentration, T_c, is the time required for water, which falls on the farthest catchment point, to travel to the catchment outlet. This assumes that the entire catchment is contributing to the flow at the catchment outlet, and that the peak of flow has been reached (Shaw, 1994). The value of the runoff coefficient depends on the catchment's characteristics and can vary between 0.05 for sandy catchments, to 0.95 for impervious urban areas (Shaw, 1994).

Gottschalk and Weingartner (1998) describes the runoff coefficient as the amount of rainfall that appears as quick runoff. Hebson and Wood (1982) describe *CA* as the catchment area contributing to peak runoff, *C* being the fraction of the catchment area (*A*) active in contributing to quickflow. This is demonstrated in Figure 3.2 as described by Newson (1995), for a time-dependent *C*. Chow *et al* (1988) define a catchment's runoff coefficient as the ratio of *R*/*M*, where *M* is the measured rainfall and *R* is the corresponding depth of runoff. Beven (2001) indicates that *C* must give account of the antecedent catchment conditions, varying from storm to storm for the same catchment, and from catchment to catchment for a given storm type.

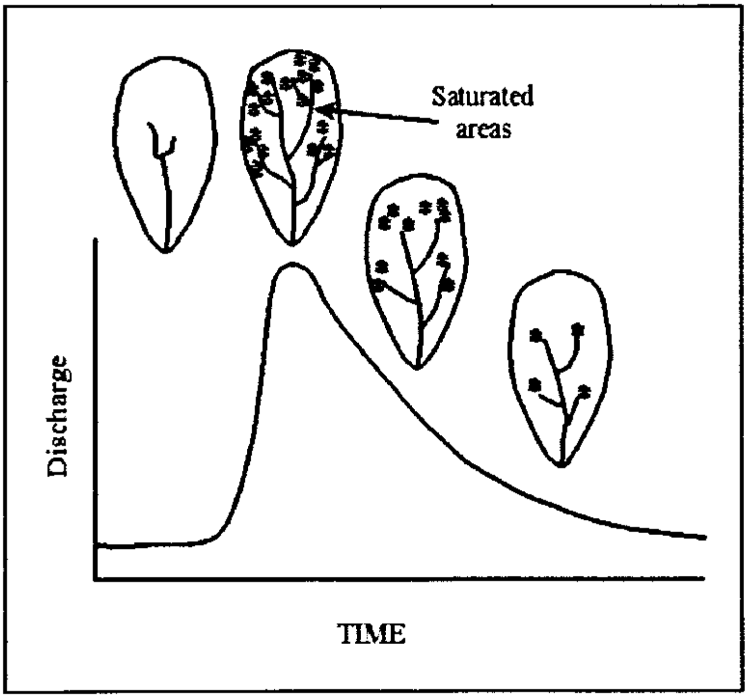

Figure 3.2: Presentation of a changing contributing area to runoff (after Newson, 1995)

Although the runoff coefficient is traditionally assumed to be a constant, Gottschalk and Weingartner (1988) use a stochastic Beta distribution function to describe a varying runoff coefficient C over time, where $0 \leq C \leq 1$, or a varying catchment area that contributes to the storm hydrograph.

In this study the runoff coefficient C establishes the fraction of measured rain that contributes to the observed hydrograph (Figure 3.3) as defined by Beven (2001):

$$a' + b' + C = 1$$

where a' = the fraction of rain lost from runoff due to evaporation and evapotranspiration, and

b' = the fraction of rain lost from runoff due to deep groundwater losses.

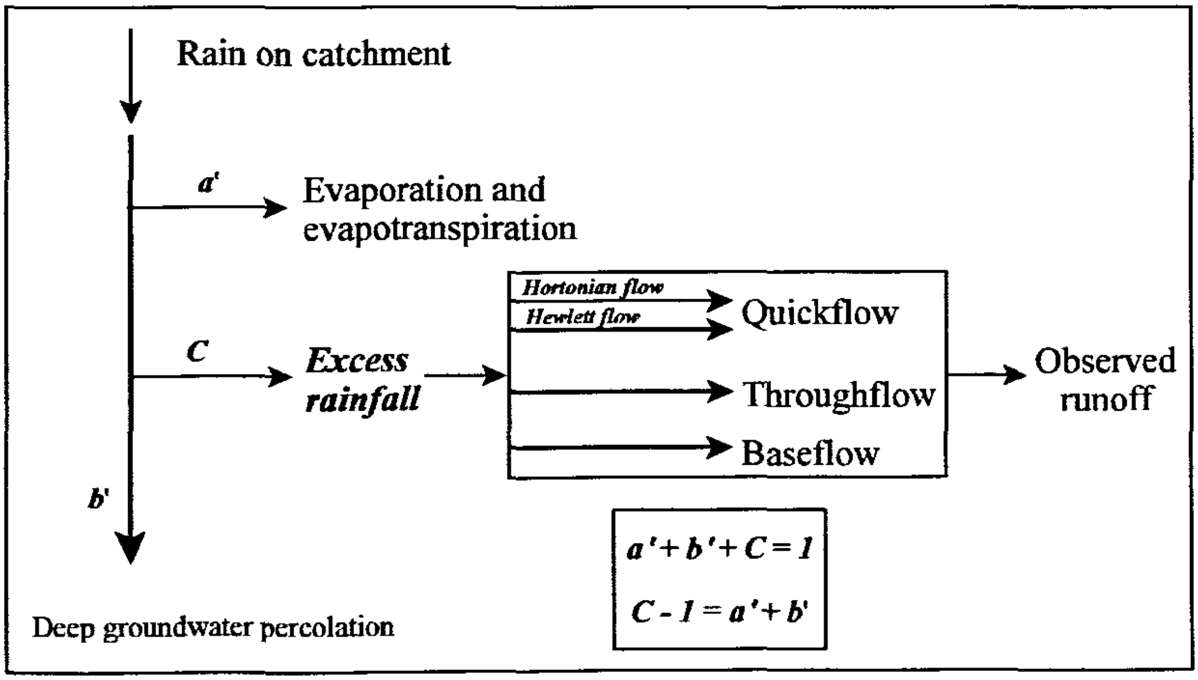

Figure 3.3: Partitioning of the observed runoff into different flow components.

Thus, $1 - C$ will account for the undetermined losses that occur while water moves over/through the catchment from rainfall to streamflow. These processes of loss include the evaporation; evapotranspiration; as well as percolation into deep groundwater resources, which does not form part of the daily hydrological cycle (Paragraph 2.4). The runoff coefficient will vary among different catchments and rain storm types.

3.3. Response functions

The triangular three parameter approach (Shaw, 1994) is an idealized hydrograph model that is described by the time to peak (TTP), the time to recede (TR) and the peak flow of the hydrograph (Figure 3.4). In this study it is recognized that the characteristic unit hydrograph is neither triangular, nor the same for each flow component.

The concept of the unit hydrograph is adapted in this study to represent a *response function* from a catchment for an individual storm event that lead to river runoff from an identifiable pathway. The unit hydrograph concept (Shaw, 1994) links excess rainfall to river runoff through one direct pathway, using a set of parameters (the time to peak, the time to recede and the peak runoff) interrelated by a mathematical function. This study extends this concept to several preferential pathways with very different response functions. These include the quickflow pathways; the

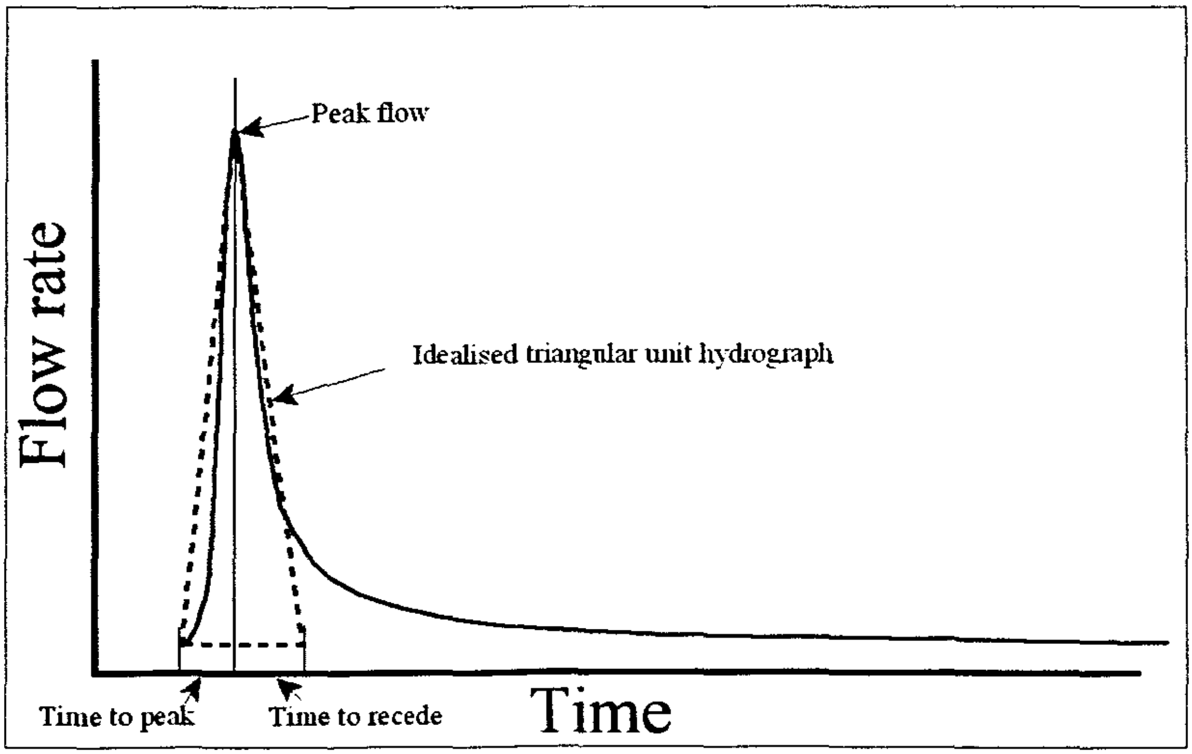

Figure 3.4: The triangular idealized unit model of the unit hydrograph estimations, using the time to peak, the time to recede and the peak flow.

throughflow pathways; the baseflow pathways; as well as the channel flow pathways. It attempts to overcome some of the weaknesses on the unit hydrograph model (described in Paragraph 3.1). The spatial features of the catchment replaces the mathematical function which relates the time to peak, the time to recede and the peak runoff in the traditional unit hydrograph calculations. It introduces the concept of different pathways of different flow components for the estimation of the hydrograph. The end result will be the convolution of the individual storm hydrographs for each of the flow components, from spatial catchment information, to derive the river runoff.

The response in the river flow to a rainfall event in the catchment, as described in terms of a hydrograph, is represented by a response function. A hydrograph is the response that is *measured in the observed streamflow after a rain event in the catchment*. However, the responses of the different flow components to a rainfall event *cannot be easily measured* individually. They can only be derived from the observed hydrograph using hydrograph analysis. They will be referred to as the different *response functions* for the different flow components. After scaling them to conserve the total rainfall, they will be called the *storm hydrographs* of the different flow components.

3.4. The instantaneous unit hydrograph

The concept of the unit hydrograph (UH) was initially described by an American engineer, Sherman, in 1932 (Shaw, 1994). Subsequently, Nash (1957) proposed the concept of an instantaneous unit hydrograph (IUH), for calculating the total runoff, using a cascade of linear reservoirs to route the excess rainfall down the catchment. The rainfall stems from one unit of instantaneous rainfall that is applied uniformly over the entire catchment.

Different IUH models have been developed for various applications, some of which are summarized by Franchini and O'Connell (1996).

A further development on the IUH concept was the geomorphological instantaneous unit hydrograph (GIUH) described by Rodriguez-Iturbe and Valdes (1979). The GIUH is a statistical probability function that describes the distribution of travel times for a water drop falling on any position in the catchment and flowing to the catchment outlet. It is summarized by Francini and O'Connel (1996) as: "The basic idea of the GIUH is that the distribution of arrival times at the basin outlet of a unit instantaneous impulse injected throughout a channel network, is affected both by the underlying natural order in the morphology of the catchment and the hydraulic characteristics of the flow along the channels themselves . . . the underlying natural order in the morphology is represented by the Horton ratios which, in turn, are based on a classification of the channel network of the catchment according to Strahler's ordering scheme, whereas the holding time of a drop of water within a stream of a given order is represented by means of an exponential law which is, however, a conceptualizing of the true flow dynamics."

3.5. Spatial modelling

The digital spatial map has its origins in the mathematical matrix (often referred to as a *raster* or a *grid*), where each individual element in the matrix represents a square (or a rectangle) on the ground in the real world (called a pixel, from PICture ELement, or called a cell). The different pixels contain digital values, representing characteristics of the square that it represents in the real world. These digital values can represent land use characteristics, or soil types, or mean heights above sea level, etc. The matrix containing the heights above sea level, called the Digital Elevation Model (DEM), is of special importance to spatial modelling of a catchment's hydrology.

The DEM is used to derive the slopes at each point in the catchment, the flow direction of water in each pixel (the aspects) and the river courses (from flow accumulation grids). The flow directions of water from each pixel will provide the travel paths that water travels from each pixel to the catchment outlet. These concepts on spatial modelling will be illustrated in Chapter six.

3.5.1. The geomorphological response function

Using a DEM, the cumulative travel distance of water from each point of impact on the catchment to the outlet can be calculated by determining the vector describing the flow path. The frequency histogram of the cumulative travel path lengths is a reflection of the geomorphological characteristics of the catchment. It is referred to as the *geomorphological response function* for a catchment, because it is a representation of the catchment geomorphology's influence on the observed hydrograph of the catchment.

The effect of the catchment shape on the hydrograph is described by Gordon, McManon and Finlayson (1992). Examples are shown in Figure 3.5.

The effect of the catchment's shape on the hydrograph will be dealt with inherently within the methodology of the unit hydrograph construction from spatial information. This is accomplished by considering the paths that water flows from each catchment segment to the outflow.

3.5.2. Replacing flow paths with flow time

The first implementation of a unit hydrograph based on spatial information was initially implemented by Ross (1921) who split the catchment up into different zones (Figure 3.6). The travel time of water from each zone to the outlet determined the area (and position in the catchment) of the zone. The amount of runoff generated from each zone was routed through the different zones to the outlet. The delays of the runoff from each zone of the catchment can then be presented in a time area histogram, to produce a flow hydrograph (Figure 3.6).

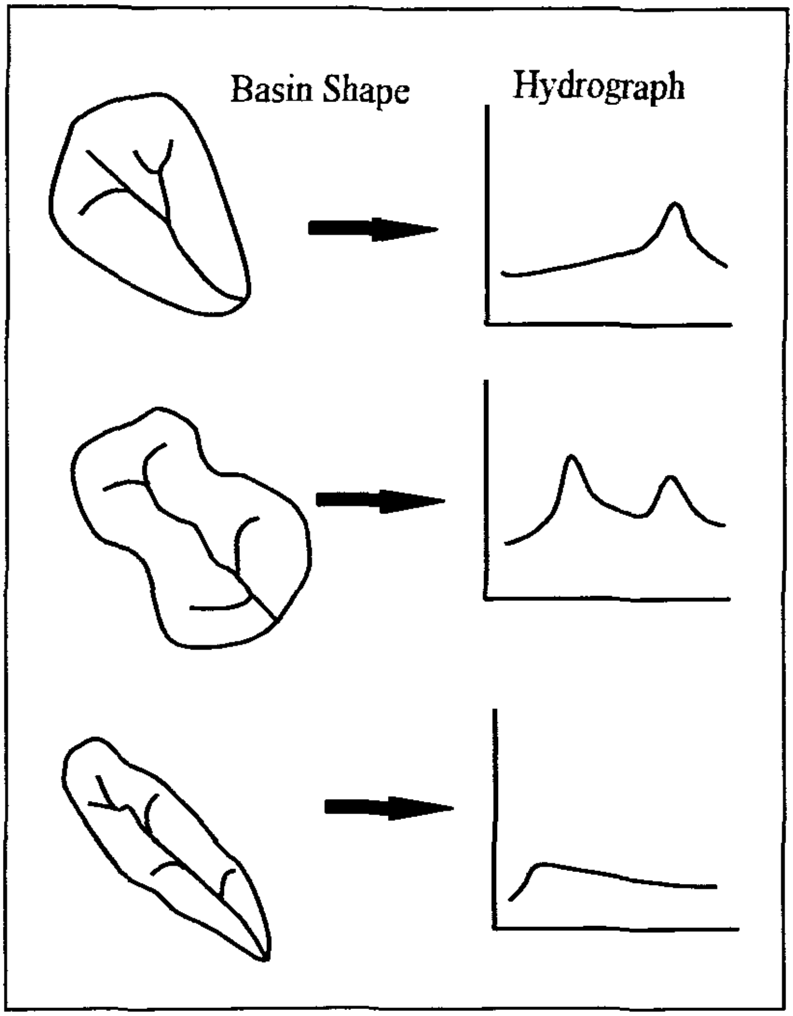

Figure 3.5: Demonstration of the effect of catchment shape on the hydrograph (after Gordon, *et al*, 1992).

The time that water takes to run over or along an element of a flow path (or a pixel) in a DEM, can be estimated by using conventional water flow equations. Thus, the cumulative travel distances to the catchment outlet can be replaced by the cumulative travel times along the flow paths. Calculating the cumulative travel times for each pixel, along the flow paths, will result in an array of travel times that will provide a more realistic representation of the unit hydrograph.

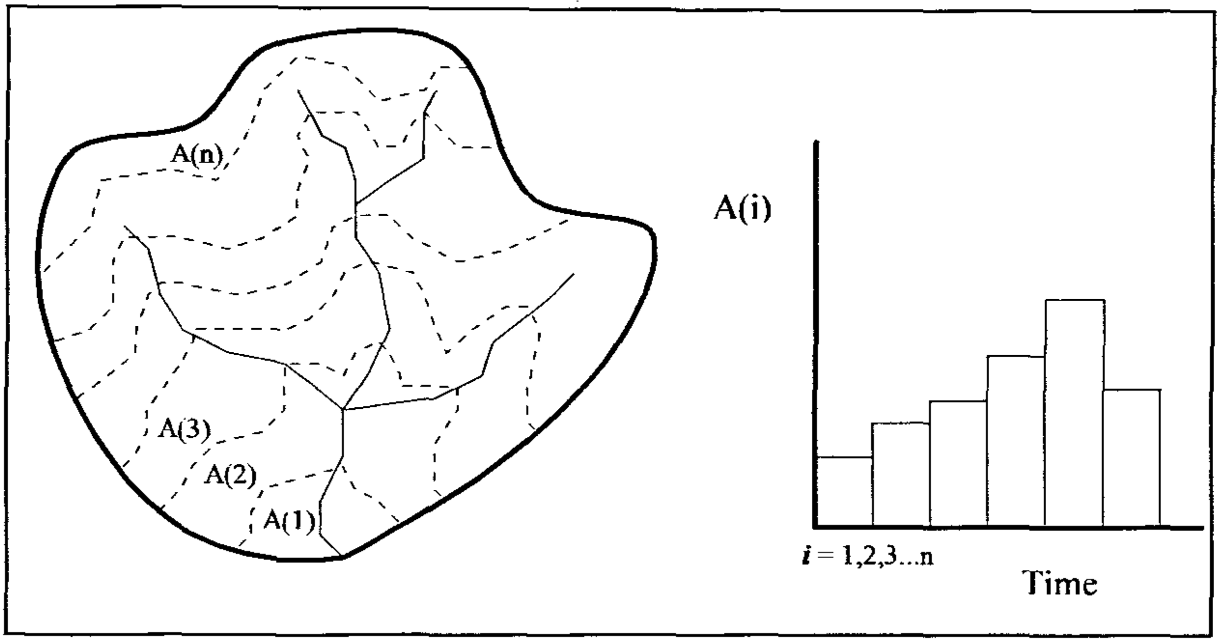

Figure 3.6: A time area histogram can be constructed by dividing the catchment into n areas (A) at the different travel times from the outlet (after Beven, 2001).

3.5.3. The travel time response function

If the velocity of flow across a flow path segment can be estimated, then the time taken to flow across the segment in the flow direction is given by:

$$T = \frac{D}{V}$$

where T = travel times

D = travel distances, represented by the (rectangular) pixel dimensions and

V = travel velocities.

A cumulative summation of travel times along the entire path length gives the total travel time that water will take from each location to reach the outlet. The frequency histogram of the cumulative travel times is then referred to as the *travel time response function*, which is assumed to represent the unit hydrograph response.

Travel velocities of water over each pixel can be estimated, making use of the conceptualized flow paths of water over the pixel.

3.5.4. The instantaneous unit hydrograph in the spatial arena

The concept of the IUH has been extended to the spatial arena with the evolution of GIS and grid-based DEM's, as described in the previous three paragraphs. The initial concepts of Nash (1957) that is of routing a drop of water down the catchment through the river network; was extended by following a drop of water from each pixel represented in the catchment, down to the river, tracing the routes indicated by the DEM of the catchment.

Kelbe *et al* (1996) implemented this spatial modelling technique using a GIS and a DEM. The DEM for the catchment was used to define the flow paths of water down the catchment, along the paths of steepest topographical gradient. They used flow direction and pixel dimensions to estimate flow path lengths. A raster grid of the total path lengths from each source area (or pixel) in the catchment to the outlet, was used to calculate the frequency histogram of cumulative path lengths, or the geomorphological response function. The geomorphological response function was then compared to observed flow hydrographs caused by isolated high intensity, short duration storm events. They were effectively investigating only the quickflow component.

The studies of Kelbe *et al* (1996) determine not only the distances that water travels to the catchment outlet, but also the travel times of water flowing over each individual pixel. They applied the flow lengths, the slopes, the aspects and the pixel's land use in an adaption of Manning's equation. They then summed the travel times to the catchment outlet along the flow paths. The frequency histogram of the cumulative travel times (the travel time response function) is then assumed to represent the hydrograph.

The equivalence between the unit hydrograph and the time response function rests on the assumptions of the unit hydrograph, namely that one unit of uniform excess rainfall falls on the entire catchment in one time step. Kelbe *et al* (1996) used high intensity rain storms of short duration which fell on a relatively small research catchment (3.2 km^2), to minimize errors in uniformity of rainfall and mixing of flow components. They concluded that these two factors contributed to the successful implementation of the analogy between the observed hydrographs and the travel time response functions.

Muzik (1996) used similar arguments to explain, in simple mathematical terms, how the frequency histogram of the cumulative travel times is in fact an estimation of the hydrograph.

The travel time response function can be derived for any catchment from a DEM in most grid-based GIS software packages. However, the underlying assumptions of this unit hydrograph need careful investigation and refinement. One of the underlying assumptions of this approach is that the summation of travel times along the travel paths indicates that the flow in each pixel is independent from the flow in every other pixel (Maidment *et al*, 1996). However, interdependency of flows amongst pixels is introduced to this model by considering the catchment area contributing runoff to each pixel. It has been discussed (Paragraph 2.6) how the catchment area of each pixel influence the flow velocities (and flow times) along the flow paths.

3.6. The conceptual model

This study utilizes the concept of different preferential flow paths to estimate the time response functions of different flow paths, for various kinds of storm events in a catchment.

Previous studies (Kelbe *et al*, 1996; Muzik, 1996) have assumed a single pathway for each location of the catchment (i.e., each location in the catchment can lead water to the outlet through only one pathway). The partitioning of the flow through the various conceptual pathways is controlled by the dominating processes for a unit of excess rainfall. Low infiltration leads to a greater proportion of quickflow. High infiltration and percolation rates promote more subsurface flow. These pathways are interrelated and dependent on rainfall and catchment characteristics.

3.6.1. Singularity pathway model

Lindsay, Kholer and Paulhus (1972) have described the features of an elemental hydrograph for a catchment, that contains only one flow path from every location in the catchment, called a singularity pathway model (Figure 3.7). This singularity model assumes that intercepted rainfall is stored in the catchment before runoff can proceed. The discharge rate $I(t)$ will increase until it reaches the uniform rainfall rate I and the detention volume (area above the discharge curve in Figure 3.7) becomes constant. At this point the system is in equilibrium until the uniform rainfall rate changes.

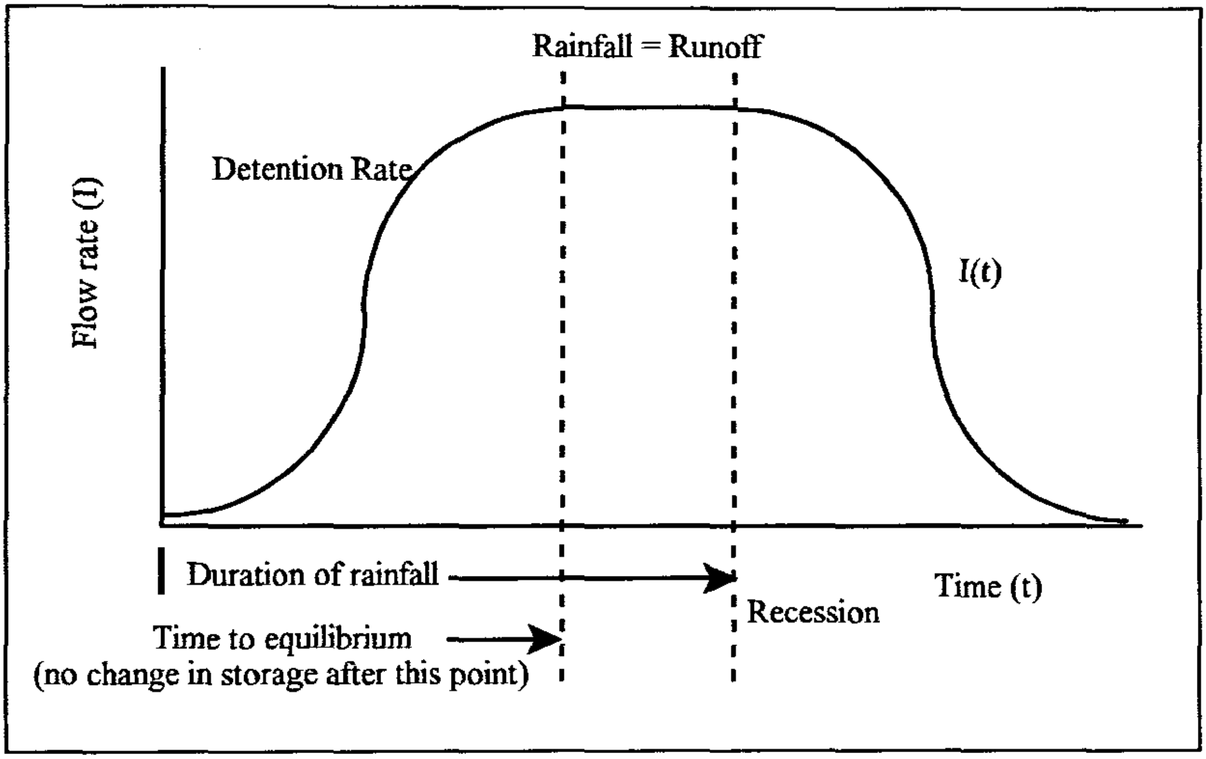

Figure 3.7: Conceptual model of discharge I(t) for a single pathway model from a small catchment under uniform rainfall rate I (after Lindsey, Kohler and Paulhus, 1972).

The shape of the discharge curve $I(t)$ (the recession limb of the hydrograph) for a uniform rainfall rate I is dependent on the physical characteristics of the drainage area that determine the pathway that the intercepted rainfall follows to the catchment outlet (Figure 3.8). For a singular pathway model, the characteristic summation curve (S-curve) should be the inverse of the recession curve. In reality, the detention storage occurs in different reservoirs (surface detention, soil moisture and groundwater). These reservoirs each have very different rates of recharge and discharge. Consequently, the summation curve is generally very different to the recession curve when multiple pathways through different reservoirs exist.

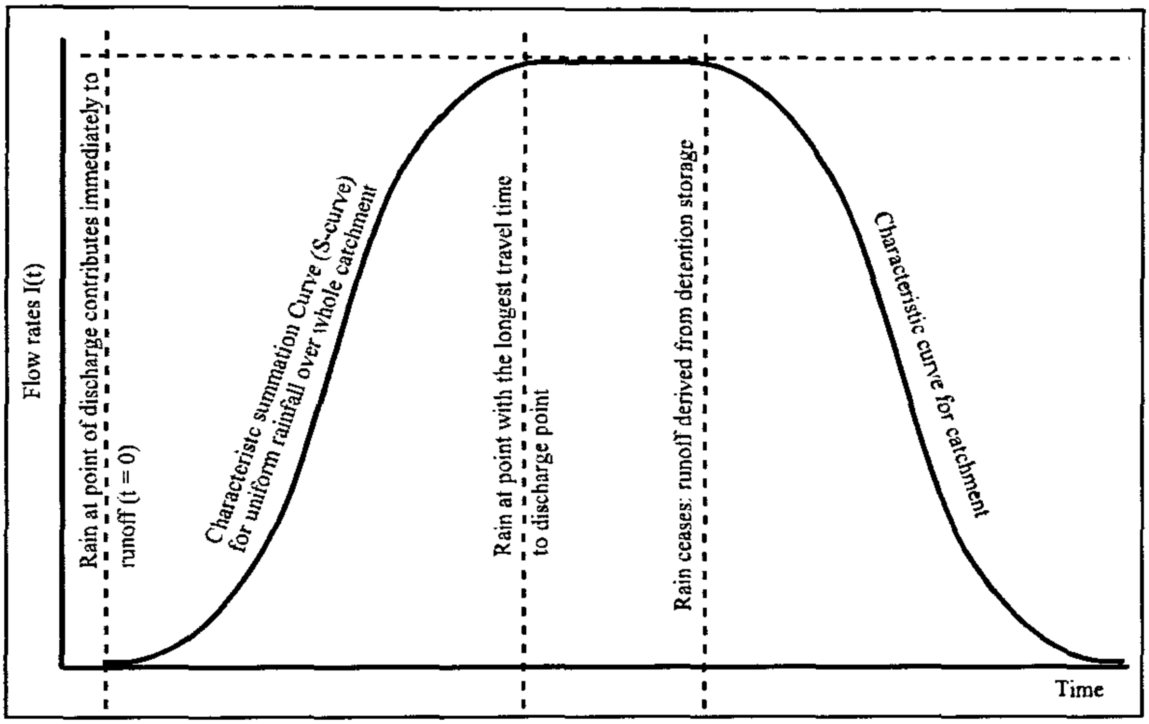

Figure 3.8: Concepts of the singular pathway response function.

The singularity model can be equated to the elemental hydrograph for surface flow described by Lindsay *et al* (1972). This model has been frequently used to simulate the rising limb and the time to peak of small catchment response functions.

In a multiple pathway system it is proposed that several of the singularity models can be superimposed for each catchment segment, if the pathways are well defined. This concept is applied in the development of a multiple pathway model in this study.

3.6.2. Multiple pathway model

Rainfall impinging on a dry soil surface will be expected to infiltrate and percolate until the infiltration capacity is exceeded. It will then be likely that some of the flow will be diverted along the surface pathlines, as well as the subsurface pathlines. These changes between the pathlines are generally dependent on the rainfall regime, as the geomorphological features are static.

Low rainfall intensities (smaller than infiltration capacity) will invariantly induce flow through the subsurface pathways. When saturation is achieved in the subsurface zones (or infiltration capacity is exceeded), many of the pathlines linked to subsurface pathways can switch to surface pathways. The switch is usually progressive, leading to more and more pathlines changing between different conceptualized flow pathways.

This study examines the pathways in order to develop a spatially based model of catchment runoff components. It assumes that the discharge hydrograph is composed of several well-defined flow components. These components have been attributed to the predominance of different hydrological processes that can force the flow of water through the catchment to follow a predominance of pathways. The Hortonian, Hewlett, throughflow (unsaturated) and baseflow (saturated) pathways would create distinctly different response functions for hill slope processes. It is conceptualized that intermixture of water along different flow pathways occurs in the river and not along the hill slopes of the catchment. Once the flow reaches the bottom of the hill slope, all components become channel flow.

Hydrograph analysis suggests that it is possible to simulate the composite discharge response function in the river by superimposing the four characteristic response functions for each pathway (Paragraph 3.1). The dominance of the different hill slope pathways is a function of the different storm types. For example, rain storms of low intensity and long duration will induce minimal Hortonian response; while the baseflow response function will play a significant role in the total flow hydrograph.

The shape of the response function curve for each pathway will be dependent on the physical characteristics of the catchment, and the processes that govern the flow along the pathway. The main contributing factors controlling to path lengths are:

1) the shape and size of the contributing area, and
2) directions of flow in pathway segments that are related to geomorphological and geological slopes.

The times taken to travel the full path lengths are affected by several other factors that include:

1) hydraulic gradient,
2) hydraulic conductance of the medium through/over which the water flow, or resistance to flow over/through the medium (influenced mainly by land use, soil types and geology, as well as antecedent conditions), and
3) the amount of upstream water that is accumulating and contributing to the flow at each point along the pathway to the outlet. This increases the depth of flow over a surface or induces saturation with increasing upstream flow. It will also determine at which point that flow become channel flow.

3.6.2.1. Hortonian quickflow on overland flow

The Hortonian S-curve (or response function) will be directly related to the catchment size, shape, slope and surface roughness. An example of a response function of Hortonian flow is given in Figure 3.9 for a small urban catchment in Richards Bay. The Hillside culvert is situated at the outlet of a partially paved urban catchment. The measuring point of the catchment flow is indicated on the aerial photograph of the catchment in Figure 3.9. Measurements include the rainfall; runoff in the river; conductivity of surface runoff and groundwater elevation in a borehole situated within the culvert catchment area, close to the culvert. A rainfall storm of high intensity

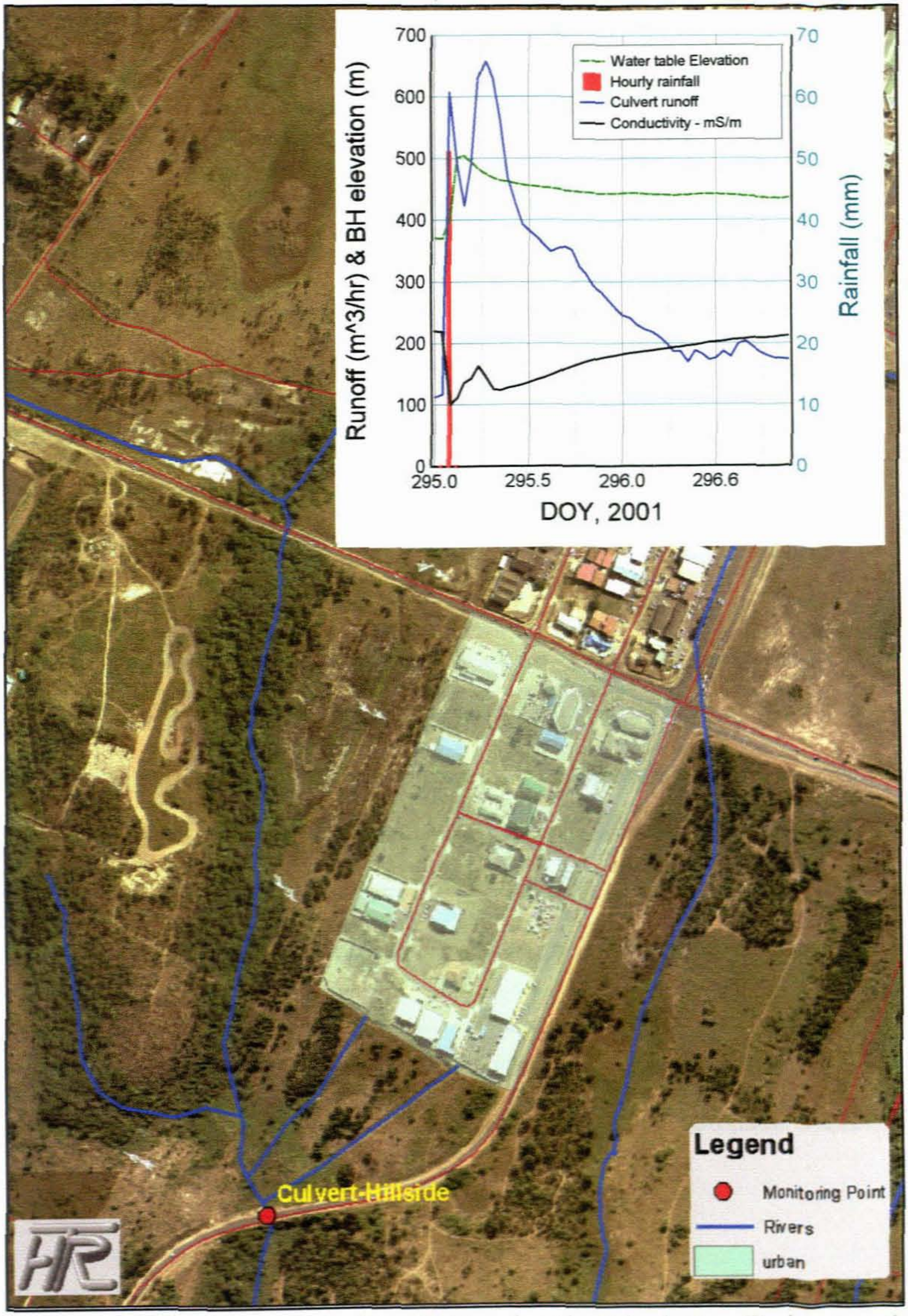

Figure 3.9: The aerial photograph of the Hillside culvert in Richards Bay. The insert graph indicates the measurements during a rainfall storm of high intensity and short duration (50 mm of rainfall in one hour).

and short duration (52 mm rainfall measured within one hour), occurred on 22 Oct. 2001 (Day Of Year 295). The inserted graph shows the rainfall, observed surface runoff and water table elevation, along with conductivity.

In this example, the rainfall on impervious area was diverted directly to the outlet point as discharge, where hourly flow measurements were being conducted (Figure 3.9). The graph indicates the Hortonian flow as the very first sharp peak in the runoff hydrograph that peaks at the same time as the rainfall. The flow causing the subsequent hydrograph peaks (six hours later) relates to proportional contributions of the (Hewlett) quickflow, the throughflow and baseflow from the pervious section of the catchment.

Electric conductivity (EC) measurements for the example on DOY 295 (inserted graph in Figure 3.9) indicate a minimum value during the time of the Hortonian flow response. EC dropped from 220 mS/m to 100 mS/m within the hour of the rainfall, indicating the presence of rainfall water at the outlet. The EC then rose slowly back toward pre-storm measurements during the time that flow changed from overland flow to storm flow. During storm flow, the EC again dropped to a minimum during quickflow conditions before increasing toward pre-storm conditions.

Studies by Mulder (1984) have indicated little or no Hortonian surface flow on the hill slopes in the Ngoye range, so it is unlikely that this flow path is important in catchments consisting of mostly pervious soils with no urban development.

3.6.2.2. Hewlett quickflow

The Hewlett concept recognizes the large role that the saturated areas have in the flow of water over the catchment slopes. It is assumed that the runoff from some variable saturated areas contributes to the quickflow response function. Manning's equation is used to describe the travel time of water along the surface pathways, as discussed in the following paragraph. Rain storms of high intensity over the entire catchment would promote Hewlett runoff from a large fraction of the catchment.

3.6.2.3. Channel flow and surface runoff

Chow *et al* (1988) indicated that channel flow velocity can be calculated by using the slope; the hydraulic gradient; the cross sectional area of the channel and Manning's *n*. Kelbe *et al* (1996) adopted this model to estimate the travel time of water over a saturated surface by using the square root of the slope; the slope length; Manning's *n* and replacing the hydraulic radius with the hydraulic depth, or the depth of water flowing over the surface. Thus the flow velocity can be equated to the square root of the slope and a coefficient (which is then related to the slope length, Manning's *n*, and a uniform hydraulic depth). Having a uniform slope length for similar sized pixels, means that only Manning's *n* changes with a change in the flow surface roughness, for different pixels:

$$\text{Overland flow velocity} \simeq (\text{slope})^{1/2} * (\text{a resistivity factor})$$

where the resistivity factor is dependent on the hydraulic depth and the surface roughness.

3.6.2.4. Baseflow

Water infiltrating into the soil surface will percolate downward from the surface through the soil structure until it reaches the saturated zone. This part of the path length is very much dependent on the antecedent conditions of the catchment. The flow pathway then flows down to the river discharge point along a slope similar to the groundwater gradient. These flow paths follow the paths of least restrictions. Rocks or impermeable soil structures, joints and fractures will create barriers and conduits to deviate the water from the most direct route. The travel time of water along this pathway is dependent on the depth from the soil surface to the saturated zone, the porosity (storativity) and the hydraulic gradient of the saturated zone.

In shallow water systems the baseflow is usually dominated by the saturated flow through a soil matrix. When fractured rock systems become important for baseflow, the pathways are diverted along the fractures rather than down the topographical surface. This creates a concentration of flow paths through the fractured zone.

The velocity of water moving through a cross sectional area of a porous material can be described by Darcy's Law (Shaw, 1994):

$$\text{Baseflow velocity} \simeq (dz/ds) * (\text{the hydraulic conductivity})$$

where the hydraulic gradient is dependent on the change in piezometric head (dz) along a flow pathline (ds) and hydraulic conductivity, K.

The hydraulic resistivity can be described as the inverse of the hydraulic conductivity (K), i.e., the hydraulic resistivity is $1/K$ (American Meteorological Society's electronic glossary of Meteorology: http://amsglossery.allenpress.com/glossery, 2005). Therefore, the hydraulic conductivity is a function of the soil resistivity profile along the flow pathline.

3.6.2.5. Throughflow

Flow through the unsaturated soil structure is controlled by the infiltration rate of the soils, the depth of the unsaturated zone, the type of soils and the macropore development of the soil structure. It will also be affected by land use, where the land use plays a role in the development of macropores. Flow will take place from the point of infiltration, down into the soil structure and along the paths of least resistance in the unsaturated zone. These paths of least resistance are often the burrows and decaying roots that develop a network of macroscopic subterranean channels, forming the macropore structure of the soil.

Determination of the throughflow travel velocities can be equated to the calculation of either the surface flow processes in the macropores or the flow through porous media based on a resistance model down a gradient. It has been indicated that both the surface and groundwater flow velocities are related to the slopes of either the surface slope or the piezometric head gradient of the groundwater. Detailed information, to derive the flow paths of throughflow to the stream through the paths of least resistance, is absent. Thus, it will be assumed that these flow paths are similar to the surface flow paths, if the macropores in the soil structure are well developed and generally close to the surface. The average hydraulic gradient is assumed to be similar to the slopes of the catchment surface for all throughflow pathways in this study. Thus the conceptual throughflow pathways are also related to the surface slopes, via a coefficient that is dependent on the amount of restriction against water flow through the soil.

3.7. Flow velocities and flow times

The path length of quickflow can be derived from the surface topography. However, the flow velocity will vary along the pathway due to changes in surface features such as the slope and surface roughness. The DEM has been used to determine the most probable pathway from the direction of the steepest gradient. The gradient can be used in conjunction with other surface features to determine the flow rate (the velocity). Other characteristics of the soil and land use can be used to derive an estimate of the resistance (or resistance coefficient) to the flow rate.

3.7.1. Resistance along the travel pathways

As indicated (in Paragraph 3.6.3), the cumulative travel time of water down a flow path is given by:

$$T_j = \sum_{i=j_{origin}}^{i=Outlet} \frac{D_i}{V_i}$$

Where

i, j = the i^{th} catchment segment along the j^{th} pathway, varying from the origin to the catchment outlet.

D_i = the distance that the water travels over catchment segment i

V_i = the average velocity at which the water flows over/through catchment segment i

T_j = Total flow time of water along pathway j to the outlet over every catchment segment i.

The distances D_i are a function of the model resolution (the pixel dimensions). The travel velocities V_i are a function of the physical properties of the catchment at the pixel location (as described in Paragraphs 2.5.1 and 2.5.2), namely the slope gradient (which is again a function of the catchment topography) and a coefficient, indicating *resistivity or resistance*, caused by land use, soil types, etc. This resistance is indicated by the depth of flow and a surface roughness along the surface flow pathways, or the permeability of the soil along the saturated subsurface pathways. The resistance of the throughflow pathway has been described in Paragraph 3.7.2.5 and the role of macropore development in this regard has been highlighted. These measurements of resistance to flow depend on local conditions within the pathline segment (or pixel), but they exclude the flow conditions upstream of the pixel.

Calculating travel times over individual segments of a flow path (pixels), has been done by Olivera and Maidment (2005) and Maidment *et al* (1996). The cumulative travel times (from each pixel to the catchment outlet) are calculated as the sum of the travel times over individual pixels along the travel pathways. This summation indicates that the flow of water over individual pixels is independent of upstream flow conditions. However, flow of water in each pixel is strongly dependent on the amount of water flowing through the pixel. For example, a river pixel contains more flow, with less resistance, than a catchment boundary pixel with the same slope, where there is little inflow and more resistance against flow.

Calculating the number of pixels which contribute water to a particular pixel, provides an estimate of the discharge contribution to flow from that pixel. The contributing area of each pixel is a model parameter that incorporates the morphology of the upstream catchment into the estimation of the resistance against flow over/through each pixel via the volumes and pathways. The upstream catchment area of a pixel is a calculable parameter, and its effect on the resistance can be incorporated into the model.

3.7.2. Hydrograph recessions and travel times

The determination of the flow velocities (and thus the flow times) for each pathway segment (pixel) is, for all flow components, related to the hydraulic slopes and a resistance coefficient. This coefficient will vary for the different flow components and will depend mostly on the degree of friction against the flow of water over/through the soil.

This resistance against movement of water along the flow components' pathways, is inherent in the rising limb and the recession curve of the observed flow hydrograph as a factor that indicates a delay or acceleration in movement of water along the pathlines. A longer travel time of water through the catchment will result in a flatter rising limb and recession curve of the hydrograph. Similarly, a quicker travel time of water through the catchment will result in a steeper rising limb and recession curve of the hydrograph. Therefore, it can be assumed that the recession curve of each flow component can be related to the travel times of each flow component. Quickflow travels the quickest down the catchment slopes and causes the sharp high peak in the storm hydrograph. The recession of this peak is much quicker than the recession of the flow during baseflow conditions, when the slower moving water finally reaches the catchment outlet. Thus, if there is a lag or an acceleration in the movement of water down the catchment slopes (caused by the different friction processes), it should influence the recession rate of the flow path's response function.

3.7.3. Quickflow discharges into river flow

One of the underlying assumptions of the method suggested above, is the independence of the flow amongst different pixels. The calculation of cumulative flow times along each pathway from the individual flow times over each pixel, suggests that the flow in each pixel is independent from the flow in every other pixel (Maidment *et al,* 1996). However, water that flows along the surface down the catchment slopes, gathers together more and more to form rills and gullies before forming little streams which ultimately converge to bigger streams. In this way the surface flow becomes river flow in a gradual natural transition process, changing the restriction of the flow in a gradual manner, although the pathlines remain the same. Therefore the flow in individual pixels is dependent on other pixels in that it is influenced by the amount of upstream flow.

This model suggests that, as the upstream area, contributing to a pixel's flow, increases; the effect of surface flow restriction on the flow velocity decreases. So this transition from surface (or "laminar sheet") flow to river flow is modelled by using the amount of contributing area of each pixel.

3.8. Model of the conceptual flow processes using a spatial derived response function

The model, presented in this report, is based on the concepts of a unit hydrograph for each flow component, depicting each preferential pathway represented above, by incorporating the physical properties of the catchment, which include the following:

1) The slopes derived from a catchment's DEM will define the flow pathlines of water flow through the catchment in order to determine the directions and distances travelled and the travel times of water flowing down the catchment slopes.

2) The travel times of flow response to a rain event will be weighted according to the resistance to flow and the upstream area contributing to the flow through each pixel.

3) The frequency histogram of the cumulative travel times of water down the catchment slopes, will define a response function for each characteristic flow component (surface and subsurface flow) for a catchment, per unit of rainfall.

4) The rainfall rate and duration of different rain events will define the probability of flow through the surface or subsurface flow paths, by partitioning the excess rainfall into the different preferential pathways.

In summary, this research develops a model whereby the spatial information of hill slopes in a small headwater catchment is used to generate the different flow components of river flow in the catchment. Most of the information necessary to derive the travel times, as well as the travel paths of each flow component, can be derived from standard catchment spatial information; i.e., the slope and direction of flow, the land use and the soil type. Observed flow data is utilized to interpret the hydrograph, as well as to verify and validate the model for a research catchment in the Ngoye hills of Zululand.

****

4 Description of the study catchment

The identification of different flow regimes in observed storm hydrographs for the separate flow paths, can only be done in small headwater catchments where there is insufficient time to complete the mixing of flow from different areas and different flow components. A suitable site for establishing the model is the University of Zululand's research catchments in the Ngoye hills, the Ntuze River catchments (Figure 4.1). The identification of different flow regimes in the catchments has been presented by Kelbe *et al* (1996). The model development has been based on measurements and observations from these nested subcatchments.

River runoff processes and water quality studies have been conducted in the Ntuze River research catchments of the University of Zululand since 1974 (Hope and Mulder, 1979). These studies have been used to evaluate existing hydrological models and to verify (or calibrate) new models (Hope and Mulder, 1979). These research catchments have also been used to study the impact of land use on catchment runoff (Kelbe and Snyman, 1993) and hydrological response to high intensity and short duration storms depicting quickflow conditions (Kelbe and Germishuyse, 1999). These research catchments were intensively monitored for hydrological processes (including water quality analysis) in a manner that is suitable for the validation of the model described in this study. Consequently, the small nested catchments monitored by sharp crested, compound V-notch weirs in the Ntuze River, code named W1H016, W1H017 and W1H031 respectively, were chosen for this study.

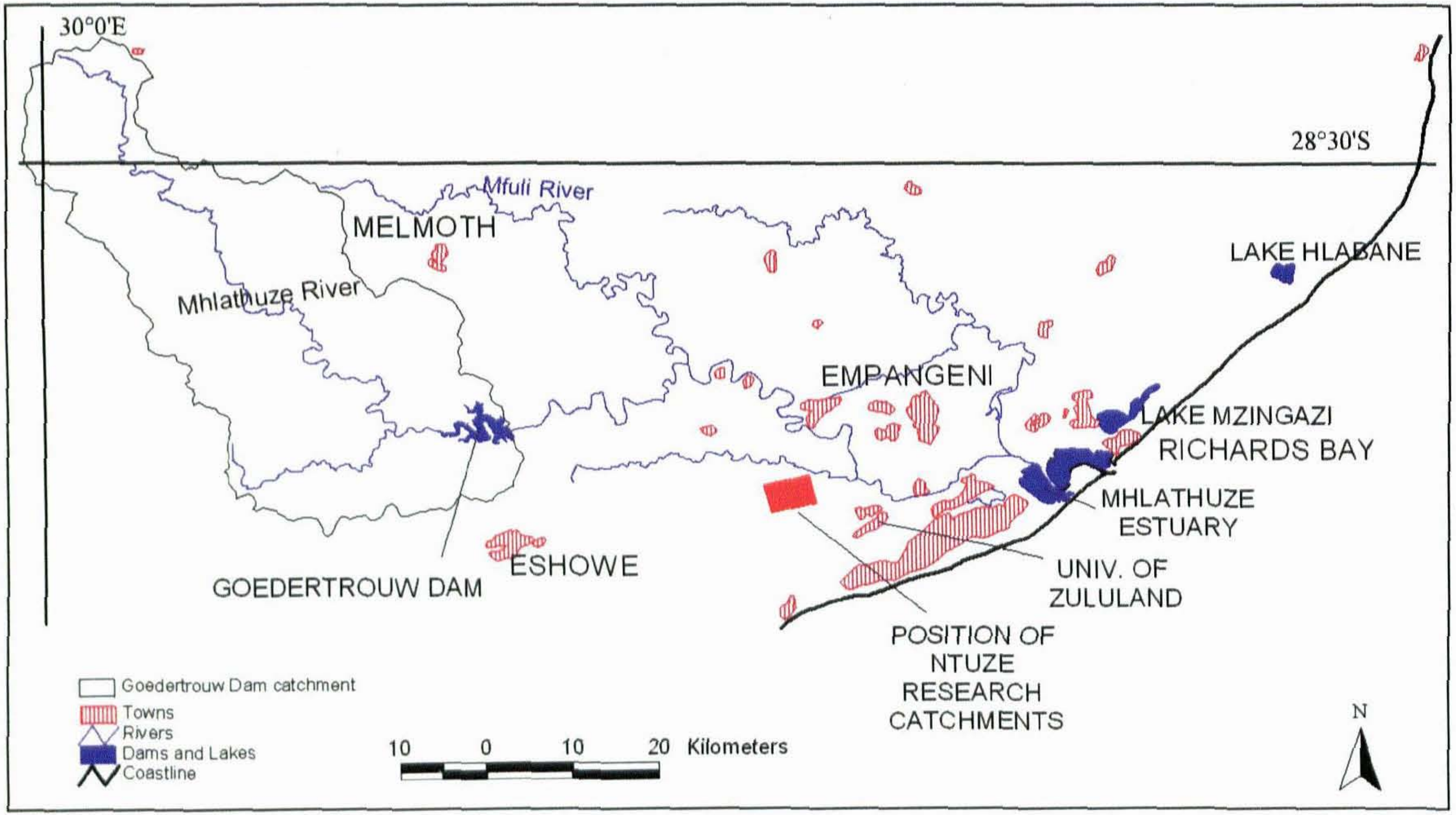

Figure 4.1: Placement and settings of the research catchments.

The model has subsequently been evaluated in its application to the much larger catchment of the Goedertrouw Dam (now also known as Lake Phobane). Details of the Goedertrouw Dam catchment are provided in a later chapter.

4.1. Location and setting

The study areas are situated on the northern coastal region of northern Kwa-Zulu/Natal, South Africa. Figure 4.1 shows the location of the Ntuze catchments and the Goedertrouw Dam catchment. The catchment of W1H017 is a subcatchment (situated in the headwaters) of the catchment of W1H016. The catchment of W1H031 lies adjacent to the catchment of W1H016 (Figure 4.2.). The confluence of the rivers from W1H031 and W1H016 feeds into the perennial Ntuze River. Table 4.1 lists the catchment sizes.

Table 4.1: Catchment sizes:

Catchments	**Ntuze research catchment areas (km^2)**		
	W1H016	**W1H017**	**W1H031**
Catchment size	3.2	0.78	3.1

4.2. River flow measurements

The Ntuze weir gauging stations were equipped with autographic water level recorders and continuous electronic flow monitoring devices (recording hourly average data). (Simultaneously, rainfall data was measured on an hourly basis at each weir.) These hourly records are available from 1989 to 1996. Rivers in the Ntuze catchments usually keep flowing throughout the year, including the dry winter months of June and July. Table 4.2 lists hydrometeorological values of the research catchments.

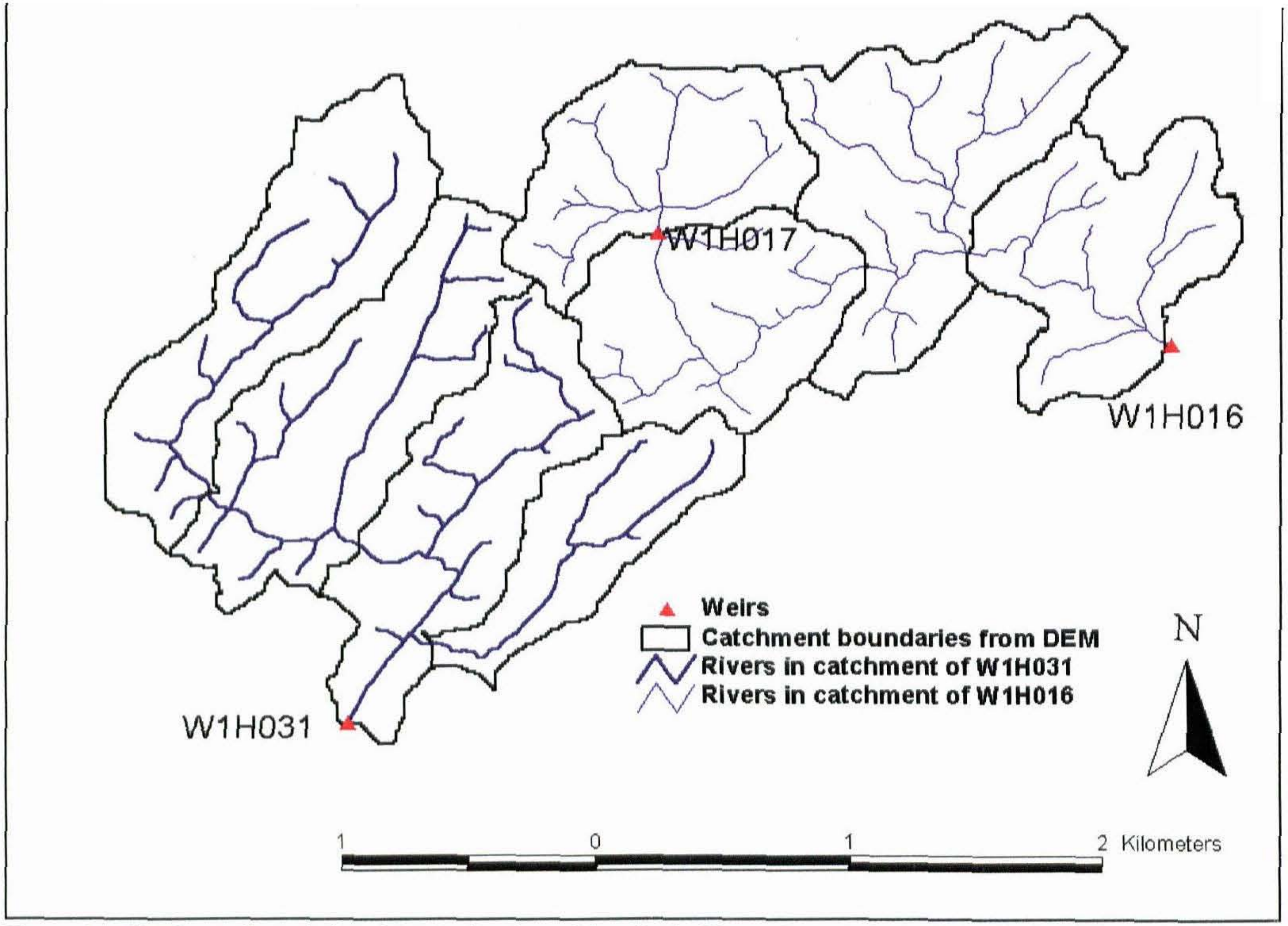

Figure 4.2: Catchment boundaries, rivers and weir positions in the Ntuze river catchments.

4.3. Rainfall climate

Hot and humid conditions characterize the climate of the area during the summer months from October to March. Rainfall varies between 1000 and 1500 mm/year, while evaporation has a slightly smaller range (Table 4.2).

Table 4.2: Climatic information of the research catchments.

Catchments	Ntuze research catchments' climatic data (mm/year)
Annual Rainfall *	1000 - 1500
Annual Evaporation *	1300 - 1400
Annual Runoff *	200 - 500

* Source: Midgley, Pitman and Middleton (1994)

Hope and Mulder (1979) indicate that the mean monthly rainfall is between 235 and 215 mm per month during wet summer months (October to March), and mean monthly rainfall of 70 to 75 mm during the drier winter months (April to September). They estimated the area's mean annual rainfall at 1800 mm, which is much higher than the figures listed in Table 4.2. However, Hope and Mulder (1979) acknowledge that their estimates are based on a rather short period of observations - all rain gauges were installed during 1976 (Hope and Mulder, 1979).

Hourly rainfall measurements were obtained from the flow gauging stations (at the catchment outlets). It is assumed that the small sizes of the catchments allow the use of rainfall measured at the catchment outlets as a true representation of the catchment rainfall.

Rainfall often occurs as high intensity short duration rainfall storms during the summer months while lower intensity storms generally occur throughout the year. Figure 4.3 displays the relationship between the rainfall duration and rainfall intensities measured at W1H016, for storms shorter than 24 hours in duration, and storms with more than 5 mm rain per day. These storms were classified arbitrarily into high or low rainfall intensity classes, as well as long or short duration classes, as indicated by the vertical and horizontal red lines in Figure 4.3. This ensured the inclusion of the full spectrum of rain storms, that occur in the research catchments, into the rainfall types.

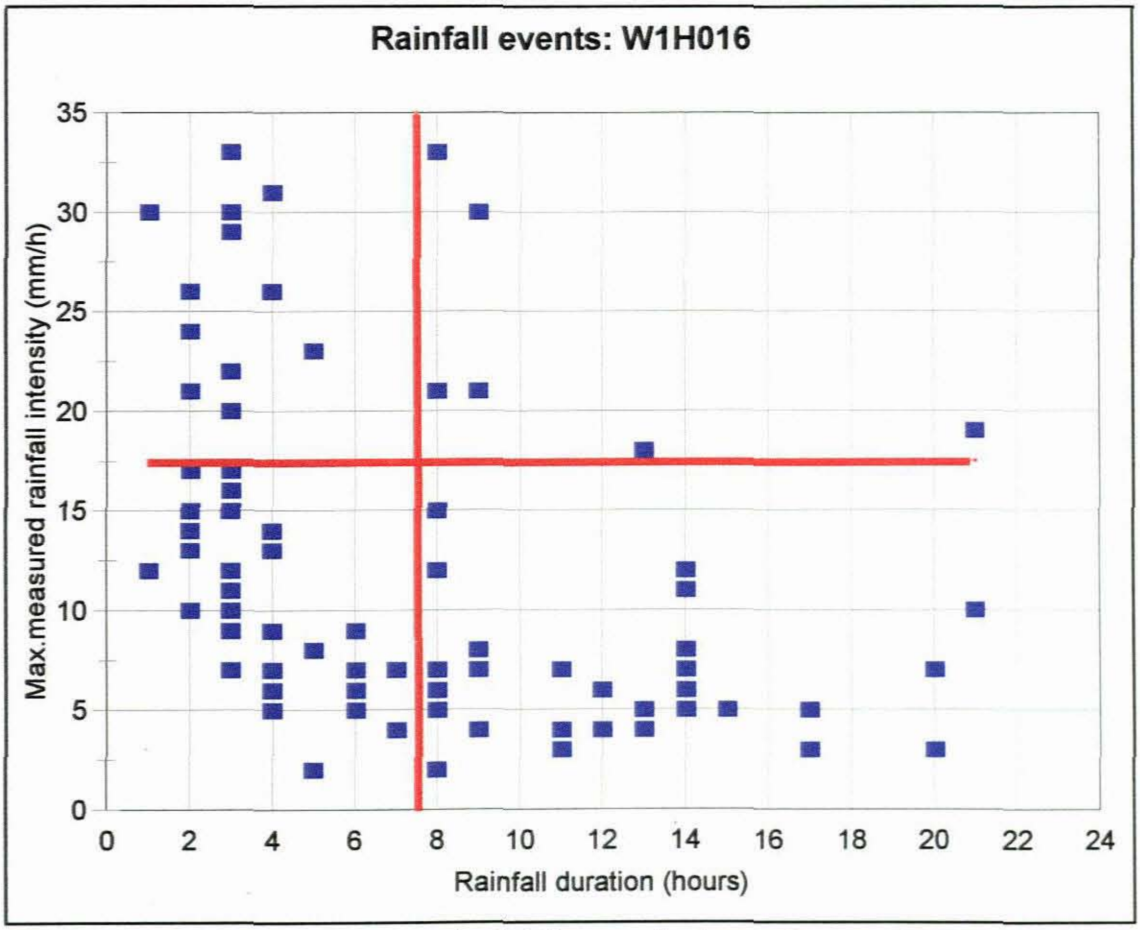

Figure 4.3: Partitioning of measured rainfall storms in the catchment of W1H016.

4.4. Morphology and geology

The topographical features of the catchment have been captured in a DEM for the entire Ntuze catchment from 5m and 20m contours (Figure 4.4). The topography of the catchments was surveyed by the Department of Survey, University of Natal, Durban in 1982. This information was supplemented by field visits to derive a 10m by 10m DEM for the catchments. Catchment boundaries and rivers derived from the DEM (Figure 4.2) and those derived from observations were closely correlated, as described by Kelbe *et al* (1996). Table 4.3 lists the morphological information of the research catchments.

The catchment of W1H017 drains into the catchment of W1H016 (Figures 4.2 and 4.4). In the catchment of W1H031 there are a number of tributaries which flow parallel to each other, with

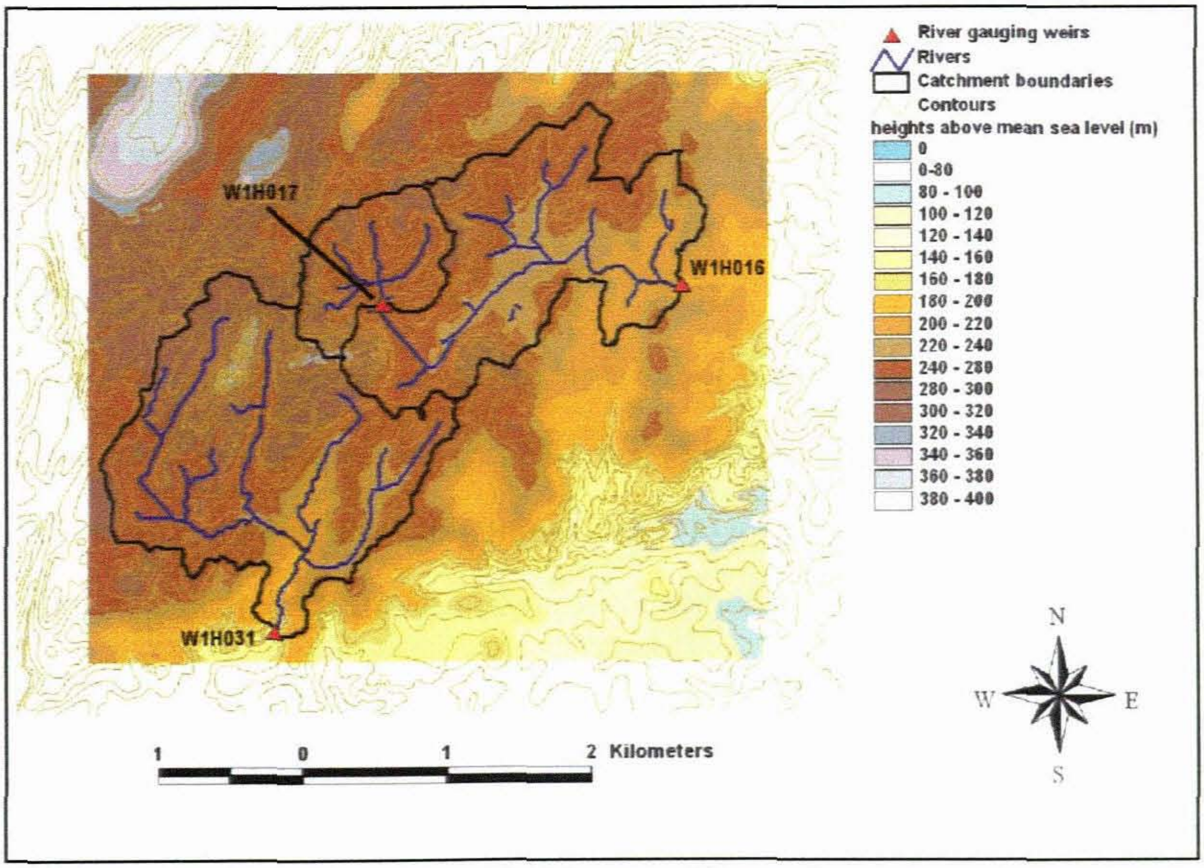

Figure 4.4: The Digital Elevation Model of the Ntuze River catchments.

the confluence situated just upstream of the outflow of the catchment at the weir W1H031.

Table 4.3: Morphological information of the research catchments and the DEM of the catchments.

Catchments	**Units**	**Ntuze research catchments**		
		W1H016	**W1H017**	**W1H031**
Catchment size	km^2	3.2	0.78	3.1
DEM: highest point	m.a.m.s.l.	342	342	350
DEM: lowest point		210	260	165
DEM scale		10m by 10m pixels		

The catchment of W1H017 has almost a circular shape, while the shape of the catchment of W1H016 is more elongated (Figure 4.4). The parallel drainage system in the catchment of W1H031 causes it to react with a flow response similar to that of a circular shaped catchment. Mulder and Kelbe (1992) showed that the hydrographs for the catchments of W1H016 and W1H031 were related to the form of the river network.

4.4.1. DEM calculation: Input

Five metre digitized contour vectors were transformed from an arbitrary chosen coordinate system, to the Transverse Mercator projection, on the GRS80 spheroid, with central meridian 31 degrees East, and reference latitude 0 degrees (the LO 31 coordinate system). The 5m contours were supplemented with 20m contours from the 1:50 000 topographical maps (Chief Directorate: Surveys and Mapping, http://w3sli.wcape.gov.za/SURVEYS/survmain.htm, 2005). The two sets of contours were carefully overlaid to create a data set from which a DEM with a spatial resolution of 10m by 10m grid pixels was derived.

4.4.2. DEM calculation

In previous research done on the Ntuze catchment, a DEM of the catchment was created in IDRISI 3 (Kelbe *et al*, 1996, Kelbe and Snyman, 1993). This model was created in an arbitrary chosen coordinate system which was at an angle of 13.8 degrees north west from north. Updating the DEM from the old IDRISI 3 format to the IDRISI 32 Release 2 file format, involved the transformation of the coordinate system from the arbitrary chosen system to an internationally recognized coordinate system, which is required in the later releases of IDRISI. This involved rotating the coordinate system of the images containing the DEM through 13.8 degrees. Modules in IDRISI were applied to assist in the image rotation, but with no success. However, individual contour vectors were transformed successfully. The IDRISI 32 release II module, called INTERCON, was used to calculate the transformed DEM used in this study (Figure 4.4).

The calculated DEM was created for a pixel resolution of 1m by 1m. It was then contracted to a 10m by 10m DEM (using the means of every ten pixels). The 10m by 10m DEM was smoothed with a mean pass filter to reduce the pits in the DEM. The remaining pits and loops in the DEM were then removed with an IDRISI module, called PIT REMOVAL.

4.4.3. Evaluation of the DEM

The DEM in this study was to be used to derive flow paths and times based on the slopes of specific surfaces. The process of generating a DEM often produces pits and flat areas that create zero slopes. These flat areas have a big influence on the estimations of flow times. Consequently, special attention needs to be given to the flat areas. These need to be either removed from the DEM, or the zero slopes need to be replaced with very small values (this second option preserves the original DEM's altitudes).

Flat areas with zero slope in the DEM were mostly restricted to flood plains, hilltops and areas outside the research catchment boundary. The calculated catchment boundaries and derived rivers compared favourably with the digitized rivers and catchment boundaries derived from aerial photographs.

4.5. Soil types

The soil types are published by Midgley, Pitman and Middleton (1994) for the whole of South Africa. They list the soil types of the study area as predominantly "sandy clay-loam to sandy clay." Soil types of the catchment were also classified by Hope and Mulder (1979) according to the Binomial system of Southern African soil types (Experiment Station of the South African Sugar Association, 1984) (Figure 4.5). Identified soils included Hu16 (Hutton), Fw/We13 (Fernwood/Wesleigh) and Cv16 (Clovely). Rocky soils and some rock outcrop also occur in the catchment (Figure 4.5).

4.6. Land use

Land use surveys of the catchment done in 1995 were used to create a land use map (Kelbe *et al*, 1996). The land use varies from extensively informal (subsistence) agriculture for most of the catchment area of W1H016, to a pristine nature reserve situated in W1H031's catchment (Figure 4.6). Table 4.4 lists the proportions of land uses of the catchments.

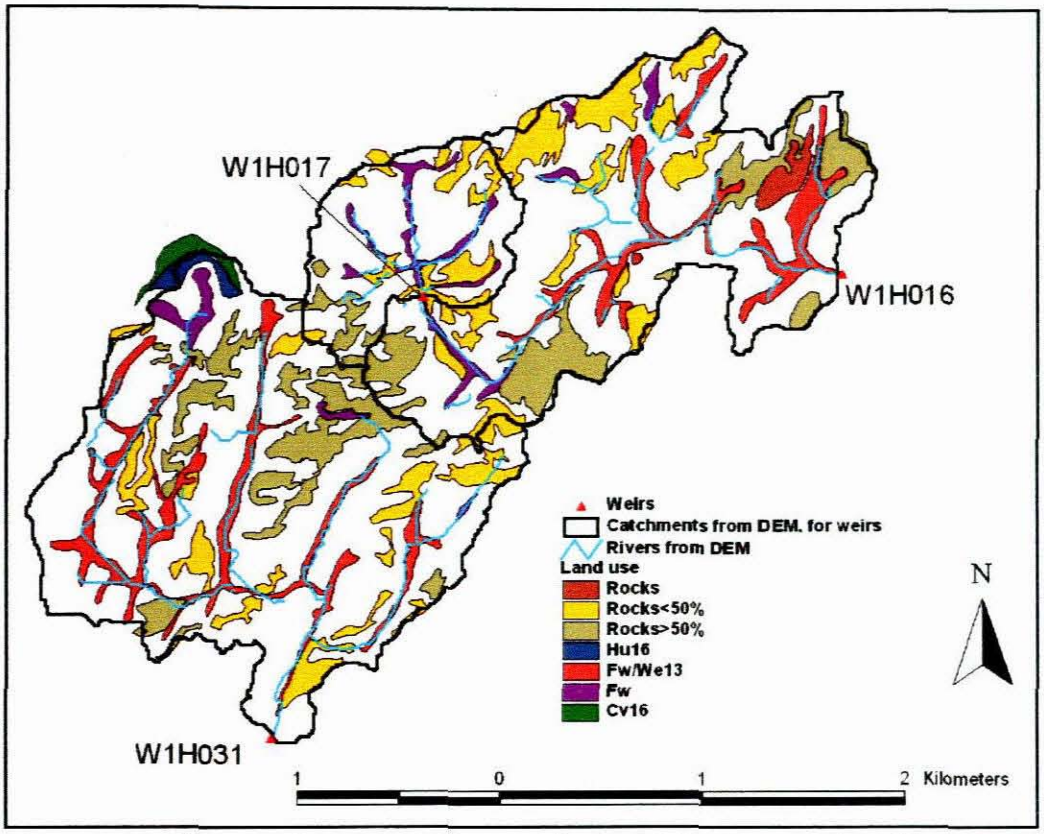

Figure 4.5: Soil types of the Ntuze River catchments (after Hope and Mulder, 1979).

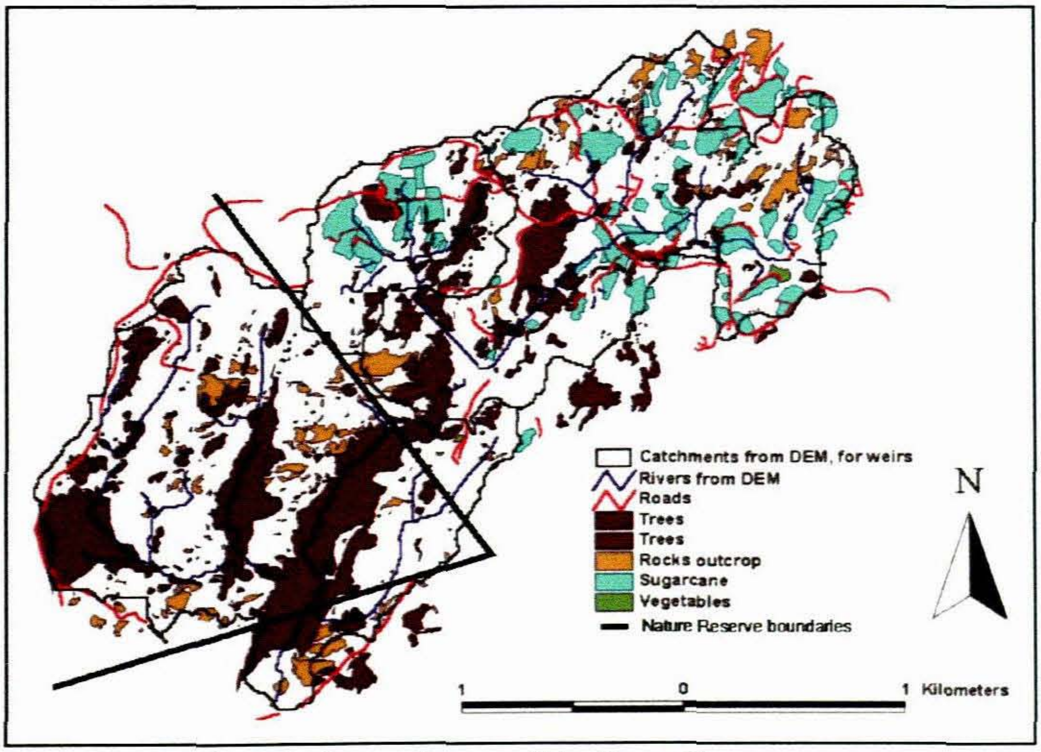

Figure 4.6: Land uses in the catchments of the Ntuze River.

Table 4.4: Land use of the Ntuze Research catchments.

W1H016		W1H031	
trees	15%	trees	30%
grass	60%	grass	63%
rocky soils	5%	rocky soils	5%
sugarcane	15%	roads	2%
roads	4%		
human living	1%		

****

5 Hydrograph analysis

The conceptual model of the river runoff recognizes several characteristic flow regimes based on separate flow paths. This thesis reports on the development of a spatial model which simulates different hydrological flow components. Calibration of this spatial model is accomplished, like all hydrological models, by comparison of the model results to the observed flow hydrographs. Model calibration is also accomplished by comparisons between the simulated flow hydrographs' characteristics and those of observed hydrographs. This chapter describes the derivation of hydrograph characteristics, from observed flow data, used during the calibration of the spatial model.

The occurrence of separate flow regimes is dependent on the dominance of hydrological processes during the storm events. It has already been established that Hortonian flow processes are unlikely to occur in the study area. The exceptions are special conditions like impervious surface structures, such as roads, pathways and exposed impervious rock (Figure 4.5).

The proportion of quickflow from long duration, low intensity storms is expected to be low in comparison to short duration, high intensity storms, if it is assumed that most of this rainfall will be absorbed into the soil. Similarly, short duration, high intensity rain storms would be expected to produce more quickflow. Consequently, the hydrograph analysis is based on the different classes of rainfall.

5.1. The hydrograph features and the catchment characteristics

Many researchers have connected the hydrograph features, like to the time to peak (TTP) and the time to recede (TR), with the topology and form of the catchment. Snyder (1938) related the TTP to the catchment length; the distance from the outlet to the catchment's centroid and a regional coefficient. He distributed the width of the hydrograph around the time of peak flow with one third before the peak flow and two thirds after the peak flow.

Jena and Tiwari (2006) modelled the unit hydrograph of two medium-sized catchments ($158km^2$ and $69km^2$, respectively) with geomorphological parameters of the catchments, such as channel and basin parameters. They used a correlation matrix between the unit hydrograph parameters (TTP, TR, peak flow, etc.) and the geomorphological parameters to select those parameters that best described the unit hydrograph. Their geomorphological parameters included an extensive list of catchment characteristics that included the catchment length ratios, basin shape factors, the number of streams per unit area, etc. All of these parameters are calculated with ease in a GIS. However, these spatial parameters are inherently included in the modelling of the unit hydrograph if every flow path from every entry point to the outlet is included in the modelling process.

5.2. Observed storm characteristics

Different storm types were chosen for hydrograph analysis. An extensive list of all storm events were used to ensure that the full spectrum of rain storm types were included in the analysis. Rain storms of more than 5 mm rainfall per day and shorter than 24 hours in duration were considered.

The storms were classified into the following types, based on the analysis in Paragraph 4.3 (Figure 4.3):

1. **High** intensity and **long** duration storm rainfall.
2. **High** intensity and **short** duration storm rainfall.
3. **Low** intensity and **short** duration storm rainfall.
4. **Low** intensity and **long** duration storm rainfall.

The division between high and low rainfall intensities were arbitrarily chosen at ± 17 mm/hour for maximum observed rainfall intensities. Similarly, the division between the long and short duration rainfall events were arbitrarily chosen to fall between seven and eight hours of rainfall (Figure 4.3). Another criterion placed on storms selected for recession analysis, was a fairly long dry period after the rainfall event, to ensure that a significant period of recession after the storm event, was analysed.

Tables 5.1, 5.2 and 5.3 lists examples of storm characteristics measured in the catchments of W1H016, W1H017 and W1H031 respectively. The observed flow after the storm, for those storms listed in the tables, was observed, either until a follow-up rain event caused a rise in the flow hydrograph, or until the flow at the catchment outlet returned to the same flow conditions prior to the rain event. The duration of the storm flow (as listed) includes the time from the beginning of the rainfall event until the flow returns to pre-storm conditions. However, for most of the storms examined, the flow recession process was interrupted by follow-up rain events.

Table 5.1: Examples of storm characteristics in the catchment of weir W1H016.

Storm types	Date	Total rain for the event	Duration of rainfall event	Maximum measured rainfall intensity	Observed flow rate before storm	Observed peak flow rate	Observed flow rate after storm	Duration of storm flow
	Units:	mm	hours	mm/hour	m^3/hour	m^3/hour	m^3/hour	hours
Low Intensity, Long Duration	25 Jan 1990	47	13	12	45	883	95	> 76
Low Intensity, Short Duration	6 Apr 1990	17	2	15	140	618	140	52
High intensity, Short duration	27 Dec 1995	30	1	30	365	3005	365	51
High intensity, long duration	15 Dec1989	51	10	17	177	4592	200	> 135

Table 5.2: Examples of storm characteristics in the catchment of weir W1H017.

Storm type	Date	Total rain for the event	Duration of rainfall event	Maximum measured rainfall intensity	Observed flow rate before storm	Observed peak flow rate	Observed flow rate after storm	Duration of storm flow
	Units:	mm	hours	mm/hour	m^3/hour	m^3/hour	m^3/hour	hours
Low Intensity, Long Duration	29 Oct 1994	20	10	3	27	149	29	64
Low Intensity, Short Duration	4 Dec 1993	45	6	11	8	462	35	> 45
High intensity, Short duration	1 Mar 1995	86	4	36	0.6	1036	9	> 45
High intensity, long duration	13 Oct 1994	61	19	21	19	521	19	80

Table 5.3: Examples of storm characteristics in the catchment of weir W1H031.

Storm type	Date	Total rain for the event	Duration of rainfall event	Maximum measured rainfall intensity	Observed flow rate before storm	Observed peak flow rate	Observed flow rate after storm	Duration of storm flow
	Units:	mm	hours	mm/hour	m^3/hour	m^3/hour	m^3/hour	hours
Low Intensity, Long Duration	26 Apr 1990	34	12	4	42	886	70	> 85
Low Intensity, Short Duration	29 Jan 1991	13	4	8	188	463	188	45
High intensity, Short duration	10 Jan 1994	64	3	52	90	3682	90	170
High intensity, long duration	4 Dec 1993	49	8	13	50	1660	90	> 130

5.3. Storm flow duration and time to peak

The time to peak (the time from the beginning of the rainfall event, to the peak of the observed hydrograph); as well as the time to recede (the time from the peak flow until the stream returns to pre-storm conditions) were derived for each storm event. The total durations of the storm flow, as observed in the hydrographs, are listed in Tables 5.1 to 5.3. The beginning of each event was assumed to coincide with the start of the rainfall event, which, for most storms, was also the time of the initial rise in the observed hydrograph.

Times to peak for 29 storms of short duration and high intensity, measured in each of the catchments of W1H016, W1H017 and W1H031, were determined by Kelbe and Germishuyse (1999). The times to peak listed by Kelbe and Germishuyse (1999) were used to find the most frequently observed TTP. This TTP of storm hydrographs was used for the TTP of the quickflow component (Table 5.4). The TTP for throughflow and baseflow (listed in Table 5.4) was estimated for application in the hydrograph analysis, using the following *assumptions*:

1. The TTP for the fastest flow component present (be it the quickflow or throughflow component) coincides with the observed TTP.
2. The TTP for the throughflow is twice as long as the TTP for the quickflow.
3. If quickflow is present, the TTP for the baseflow is three times as long as the TTP for the quickflow, otherwise TTP for baseflow is twice as long as TTP for throughflow.
4. All storm flow components present start flowing at the beginning of the rainfall event.

Assumption four can be justified by noting the increase in observed flow at the catchment outlet, even during the first hour of a rain event, for all storm types and weirs.

Assumptions regarding the TTP were made as an interim arrangement. It is now stated that the spatial model's time response functions calculate the peak of each flow component implicitly. The TTP estimated by the spatial model is not directly affected by any assumptions made during the hydrograph analysis about the times each flow component might peak, but rather by the processes that governs the flow down/through the catchment slopes, as described in Chapter eight. The spatial model applies physical principles (flow velocities) to determine the entire flow hydrograph.

The four assumptions listed above were only regarded during the empirical analysis of the hydrograph separation. Changes to these assumptions will result in changes to the division of excess rain among the flow components in the observed hydrograph. However, these divisions of excess rain among the flow components were calibrated again during the final model runs, via a process of comparisons between observed and simulated storm flow hydrographs.

The analysis of the TTP and TR were supplemented with information derived by Hope and Mulder (1979) for the catchments of W1H016 and W1H017 to estimate storm flow durations. Hope and Mulder (1979) analysed rainfall events from 1977 and 1978 and found that the TTP for average rainfall events was between six and eight hours for the catchment of W1H016, and three to five hours for the catchment of W1H017, which are similar to values calculated from the storm analyses described in this research. Hope and Mulder (1979) observed that the ratio of the TR and TTP for the catchments were:

For the catchment of W1H016: $\frac{TR}{TTP}$ = 1.5 to 1.8 (average 1.65) and for the catchment of W1H017: $\frac{TR}{TTP}$ = 0.9 to 1.2 (average 1.05)

Although no analysis was done by Hope and Mulder (1979) for the catchment of W1H031, it was assumed that the ratio would be similar to W1H017, as both catchments have a similar shape, and the two catchments' sizes are within the same order of magnitude (3.2 and 0.7 km^2 respectively):

For the catchment of W1H031: $\frac{TR}{TTP}$ = 1.05.

These ratios were used to calculate the TR (in hours) from the TTP (in hours) for both the quickflow and throughflow components. The total times to peak and recede again (total flow time) of each flow component, are listed in Table 5.4.

It is expected that the TR is a function of the catchment shape and size and not of the storm type. Hence it is anticipated that the total storm flow duration remains constant for a given catchment, for one unit of rainfall.

Table 5.4: TTP and TR (all values in hours), as derived by Kelbe and Germishuyse (1999), Hope and Mulder, (1979) and the assumptions listed in Paragraph 5.2.

Weir	TTP: Quickflow	Duration of quickflow (TTP + TR)	TTP: throughflow	Duration of throughflow (TTP + TR)	TTP: baseflow (hours)	Duration of quick and throughflow
	Derived from Kelbe and Germishuyse, (1999)	Derived from Hope and Mulder (1979)	Derived from assumption one	Derived from Hope and Mulder (1979)	Derived from assumption three	Derived from Hope and Mulder (1979)
W1H016	4	7	8	13	12	20
W1H017	3	6	6	12	9	18
W1H031	3	6	6	12	9	18

5.4. Methods of separating flow components

Ward and Robinson (2000) described some of the traditional methods for separating slower and quicker moving flow components of river runoff. Most of these separation techniques rely in some or other way on the time of arrival of water at the stream channel (Ward and Robinson, 2000). Most techniques also make use of a straight line projection from the beginning of stream flow rise to the point where it intersects a specific condition on the falling limb of the hydrograph, to separate a quicker flow component from a slower flow component (Figure 5.1). The slope of the straight line will depend on the separation technique and interception point. Different techniques incorporate different processes, which affect the flow down the catchment to the rivers, e.g., the impact of bank storage on the different flow components. Separation techniques which use water quality characteristics (like temperature, conductivity and ionic composition) are also described by Ward and Robinson (2000).

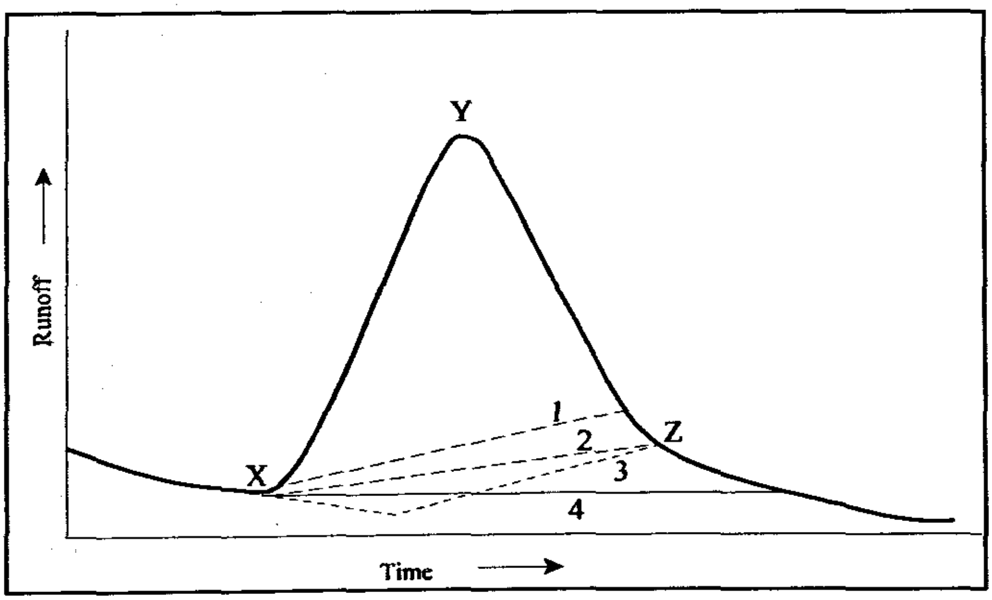

Figure 5.1: Different methods of baseflow separation, indicated by the different straight lines (after Ward and Robinson, 2000).

Figure 5.1 illustrates the graphical separation methods between quicker and slower moving flow components. Line 1 indicates a separation which starts at the rise of the hydrograph (point X) and is extended to some point after the peak of the hydrograph (point Z). The position of point Z can be established to fall on a point N time units after the peak of the hydrograph (line 1). N can vary with catchment size, or can be chosen as the point of highest curvature close to the bottom end of the recession limb (line 2). Another method (line 3) is to extend the recession curve prior to the storm hydrograph until the time of the peak in the hydrograph (point Y), followed by another straight line upwards to the arbitrarily chosen point Z. The simplest of the separation methods (line 4) is to draw a straight horizontal line along the base of the hydrograph from the start of the rising limb (point X) until it intersects with the storm hydrograph again (Ward and Robinson, 2000).

Wilson (1983) indicated that the choice of separation technique depends on the data available and he suggested the use of a "master depletion curve" if a continuous record of streamflow is available over a period of a few years. He indicated how the "master depletion curve" of a weir can be utilized to separate the baseflow from the quicker flow components observed at the same weir.

5.5. Flow separation method applied in this study

The four flow regimes have distinct different flow rates that produce different characteristic hydrographs shown schematically in Figure 5.2. The shape of the individual flow component's hydrographs is defined by their magnitude Q_i, duration T_i, time to peak and recession rate for flow component *i*. The occurrence and magnitude of each hydrograph is dependent on the partitioning of rainfall into the different flow paths. For example, in many storm events of low

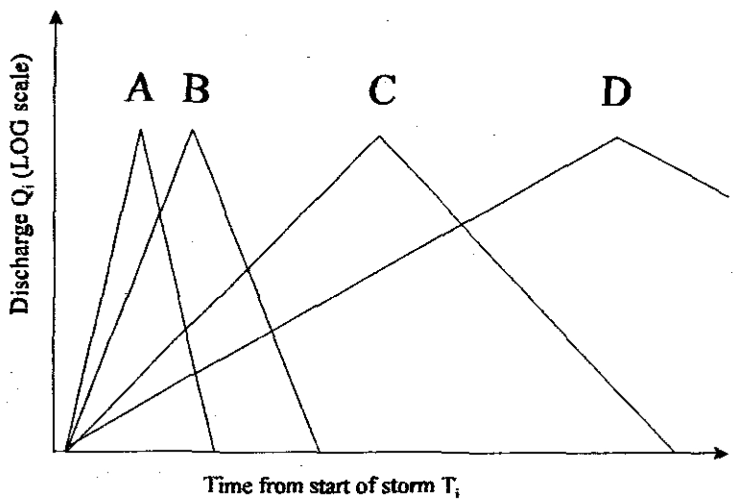

Figure 5.2: Conceptual diagram of individual storm flow response functions for overland flow (A), quickflow (B), unsaturated throughflow (C) and saturated baseflow (D). The observed flow is a composite of the four scaled response functions.

intensity, neither the overland flow (curve A) nor the quickflow (curve B) are likely to be detectable and consequently the observed storm flow will be a composite of curves C and D.

Schulz (1976) described the method of separating the individual storm hydrographs. The model assumes that each flow component present in the observed flow hydrograph, will each have a unique recession rate which is constant for each flow component. This assumption is then implemented firstly by the observation of a recession rate.

It is then followed by the assumption that the particular flow component occurs in the observed hydrograph at that observed recession rate from the assumed time of the peak flow.

Schulz (1976) used the reservoir routing model to define the recession curve of each flow component:

$$Q_t = Q_0\, K_{rec}^{\,t}$$

Where Q_t = the discharge at some time t (or $0 + t$)

Q_0 = the discharge measured t time units earlier

K_{rec} = the recession constant

t = the time interval between Q_t and Q_0

The presence of each flow component (A, B, C or D) in the storm hydrograph is indicated by a unique recession rate. Thus, based on this model, the equation will plot as a straight line on a semi-log graph, provided K_{rec} is constant. The K_{rec} can also be solved by taking a unit time step ($t = 1$):

$$K_{rec} = \frac{Q_1}{Q_0}$$

K_{rec} is determined as a constant value for those parts of the hydrograph that plot as straight lines on the semi-log graph. Different flow components will have different recession rates, thus plotting with straight lines at different angles on the semi-log graph. These are then extrapolated back in time to the estimated TTP of the flow component. The recession of each flow component is determined to distinguish between different parts in the hydrograph, each part having different recession rates.

Applying this flow component separation technique to an observed hydrograph is a purely mathematical exercise, but subjectivity does play a role to some extent. Results from the studies of Kelbe and Germishuyse (1999) were used to guide the analysis around subjective decisions.

They identified changes in water quality measurements (pH, conductivity and turbidity) that they interpreted as flow from different pathways in the observed hydrographs in the catchments of W1H016, W1H017 and W1H031, in the Ngoye hills, which supported the conceptual model of different pathways.

Assumptions regarding the times to peak of each flow component (Paragraph 5.2) were necessary. The hydrograph separation method described above assumes that the different flow components peak at the same time as the observed peak in the hydrograph. However, this assumption did not fit the observations from the research catchments. Assumptions described in Paragraph 5.2 were made as an interim arrangement. These assumptions were replaced in the spatial model by estimations of the travel time of water flowing down the catchment slopes.

5.5.1. *Antecedent flows*

Most of the storm flow hydrographs which were analysed, include some flow in the river prior to the storm (or antecedent flows). The observed hydrographs had to be normalized for antecedent flow conditions before the flow component separation. The reason for the normalization is that; once the flow is classified into different flow components, the amount of water that belongs to each flow component is estimated. Large amounts of baseflow that are present in the river from a time prior to the observation of the storm hydrograph, will continue throughout the event and thereafter. This baseflow, already present in the river, must be separated from the baseflow which occurs in the river due to the rain event.

Normalization of the observed flow hydrographs was achieved by subtracting a declining flow from the observed flow hydrograph from the first time step of increasing flow in the hydrograph.

The rate of this declining flow is assumed to be similar to the river's long term recession during dry winter catchment conditions, discussed in Paragraph 5.6.

5.5.2. Baseflow

The antecedent conditions are often associated with baseflow. This becomes the only period in most observed storm hydrographs where one of the flow components (baseflow) can be uniquely identified and its recession rate determined.

The flow component separation method applied here, is based on the assumption that each flow component can be associated with a distinctly different recession rate after it has reached a peak flow during a storm event. These different recession rates can be observed in the hydrograph by plotting the observed flows along a log y-axis, against time, on a linear x-axis, *since the start of the storm* (Figure 5.3). The part of the graph which depicts the start of only baseflow conditions after the storm event, is under discussion here. Drawing a straight line over the log-graph and extending the line back in time, the flow values on the line indicate the values of the baseflow hydrograph. The constant recession rate of the baseflow is indicated by the slope of the straight line. The baseflow recession is then extended back to the time of the assumed peak of the baseflow (Figure 5.3).

Assumptions regarding the time of the baseflow peak were made, as listed (Table 5.4) and discussed in Paragraph 5.2. The rising limb of the baseflow component was estimated by drawing a straight line from the flow rate at the start of the flow storm hydrograph to the flow rate at the TTP of the flow component, on a *normal axis*. Flow rates along this line were assumed to represent the rising limb of the baseflow hydrograph.

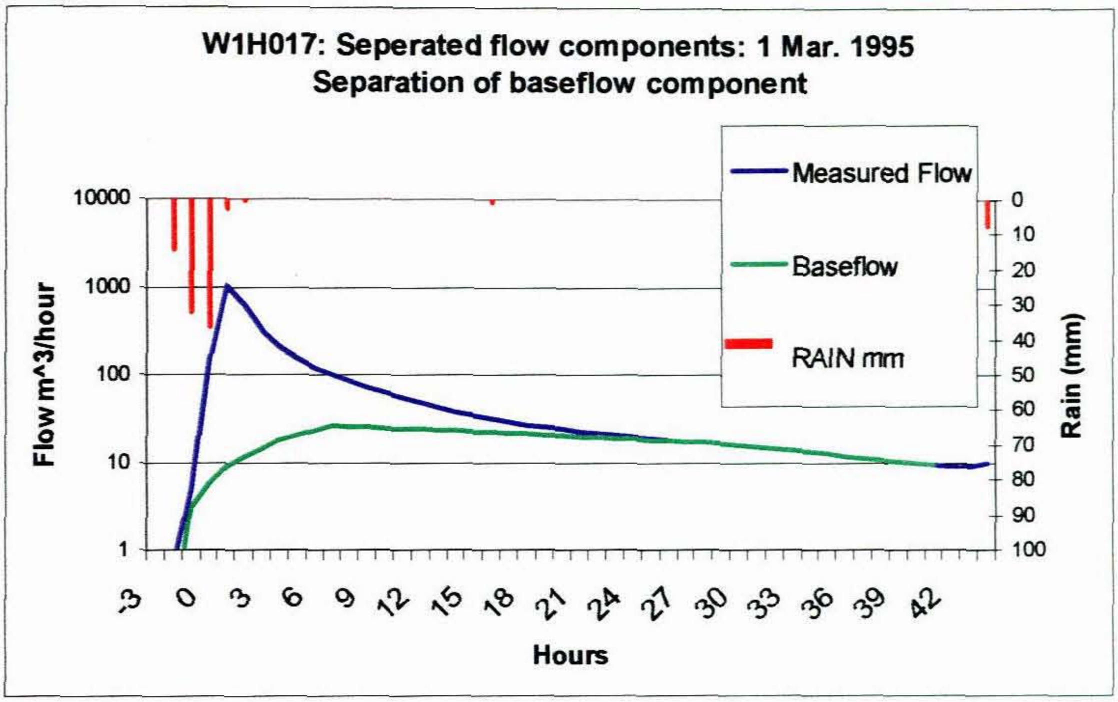

Figure 5.3: A graphic display of the separated baseflow component from the observed flow, calculated during flow component analysis.

5.5.3. Throughflow

Once the baseflow hydrograph has been determined and subtracted from the observed hydrograph, the residual flow is a combination of the throughflow and quickflow. The same separation process can then be applied to the residual flow, in order to extract the throughflow in a similar manner to baseflow. The hydrograph of the throughflow will be delineated by its distinctly different recession rate. Like in the case of the baseflow hydrograph calculation, it is the "tail end" of the graph which is considered here (Figure 5.4). This recession rate is indicated by the slope of the straight line through the log graph of the residual flow along the tail end.

Again the straight line is extended back in time to the TTP of the throughflow (assumptions in Paragraph 5.2), and the hydrograph of the throughflow is calculated using its estimated recession rate. The rising limb of the throughflow was again estimated by drawing a straight line from the

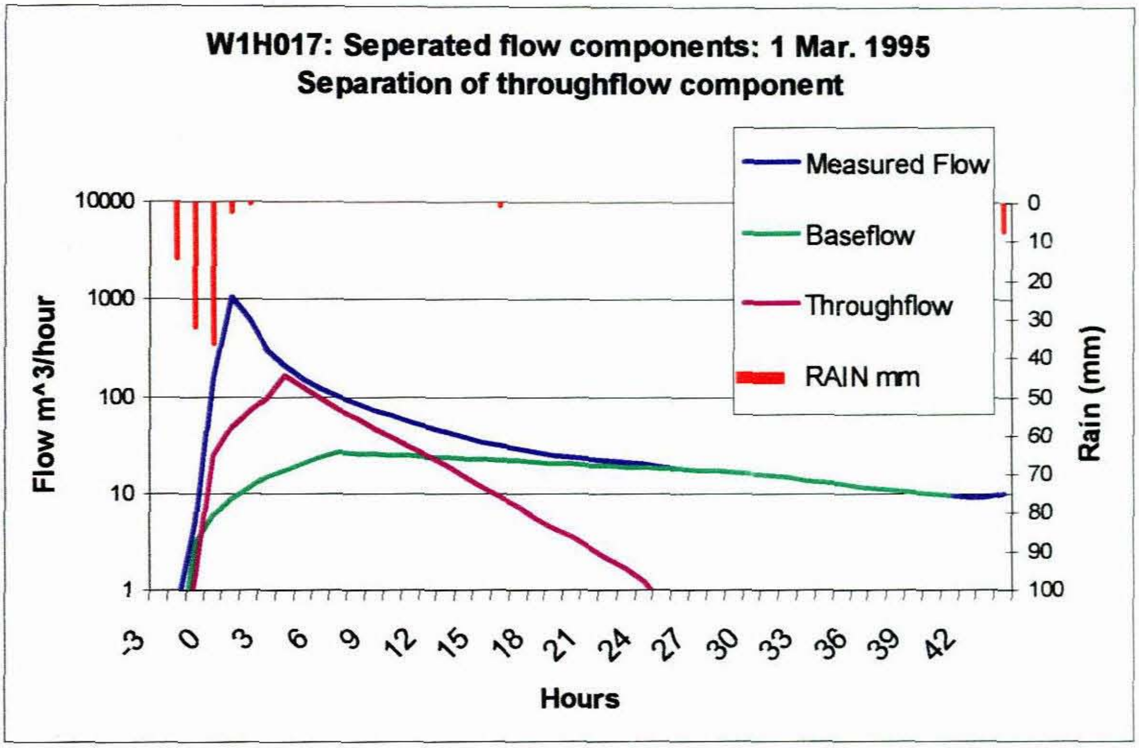

Figure 5.4: A graphic display of the observed flow, as well as the separated throughflow and baseflow components, calculated during flow component analysis.

flow rate at the start of the storm flow to the flow rate at the TTP of throughflow. Flow rates along this line were assumed to estimate the rising limb of the throughflow. Then, once the recession rate is determined and the throughflow is calculated, it is subtracted from the residual flow to provide an estimate of the quickflow's hydrograph (Figure 5.4.).

5.4.4. Quickflow

If there is any significant flow after subtracting the baseflow and throughflow hydrographs from the observed storm flow, it is assumed to represent the hydrograph of the quickflow (which is assumed to be a combination of Hortonian and Hewlett flow). Ideally, the quickflow should indicate a constant rapid decline in flow (Figure 5.5).

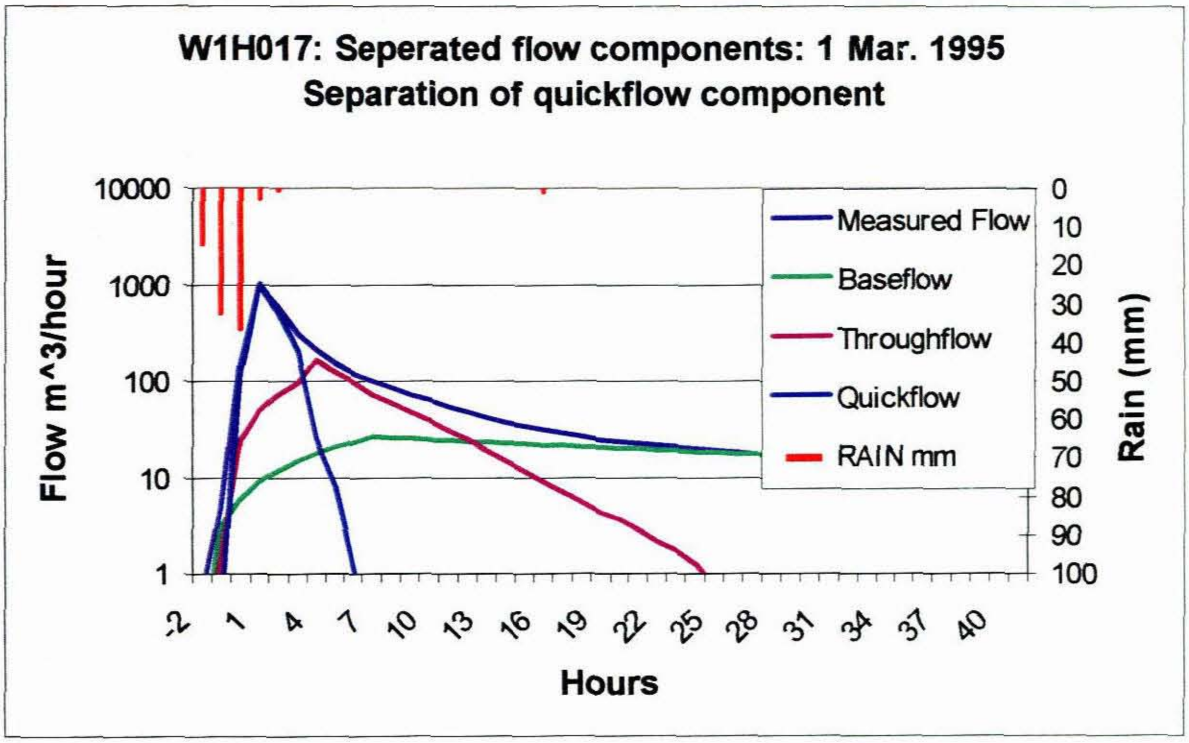

Figure 5.5: A graphic display of the observed flow, as well as the separated baseflow, throughflow and quickflow components, calculated during flow component analysis.

5.6. Results from the hydrograph analysis

5.6.1. Storm flow durations

Based on the flow component separation analysis of observed hydrographs, the TTP and TR for each flow component were noted again (Table 5.5) in order to compare them to estimations from Kelbe and Germishuyse (1999) and Hope and Mulder (1979), listed in Table 5.4. Tables 5.6 to 5.9 list the individual values for the indicated rainfall types. The quickflow component was not observed for most storms of low intensities.

Table 5.5: The mean values (over different rainfall types) of time to peak (TTP) and time to recede (TR) of each catchment, estimated during the flow component separation analysis.

Weir	Observed TTP: (hours)	Duration of quickflow: (TTP + TR) (hours)	Duration of throughflow: (TTP + TR) (hours)
W1H016	6	13	36
W1H017	5	13	23
W1H031	7	12	40

Table 5.6: TTP and TR estimated for the ***high intensity, short duration*** *rainfall type:*

Weir	Observed TTP: (hours)	Duration of quickflow: (hours)	Duration of throughflow: (hours)
W1H016	2	9	37
W1H017	3	6	17
W1H031	2	7	18

Table 5.7: TTP and TR estimated for the ***high intensity, long duration*** *rainfall type:*

Weir	Observed TTP: (hours)	Duration of quickflow: (hours)	Duration of throughflow: (hours)
W1H016	3	17	31
W1H017	5	20	32
W1H031	7	16	90

Table 5.8: TTP and TR estimated for the ***low intensity, short duration*** *rainfall type:*

Weir	Observed TTP: (hours)	Duration of quickflow: (hours)	Duration of throughflow: (hours)
W1H016	4		43
W1H017	4		15
W1H031	8		28

Table 5.9: TTP and TR estimated for the ***low intensity, long duration*** *rainfall type:*

Weir	Observed TTP: (hours)	Duration of quickflow: (hours)	Duration of throughflow: (hours)
W1H016	15		31
W1H017	9		27
W1H031	9		26

The TTP listed in Table 5.5 differs substantially from the observed TTP indicated in Table 5.4. The storm duration listed in Table 5.4 also differs from the observed storm flow durations listed in Table 5.5. A possible reason for this might be a difference in sampling method when storms were picked for analysis. For example, Kelbe and Germishuyse (1999) examined short duration storms. In this study some effort was made to ensure that representative storms from the four chosen rain storm types were selected. From Tables 5.6, 5.7, 5.8 and 6.9 it is also apparent that the TTP for the different storm types ranges over small values for the higher intensities storm types (two to seven hours), while the TTP for low intensity storm types ranges between four and fifteen hours. It is thus proposed that the TTP is a function of the storm type. This is because the high intensity storms will have a significantly higher proportion of quickflow, where as the low intensity storms will have little or no quickflow.

5.6.2. Recession constants and percentage of water from each flow component

Based on the separation of the three flow components, the percentage of water volume in each flow component was estimated (Table 5.10) as well as the recession rates (or recession constants) for each flow component (Table 5.11). Table 5.12 shows the same information as Tables 5.10 and 5.11, but ordered according to flow components and storm types.

The antecedent flows observed in the river prior to the storm hydrograph, were not included in the estimation of the percentage of baseflow in the storm hydrograph.

Table 5.10: Percentages of water in each of the flow components, for each of the catchments, during different storm types. Percentages are rounded to the nearest 10%

Catchment: flow component	High intensity, long duration	High intensity, short duration	Low intensity, short duration	Low intensity, long duration
W1H016: quickflow	60%	30%		
W1H017: quickflow	40%	50%		
W1H031: quickflow	40%	50%		
W1H016: Throughflow	20%	40%	50%	50%
W1H017: Throughflow	40%	30%	50%	50%
W1H031: Throughflow	40%	20%	50%	50%
W1H016: Baseflow	20%	30%	50%	50%
W1H017: Baseflow	20%	20%	50%	50%
W1H031: Baseflow	20%	30%	50%	50%
Mean: Quickflow	50%	40%		
Mean: Throughflow	30%	30%	50%	50%
Mean: Baseflow	20%	30%	50%	50%

Table 5.11: Recession constants for each of the catchments, during different storm types.

Recession Constants:	High intensity, long duration	High intensity, short duration	Low intensity, short duration	Low intensity, long duration
W1H016: quickflow	0.66	0.55		
W1H017: quickflow	0.59	0.35		
W1H031: quickflow	0.73	0.64		
W1H016: Throughflow	0.81	0.82	0.8	0.79
W1H017: Throughflow	0.86	0.73	0.71	0.77
W1H031: Throughflow	0.92	0.85	0.78	0.82
W1H016: Baseflow	0.98	0.98	0.98	0.99
W1H017: Baseflow	0.97	0.97	0.98	0.99
W1H031: Baseflow	0.99	0.99	0.99	0.98
Mean: Quickflow	0.66	0.51		
Mean: Throughflow	0.82	0.82	0.76	0.79
Mean: Baseflow	0.98	0.98	0.98	0.99

Table 5.12: Recession constants and percentages of flow for each component, listed for the catchments of W1H016, W1H017 and W1H031, for the different storm types.

QUICKFLOW		High intensity rainfall		Low Intensity rainfall	
		Recession Rates	% of total flow	Recession Rates	% of total flow
Short duration rainfall	W1H016	0.55	30%	(No quickflow)	(No quickflow)
	W1H017	0.35	50%		
	W1H031	0.64	50%		
Long duration rainfall	W1H016	0.66	60%	(No quickflow)	(No quickflow)
	W1H017	0.59	40%		
	W1H031	0.73	40%		

THROUGHFLOW		High intensity rainfall		Low Intensity rainfall	
		Recession Rates	% of total flow	Recession Rates	% of total flow
Short duration rainfall	W1H016	0.82	40%	0.80	50%
	W1H017	0.73	30%	0.71	50%
	W1H031	0.85	20%	0.78	50%
Long duration rainfall	W1H016	0.81	20%	0.79	50%
	W1H017	0.86	40%	0.77	50%
	W1H031	0.92	40%	0.82	50%

BASEFLOW		High intensity rainfall		Low Intensity rainfall	
		Recession Rates	% of total flow	Recession Rates	% of total flow
Short duration rainfall	W1H016	0.98	30%	0.98	50%
	W1H017	0.97	20%	0.98	50%
	W1H031	0.99	30%	0.99	50%
Long duration rainfall	W1H016	0.98	20%	0.99	50%
	W1H017	0.97	20%	0.99	50%
	W1H031	0.99	20%	0.98	50%

The separation of flow components is based on estimations that depend on certain assumptions about the governing processes of flow down the catchment slopes and along the rivers (Chapters two and three). These assumptions are often violated due to the complexity of flow down catchment slopes. It has been indicated that the pathline of a water particle can deviate from the proposed model by moving to another preferential group of pathlines (or flow component) to another (Paragraph 3.6.2). For this reason all estimated proportions of flow belonging to a flow component were rounded to the closest 10%. Mean percentage values of the flow separation over the three research catchments were calculated from the original percentage values, before rounding (listed in the last three rows of Tables 5.10 and 5.11). These means were utilized when the model was applied to the larger catchment of the Goedertrouw Dam.

There is considerable variability between the recession constants of the quickflow and throughflow for different weirs and different storm types. A possible explanation for this phenomenon could be the transmission of errors during the separation procedure for the flow components. The baseflow component is separated first from the total observed flow (this estimation being possibly the most accurate estimation). In the next step the throughflow is separated from the residual flow. Thus, errors in the baseflow estimation are transmitted to the throughflow estimation. Quickflow is calculated as the total flow minus the baseflow minus the throughflow, and is therefore affected by errors in both the baseflow and throughflow estimations.

However, the difference in quickflow recession rates could also indicate differences in catchment characteristics that enhance the surface processes. For example, the catchment of W1H017 has a higher relative proportion of exposed granite rock outcrop compared to the catchments of W1H016 and W1H031. This can cause a much greater surface flow rate.

Rainfall events of high intensity will yield considerable more quickflow than the rainfall events of lower intensity, where there is very little or often no quickflow observed. Recession rates of quickflow generally do not exceed a value of 0.7.

Recession rates of throughflow vary between 0.7 and 0.9. The lower recessions rates (i.e. initial higher flow rates) are detected when rain falls on a wet catchment. During this type of storm, the macropores fill up quickly and provide a route for water to flow more rapidly along this pathway.

The baseflow recession rates, for all storm types, are almost identical, ranging between 0.97 and 0.99 (Table 5.12).

An example of the separated flow components for each of the different storm types in shown in Figure 5.6, for W1H016; Figure 5.7, for W1H017 and Figure 5.8, for W1H031.

5.7. Long term recession constant of baseflow

To verify that the analysed storms were "completed" storms, and not prematurely truncated (due to follow-up rainfall events), the long term recession constants were calculated over a dry winter season, for each catchment. The flow at the three weirs during the dry winter months of May to August was investigated, during each year when continuous flow records were available. The drought during 1993 caused the flow over the weirs of W1H016 and W1H017 to cease, and thus no long term recession data is available from this year. Missing data in the records of weir W1H016, during the winter months of 1994, prevented comparison of information from other weirs during this time period. Many rainfall events during the winter months of 1989 to 1992 prevented these years from providing good data for the investigation into a long term recession.

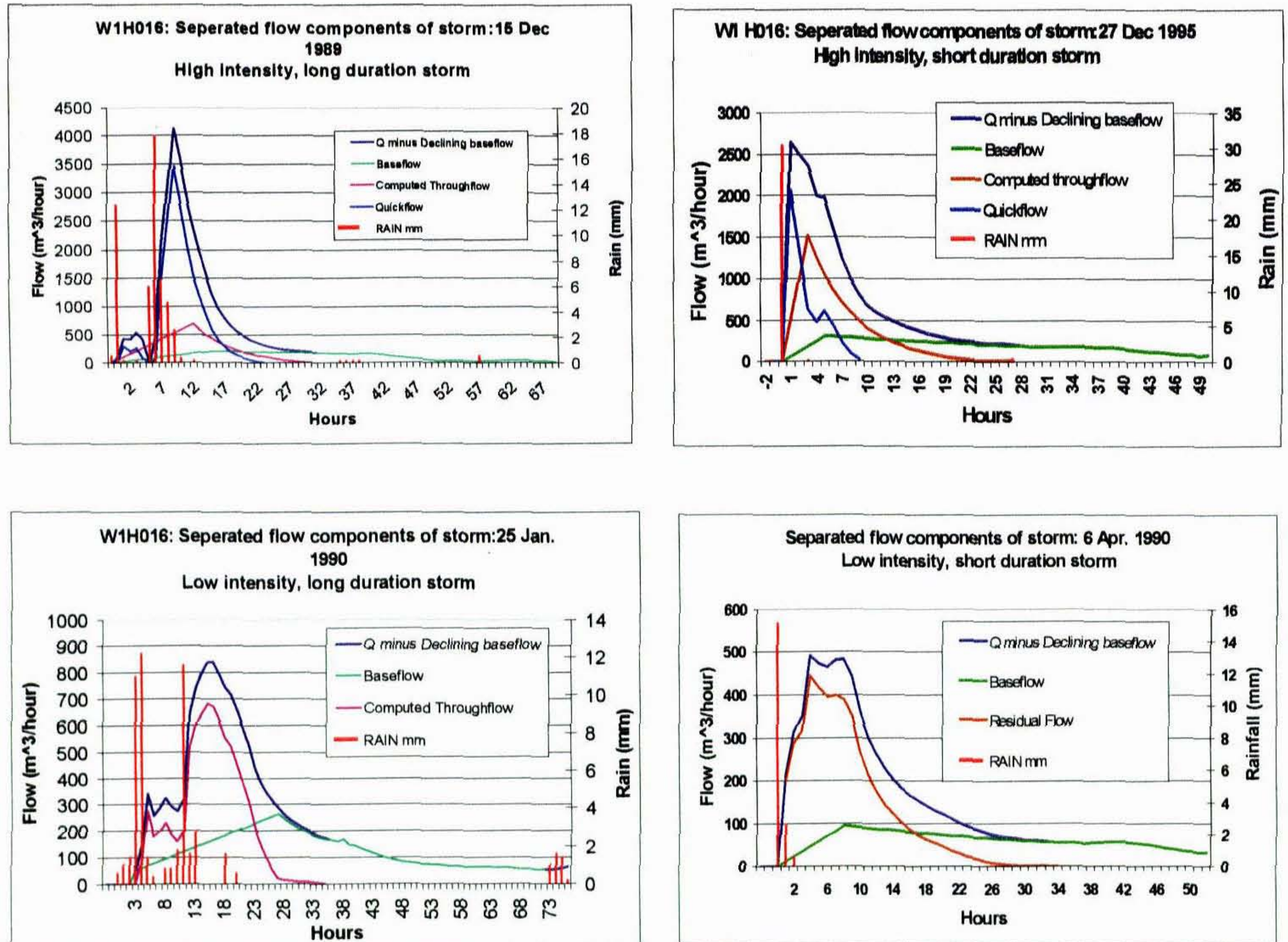

Figure 5.6: Separated flow components for the four different rainfall types, in the catchment of W1H016.

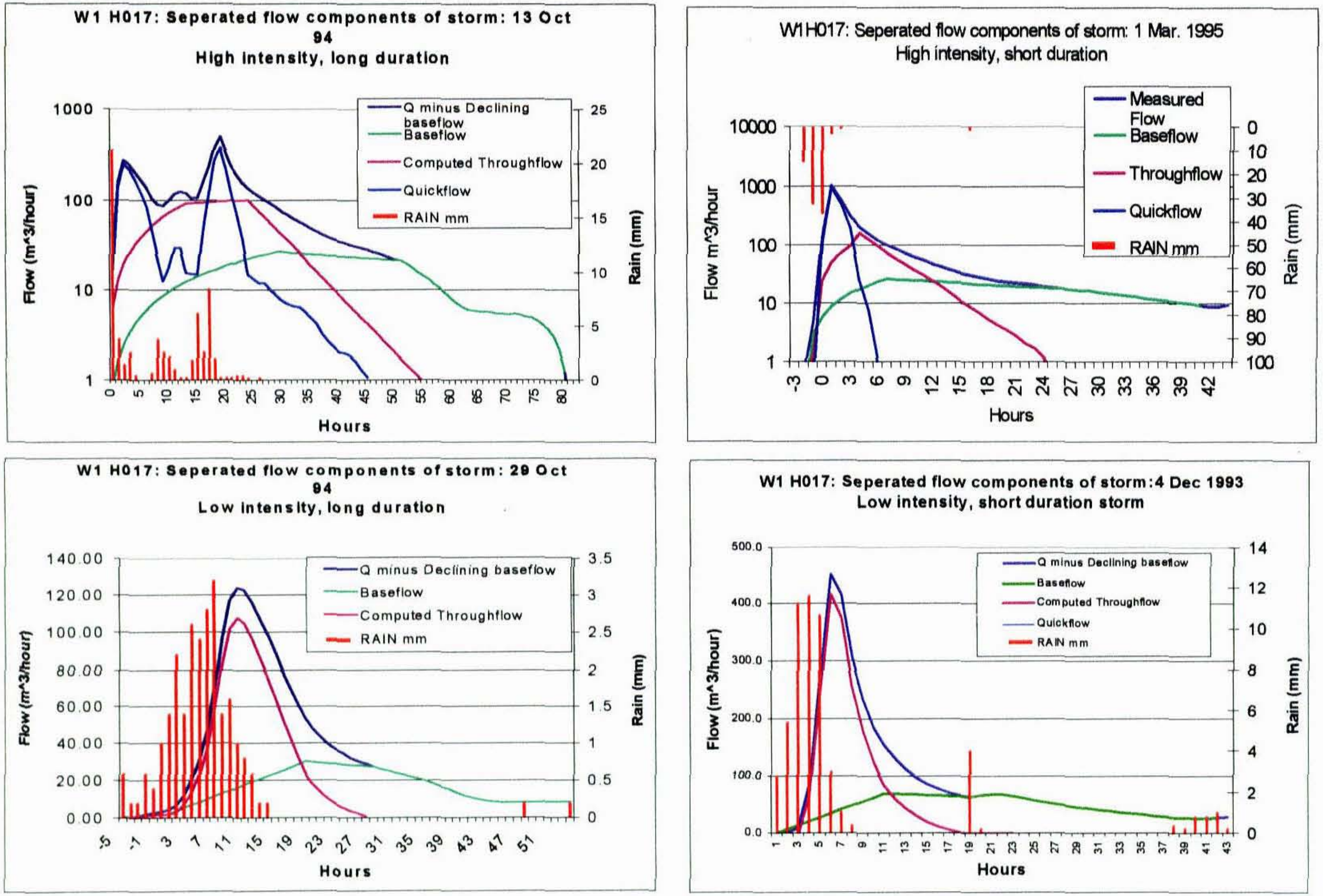

Figure 5.7: Separated flow components for the four different rainfall types, in the catchment of W1H017.

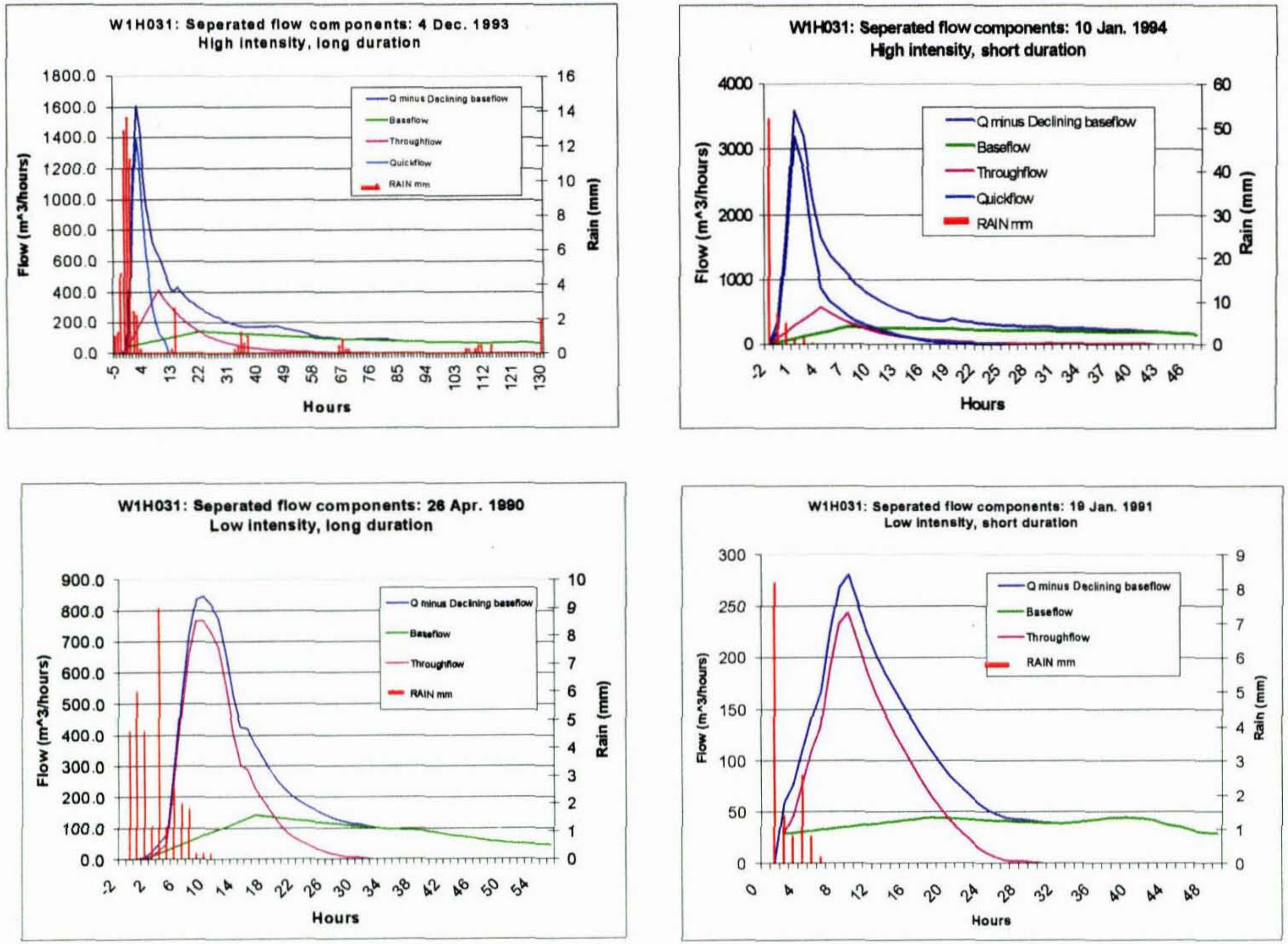

Figure 5.8: Separated flow components for the four different rainfall types, in the catchment of W1H031.

Thus, the flow measured during the winter months of 1995 was utilized. The estimates of baseflow recession rates from this information indicate typical conditions at the end of a dry winter period when groundwater resources have been depleted.

For the catchments of W1H017 and W1H016, some hourly recession rates that are greater than one, occur mostly during the night hours between 20H00 in the evening and 10H00 the following morning. Recession rates lower then one are observed during the day from around 10H00 until about 19H00 at night. This change in flow rates on a diurnal base could possibly be caused by evaporation and/or evapotranspiration from the streams during the day, and allowed greater flow to occur at night.

The average long term recession rates, filtered for diurnal effects, are listed in table 5.13. The long term recession constants compare well with the baseflow recession constants calculated from observed storms (Table 5.11).

The work of Wittenberg and Sivapalan (1999) indicated that the baseflow recession rate is not constant, but that it changes with time. They related this change of the baseflow recession rate to the seasonal change of evapotranspiration. Changes of potential evapotranspiration are commonly related to winter and summer seasons, which then influences the baseflow recession rate. In this research, most of the storms used for the hydrograph analysis, occurred during summer conditions, therefore a constant evapotranspiration (and therefore a constant flow recession for each flow component) are assumed. The seasonal change in baseflow recession should be included in future development.

Table 5.13: Long term recession constants for different catchments during dry seasons.

Long term recession constants	W1H031	W1H031	W1H016	W1H017
Calculated over dry period during drought:	25 May 1994 to 28 June 1994	4 May 1995 to 15 June 1995	30 April 1995 to 16 June 1995	1 June 1995 to 17 June 1995
Total rainfall during this period: (mm)	17	31	78.4	No rainfall available
Average **recession constant** during this period:	**0.9997**	**0.9986**	**0.9985**	**0.9989**
Mean flow during this period: (m^3/hour)	4.4	126	98	13
Max flow during this period: (m^3/hour)	7	363	615	10
Min flow during this period: (m^3/hour)	3.5	57	34	20
Flow at start of period: (m^3/hour)	5.1	318	615	20
Flow at end of period: (m^3/hour)	3.5	57	43	12

Figure 5.9 displays the long term constant recession rate along with the measured flow and rainfall for the period used in the analysis. The green recession line (Figure 5.9) was scaled to display parallel to the observed flow line, for clear display.

5.8. Initial estimation of excess rainfall

When a rain storm occurs on a catchment, a certain percentage of the water is allocated to evaporation and evapotranspiration, and a minor percentage also to deeper groundwater storage. This proportion of rainfall does not contribute to the observed storm hydrograph caused by the rainfall event. The excess rainfall is that percentage of the rainfall which contributes to the flow at the catchment outlet (Figure 2.4).

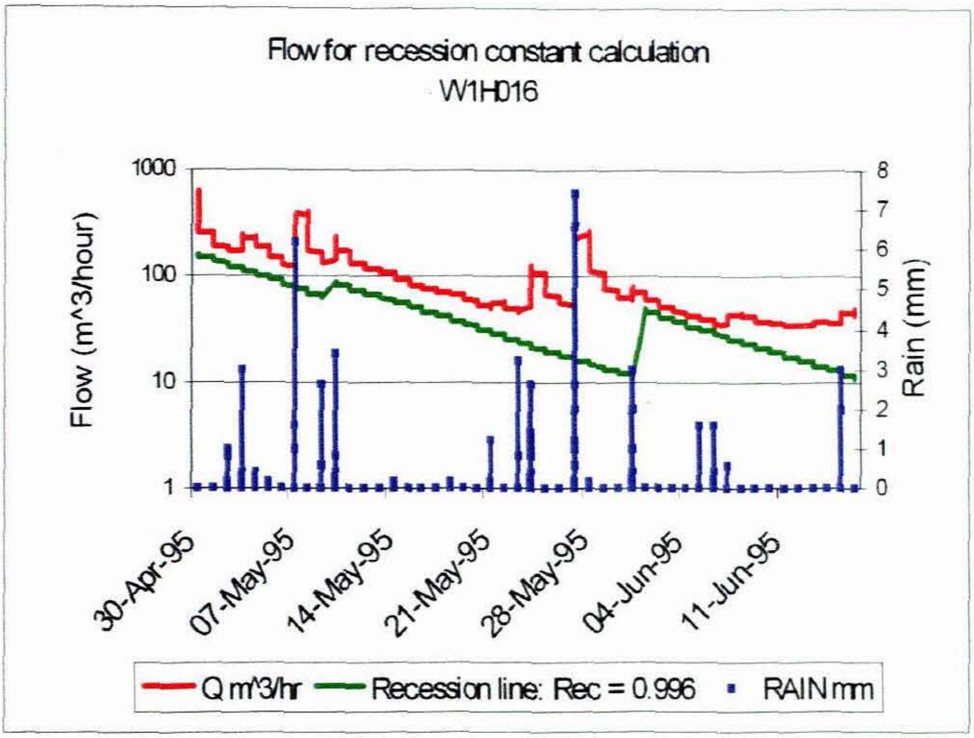

Figure 5.9: Flow recession rates for a long dry season.

Pre-event baseflow was estimated by assuming a constant flow rate for the baseflow component throughout the storm event. This flow rate was assumed equal to the flow rate at the beginning of the storm hydrograph. Pre-event baseflow was eliminated from the estimation of excess rain.

The percentage excess rainfall for different observed storms was determined using the observed flow rates, from which pre-event baseflow was deducted, and the corresponding observed rainfall records. Flow rates (in m^3/hour) were converted to units of mm/hour (using the catchment sizes) to match the units of the rainfall records (mm/hour). The total flow of each storm event (from the start of the rising limb of the hydrograph to the point where flow from the storm event returned to pre-storm conditions) was compared to the total rainfall of the event. These are listed in Table 5.14 for each of the research catchments. The data from each weir's catchment is ranked for rainfall type and increasing rainfall storm durations.

Table 5.14: Rainfall measurements and calculated percentages of excess rainfall for different storms.

Dates	Measured rain	Excess Rainfall	Duration of rainfall event	Maximum measured rainfall intensity	Rainfall type	% Excess Rainfall	Mean % Excess rainfall
	(mm)	(mm)	(hours)	(mm/hour)		%	%
				W1H016			
27 Dec 1995	30.4	8	1	30	Short dur, high int	**27%**	**14 %**
12 Nov 1992	35.6	2.4	2	21	Short dur, high int	**7%**	
1 Mar 1995	60.2	2	4	30	Short dur, high int	**4%**	
22 Jan 1994	45.4	3.0	5	22	Short dur, high int	**7%**	
10 Jan 1994	45	6.0	6	22	Short dur, high int	**15%**	
23 Oct 1995	45.2	10.7	4	29	Short dur, high int	**24%**	
6 Apr 1990	17.8	2.3	2	15	Short dur, low int	**13%**	**14%**
30 Oct 1989	19	6.4	2	17	Short dur, low int	**34%**	
16 Mar 1993	25.2	0.3	4	13	Short dur, low int	**1%**	
6 Feb 1990	34.8	2.7	9	11	Long dur, low int	**8%**	
24-25 Jan 90	47.4	5.3	13	12	Long dur, low int	**11%**	**11 %**
14 Feb 1990	49	11.2	8	17	Long dur, high int	**23%**	**22%**
15 Dec 1989	50.6	10.7	10.0	17	Long dur, high int	**21.1%**	
Mean % excess rainfall for the catchment of W1H016:						**15%**	**15%**
				W1H017			
13 Nov 1992	24.6	0.7	2	20	Short dur, high int	**3%**	**13 %**
23 Oct 1995	41.6	9.5	2	39	Short dur, high int	**23%**	
13 Jan 1996	46.4	11.4	3	31	Short dur, high int	**25%**	
10 Jan 1993	31.2	1.3	4	19	Short dur, high int	**4%**	
15 Mar 1993	38.4	1.8	4	26	Short dur, high int	**5%**	
16 Jan 1996	57.8	15.0	4	32	Short dur, high int	**26%**	
1 Mar 1995	85.8	4.6	4	36	Short dur, high int	**5%**	
9 Mar 1994	24.4	1.4	2	14	Short dur, low int	**6%**	**13 %**
27 Dec 1995	27	7.8	2	16	Short dur, low int	**29%**	
30 Mar 1994	29.8	1.8	2	15	Short dur, low int	**6%**	
4 Dec 1993	44.6	4.9	6	11	Short dur, low int	**11%**	
29 Oct 1994	20	2.6	10	3	Long dur, low int	**13%**	**13 %**
13 Oct 1994	61	7.8	19	21	Long dur, high int	**13%**	**13 %**
Mean % excess rainfall for the catchment of W1H017:						**13 %**	**13%**

Dates	Measured rain	Excess Rainfall	Duration of rainfall event	Maximum measured rainfall intensity	Rainfall type	% Excess Rainfall	Mean % Excess rainfall
	(mm)	(mm)	(hours)	(mm/hour)		%	%
W1H031							
6-7 Apr 1990	24.2	9.7	2	22	Short dur, high int	40%	20%
13 Nov 1992	30.6	1.6	2	28	Short dur, high int	5%	
23 Oct 1995	46.4	11.7	3	40	Short dur, high int	25%	
10 Jan 1994	64	14.5	3	52	Short dur, high int	23%	
22 Jan 1994	45.6	3.5	4	35	Short dur, high int	8%	
1 Mar 1995	105	8.3	4	38	Short dur, high int	8%	
13 Jan 1996	44.8	12.8	7	20	Short dur, high int	29%	
15 Feb 1990	62	13.5	7	30	Short dur, high int	22%	
29 Jan 1991	13	1.4	4	8	Short dur, low int	11%	18%
30 Oct 1989	8.3	8.3	4	17	Short dur, low int	25 %	
4 Dec 1993	49	8.8	8	13	Long dur, high int	18%	18%
26 Apr 1990	33.6	4.2	12	4	Long dur, low int	12%	12 %
Mean % excess rainfall for the catchment of W1H031:						19%	19%
Mean % excess rainfall for the three catchments:						15%	

There is considerable variation in the percentage excess rainfall within the different storm types. There is no correlation between the storm types and the excess rainfall. This indicates that the variation in excess rainfall does not depend only on the storm type. This model is built on the assumption that there is a direct relationship between the rainfall and runoff. However, the catchment rainfall estimation by point measurements may not be sufficiently accurate for this comparison.

The mean percentage of excess rainfall per storm event calculated over the three catchments is 15%. Thus, the value of 0.15 was used as a first estimation of the fraction of excess rainfall (or the runoff coefficient *C*) during the spatial model's application with observed rain storms in the catchment of the Ntuze River.

5.9. Summary

This chapter describes the analysis of observed flow hydrograph in an attempt to derive attributes that verify the important features of storm runoff incorporated in the spatial model. Important catchment information has been extracted from the observed hydrographs. The partitioning of the total observed river flow into flow components provides estimates of the percentage of storm water that belongs to the different flow components, for the different storm types.

The estimation of the recession constants, for different observed flow storm types, provides catchment information that will be vital in the development and verification of the response functions derived from spatial information (or the GIS storm hydrograph).

****

6 Spatial information and modelling

This chapter describes the preparation of the spatial information (development of the DEM and the derived information) to determine the physical pathways for the various flow components in order to implement the conceptual model of flow mechanisms. It describes the deduction of the physical pathways of the different flow components, from the point of rainfall impact on the catchment, to the outlet.

6.1. Analysing the DEM

A raster (or a raster image, or a grid) is a matrix in which each element represents a rectangular area on the earth. Each element is called a pixel in GIS. For the special case of the DEM, each pixel contains the mean height of the land surface above mean sea level, within its demarcated area. The DEM is an interpolated surface, calculated from the elevation contours of the catchment. GIS software packages interpolate between the rasterised contours (i.e., vector contours that are overlaid on the matrix) to create a value for each pixel of the complete matrix. Various methods are used for DEM estimations, using different inter- and extrapolation techniques.

The scale of the DEM resolution must be chosen with care. The pixels' resolution must be fine enough to describe the detail of the geomorphological features that need to be analysed.

However, a very detailed resolution can lead to time-consuming calculations while not adding much information to the catchment knowledge. The ideal DEM scale will describe the catchment slopes which direct water to the rivers, as well as the river courses and any river and catchment features that are of importance to the river runoff contribution.

The capabilities of DEM analysing software includes the ability to calculate *slopes*, *aspects* (the direction that the steepest slope is facing) and hence the *flow directions* that water would follow from each pixel to one of eight neighbouring pixels (Figure 6.1). From the *flow accumulation grid* (indicating the number of upstream pixels flowing into each pixel), the *courses of rivers* are determined (Figure 6.1). These functions are built into most GIS packages. Different software packages utilize different techniques to do these calculations.

The DEM is used to calculate the flow directions through each pixel. Figure 6.1 illustrates how the flow direction through each pixel can be utilized to determine the different flow paths of water down the catchment slope. Slope lengths of each pixel (L) are derived from the rectangular pixel

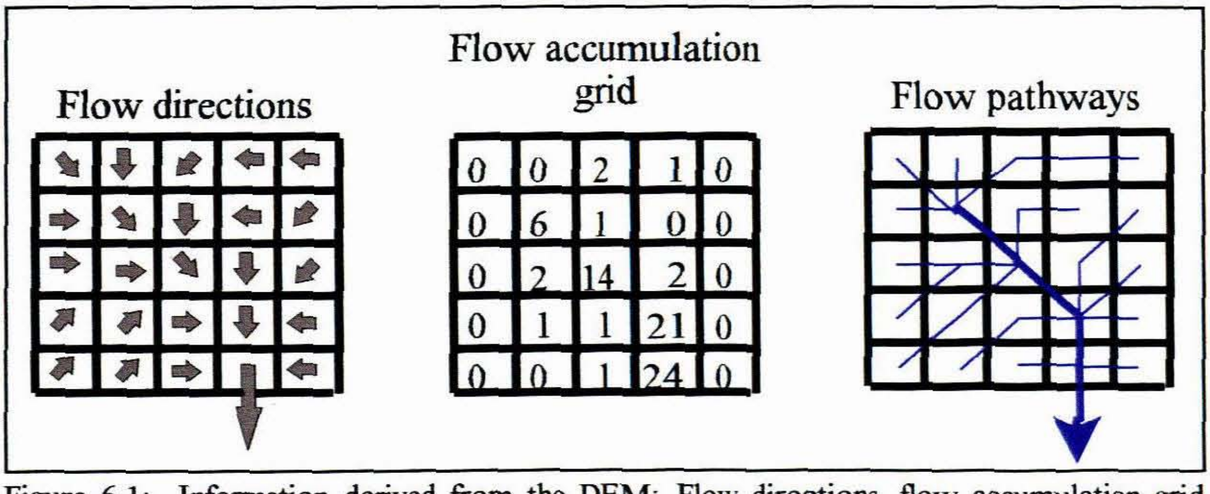

Figure 6.1: Information derived from the DEM: Flow directions, flow accumulation grid (indicating the number of upstream pixels flowing into each pixel) and flow pathways, from which the river courses area deducted.

dimensions (x, y) and flow directions:

$L = x$ or $L = y$

for up, down, right or left flow directions, and

$$L = \sqrt{x^2 + y^2}$$

where flow direction is diagonal across the pixel.

In particular, travel directions of flow paths (see the flow pathways or river courses in Figure 6.1) are combined with the flow distances, to derive the *cumulative travel distances* that water flows from any pixel in the catchment to the outlet (Figure 6.2). This calculation provides a grid of which every pixel contains the cumulative distance from the pixel to the catchment outlet. The furthest pixel from the catchment outlet in Figure 6.2 is the top right-hand corner, although it is not the furthest point by line of sight.

If the flow velocities of water over individual pixels are known, the flow times of water over individual pixels can be deducted (time = length / velocity). The *cumulative* flow times of water from each pixel to the catchment outlet are calculated in a similar way to *cumulative* flow distances, once the velocity profile has been determined.

For the special case where the flow velocities equal a unit velocity (one) for each pixel of the catchment, the histogram of the cumulative flow times will then be equivalent to the histogram of the cumulative flow distances. The response function describing this histogram of travel lengths will be referred to as the *geomorphological response function* (Figure 6.2). It will be a unique function for each catchment and will generally be invariant for a particular flow surface.

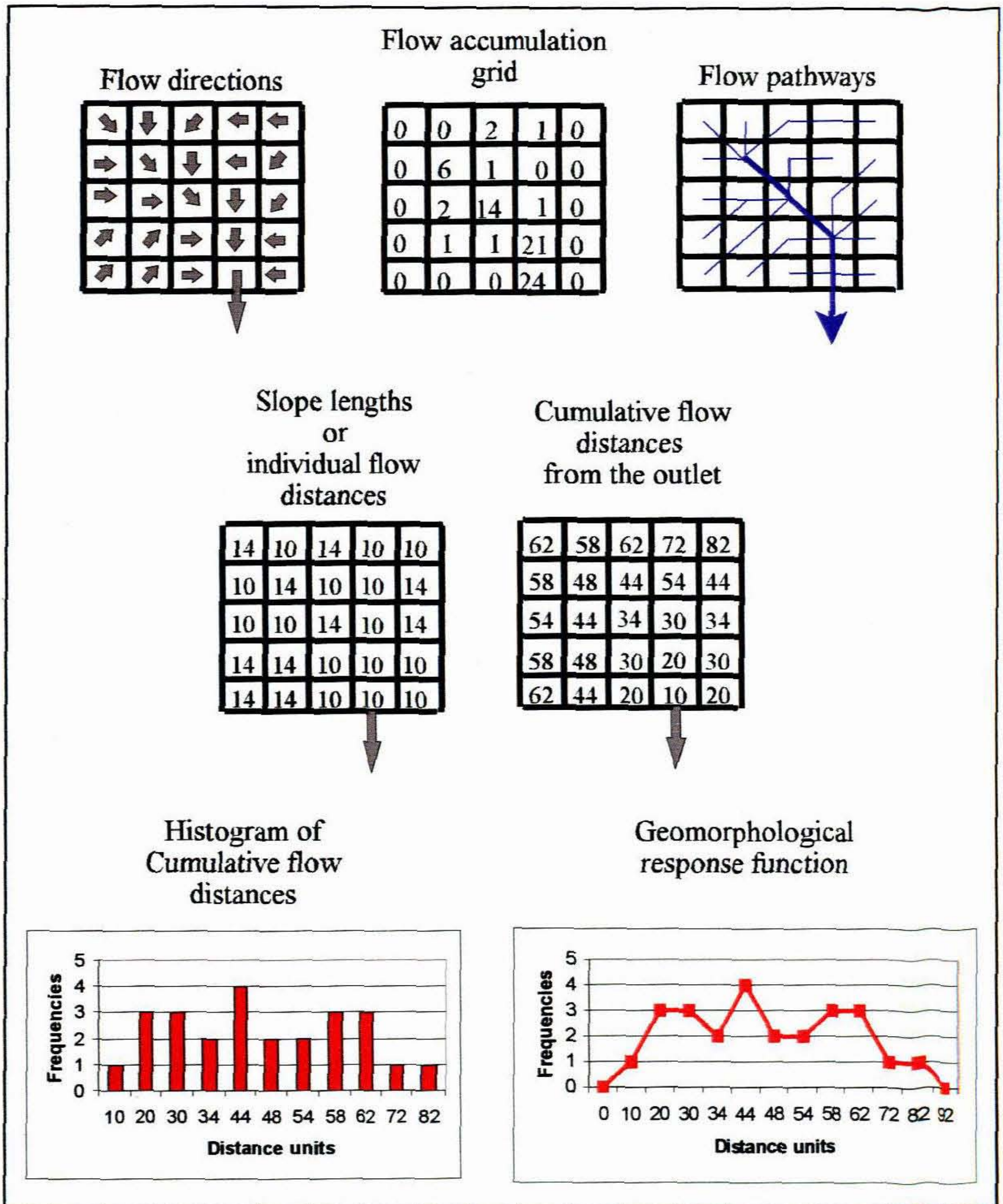

Figure 6.2: Slope lengths are calculated from the flow directions. Slope lengths and flow directions are then used to determine the cumulative travel distances. The arrows indicate the flow exit point from the catchment.

Hence, the geological response function for overland flow could be different to the flow surface for groundwater, where there may be geological features that redirect the flow pattern.

Where the cumulative travel distances have been replaced with the estimated cumulative travel times, the response function of the resulting histogram will be referred to as the *travel time response function*. This function, estimated for one unit of excess rainfall, will be equated to the unit hydrograph for the flow surface.

6.2. Software to determine cumulative travel distances and times

GIS software packages can be vector-based or raster-based. Vector-based GIS software (such as Arcview) analyse the point, line and polygon features. Tables, containing information that relates to the features, can be manipulated, e.g., the selection of certain land uses. Numeric values in these tables can be manipulated, like multiplying the contour heights to change units, etc. Vector-based GIS software can also perform spatial calculations on the vectors, like calculation of distances from a vector that represents a river, or the area within a polygon vector. Vector-based GIS software can often layer the raster images or grids as backdrops, from where manual digitizing of vectors can be performed.

Raster-based GIS software (such as IDRISI and the Spatial Analyst extension of Arcview) includes the capability to display raster grids and also to conduct mathematical and statistical operations on the grids. These operations include a wide variety of calculations on each pixel element (like calculating the inverse of each pixel's value, or determining each value as a percentage value), as well as summary information, like the area covered by pixels of similar identity. Raster-based GIS software also includes some matrix algebra, like the sum of corresponding pixels in two or more grids.

Raster-based GIS software packages, which include functions that calculate and analyse a DEM, usually have some built-in functions that calculate slopes and aspects, as well as flow accumulation grids. However, software which determines the cumulative travel distances of flow down the catchment slopes, is not readily available. IDRISI 32 could also not provide an estimate of these cumulative travel distances.

This study utilized the IDRISI 32 release II software (available from Clark Labs: http://www.clarklabs.org/), in conjunction with the TOPAZ software (available free from the internet: http://duke.usask.ca/~martzl/topaz/index.html) to determine the cumulative distances of flow pathways. Olivera and Maidment (2005) state that Arc/Info GRID can also be utilized to derive this response function, using Arc/Info's function FLOWLENGTH. FLOWLENGTH is also equipped to provide cumulative travel times down the travel pathways to the outlet, as weighted travel distances. However, Arc/Info was not available for this research because of cost.

6.2.1. An overview of TOPAZ

TOPAZ was utilized in this study to calculate the cumulative distances of pathways from any point in the catchment to the catchment outlet.

The TOPAZ program operates outside a GIS. It analyses topographic parameters of a catchment for use in spatial hydrological modelling. Its input is a DEM created in a GIS of the user's choice. It analyses the DEM with tools not supplied by commercial GIS packages, and rewrites the output for exporting to the user's GIS. It was developed by the United States Department of

Agriculture, Agricultural Research Service (Garbrecht and Martz, 2003, http://duke.usask.ca/~martzl/topaz/index.html). Easy import and export of IDRISI files to and from TOPAZ is built into the software.

According to the TOPAZ Overview documentation: "The overall objective of TOPAZ is to provide a comprehensive evaluation of the digital landscape topography with particular emphasis on maintaining consistency among all derived data, the initial input topography, and the physics of the underlying energy and water flux processes at the landscape surface. TOPAZ overcomes some limitations of existing DEM processing methods and includes a number of new topographic processing features that are relevant to hydraulic and hydrological analyses."

Examples of TOPAZ applications include:

1. drainage network generation and watershed segmentation
2. analysis of DEM resolution on generated network and subcatchment characteristics;
3. flownet generation and subcatchment parameters quantification for the Agricultural NonPoint Source model and,
4. a model interface between TOPAZ and a hydrological model. The interface has been applied for irrigation system development in Turkey and for the analysis of scaling effects in a Canadian research program.

(From: http://duke.usask.ca/~martzl/topaz/index.html.)

6.2.2. Utilizing TOPAZ in the research project

To produce a geomorphological response function, the flow path distance from each pixel to the catchment outlet is needed.

The calculation of a DEM from contours is prone to interpolation problems that can lead to pits and flat area in the calculated DEM surface. The DEM, as calculated in IDRISI before removal of pits or flat areas, was imported into TOPAZ. TOPAZ then made some adjustments (see Paragraph 6.2.3) before a full DEM analysis was performed. The full analysis included the calculation of cumulative distances from each pixel to the catchment outlet. Output from TOPAZ (a grid with pixel values that indicates the distance from each pixel to the catchment outlet) was rewritten to IDRISI 32 file format for further modelling and analyses.

6.2.3. Depressions, slopes and aspects in TOPAZ

Although TOPAZ provides outflow from depressions and flat areas, the software does not adjust the DEM to eliminate flat areas. It simply identifies them, and provides flow directions (or aspects) for those pixels which are situated on flat areas. Consequently, zero slopes give extremely large travel times in the proposed model of surface flow (Manning's equation) and subsurface flow (Darcy's Law). While TOPAZ diverted flow through pits and depressions, the zero slopes caused unrealistic high travel times. Thus, the zero slopes had to be adjusted to estimate the travel times. Slopes calculated in IDRISI 32 were determined after IDRISI adjusted the original DEM for depressions and loops in flow paths. This slope grid, with eliminated areas of zero slopes, was utilized in conjunction with the TOPAZ travel distances and flow directions to determine the travel velocities.

6.2.4. Travel distances indicated by TOPAZ following the travel pathways

The histograms of the travel distances calculated in TOPAZ GIS software provided the statistics given in Table 6.1. Figures 6.4, 6.5 and 6.6 gives the frequency histograms of the cumulative travel distances from each pixel to the catchment outlet, which is called the *geomorphological* *response functions,* sketched in the graph next to the DEM of each catchment.

Table 6.1: Mean and maximum travel distances for the different catchments.

Weir	Mean distances travelled (metres)	Maximum distances travelled (metres)
W1H016	2157	4067
W1H017	631	1131
W1H031	2155	4168

6.3. Fractured rock

As shown above, the geomorphological response function of a flow surface will depend on the flow directions and the flow distances to the outlet, cumulated along the flow paths of the surface. In the case of a fractured rock network in the underlying soil-and-rock matrix of a catchment, the flow directions and flow distances along the fractures will be determined by the positions and lengths of the fractures. These fractures can create flow paths that differ substantially from flow pathways through the soil matrix surrounding these fracture. (See discussion in Paragraph 2.2.4). The fracture's unique characteristics changes the flow network along the baseflow pathways to flow along the network of fractures in the bedrock. It is suggested that the flow along fractured rock can be simulated as a network of flow paths, integrated in the baseflow pathways, where the baseflow surface is directly influenced by the fracture network (Beven, 2001).

If the fractures can be established, the flow paths can be deducted from the positions of the fracture network, in conjunction with the hill slopes. Flow directions along the fractures will be determined by the piezometric heads on the two edges of each fracture, since water flows from higher potential head toward lower potential head.

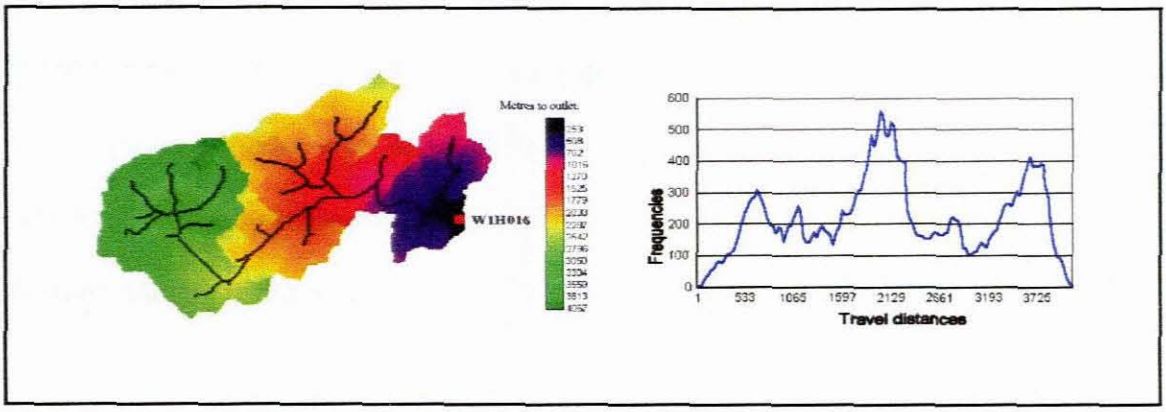

Figure 6.3: Map of the travel distances from each pixel to the outlet at W1H016, with its unique geomorphological response function.

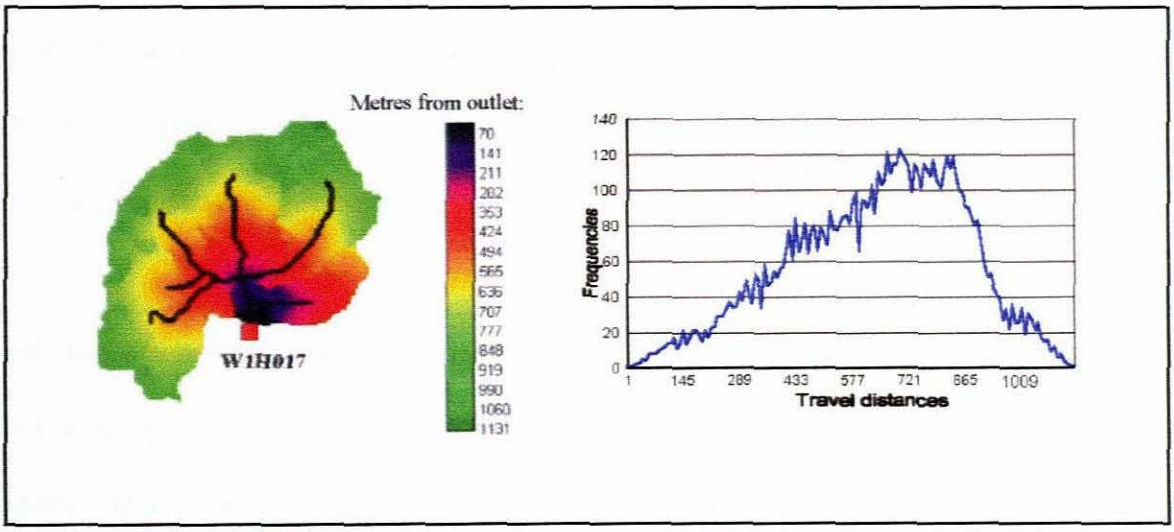

Figure 6.4: Map of the travel distances from each pixel to the outlet at W1H017, with its unique geomorphological response function.

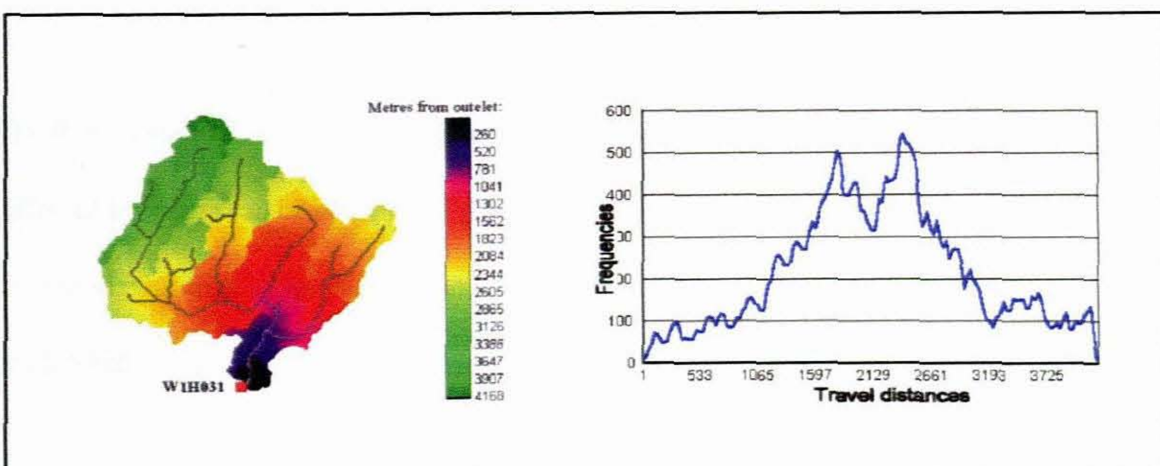

Figure 6.5: Map of the travel distances from each pixel to the outlet at W1H31, with its unique geomorphological response function.

It can generally be assumed that flows along the fractures will generally tend to flow away from the catchment boundaries toward the river system, until it crosses one of the main rivers, from where the flow follows the course of the river. This assumption can be applied in the absence of detailed fracture network information.

Figure 6.6 displays the case of a flow surface, similar to the flow surface demonstrated in Figure 6.1, with a simple fracture network added, indicated with green lines. This fracture network consists of two straight lines. It is assumed that flow directions along the facture network will be toward the main rivers. Thus, the flow directions of the baseflow surface is changed by routing the flow paths along the fractures in the direction of the main rivers. When it crosses a river, it will flow along the river to the outlet.

Differences between the two sets (from Figures 6.2 and 6.6) of flow directions and cumulative flow distances to the outlet are indicated in Figure 6.6 with red arrows and red cumulative distance values. The geomorphological response function illustrated in Figure 6.6 indicates a slightly different function from the same function illustrated in Figure 6.2. This is due to the re-direction of flow paths along the fracture network toward the rivers.

The flow velocities along the fractures can be estimated if the hydraulic conductivities along the different fractures can be established (Paragraph 2.5.2). If flow velocities along the fractures are estimated, the time response functions, which include flow from a fracture network, can be established.

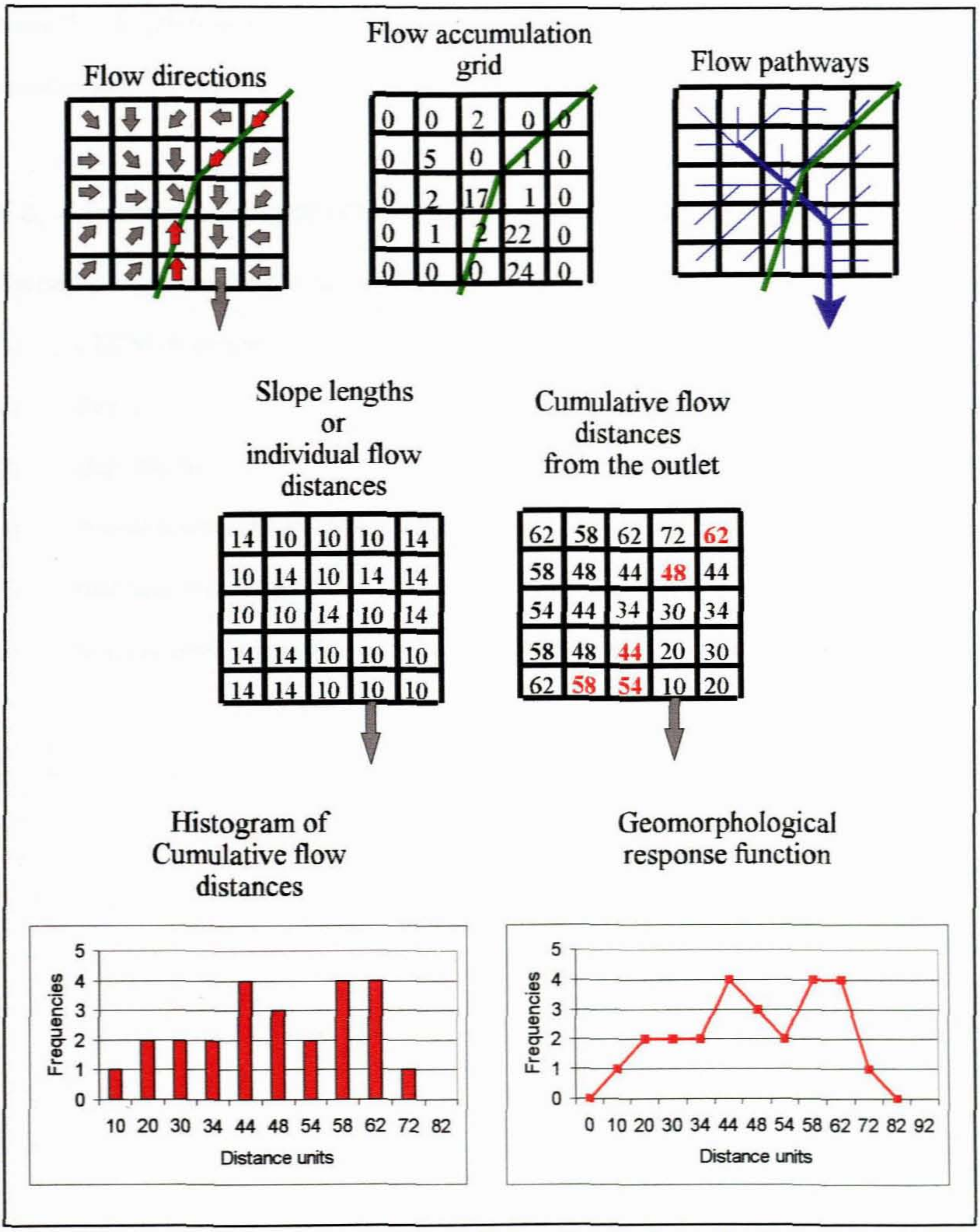

Figure 6.6: Surface information derived from a flow surface (similar to the flow surface of Figure 6.2) to which a fracture network has been overlaid (indicated with green lines). The differences between this flow surface and the flow surface from Figure 6.2 is indicated in red arrows (flow directions) and red values of cumulative distances.

No substantial evidence could be found indicating the existence of a fractured rock network in the research catchments of the Ntuze River, so the concept could not be verified in the model development.

6.4. Summary of spatial information needs of the model

Spatial information needed to estimate the geomorphological response function, is:

1) a DEM (at an appropriate scale),
2) slopes,
3) slope lengths,
4) flow directions of water from each pixel,
5) flow accumulation grid and
6) flow distances from each pixel to the catchment outlet.

****

7 Determination of the storm hydrograph using spatial information

The geomorphological response function can be adjusted for translation velocities along the pathway. This function is referred to as the *travel time response function* and has been equated to the observed hydrograph's features. Applying these arguments, it is possible to derive equivalent response functions for each of the different flow component's pathways, if the corresponding velocity profile along the pathways can be derived, in conjunction with the geomorphological response function.

For a two-dimensional surface, flow is constrained to movement along the surface plane and does not infiltrate into the subsurface soils structure on a different plane in the two-dimensional system. These pathlines are generally unique and finite. They are a direct function of the features in the surface plane. For a three-dimensional system, subsurface processes are also considered and flow can infiltrate the soil structures. For the three-dimensional system, the response function is no longer unique and can contain an infinite number of pathlines. However, it has been shown that there are usually preferential pathlines that can be grouped together (into pathways, as described in Paragraphs 2.4 and 3.6.2) and conceptualized as the dominating hydrological processes.

This chapter describes the determination of the travel times of water along the different flow component's pathways to derive the travel time response functions of each flow component. The sum of the flow components' response functions is then compared to observed storm hydrographs, for the different rain storm types.

7.1. Calculation of travel times over individual pixels

The time taken to traverse across each pixel, cumulated along the flow paths, will provide a raster grid of cumulative travel times. The histogram of travel times will represent the *travel time response function*. Flow equations were utilized to calculate the travel time of water across each individual pixel for the different flow processes.

The velocity profile along the individual pathways can be calculated for different conceptual flow pathways, assuming the following processes:

1. Open channel flow obeys Manning's equation (Chow *et al*, 1988)
2. Surface flow pathways obey an adaption of the Manning's equation (Kelbe *et al*, 1996)
3. Throughflow pathways can be conceptualized as a combination of Manning's equation and Darcy's law for saturated conditions
4. Baseflow pathways obey Darcy's Law for saturated conditions (Todd, 1980).

7.1.1. Open channel flow

Pixels that contain a river course are assumed to conform to a travel time derived from open channel flow theory. The travel times of water along an open channel segment can be estimated from Manning's equation (Chow *et al*, 1988), written in the following form:

$$T = \frac{Ln}{R^{2/3}S^{1/2}} \qquad \text{(equation 7.1)}$$

where T = travel time (in seconds) across a pixel,

L = dimension of a pixel (in metres), straight or diagonally across the pixel,

n = Manning's n (a roughness coefficient),

R = the hydraulic radius of the channel (in metres), and

S = slope of the channel (in fractions, with arbitrarily assigned minimum slope of 0.001).

The hydraulic radius R is the cross sectional area of flow divided by the wetted perimeter (Chow *et al*, 1988). This radius can be approximated for shallow flow in relative wide channels by the flow depth. A detailed description follows in Paragraph 7.2.

Both the hydraulic radius of the channel (R) and Manning's n are assumed to reflect the mean river conditions in the channel segment represented by the pixel. In reality, these values will change during the course of the storm as the flow increases or decreases. These changes over time have not been incorporated into the model.

A value of 0.029 was used for Manning's n in the Ntuze channels, which represent a value for streams that are clean, straight, in full stage and with no pools (Chow *et al*, 1988 and Wilson, 1983). These are the assumed river conditions during storm flow in the research catchments. It was assumed that the flow depths during storm conditions can be represented by a depth of 0.1m over an average channel segment. The hydraulic radius R and the influence of catchment morphology on the values of R will be discussed in Paragraphs 7.2.1 and 7.2.2.

7.1.2. Surface flow and saturated overland flow

The flow equation derived for open channel flow (equation 7.1) was adapted for surface flow, by replacing the hydraulic radius of the channel with the hydraulic depth of water flowing across a pixel of known dimensions, in a manner similar to that used by Kelbe *et al* (1996). Initially, it was assumed that the hydraulic depth can be derived from one unit of excess rainfall for a uniformly distributed rainfall of short duration and high intensity over the entire catchment. Assumed values for Manning' *n* are listed in Table 7.1 for the surface flow conditions (taken from Chow *et al*, 1988 and Wilson, 1983).

Table 7.1: Values used for Manning's n. (From: Chow et al, 1988 and Wilson, 1983.)

Surface conditions	n
Natural forests	0.1
Eucalyptus	0.1
Sugarcane	0.07
Subsistence farming	0.04
Rocks	0.01
Roads	0.02
Human living	0.02
Grassland	0.04

Travel times for surface flow across every pixel were calculated in seconds for the 10m by 10m pixels of the Ntuze River catchment. Calculated travel times for water travelling across individual pixels range from near-zero to 13900 seconds (3.8 hours), with the mode between 100 to 120 seconds (1.7 to 2 minutes).

7.1.3. Baseflow

An estimate of the travel velocities of groundwater flow can be derived by making use of Darcy's Law. Maidment *et al* (1996) applied the following equation to estimate the baseflow velocities in each pixel using an adaption of Darcy's Law:

$$T = \frac{L}{KS} \qquad \text{(equation 7.2)}$$

Where T = flow times over each pixel,

L = distance of flow over pixel,

S = the slope of the piezometric head, and

K = the hydraulic conductivity.

The slope must be derived from a pieziometric surface that is generally unknown for the baseflow calculations. Thus, it is assumed that the water table surface can be estimated from the topographical surface. A smoothed surface profile was created by replacing each pixel in the surface DEM with the mean of the pixel and its eight surrounding pixels. Calculated heights of the water level that are above the topographical surface were limited to a depth of 0.1m below the surface level. The resultant surface was smoother than the surface of the DEM. Gradients generated from this surface of the saturated zone gave a mean slope of 0.183, which is slightly lower than the topographical surface mean slope of 0.203.

Hydraulic conductivity of the deeper soils is difficult to establish, even with substantial field investigations, and estimated values often range over a few orders of magnitude. Shaw (1994) indicated a range of values for hydraulic conductivity that range between 1 and 10 metres per day, for water flow in sandy conditions. A hydraulic conductivity of 1 m/day will be assumed in the study area for the sandy soils in the research catchments.

Calculating the velocity of water through the catchment using Darcy's Law for saturated flow, provides flow times across individual pixels that fall between 50 and 70 days. These initial calculations (using equation 7.2) assumed a hydraulic conductivity of 1 m/day (for sandy slopes) and an average groundwater gradient of 0.2 across a pixel length of 10m (or 14m for the diagonal).

These flow time estimations are unrealistically long. The model simulates the storm hydrographs with an hourly time step, over a period of a few days. However, estimated flow times of 50 to 70 days over 10m segments could explain the perennial water flow in the main channels of the research catchments during the drought of 1993, which was finally broken in the rain season of 1994/1995.

Beven (2001) has suggested that the rapid response reaction of baseflow to a rainfall event (similar to those observed by Kelbe and Germishuyse, 1999, illustrated in Figure 2.3), can be explained by a pressure wave that translates much quicker through the saturated soils than the traditional estimated flow velocities of water through the saturated zone (Paragraph 2.3). Based on the wave translation theory (Beven, 2001), a new approach was applied to the calculation of baseflow velocities. *It is assumed, particularly for high intensity storms,* that the infiltrating rainfall creates a wetting front that induces a pressure wave, which causes a much quicker response in the groundwater discharge. This has been incorporated into the model as an "adapted" hydraulic conductivity. The adapted hydraulic conductivity could possibly emulate the theory of a pressure wave that is translated across the catchment through the saturated zone, creating travel times that are much faster than the traditional estimations of groundwater flows. Estimated baseflow travel times, as calculated from the analysis of observed storm hydrographs (Chapter five) were utilized to derive an estimate for an adapted hydraulic conductivity, K_a.

7.1.4. Throughflow

The throughflow is conceived as a mixture of unsaturated flow through the soil matrix and surface flow within the macropores (miniature pipes). The unsaturated matrix flow can be estimated using Darcy's Law, with appropriate unsaturated values for the hydraulic conductivity K, while the surface (macropore) flow is better described by Manning's equation. However, the proportion of flow in each pathway is unknown. Both equations are of the same form (if $K \equiv R^{2/3}/n$) and a proportionality factor is introduced to describe the partitioning between the pathways:

$$T = a\frac{Ln}{R^{2/3}S^{1/2}} + b\frac{L}{KS} \qquad \text{(equation 7.3)}$$

where T = the travel times,

a and b are proportionality constants, $a+b=1$, $0 \leq a,b, \leq 1$

L = the slope length,

n = Manning's n,

R = hydraulic radius,

S = the slope gradient, and

K = the conductance of the flow.

Ward and Robinson (2000) recognized that throughflow can be influenced by a "piston replacement" or "translatory flow," which in concept differs slightly from the pressure wave theory described by Beven (2001). They described translatory flow as a relatively quick reaction of the water table to rainfall, due to percolation in the zone of aeration, where water moves along preferential channels such as cracks and decayed root channels, or macropores. The translatory flow theory explains the quick reaction of water tables to rainfall events in low-permeability soil types. This quick reaction is due to a quicker flow velocity of water through the macropore zone than traditionally estimated for flow through the topsoil matrix.

In the unsaturated soil zone, where the throughflow occurs, no pressure wave can be translated, as described for the saturated groundwater flows. Flows along the throughflow pathways will rather flow under gravity and along preferential channels through the soil macropore structure, in a manner similar to the surface overland flow. For the application of this version of the model, it is assumed that macropore flow completely dominates throughflow in the Ntuze research catchment, so that $a = 1$ and $b = 0$ (in equation 7.3) for the throughflow component. For catchment slopes, where it is known that no macropore development occurs, this needs to be revised.

7.2. The catchment morphology and the hydraulic radius

7.2.1. Hydraulic radius of overland flow and channel flow

The hydraulic radius R for open channel flow is described as the wetted area (the width W times the depth d) over the wetted perimeter, $W + 2d$ (Chow *et al*, 1988) as illustrated in Figure 7.1. It then follows that, if the depth d is very small compared to the width W, the hydraulic radius can be simplified to the depth of the rivers d:

$$R = \frac{Wd}{W+2d} \cong \frac{Wd}{W} = d \text{, for } W >> d$$

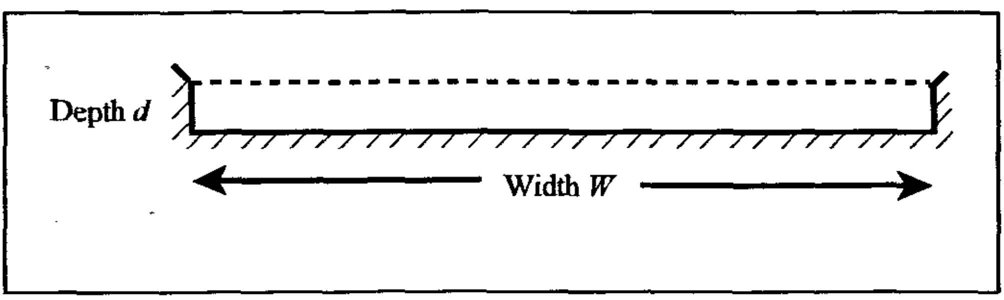

Figure 7.1: A graphic representation of the cross section of a riverbed, as conceptualized in the calculation of a hydraulic radius.

In this model the pixel width is used to estimate the river widths W, for main rivers. When river depths (d) and river widths (W) have similar values, the estimation of the hydraulic radius needs to be revised, because the assumption of $W + 2d \approx W$ will not apply.

7.2.2. Contributing areas

The effect of the river network on the storm hydrograph has been studied and mathematically expressed by many researchers (e.g., Hromadka and Whitley, 1999; Lin and Wang, 1996; Rodriguez-Iturbe and Valdes, 1979). Most of these theories are based on, or refer to, the theory of Nash (1957).

The river network can be delineated from the DEM of a catchment, with modules in a GIS that make use of the contributing area to each pixel. Rivers can be categorized, using a DEM and GIS software, according to the contributing area of each river segment. The contributing area of each pixel in the catchment was investigated for a possible linkage between the form of the storm hydrograph and the river network morphology. The frequencies of the contributing areas to each pixel were plotted against the contributing areas (Figure 7.2) for all three catchments. The distribution is nearly identical for all three research catchments. The plot indicates that a large percentage of the pixels (~ 20%) in the research catchment area have an upstream area of only 100 m^2 (or one 10m by 10m pixel), which represents the catchment boundaries. Moving along the positive X axis (towards larger contributing areas), there is a sharp drop in the frequencies, which follows an exponential decline. It extends to a "tail" end of the graph, where the larger catchment areas are assigned to a very few pixels (only those in the main river channel close to the catchment outlet).

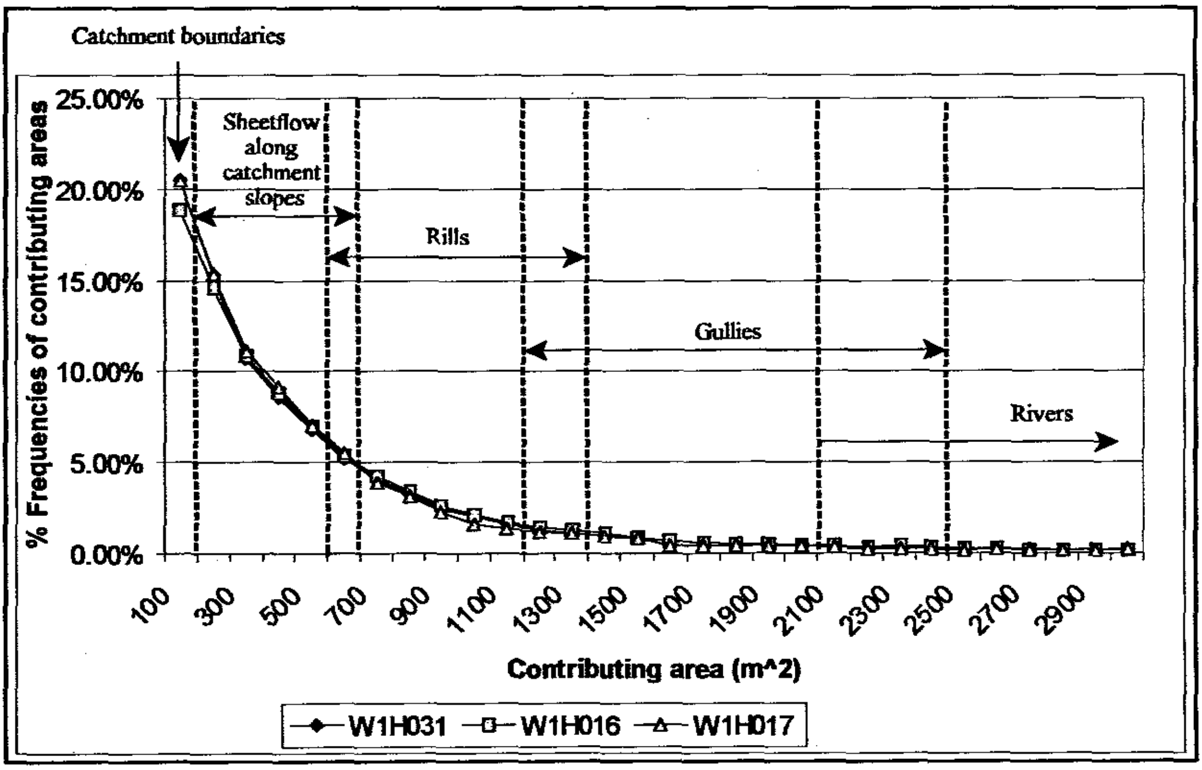

Figure 7.2: Frequencies of contributing areas (expressed in percentages of total frequencies) plotted against the contributing areas (in m^2) and the geomorphic features they could represent.

Figure 7.2 indicates that there is a gradual change in the frequencies as the contributing area increase. As the contributing area of the catchment segments increase, flow processes in those catchment segments will change (Paragraph 3.7.1). Thus, the gradual change in frequencies (Figure 7.2) could possibly indicate the *gradual change* in flow rates which take place as water flow from the catchment boundaries over the hill slopes, gradually forming rills; then deeper gullies; and finally joining the main river which flows to the outlet. This change in flow processes results in a *gradual change in flow times* across different catchment segments.

Flow time of water is a physical characteristic which depends on a number of physically measurable variables: flow length (L); the slope (S); the friction against flow (Manning's n) and the flow depth (or R). As the water moves from the catchment boundaries into rills, forming gullies and joining the main rivers, the flow length and slope stays constant over each catchment segment. However, both the friction against flow (Manning's n) and flow depth (or R) will change as flow processes change from surface flow to flow along rills, to flow along deeper gullies and finally to the flow along the main rivers.

For the purpose of this study, Manning's n was assumed a constant value for each land use, for each catchment segment, because it's values are derived from unchanging land use. The gradual change in flow depth R will be discussed in the following paragraphs.

7.2.2.1. Adapted hydraulic depths

When a given amount of excess rain falls on a catchment, laminar sheet flow may take place, described previously as infiltration excess surface flow (Paragraph 2.2). As the water moves down the catchment slopes, gradually more rills and gullies start to form, depending on the upstream area of each catchment segment. As soon as water reaches the rills and gullies, the travel times change, influenced by the depth of flow, according to Manning's equation (as described in Paragraph 2.6). Therefore, the contributing area was used to estimate a change in the hydraulic radius in each part of the catchment.

An increase in contributing area will result in a reduction in travel times across pixels (Paragraph 3.7.1). It was also shown that an increase in contributing area will also result in an increase in the hydraulic radius. Hence, generally *quicker travel times* should be assigned to pixels where flow occurs in a manner similar to concentrated flow, rather than sheet flow. This should generally occur in pixels with larger contributing areas. On the other hand, generally *longer travel times* should be assigned to pixels closer to the catchment boundaries. Thus, the travel times along the flow paths should be scaled according to the contributing areas.

The hydraulic radius (R) in Manning's equation (or the hydraulic depth) has been related directly to the upstream area of each pixel, for a spatially uniform rainfall event over the entire catchment. The initial assumption that the overland flow has a unit depth R (Paragraph 7.1.2) is changed by scaling the flow depth, according to the contributing area.

The model developed in this research suggests that

$$R_a = R(\frac{a}{C_Q})^m \qquad \text{(equation 7.4)}$$

where R_a = the hydraulic radius, adjusted according to the contributing area of each pixel (in metres).

R = the hydraulic radius or depth for one unit of excess rainfall (in metres),

a = the area contributing to flow through each pixel (in m^2),

C_Q = a spatially invariant normalization coefficient of the contributing area a (in m^2),

m is a calibrated constant.

The function of C_Q is to normalize the contributing area a for pixel scale. The coefficient C_Q was given the mean value of the spatially variant a values throughout each catchment: $C_Q = 22300$ m^2 in the catchment of W1H016, and $C_Q = 23000$ m^2 in the catchment of W1H031. The spatial mean value of a/C_Q over the entire catchment is 1. For pixels with no contributing area (e.g., pixels on the catchment boundaries, where $a = 100$ m^2) the value of a/C_Q is a very small value, i.e., 100/23000 = 0.0043. For pixels at the outlet (where the contributing area of the pixels is close to the entire catchment) the value of a/C_Q will be much larger than one. For the outlet of the catchment of W1H016, $a/C_Q = 3252700/22300 = 145.8$. Pixels, where a/C_Q is larger than the initial estimate of the hydraulic radius R, occur along the rivers and streams of the catchment.

These calculations are a mathematical interpretation of the gradual change that occurs in the depth of flow, from the catchment boundaries to the catchment outlet.

Substituting equation 7.4 (R_a) in equation 7.1 (for R) implements an adjusted concept about the resistance against flow caused by the hydraulic radius. The adapted hydraulic radius R_a is a mere scaling of the hydraulic radius R. It brings about a scaling of the travel times along the conceptualized travel pathways of sheet flow. Adapted travel times of quickflow over pixels (for both overland flow and channel flow) are estimated as:

$$T = \frac{Ln}{R_a^{\ 2/3} S^{1/2}} = \frac{Ln}{R^{2/3} S^{1/2}} * (\frac{C_Q}{a})^{2m/3} \qquad \text{(equation 7.5)}$$

The implementation of equation 7.5 which resembles equation 7.1 will be the spatially uniform values of $a = C_Q = 1$.

7.2.2.2. Adapted hydraulic conductivity

A similar implementation of equation 7.4 was applied to the baseflow (equation 7.2) where an adaption of the hydraulic conductivity is suggested:

$$K_a = K(\frac{a}{C_B})^{m_K} \qquad \text{(equation 7.6)}$$

Where K_a = an adapted hydraulic conductivity (in m/day),

K = the traditional estimation of the hydraulic conductivity (in m/day),

a = the contributing area of the pixel (in m^2),

C_B =a spatially invariant scaling coefficient of the contributing area a (in m^2) and

m_K is a calibrated constant.

The value of a/C_B again varies throughout the catchment in a similar manner to the a/C_Q. The adapted hydraulic conductivity K_a, is normalized, in a manner similar to the adapted hydraulic radius R_a. However, the adapted hydraulic conductivity can be interpreted as the conductance of a pressure wave, which is translated through the saturated zone of the catchment as soon as rainfall enters the saturated soil zone during a rainfall event (Paragraph 2.3).

Equation 7.6 is then substituted in equation 7.2 to estimate the adapted travel times of baseflow down the catchment slopes. Adapted travel times of baseflow are suggested:

$$T = \frac{L}{K_a S} = \frac{L}{KS} * (\frac{C_B}{a})^{m_K} \qquad \text{(equation 7.7)}$$

Where T = the estimated travel times of baseflow (in days),

L = the slope length (in metres),

K = the traditional estimation of the hydraulic conductivity for the groundwater flow, for the research catchments estimated at 1 m/day,

S = the slope of the groundwater gradient,

a = the contributing area to the pixel (expressed in a dimensionless number of pixels),

C_B = a spatially invariant scaling coefficient of the contributing area a (in m^2), and

m_K is a constant exponent to be determined.

The concepts of an adapted hydraulic radius and conductivity are also referred to as a *time lag* in the flow down the catchment slopes by Maidment *et al* (1996) and Muzik (1996). However, this research's estimations of flow times are dependent on the catchment's morphology, and not only on the land use or soil types.

Equations 7.4 and 7.6 have a profound impact on the estimation of the travel times and the form of the simulated response functions. Therefore, the influence of contributing areas on the estimation of travel times and cumulative travel times, was investigated. Figure 7.3 displays a map of the catchment showing the distribution of the inverse of the percentage of contributing areas (100/a). Since the travel times in rivers are proportional to $1/a$, the rivers will show substantially lowered travel times, resulting in quick conductance of water along these channels. On the other hand, the travel times along the slopes and catchment boundaries will be slowed.

Figure 7.3 indicates different sections of each catchment's rivers, where the factor $1/a$ can be interpreted as defining flow types. Those pixel where $1/a < 1$ are classified as channels, which can be classed into different order streams (Figure 7.3). The different classes can be compared to the first, second and third order streams of Strahler (Strahler, 1964). This concept can be used

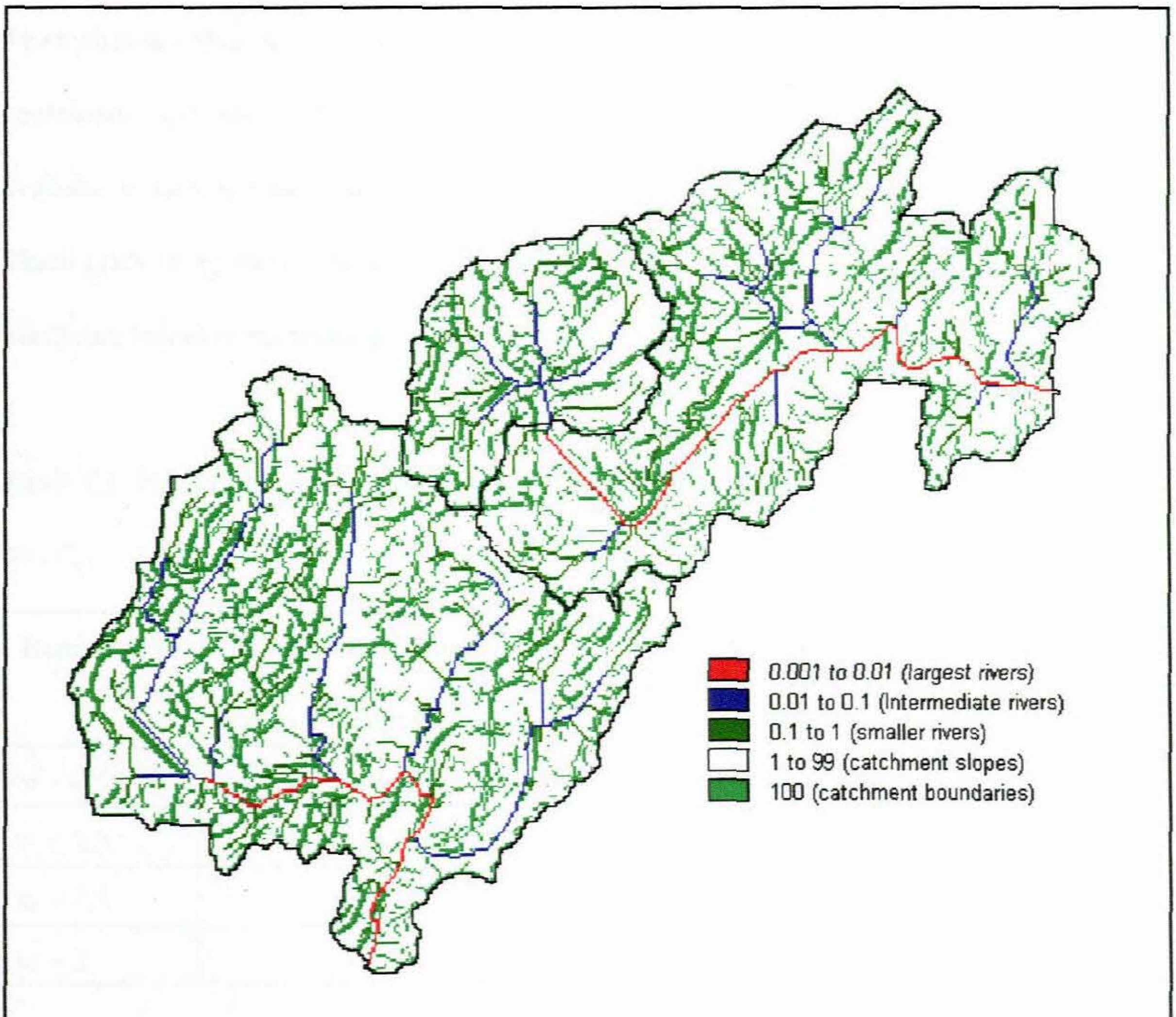

Figure 7.3: A map of the Ntuze research catchments, indicating the inverse of the percentage contributing areas of each pixel, or (one pixel area)*100/a.

to determine the change in the flow patterns from distributed flow to rills, gullies and stream flow, as suggested in Figure 7.2.

7.2.3. The exponent of the adapted hydraulic radius

The exponent m in equation 7.4 and it's effect on both the adapter hydraulic radius R_a and the calculated travel times (equation 7.5) was investigated.

$$R_a = R(\frac{a}{C_Q})^m \qquad \text{(equation 7.4)}$$

The hydraulic radius R for unit flow was set to 0.001 m (1 mm excess rainfall). A GIS raster grid containing each pixel's contributing area (a) was applied to equation 7.4 (using matrix algebra available in GIS software packages), to calculate R_a, for different values of the exponent m. These grids of R_a were compared for different values of m. Table 7.2 lists the minimum and maximum values in the raster grids of R_a for corresponding values of m.

Table 7.2: Values of R_a (in metres) for corresponding values of the exponent m when $R = 1$ mm and $C_Q = 22600$.

Exponent m	Minimum R_a (for $a = 1$) (at catchment boundary)	Maximum R_a (for a at the outlet)	
		W1H016 and W1H031	W1H017
$m = 0.5$	1×10^{-4}	0.013	0.006
$m = 1.0$:	1×10^{-5}	0.17	0.04
$m = 1.5$:	1×10^{-6}	2.24	0.27
$m = 2$:	1×10^{-7}	29.27	1.7

For a given m, the distribution of the values of R_a in the grid varies in an exponential fashion (Figure 7.4). As the number of contributing pixels a increases for a given m, the corresponding frequencies decrease. The frequency distribution of contributing areas (on a log Y axis) was compared to the adapted hydraulic radius R_a (for different values of m) on the second Y axis (Figure 7.4, with the second Y axis as a normal axis, decreasing from the maximum at the bottom to the minimum at the top).

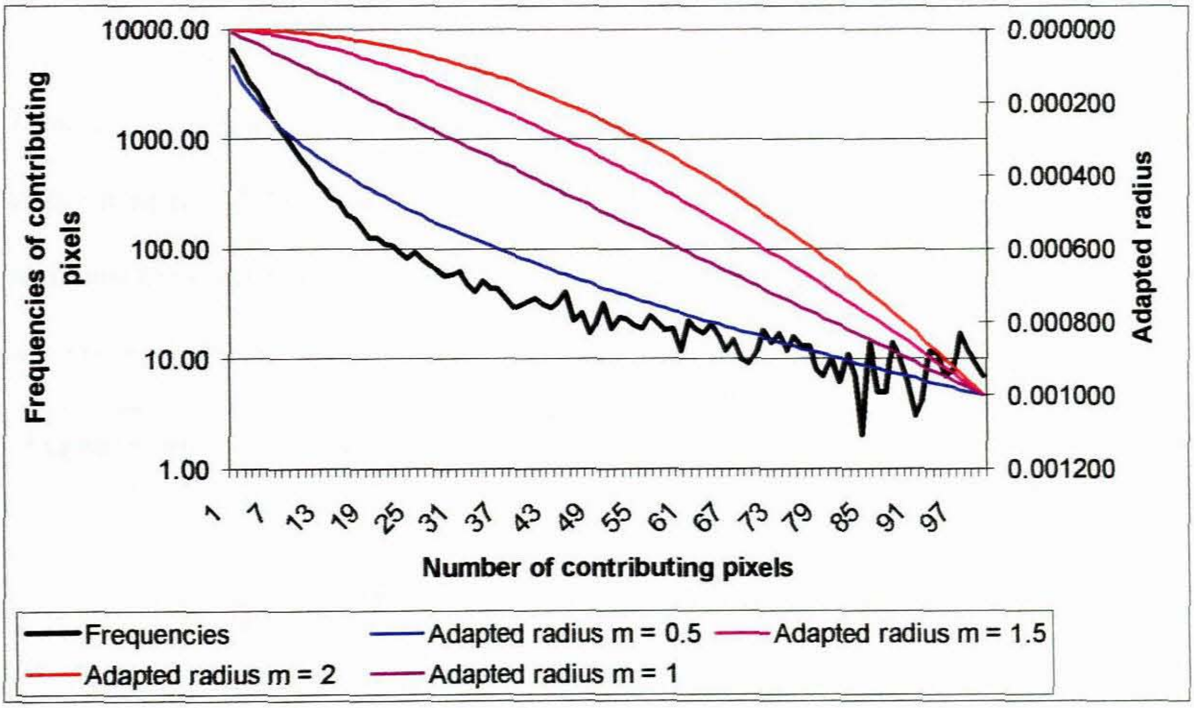

Figure 7.4: Frequencies of contributing area, and the adapted radius, for different values of m for the Ntuze research catchments (plotted for 95% of the catchment area).

Figure 7.4 suggests that the distribution of the adapted radius for $m = 0.5$ is closest to the frequency distribution of contributing areas. However, the influence of a change in the exponent m on the resultant travel times must also be considered. Thus, equation 7.5 (travel times over individual pixels) was evaluated for different values of m.

Table 7.3 indicates the resultant travel times over individual pixels for different values of the exponent m. Maximum travel times over very flat areas can approach infinity. The second column in Table 7.3 lists these calculated maximum travel times. To eliminate the effect of flat areas, maximum travel times of 10 000 seconds (2.7 hours) were assigned to the few pixels which contained very high calculated travel times. Corresponding mean travel times are listed in the third column (Table 7.3). (The *mean* travel time of each grid was calculated in the absence of a module to calculate the *median* travel time of each grid.)

Table 7.3: Travel times (in seconds) over individual pixels along the quickflow pathways, for different values of the exponent m. Mean travel times (third column) were calculated after maximum travel times of 10 000 seconds were assigned to a few pixels estimating a travel time more then 10 000 seconds.

Exponent m	**Maximum travel times calculated**	**Mean travel times over one pixel**
$m = 0.5$:	84700 s	752s = 12.5 min
$m = 1.0$:	515000 s	2327s = 38 min.
$m = 1.5$:	3.1×10^6 s	3847s = 64 min.
$m = 2.0$:	1.9×10^7 s	3950 s = 65.8 min.

The important issue at hand is that the distributions of the travel times change as the exponent m changes (Figure 7.5). Pixels with smaller travel times (faster flowing water) will be associated with pixels along the main channels. If flow rates (or rather travel times) are the delineator of channel flow, then a change in m will bring about a change in classification of channel pixels.

The amount of pixels with a short estimated travel time, should be similar to the amount of river pixels in the catchment. The number of river pixels from Figure 4.4 is 1843 pixels. This number is close to the starting value of the frequency graph in Figure 7.5. Figure 7.5 illustrates that generally larger values of m will result in more pixels with shorter travel times which correspond to channel flow. Figure 7.6 takes a closer look at this phenomena, and indicates the frequency distribution of travel times over of the initial 1.5 minutes, for the different values of exponent m.

Despite the relative short mean travel times estimated using $m = 0.5$ (compare travel times estimated with other values of m, from Table 7.3), closer examination of this travel time grid indicates that there are almost no estimated travel times shorter than 10 seconds (i.e., flow rates of 1 m/s, which is a mean flow rate observed in river channels) (Figure 7.6). Therefore, the case of $m = 0.5$ was not considered an appropriate value.

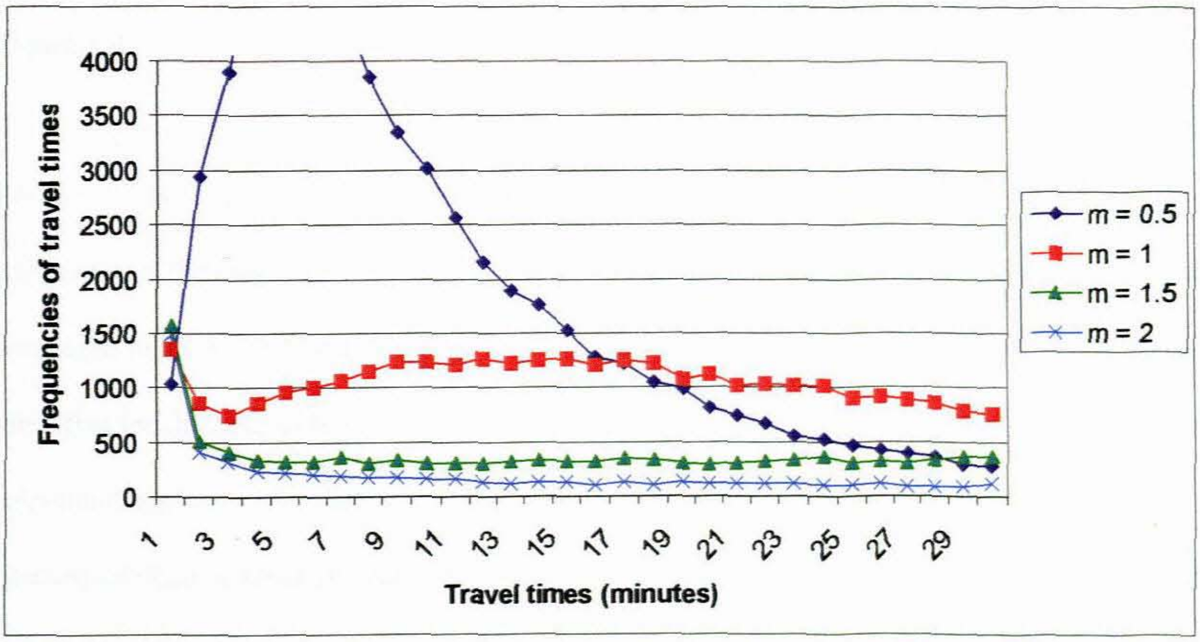

Figure 7.5: Distributions of frequency histograms for the travel times calculated from different values of the exponent m in equation 7.5.

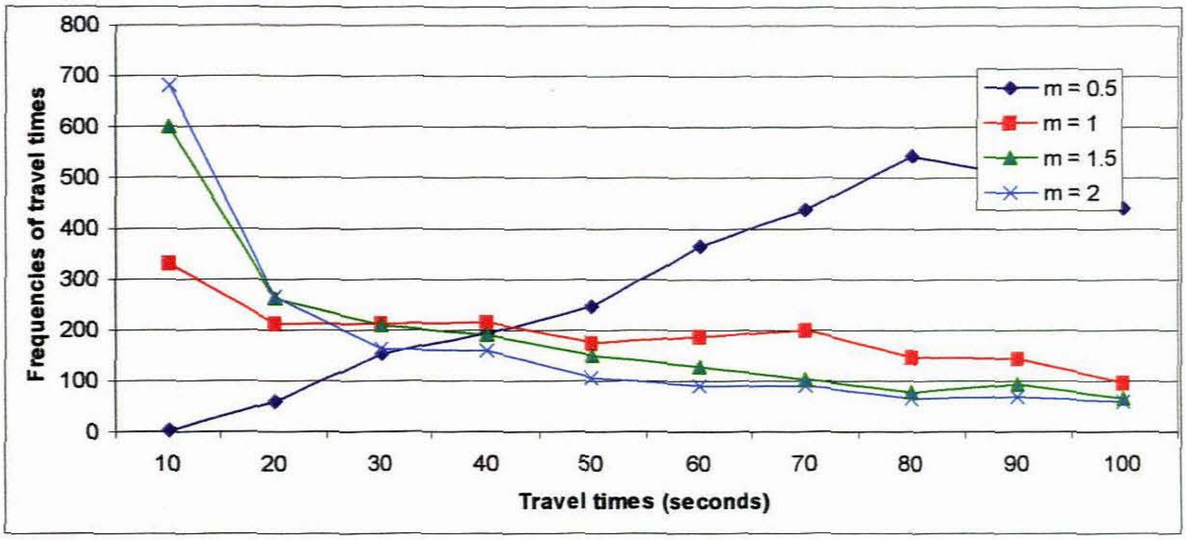

Figure 7.6: Distributions of frequency histograms for the travel times, calculated for the different values of the exponent m in equation 7.5, *within the first 100 seconds.*

The rivers were eliminated from the rest of the catchment using the criteria of pixels with travel velocities of 1 m/s or faster (10 seconds/pixel), for each value of the exponent m. For the case of $m = 0.5$ almost no rivers were indicated, because very few pixels indicated travel times less than 10 seconds. The channel positions, as indicated by travel times of less than 10 seconds, for m = 1 and m = 1.5 are mapped in Figure 7.7. Compare these to the river positions shown in Figure 4.4.

For m = 1, the distribution of travel times frequencies has identified insufficient river channels, compared to the expected distribution. For m = 1.5 there is a similar classification of rivers compared to the 1:5 000 map (Figures 4.4 and 4.2). Although the classification of river channels identified for the case of m = 2 reveals a very similar set of river channels to that of m = 1.5; the calculated depths of the adapted radius R_a for the case of m = 2 (Table 7.2) was not acceptable. Consequently, it is assumed that 1.5 is the most suitable value for m in these catchments using the DEM with a spatial resolution of 10m by 10m.

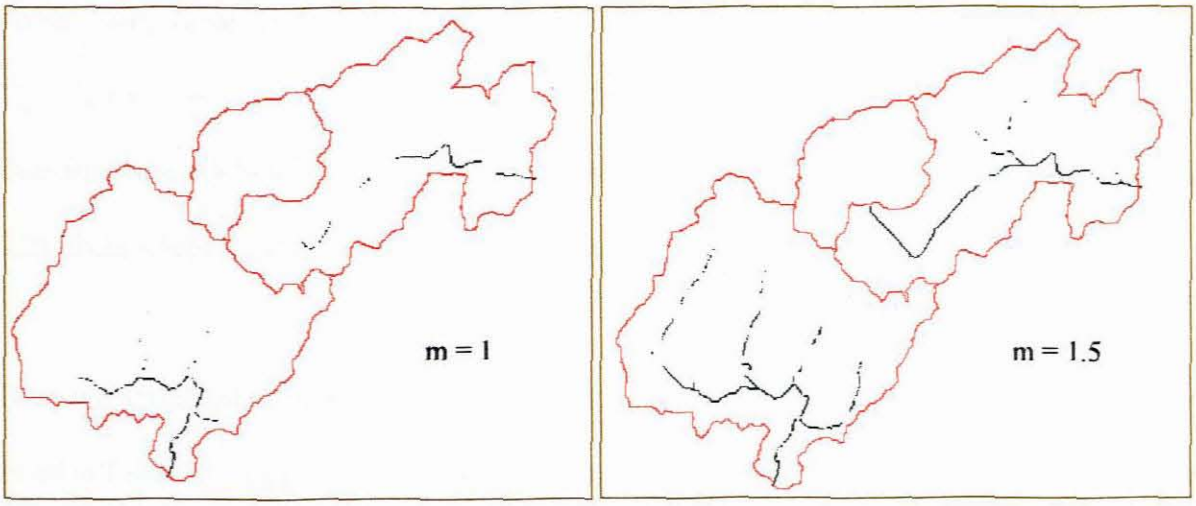

Figure 7.7: River channel pixels as identified by the criteria of travel times < 1 m/s, for the exponent $m = 1$ (left) and $m = 1.5$ (right).

For m = $^3/_2$, equation 7.5 will read as follows:

$$T = \frac{Ln}{R^{2/3}S^{1/2}} * \frac{C_Q}{a}$$

7.2.4. The exponent of the adapted hydraulic conductivity

The adapted hydraulic conductivity in equation 7.6 was examined for the Ntuze River to estimate the exponent m_K:

$$K_a = K(\frac{a}{C_B})^{m_K} \qquad \text{(equation 7.6)}$$

A constant hydraulic conductivity of 1 m/day was used, as well as $C_B = 0.01$. Slopes similar to those of a smoothed catchment surface DEM (in equation 7.7) was assumed, with a mean slope of 0.18. Travel times from the catchment slopes down to the main river channels (Figure 4.2) were calculated, while the travel times for channel flow were derived for the main channels' pixels, using equation 7.5. (The calculations of the channel's travel times assumed $m = {}^3/_2$, $C_Q = 22300$ in the catchment W1H016, $C_Q = 23000$ in the catchment W1H0131 and $R = 0.001$.) This simulates the baseflow from the catchment slopes to the main channels (mapped in Figure 4.2), from where it joins the river flow to the outlet.

Output from the calculation of travel times along the baseflow pathways over individual pixels are listed in Table 7.4. Again, unrealistically high maximum travel times were assigned to some pixels due to flat areas in the baseflow surface. Corresponding mean travel times are listed.

Table 7.4 illustrates that the smaller values of the exponent m_K provide generally longer travel times. The distributions of the different travel times shift as m_K changes. As the exponent m_K increases, more pixels have shorter travel times, with a shorter time lapse to the maximum occurrence of the frequencies.

The histograms of the frequencies for the different travel times over each pixel were plotted for the different values of the exponent m_K in Figure 7.8. For the case of $m_K = 0.5$, there are too many pixels with exaggerated travel time over individual pixels (Figure 7.8). The mode occurs at 30 to 40 hours travel time over one pixel, which is a much longer travel time than observations have suggested (Chapter five). For the cases of $m_K = 2$ and $m_K = 1.5$, there are too many pixels with a very short travel time (Table 7.4). For these values of m_K the mode of the frequencies occur at approximately one minute, which is similar to quickflow conditions. Thus, the cases of $m_K = 0.5$, $m_K = 1.5$ and $m_K = 2$ are questionable.

Table 7.4: Travel times (in minutes) over individual pixels along the baseflow pathways, for different values of the exponent m_K. Mean travel times (third column) were calculated after maximum travel times (second column)were assigned.

Exponent m_K	**Assigned maximum travel time**	**Mean travel times**	**Time of the mode of the frequencies**
$m_K = 0.5$:	41 days	135 hours	30 - 40 hours
$m_K = 1.0$:	83 hours	9 hours	45 - 70 minutes
$m_K = 1.5$:	8 hours	51 minutes	1 minute
$m_K = 2.0$:	3.3 hours	13 minutes	1 minute

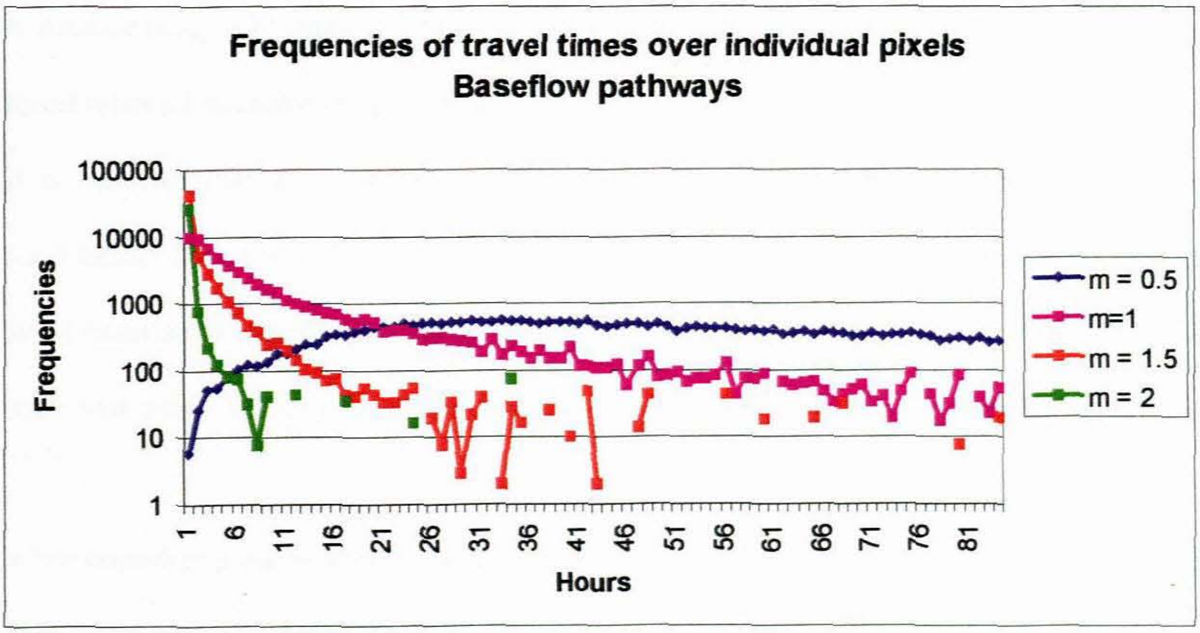

Figure 7.8: Frequencies of the different travel times over individual pixels, along the baseflow pathways, for the Ntuze research catchments.

Included in these frequencies are the travel times of flow along the main channels, which are assumed to have characteristic channel flow times (estimated from Manning's equation). These travel times are less than one hour, and should be detectable as an initial high frequency of travel times within the first hour. However, this phenomenon is only detectable in the case of $m_K = 1$ (Figure 7.9), where there was a large number of pixels with travel times less than one minute (representative of channel flow velocities of maximum 0.1 m/s). Ignoring the initial peak for river channels, brings the mode of travel times, for $m_K = 1$, to one hour (equivalent to a flow velocity of 0.002 m/s).

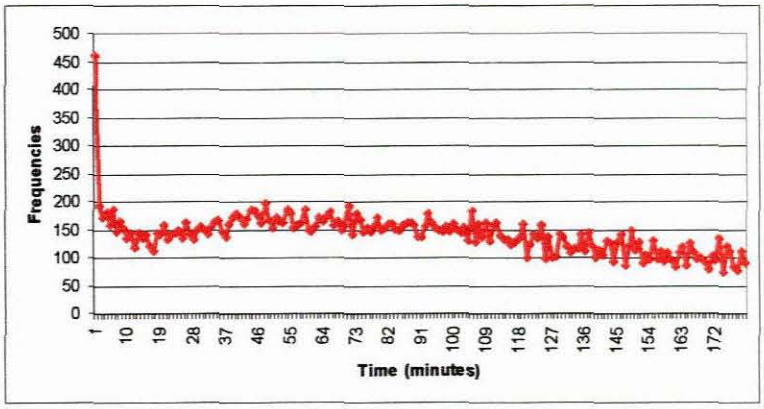

Figure 7.9: Frequencies of the travel times over individual pixels, for $m_K = 1$. The initial peak indicates travel times along the river channels.

In the case of $m_K = 0.5$, the travel times along the main channels are far shorter than the estimated travel times for the baseflow (which are all calculated in hours), and are rounded to zero values. It is expected that the travel times of baseflow through the subsoil structures should be substantially slower than the travel times of water along the main channels. However, there is a lot of uncertainty which surrounds the travel times of baseflow, when considering the pressure wave that causes velocity translation along the baseflow pathways (Beven, 2001).

When considering the time of the mode of frequencies (Table 7.4) it is clear that both the cases of $m_K = 1.5$ and $m_K = 2$ provide baseflow travel times similar to the travel times of channel flow. It can then be concluded that the case of $m_K = 1$ is the better option. The value of $m_K = 1$ was used in the present version of the model for the Ntuze catchments.

7.2.5. Effect of catchment morphology on resistance in throughflow

The calculation of travel times along the throughflow pathways is not clear. Some concepts of the throughflow pathways have been presented. It has been suggested that either the Manning's equation or Darcy's Law can be applied to estimate the travel times, or ideally a weighted combination of the two equations. The morphology of the catchment will also affect the throughflow, as in the case of the sheet flow, channel flow and baseflow. In the cases of the surface flow and the baseflow, the catchment morphology has been used to change the resistance against flow. For surface flow and channel flow, the hydraulic depth was changed. In the case of baseflow, the hydraulic conductivity was adapted according to the morphology of the catchment. For throughflow, a combination is suggested to represent the combined soil and macropore flow (equation 7.3). In the present version of the model it is assumed that no translation of a pressure wave can occur in the unsaturated zone (where throughflow occurs). Thus, the throughflow was simulated in a way similar to the quickflow processes, with appropriate parameter values. Verification of parameters for the throughflow component was complicated due to the absence of field data.

The travel times are related to the flow processes and are scaled by the adapted hydraulic radius R_a (equation 7.4). This equation contains three parameters, i.e., R, a and C_Q. R and a are physically measurable parameters. The travel times of throughflow are somewhat delayed when compared to the quicker flows of overland flow. Therefore, the coefficient C_Q should be replaced with a similar coefficient C_T which should have a similar, but slightly larger value than C_Q. Values for C_T were estimated according to derived throughflow travel times (Tables 5.5 to 5.9), to values between $(2 * C_Q)$ and $(5 * C_Q)$.

7.3. Cumulative travel times over flow pathways

The travel times over individual pixels were integrated along the flow pathways in order to calculate the cumulative travel times along each pathway for each flow component. The travel times from the starting pixel, along the travel pathway, to the outlet, were stored in the starting pixels. The histogram of these cumulative travel times represents the response function of the travel times along the preferential hydrological flow pathways and is considered in the model to represent the storm hydrograph (Refer to Figure 6.2, replacing flow distances with flow times).

7.3.1 The HYDTIME program

The TOPAZ software could only calculate the cumulative *distances* from a pixel to the catchment outlet, and not the cumulative *travel times of water* from a pixel to the catchment outlet. A model called HYDTIME was developed to calculate the cumulative travel times along the flow pathways. The software runs on the BASIC programming compiler. It consists of two different parts: a file rewriting module and the travel time calculation module. Printouts of the codes for the two modules are listed in Appendix A.

Input to the file rewriting module comprises two different IDRISI raster grid files (each rewritten to the ASCII file format). One file contains the travel times of water over individual pixels, and the other contains the flow direction of water from each pixel. The data from these two files is rewritten to a combined binary file (Appendix A1).

The module that calculates cumulative travel times down the catchment slopes, uses the binary file as input (Appendix A2). The movement of water is followed along the flow pathways down the catchment slopes, using the flow directions. The module sums the individual travel times of water over each pixel along each pathway to the catchment outlet, to calculate the cumulative travel times along these pathways. It saves the cumulative travel times from each pixel to the outlet in the originating pixel. The outlet of the catchment needs to be specified in terms of the pixel's row and column. The module outputs an IDRISI raster grid file (in ASCII file format) that contains the cumulative travel times from each pixel to the outlet, for pixels inside the catchment. Pixels outside the catchment are assigned a zero value.

7.3.2. Model limitations

During the development of the model, the Ntuze catchment was used to verify the HYDTIME model. The longest travel pathway was about 4km, which leads to maximum estimated travel times in the order of three to five days, as estimated from observed hydrographs.

HYDTIME program's limitation was discovered during the application of the GIS storm hydrograph model to the larger catchment of the Goedertrouw Dam, which utilizes a 125m by 125m DEM. The core of the problems encountered were due to the use of *integer* values (NOT real values) for travel times over each pixel during the cumulative travel time calculations.

Consider the travel time of water flowing across a river pixel of, say, 125m length to be approximately two to four minutes (for a travel velocity between 1 and 2 m/sec under storm conditions). Thus, the travel times of water over all individual pixels (not only for rivers) would be calculated in minutes. Using hourly time units meant that travel times of two to four minutes (or 0.03 to 0.06 hours) would be rounded to zero travel times over these pixels, since all calculations of cumulative travel times occur in integer values.

On the other hand, the maximum cumulative travel time of baseflow from the top catchment boundaries to the catchment outlet, will be between 20 and 60 days, or 480 to 1140 hours, which is 28800 to 86400 minutes. The HYDTIME program can unfortunately only handle integer values up to 32767 (i.e., 32767 minutes or 22 days).

Attempts to enhance the model by incorporating long integers (utilizing values up to 2,147,483,647), were unsuccessful. It seemed that the BASIC software, which compiles the program, reads random access files that contain integer values, and not those that contain long integers or real values (double precision). Modern programming software needs to be identified for enhanced capabilities and programming techniques to overcome the shortcoming. The author supposes that a similar shortcoming of software programming techniques could possibly be one of the reasons why some raster-based GIS software packages examined do not include capabilities like the calculation of water's travel distance from each pixel to a specified catchment outlet, or the calculation of water's travel times to the catchment outlet (which simply is a weighted travel distance).

This calculation of travel distances (and weighted travel distances equivalent to travel times) of water to the catchment outlet can be done in Arc/Info-Grid, making use of its function called FLOWLENGTH (Olivera and Maidment, 2005). This software runs on a UNIX operating system. However, the author of this thesis did not have access to this software package during the time of this research project.

This shortfall of HYDTIME was partly overcome by using different time units for different travel time scenarios. By changing the time units of individual pixels, cumulative travel times were controlled to fall between one and 32767 time units.

Some of the results indicating response functions of baseflow included cases of zero travel times in river pixels. However, these "zero" travel times in rivers indicate much shorter travel times in river pixels than in catchment pixels, rather than no flow.

7.4. Resultant response functions

The travel time response functions for each catchment were estimated. Although the travel time response functions still consist of frequencies, the estimated total travel times are not influenced by the conversion of flow to frequencies. The frequencies are simply scaled to represent flow rates.

Figures 7.10, 7.11 and 7.12 show the travel time response functions for the catchments of W1H016, W1H017 and W1H031, for the three different flow components. For the catchment of W1H016, the cumulative travel times along the quickflow pathways range from very small values to 105 hours (4.3 days), with a peak at two hours. For the catchment of W1H031, cumulative travel times along the quickflow pathways range over 97 hours (4.1 days). For the catchment of W1H017, the cumulative travel times of quickflow range over 50 hours (just more than two days), with a peak at three hours. These peaks are followed by a typical hydrograph recession curve, for all catchments.

Baseflow travel times were estimated to peak at six hours after the start of the rainfall event (for W1H016), and end about 40 days later. This is similar to the observed data from storms measured in the catchment.

Equation 7.5 was used for quickflow and throughflow (using hypothetical, spatially invariant values for quickflow, C_Q = 22600; for throughflow the assumed value was $C_Q * 2 = 22600 * 2 = 45200$). For baseflow equation 7.7 was used, with $C_B = 0.02$.

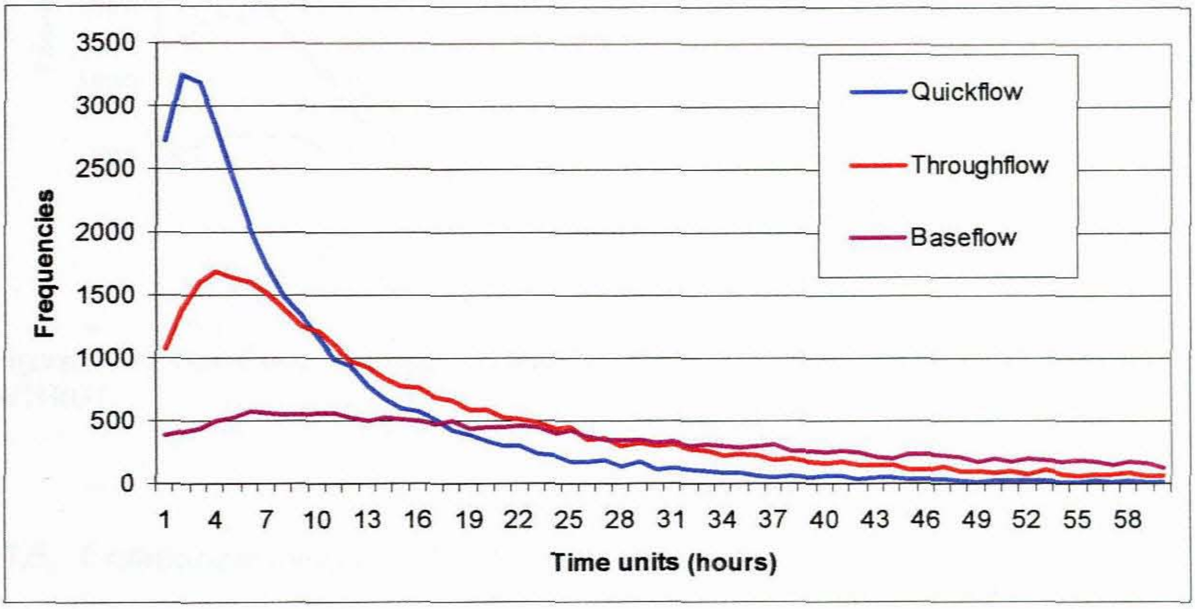

Figure 7.10: Travel time response functions of three flow components in the catchment of W1H016.

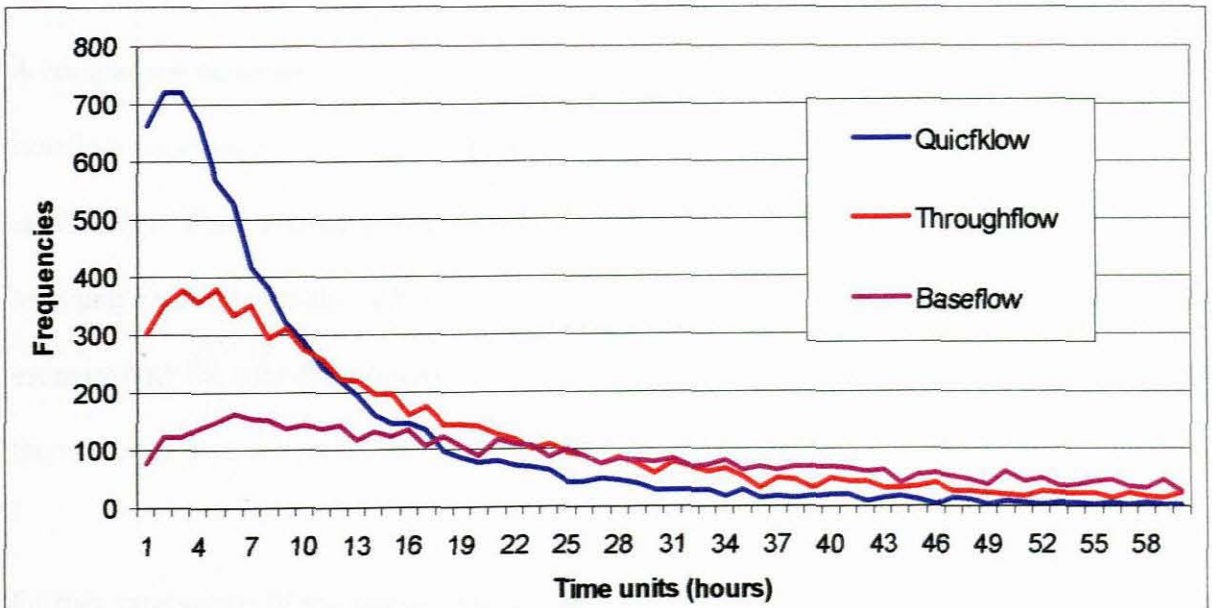

Figure 7.11: Travel time response functions of three flow components in the catchment of W1H017.

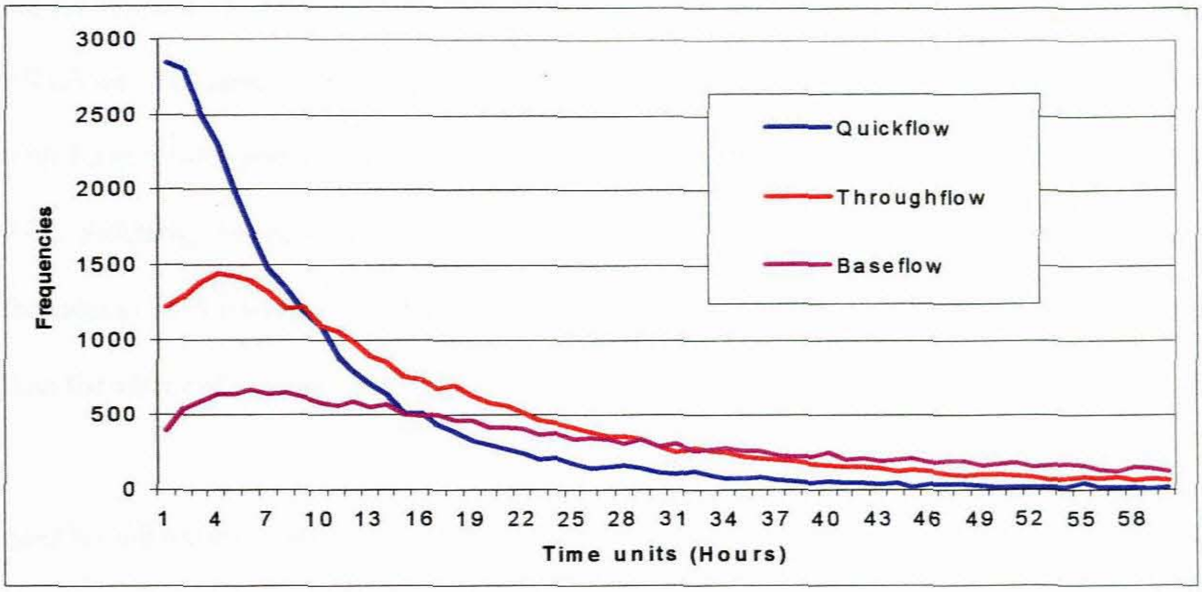

Figure 7.12: Travel time response functions of three flow components in the catchment of W1H031.

7.5. Comparison between Manning's equation and Darcy's equation

This section compares two equations that both estimate travel times of water through different medium, with different conceptual interpretation to flow.

A comparison between equations 7.5 and 7.7, which estimates travel times of overland flow and baseflow respectively, reveals that similar parameters govern both estimations of flow (Maidment *et al*, 1996). If the hydraulic conductivity K in equation 7.7 is equated to the combination of the Manning's n and hydraulic radius R (i.e., $n/R^{2/3}$), it follows that similar equations are utilized to estimate both the quickflow and baseflow of the storm hydrograph. The main difference between the two equations is the exponent of the slopes.

Further exploration of the slopes S (which have a mean of 0.2 and mode of 0.1) and the square root of the slopes ($\sqrt{S}$) (which have a mean of 0.4 and also a mode of 0.4) indicates that the ranges of S and $\sqrt{S}$ are similar. Figure 7.13 illustrates the difference in distributions of the S and $\sqrt{S}$ values. The application of these variables in equations 7.5 and 7.7 respectively, is to multiply with $1/S$ and $1/\sqrt{S}$, respectively. The peak value of $S = 0.1$ will give a value of $1/S = 10$ (Equation 7.7). Similarly, the peak value of $\sqrt{S} = 0.4$ will give a value of $1/\sqrt{S} = 2.5$ (equation 7.5). Thus, the values of $1/S$ in equation 7.7 (which estimates baseflow travel times) tend to be slightly higher than the values of $1/\sqrt{S}$ in equation 7.5 (which estimates overland flow travel times).

Another difference between equations 7.5 and 7.7. lies in the time units. Overland flow (equation 7.5) is estimated in seconds, while baseflow (equation 7.7) is estimated in days. The travel times of the two equations differ with a factor of 60*60*24 = 86400. It was analytically expected that

$$C_Q \frac{Ln}{60 * 60 * S^{1/2} R^{2/3} a} \cong C_B \frac{L * 24}{KSa} \qquad \text{(equation 7.8)}$$

where, if the $C_Q = 1000$, $C_B = 0.01$, and both sets of calculations are converted to units of hours.

These two estimations of travel times were used to derive the response functions from the topographical surface in the catchment of W1H016, i.e. a single set of slopes and slope lengths

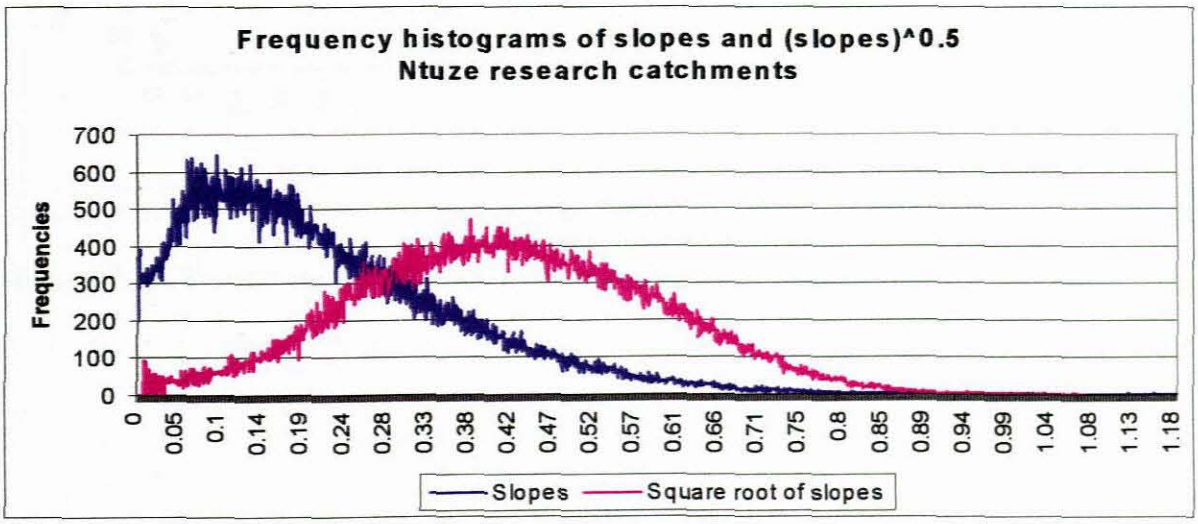

Figure 7.13: The distributions of the frequency histograms of the values of S (slopes) and $\sqrt{S}$.

for both equations. The hydraulic conductivity of the baseflow was set at a spatially invariant value of 1 m/day. Similar contributing areas (a) were utilized for both equations. Travel times were calculated from the catchment boundaries to the outlet for both equations. (This is different to the baseflow estimations in the GIS unit hydrograph model, which estimate baseflow travel times from the catchment boundary to the rivers, and not the outlet.)

Figure 7.14 illustrates the different flow response functions derived from the Manning's equation and Darcy's Law. The Manning's equation estimated more pixels with a shorter cumulative flow time, as illustrated by the relative single peak in the flow response function, occurring quite early in the hydrograph. Longer flow times are estimated with Darcy's Law, as indicated by the multiple lagged peaks in the flow response function from Darcy's equation.

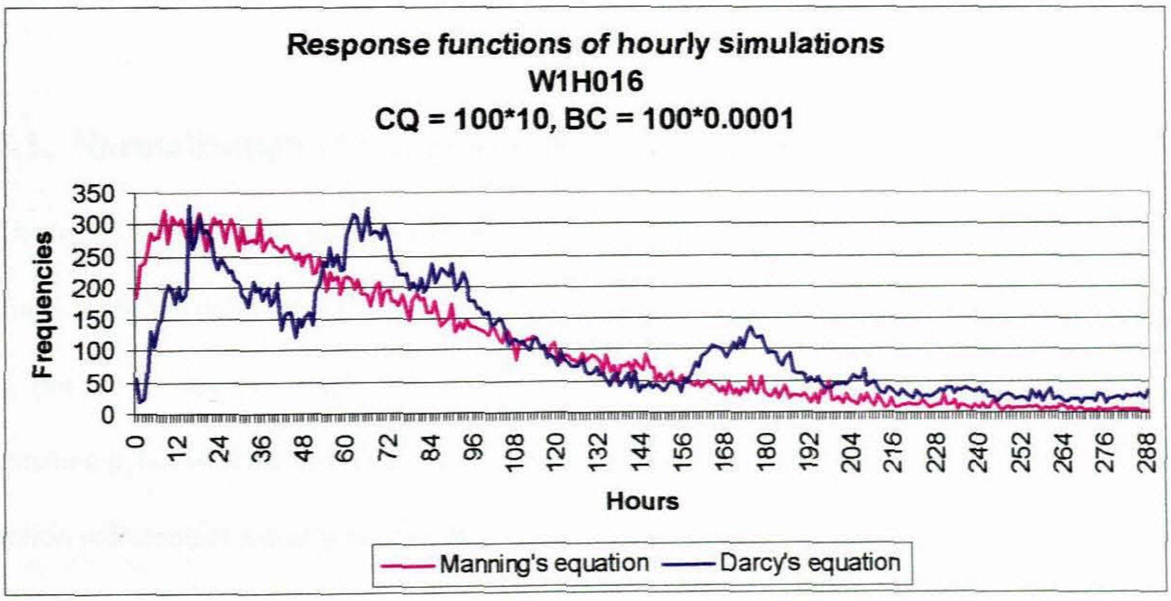

Figure 7.14: Travel time response functions showing the influence of using S and $\sqrt{S}$.

****

8 Calibration of the response functions

In Chapter seven, the travel time response function for each flow component (referred to as the response functions) was derived from spatial information. The convoluted response function, incorporating all three of the flow components' response functions, will be referred to as the *GIS storm hydrograph* (GIS SH). This chapter describes the parameters of the GIS storm hydrograph and the convolution process. The information derived from the hydrograph analysis will be utilized to calibrate the parameters of the response functions, for the different flow components, under the various rain storm types.

8.1. Normalization of frequencies for pixel resolution and catchment size

The travel time response functions are derived from the frequency histograms of cumulative travel times along the different pathways. These frequencies depend on the number of pixels present in the DEM. Say a DEM, with unit pixel resolution, is replaced with a DEM for the same catchment, but with half the pixel resolution (every four pixels are combined into one pixel). This action will result in a doubling of pixel dimensions, and a reduction of the total frequencies in the travel time response function, by a factor of four. The general relationship between a change in pixel resolution and the change in frequencies is listed in Table 8.1. This table indicates that the area of one pixel in a DEM is directly related to the number of pixels covering the catchment.

The units of the frequencies in the response functions are a number per time unit. Multiplying the frequencies in the travel time response functions by the area of one pixel, changes the response functions' units to area per time unit (e.g., m^2/hour). Multiply the (area/time unit) by the amount of excess rainfall (in metres), converts the response functions' units to volume per time unit, which is the discharge of the catchment per time unit (m^3/hour). These steps ensure that the area under the adapted time response function is equal to the amount of water that runs off the catchment along the response function's pathways.

8.2. The runoff coefficient

The *runoff coefficient* of the model is the fraction of the measured rain that causes the runoff in the river after a rain storm. The total volume of water (m^3) that should be flowing through the river outlet from a rainfall event is given by:

$$A * (Excess\ Rain) \qquad \text{(Equation 8.2)}$$

or

$$A * R_{measured} * C \text{ (in m}^3\text{)} \qquad \text{(Equation 8.3)}$$

where A = catchment area (m^2),

$R_{measured}$ = measured rainfall (in metres),

C = the runoff coefficient, $0 \leq C \leq 1$.

Excess rainfall is that proportion of rainfall that causes the observed storm hydrograph that follows the rainfall event. Therefore,

$$R_{excess} = C * R_{measured} \qquad \text{(Equation 8.4)}$$

where R_{excess} is the excess rainfall of the storm event (in metres). Consequently, the (dimensionless) runoff coefficient is given as

$$C = \frac{R_{excess}}{R_{measured}} \qquad \text{(Equation 8.5)}$$

Substitution of equation 8.5 in equation 8.3 indicates that only the excess rainfall is necessary to calculate the volume of rainfall that causes the storm hydrograph. However, estimations of excess rainfall can be difficult, and of unsure accuracy. Some methods of excess rainfall estimation are discussed by Beven (2001). The runoff coefficient in this model is a parameter that needs to be calibrated. The individual values of the time response functions are multiplied by the runoff coefficient.

The runoff coefficient has been described as a parameter changing over time (Paragraph 3.2 and Figure 3.2). In this model, it is assumed that the runoff coefficient stays constant over time. The processes that influence the values of the runoff coefficient have been discussed previously (Paragraphs 2.4 and 3.2).

8.3. Partitioning coefficients

The measured rainfall is partitioned according to the different processes (infiltration and percolation), into the different flow components (quickflow, throughflow and baseflow) as shown in Figure 3.3. The percentage of the total flow in the storm hydrograph that belongs to each flow component, for different storm types, has been estimated and listed in Table 5.10.

The excess rainfall is partitioned amongst the individual flow components, for storm type i, as follows:

$$p_i = p_{(quickflow)i} + p_{(throughflow)i} + p_{(baseflow)i} \qquad \text{(Equation 8.6)}$$

where $p_i = 1$, and

$p_{(quickflow)i}$, $p_{(throughflow)i}$ and $p_{(baseflow)i}$ are *partitioning coefficients*, that partition the excess rainfall to quickflow, throughflow and baseflow, respectively, for storm type i (Figure 8.1), and

$0 \leq p_{(quickflow)i} \leq 1$, $0 \leq p_{(throughflow)i} \leq 1$ and $0 \leq p_{(baseflow)i} \leq 1$.

Figure 8.1 indicates how the measured rain from storm type i is divided into evaporation/evapotranspiration, deep groundwater percolation and excess rainfall, which causes the observed outflow from the catchment. The runoff coefficient (C) determines the fraction of

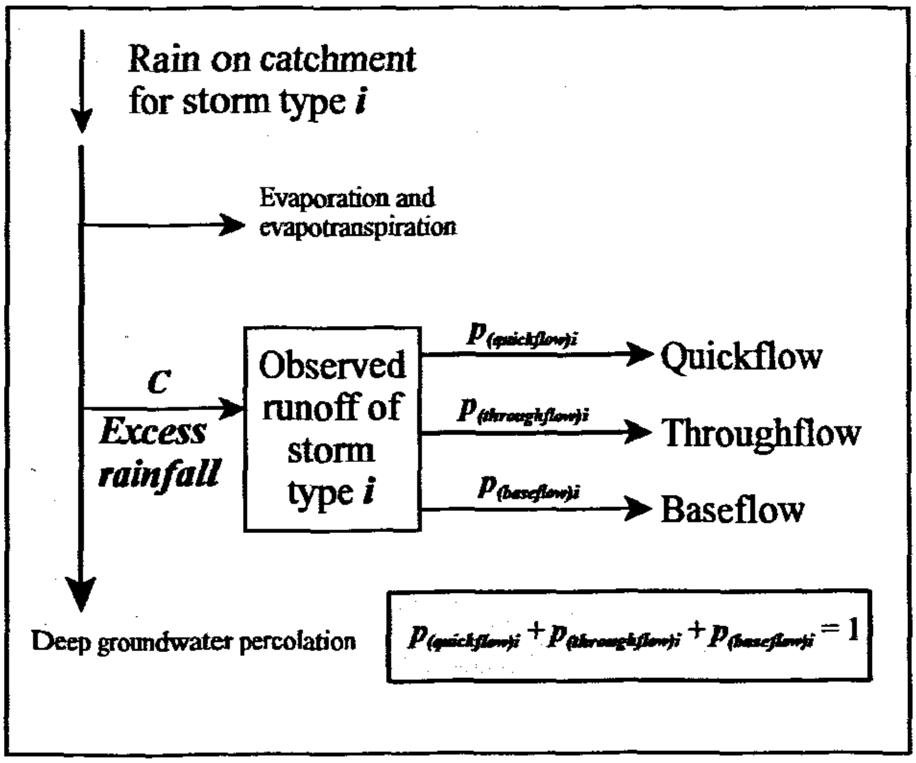

Figure 8.1: The graphical representation of the partitioning coefficients $p_{(quickflow)i}$, $p_{(throughflow)i}$ and $p_{(baseflow)i}$ from rain storm type i.

excess rainfall that is divided among the different flow components, according to the values of the partitioning coefficients.

The individual values of the time response functions are multiplied by the partitioning coefficients, and scaled by the runoff coefficient C. For storm type i, the runoff coefficient for each flow component (C_{qi} for quickflow, C_{ti} for throughflow and C_{bi} for baseflow) is related to the fraction of flow partitioned to the flow component, as well as the fraction of excess rainfall in the simulated storm type's hydrograph:

$C_{qi} = Cp_{(quickflow)i}$; $C_{ti} = Cp_{(throughflow)i}$ and $C_{bi} = Cp_{(baseflow)i}$ (Equation 8.7)

Note that the runoff coefficient C does not necessarily change only with the storm type i. Its variation depends on other processes and conditions, such as the antecedent moisture conditions of the catchment.

The values of the partitioning coefficients were established from analysis of observed storm hydrographs, for each research catchment and for every storm type (Table 5.10).

8.4. The time scaling coefficients

Different processes influence the travel times of water flowing through/over a catchment to the outlet. The more dominant processes will influence the observed hydrograph more strongly. For example, the hydrograph for an event of long duration and low intensity rainfall will be much flatter than the hydrograph of a storm event of short duration and high intensity. Similarly, the difference between the storm hydrograph of the quickflow component and the storm hydrograph of the baseflow component, lies mainly in the processes that cause flow to be concentrated along slower or quicker pathways down the catchment slopes.

The different processes dominating the travel times can be detected in the different recession curves of the runoff hydrographs for small catchments: A steep recession curve in the case of quicker travel times, and a flat recession curve in the case of slower travel times. Thus, to apply the storm hydrograph as a model to simulate different flow components, for different storm types, the recession curve of the simulated storm hydrograph needs to be calibrated to fit the recession curve of the observed hydrograph. This is accomplished in the model by partitioning the flow through slower or faster pathways, depending on each storm type.

Most of the processes that cause the difference in travel times, have been included in the model by varying the flow times along different process pathways. Interaction between the different flow components has not been included in this version of the model.

During the separation of the flow components in the observed storm flow data (Paragraph 5.5), the travel times of each flow component from beginning to end was estimated. This gave an indication of the time span for water to flow from the catchment headwaters to the catchment outlet for each flow component. During the analysis of the observed hydrographs, it was assumed that the TTP of throughflow was twice the TTP of quickflow, and the TTP for baseflow was three times the TTP of throughflow (Paragraph 5.3).

The recession rates of the unit travel time response functions, for each flow component and each storm type, will be compared to the recession rates which were estimated during the hydrograph analysis. These two sets of recession rates were based on two independent estimation methods, each having different assumptions and mathematical calculations. Time scaling coefficients, which can alter the travel times of water flowing along either of the flow pathways in a linear fashion, were incorporated in the model.

The time scaling coefficients' main function is to incorporate processes not currently included in the model. E.g., the function of these coefficients can be equated to a change in the hydraulic slope lengths L, a parameter that is found in both Manning's equation (equation 7.5) and Darcy's Law (equation 7.7). The GIS storm hydrograph model assumes that the exact path length travelled by a drop of water down the catchment slopes, is estimated by the pixel dimensions. However, the exact lengths of path lines are unknown, especially for throughflow and baseflow pathlines.

A time scaling coefficient for each flow component was introduced: T_{SQ} for the quickflow component; T_{ST} for the throughflow component and T_{SB} for the baseflow component. The time scaling coefficients are multiplied by the estimated travel times along the individual pathways. Thus, equation 7.5 is multiplied by T_{SQ} and equation 7.7 is multiplied by T_{ST}.

It is acknowledged that the processes influencing the travel times of water along the quickflow and throughflow pathways, differ. However, travel times along both pathways are estimated in the model by the same equation, i.e., Manning's adapted equation. Due to the uncertainty that surrounds flow along the throughflow component, values for the parameters L, and S were given the same values as the quickflow pathways parameters, to estimate travel times along the throughflow pathways. The differences between travel times along the quickflow and throughflow pathways are simulated in the model by assuming different n and R_a values from the two components.

The different processes dominating the travel times can be detected in the different recession curves of the runoff hydrographs for small catchments: A steep recession curve in the case of quicker travel times, and a flat recession curve in the case of slower travel times. Thus, to apply the storm hydrograph as a model to simulate different flow components, for different storm types, the recession curve of the simulated storm hydrograph needs to be calibrated to fit the recession curve of the observed hydrograph. This is accomplished in the model by partitioning the flow through slower or faster pathways, depending on each storm type.

Most of the processes that cause the difference in travel times, have been included in the model by varying the flow times along different process pathways. Interaction between the different flow components has not been included in this version of the model.

During the separation of the flow components in the observed storm flow data (Paragraph 5.5), the travel times of each flow component from beginning to end was estimated. This gave an indication of the time span for water to flow from the catchment headwaters to the catchment outlet for each flow component. During the analysis of the observed hydrographs, it was assumed that the TTP of throughflow was twice the TTP of quickflow, and the TTP for baseflow was three times the TTP of throughflow (Paragraph 5.3).

The recession rates of the unit travel time response functions, for each flow component and each storm type, will be compared to the recession rates which were estimated during the hydrograph analysis. These two sets of recession rates were based on two independent estimation methods, each having different assumptions and mathematical calculations. Time scaling coefficients, which can alter the travel times of water flowing along either of the flow pathways in a linear fashion, were incorporated in the model.

The time scaling coefficients' main function is to incorporate processes not currently included in the model. E.g., the function of these coefficients can be equated to a change in the hydraulic slope lengths L, a parameter that is found in both Manning's equation (equation 7.5) and Darcy's Law (equation 7.7). The GIS storm hydrograph model assumes that the exact path length travelled by a drop of water down the catchment slopes, is estimated by the pixel dimensions. However, the exact lengths of path lines are unknown, especially for throughflow and baseflow pathlines.

A time scaling coefficient for each flow component was introduced: T_{SQ} for the quickflow component; T_{ST} for the throughflow component and T_{SB} for the baseflow component. The time scaling coefficients are multiplied by the estimated travel times along the individual pathways. Thus, equation 7.5 is multiplied by T_{SQ} and equation 7.7 is multiplied by T_{ST}.

It is acknowledged that the processes influencing the travel times of water along the quickflow and throughflow pathways, differ. However, travel times along both pathways are estimated in the model by the same equation, i.e., Manning's adapted equation. Due to the uncertainty that surrounds flow along the throughflow component, values for the parameters L, and S were given the same values as the quickflow pathways parameters, to estimate travel times along the throughflow pathways. The differences between travel times along the quickflow and throughflow pathways are simulated in the model by assuming different n and R_a values from the two components.

8.5. Relationship between the recession rates and the time scaling coefficients

An analysis was performed to examine the relationship between the recession rates of the simulated response functions and the time scaling coefficients. Different time scaling coefficients, ranging between 0.1 and 10, were applied to the travel times of flow across the individual pixels. Corresponding response functions were calculated. These response functions are plotted for the catchment of W1H016 in Figure 8.2, which shows the range of recession curves associated with each scaling factor.

The frequencies of the simulated response functions were examined for different coefficients by scaling the peak values to a uniform value (Figure 8.2).

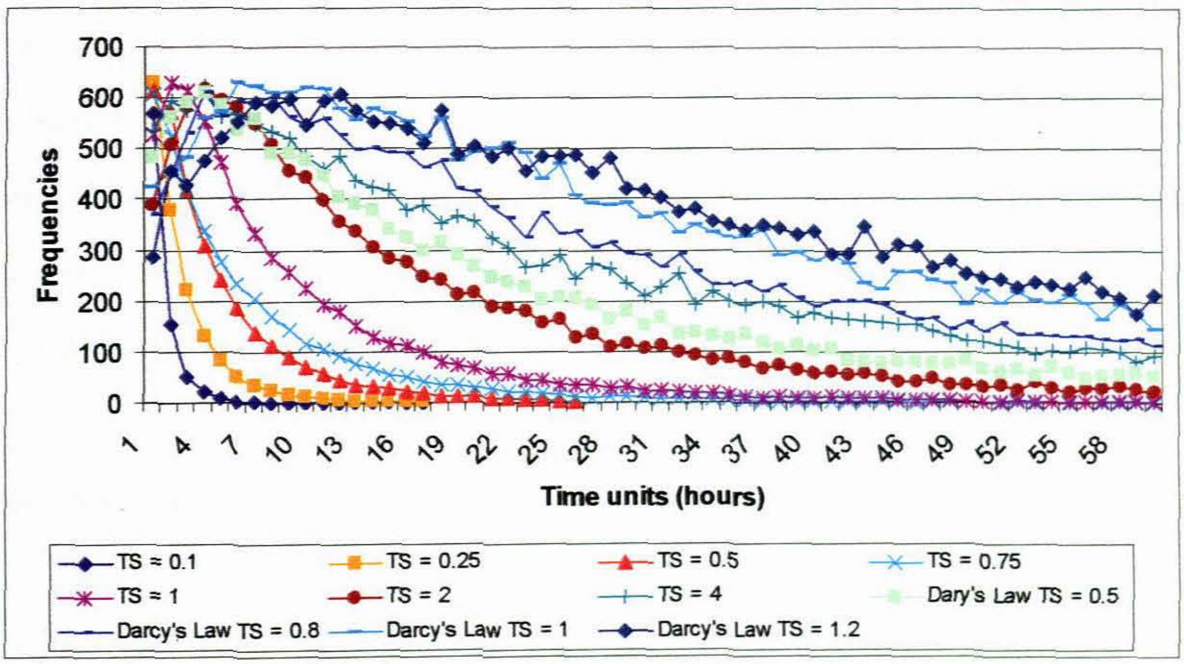

Figure 8.2: Different response functions from the catchment of W1H016, for different time scaling coefficients (TS) used in the Manning's equations and in Darcy's Law.

In evaluating the relationship between the time scaling coefficients and the recession rates, it was discovered that the three catchments indicate very similar values for the T_{SQ} and T_{ST}, as listed in Table 8.2. The (adjusted) recession rates in Table 8.2 were compared to the observed values (Table 5.11) to select the most appropriate time scaling coefficient for the different storm types.

Table 8.2: Time scaling coefficients of quickflow and throughflow for the three Ntuze River catchments, with the associated recession rates.

T_{SQ} and T_{ST} (Quickflow and throughflow)	W1H016	W1H017	W1H031
	Recession rates associated with the hydrographs		
0.1	0.39	0.31	0.37
0.25	0.62	0.66	0.69
0.5	0.81	0.82	0.85
0.75	0.89	0.85	0.89
1	0.91	0.93	0.91
2	0.96	0.95	0.97
3	0.97	0.97	0.98

For the baseflow, a similar comparison was made between the estimated recession rates (listed in Table 5.11) and the simulated values listed in Table 8.3. The mathematical relationship between the time scaling coefficients and the listed recession constants (Table 8.2) was established (using regression analysis) in order to calculate the time scaling coefficient for a given recession rate (detailed in Appendix B).

Table 8.3: Time scaling coefficients of baseflow for the three Ntuze River catchments, with the associated recession rates.

T_{SB} (Baseflow)	W1H016	W1H017	W1H031
	Recession rates associated with the hydrographs		
0.5	0.96	0.95	0.94
0.8	0.98	0.97	0.97
1	0.99	0.98	0.98
1.2	0.99	0.99	0.99

8.6. Flow component calibration

During the hydrograph analysis, the flow time of each flow component was estimated. This gave an indication of the time span for water to flow from the catchment headwaters to the catchment outlet along each flow path.

Making use of the recession rates calculated from observed hydrographs for the different flow components (Table 5.11), the time scaling coefficients for each flow component were calculated by the mathematical relationship between the recession rates and time scaling coefficients (Appendix B).

8.7. Results of the calibration

Four observed storms were chosen from each catchment (W1H016, W1H017 and W1H031) for each of the four different storm types, as listed in Table 5.1, to assist in the calibration process.

8.7.1. Derived values for the time scaling coefficient

Values for the time scaling coefficients were read from the Tables 8.2 and 8.3, by using the recession rates from Table 5.1, for the different storm types. Table 8.4 lists the recession rates with the corresponding time scaling coefficients, for each catchment and storm type.

The time response functions of the three different flow components, as well as the total flow, simulated with the parameter values in Table 8.4, are shown in Figures 8.3, 8.4 and 8.5 for the three different research catchments. These graphs represent the simulated unit storm hydrographs, which is equivalent to the catchment's response to 1 mm of excess rainfall.

Table 8.4: Recession rates (Rec K) for different time scaling coefficients (T_S) in Manning's equation and Darcy's Law. The initially assumed time scaling coefficient is listed, with the recession rates (rec K) for each storm scenario, as well as the corresponding T_S read from Tables 8.2 and 8.3.

Catchment: flow component	Assumed time scaling coefficient	High intensity, short duration		High intensity, long duration		Low intensity, short duration		Low intensity, long duration	
		Rec K	T_S	Rec K	T_S	Rec K:	T_S	Rec K	T_S
W1H016: Quickflow	**1**	*0.55*	**0.25**	*0.66*	**0.25**				
W1H016: Throughflow	**2**	*0.82*	**1**	*0.81*	**0.75**	*0.8*	**0.5**	*0.79*	**0.5**
W1H016: Baseflow	**(3)**	*0.98*	**0.8**	*0.98*	**0.8**	*0.98*	**0.8**	*0.99*	**1**
W1H017: Quickflow	**1**	*0.35*	**0.1**	*0.59*	**0.25**				
W1H017: Throughflow	**2**	*0.73*	**0.5**	*0.86*	**0.75**	*0.71*	**0.25**	*0.77*	**0.5**
W1H017: Baseflow	**(3)**	*0.97*	**0.8**	*0.99*	**1.2**	*0.98*	**1**	*0.99*	**1.2**
W1H031: Quickflow	**1**	*0.64*	**0.25**	*0.73*	**0.5**				
W1H031: Throughflow	**2**	*0.85*	**0.75**	*0.92*	**2**	*0.78*	**0.5**	*0.82*	**0.75**
W1H031: Baseflow	**(3)**	*0.99*	**1.2**	*0.99*	**1.2**	*0.99*	**1.2**	*0.98*	**1**

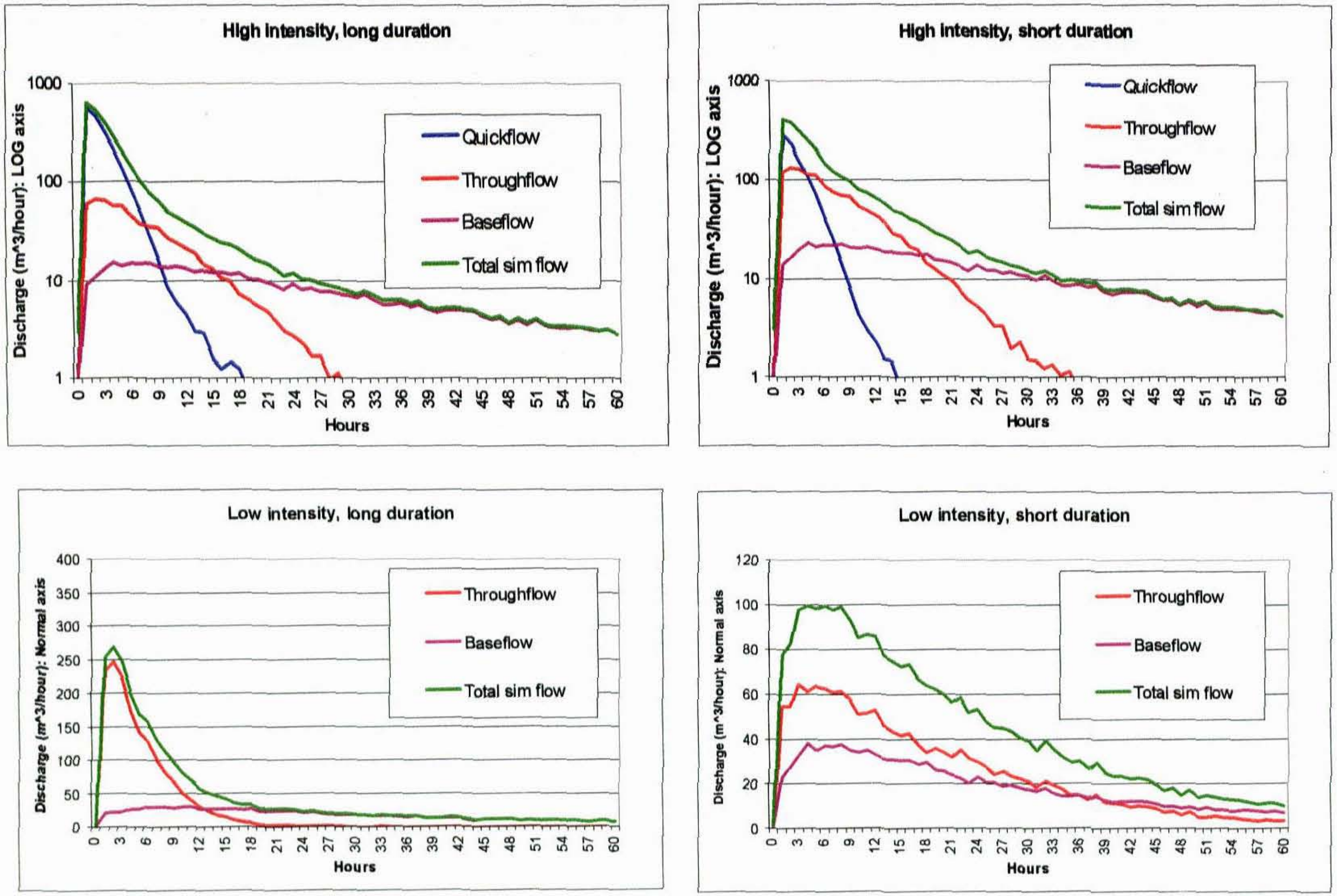

Figure 8.3: Response functions simulated for the different rainfall types, in the catchment of W1H016.

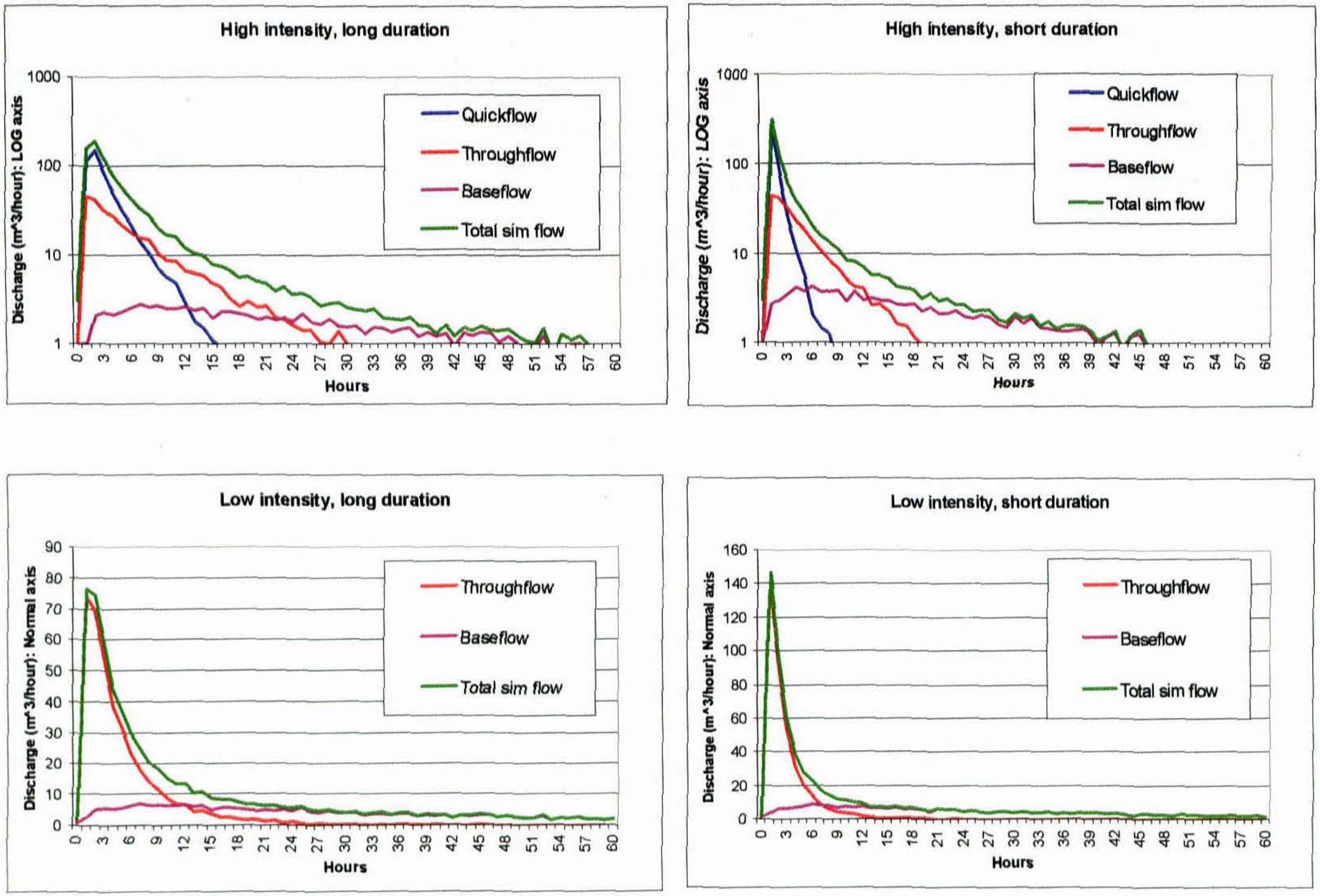

Figure 8.4: Response functions simulated for the different rainfall types, in the catchment of W1H017.

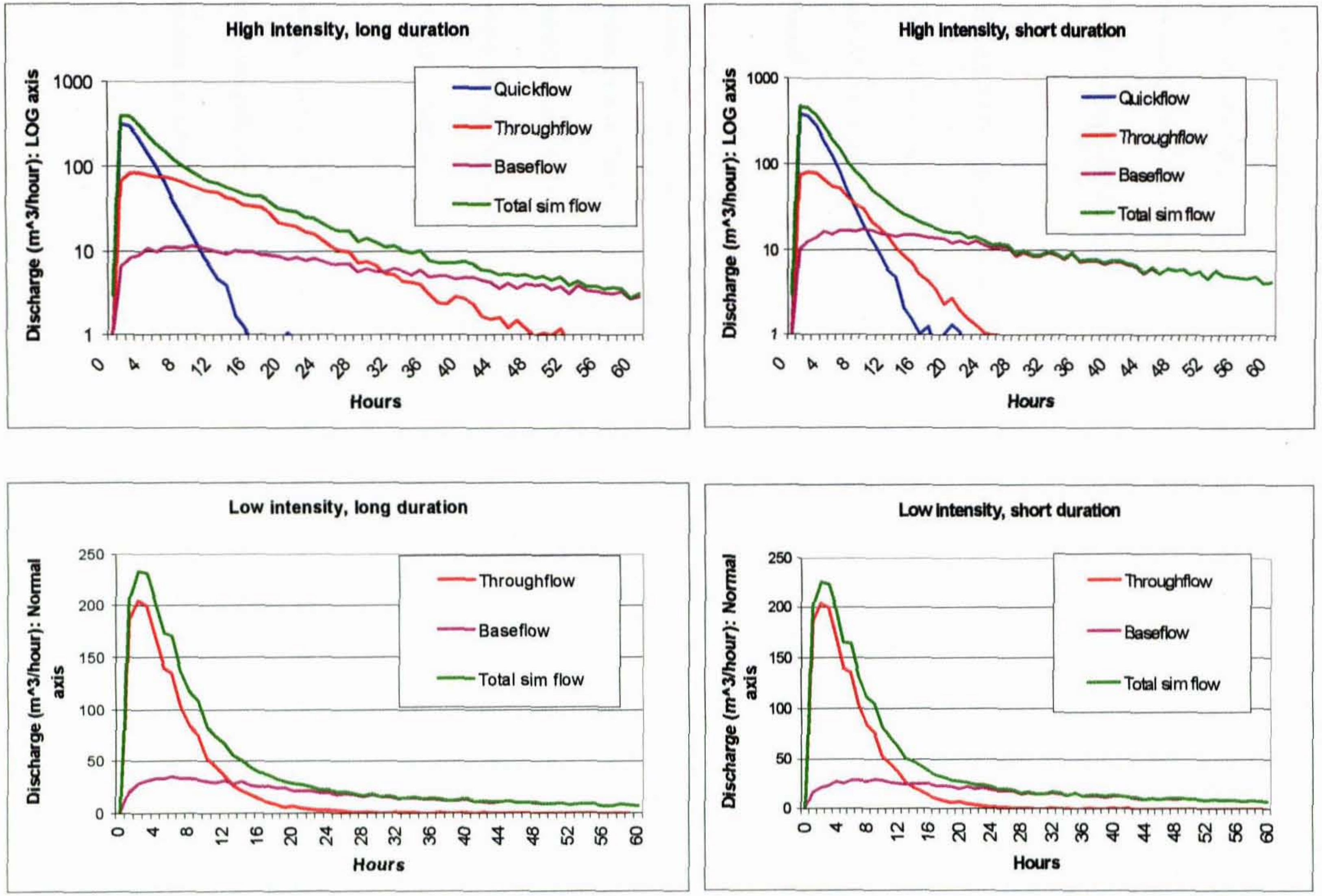

Figure 8.5: Response functions simulated for the different rainfall types, in the catchment of W1H031.

8.7.2. Derived values for the runoff coefficient

To scale the simulated unit storm hydrographs (Figures 8.3 to 8.5) to the actual runoff hydrograph, the values of the time response functions are multiplied by the runoff coefficient, as well as the measured rainfall and the partitioning coefficients (equation 8.4). The runoff coefficient is assumed to be constant for the duration of a storm event.

Table 5.14 lists the percentage excess rainfall from observed storms from each catchment. The mean fraction of excess rainfall of all analysed storms listed in this table is 0.15 (or 15%). The listed mean percentage excess rainfall (Table 5.14) of each catchment were the assumed (constant) values of the runoff coefficients used during the simulation for each individual storm.

It has been indicated that the changes in the runoff coefficient causes a change in the volumetric simulation of the storm hydrograph. The GIS storm hydrograph model (which applies a constant runoff coefficient throughout each storm event) assumes that the peak observed flow of the storm event will be the optimal point in the storm hydrograph to calibrate the runoff coefficient, if observed runoff is available.

Values for the runoff coefficients were adjusted until the peak of the simulated storm hydrograph was in close proximity to the observed storm hydrograph. Table 8.5 lists the model values for the calibrated runoff coefficients.

Table 8.5: Calibrated values for the runoff coefficients, for each storm's information.

Storm date	Rainfall type	Rainfall	Storm rain duration	Max Measured Rainfall intensity	Excess rainfall	Pre-storm Observed runoff	Peak Runoffs:		Runoff Coefficient	Ratio: (Excess Rain)/ (Measured Rain)
							Observed	GIS storm hydrograph		
		mm	hours	mm/hour	mm	m^3/hour	m^3/hour	m^3/hour		
Weir W1H016										
15 Dec 1989	Long duration, High intensity	50	10	17	10.6	175	4592	2655	0.215	0.21
27 Dec 1995	Short duration, High intensity	30.4	1	30	8.2	365	3003	3003	0.206	0.27
24 Jan 1990	Long duration, Low intensity	47.4	13	12	5.3	45	883	885	0.1	0.11
6 Apr 1990	Short duration, Low intensity	18.4	2	15	2.5	140	629	629	0.13	0.14
Weir W1H017										
13 Oct 1994	Long duration, High intensity	61	19	21	8	17	522	535	0.1	0.13
1 Mar 1995	Short duration, High intensity	85	4	36	4.6	0.5	1036	1057	0.065	0.05
29 Oct 1994	Long duration, Low intensity	21	11	3.2	2.6	27	149	149	0.14	0.13
4 Dec 1993	Short duration, Low intensity	44	6	11	4.9	8	462	476	0.125	0.11
Weir W1H031										
4 Dec 1993	Long duration, High intensity	49	8	13	8.7	48	1660	1689	0.145	0.18
10 Jan 1994	Short duration, High intensity	64	3	52	14.5	89	3682	3703	0.103	0.145
26 Apr 1990	Long duration, Low intensity	33	9	4.6	4.2	41	886	903	0.17	0.12
21 Jan 1991	Short duration, Low intensity	13	4	8.2	1.4	188	463	465	0.1	0.11

Excess rainfall was calculated using the total observed runoff and rainfall for each event. Note that the calculated ratio of the (Excess rainfall)/(Measured rainfall) is in close proximity to the runoff coefficient, where the runoff coefficient was calibrated using only one point on the observed hydrograph, i.e., the observed peak runoff. This indicates that, if the runoff coefficient is calibrated by the peak observed runoff, the largest part (though not all) of it is explained by the ratio of (Excess rainfall)/(Measured rainfall).

The part of the runoff coefficient not explained by this ratio bas been attributed to a possible change in the runoff coefficient during the course of the storm flow, explained by Gottschalk and Weingartner (1998) and Hebson and Wood (1982). It can also be attributed to the uneven distribution of rainfall through the catchment (Beven, 2001). Even through the research catchments are very small in size (±3km^2), spatial rainfall variations can occur which can cause biassed catchment rainfall estimations.

The observed rain storms of long durations are frequently composed of different rainfall events, separated by one or two hours with negligible rain (less than 1 mm in the hour). The different sections of those special rain events were allowed to have different runoff coefficients, bringing about a changing runoff coefficient during the course of the storm. This allowed more accurate simulation of the total storm hydrograph. The runoff coefficients of each storm event, in Table 8.5, are the means of these different runoff coefficients.

Changing the runoff coefficient C will have NO effect on the recession rates of the hydrograph, while applying different time scaling coefficients have a direct effect on the recession curve of the resulting storm hydrograph (Figure 8.2). The coefficients C and T_S (when kept constant for the duration of a storm) function independently of each other, influencing two different dimensions of the storm hydrograph: The runoff coefficient influences the *volume* of water that flows along the flow pathways, and the time scaling coefficients influence the *flow times* along the flow pathways, where the resistance against flow plays a role.

8.7.3. Simulated times to peak

Simulated storm hydrographs are shown in Figure 8.6 (catchment of W1H016), Figure 8.7 (catchment of W1H017) and Figure 8.8 (catchment of W1H031) for four different rain storm types. In some of the simulations there is a definite translation error in the time to peak (TTP). Note especially Figure 8.6 for the rainfall type of low intensity and short duration, and Figure 8.8, the rain type of low intensity and short duration, where there is a large discrepancy in the storm hydrograph between the simulated TTP and the observed TTP. This suggests that too much of the flow has been partitioned as throughflow.

Wetter (post-peak) catchment conditions will result in more quickflow, and thus result in a quicker response in the hydrograph, thus also a shorter TTP. There appear to be errors in the simulated GIS storm hydrograph due to the assumptions regarding the antecedent catchment conditions. Future development may consider the antecedent conditions of the catchment prior to the peak flow, to improve the predictions. Catchment conditions will change during any rainfall event (from dryer to wetter conditions) and therefore the runoff coefficient should be allowed to change. Improvements can be implemented with a change in the runoff coefficient before and after the peak runoff occurs.

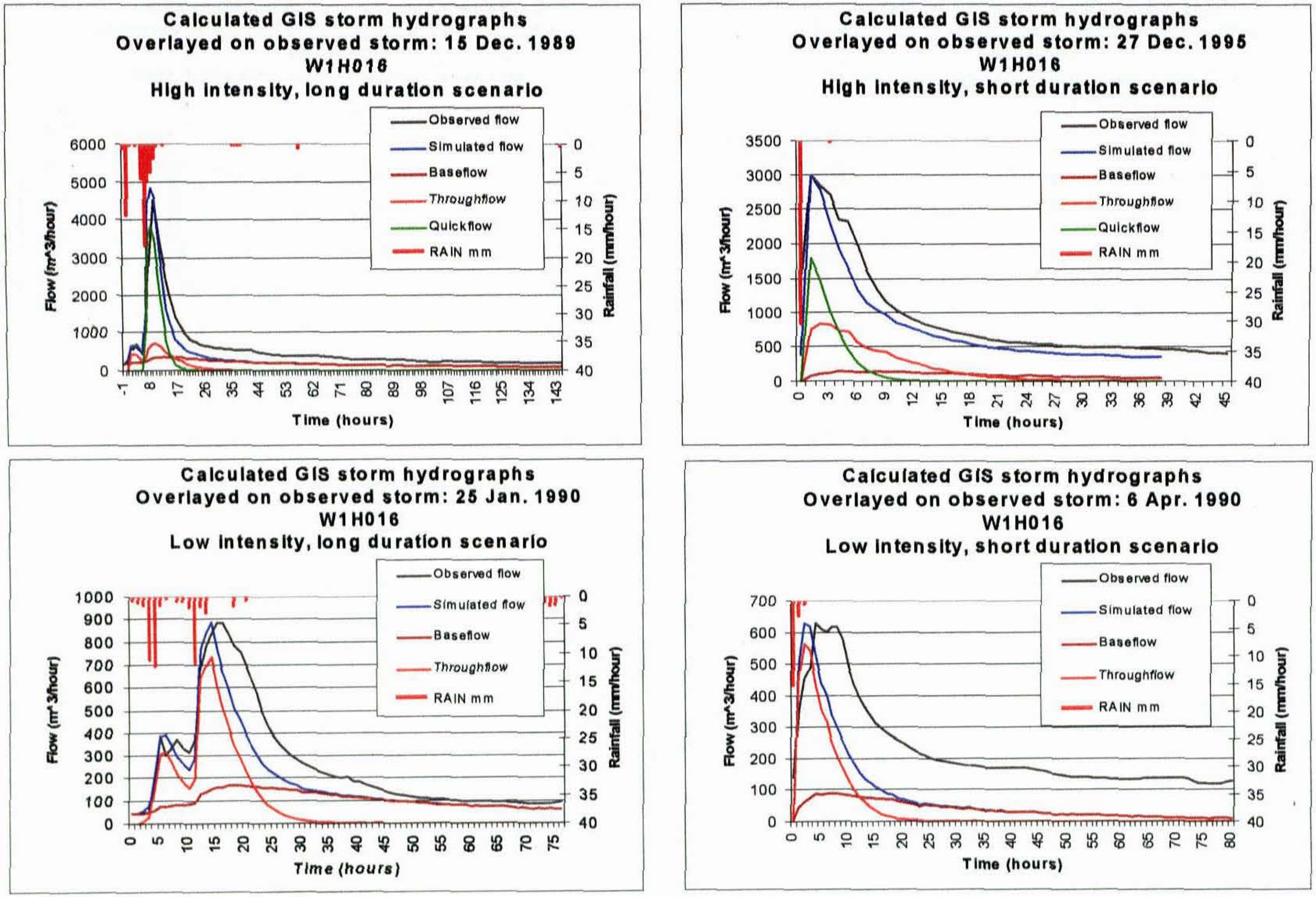

Figure 8.6: Simulated storm hydrographs in the catchment of W1H016, for the four different rainfall types

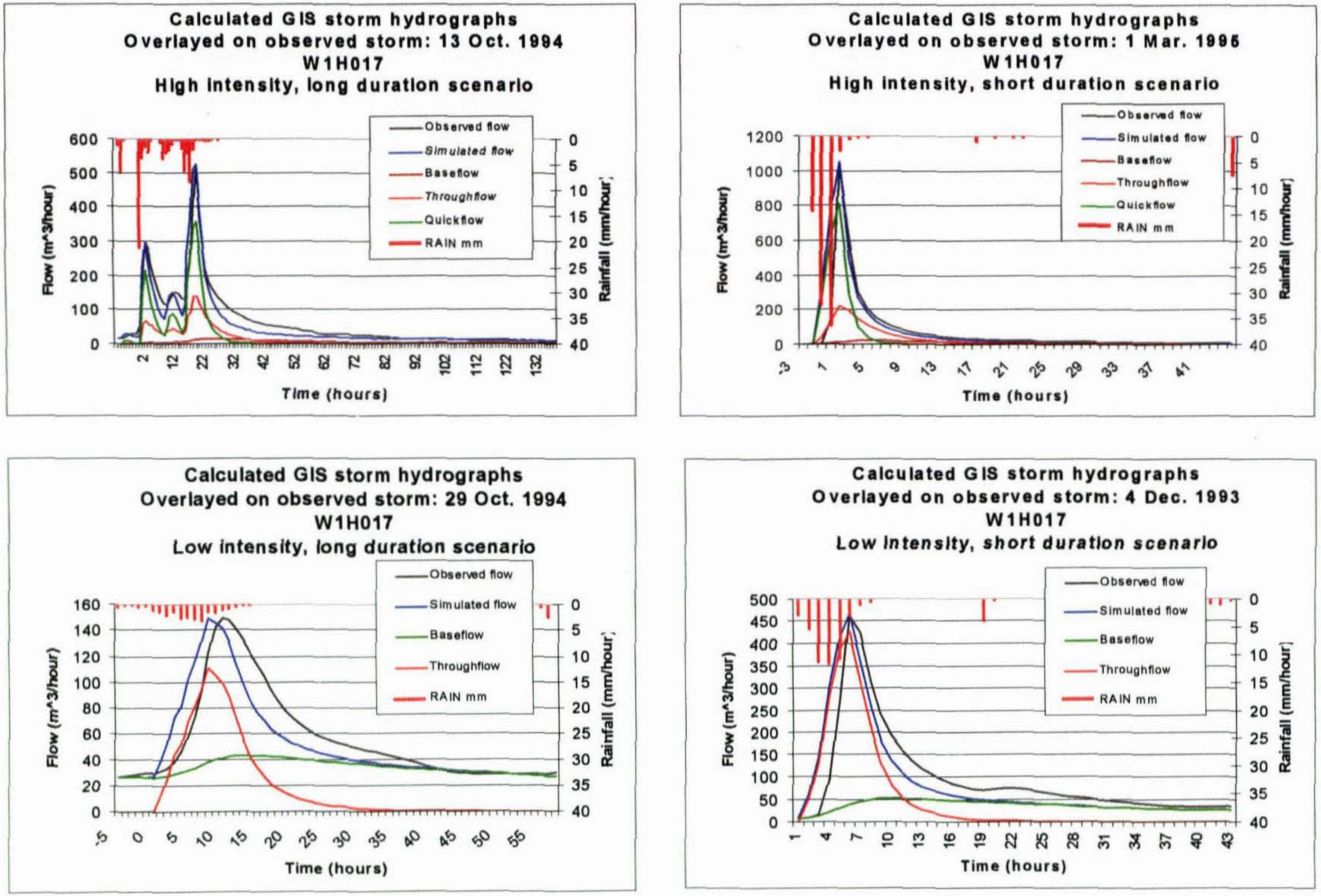

Figure 8.7: Simulated storm hydrographs in the catchment of W1H017, for the four different rainfall types.

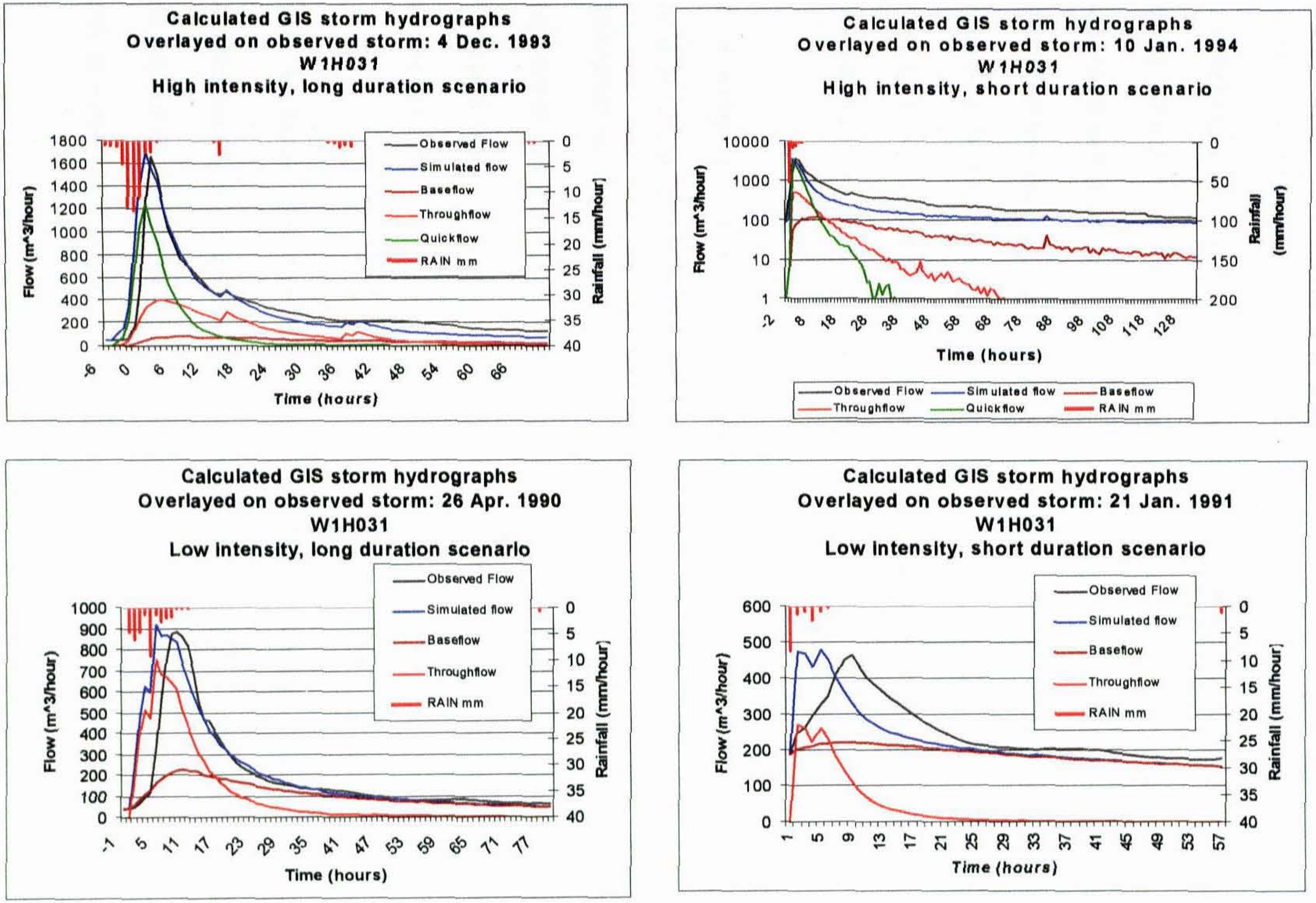

Figure 8.8: Simulated storm hydrographs in the catchment of W1H031, for the four different rainfall types.

It can be argued that the peak of a runoff event happens when the entire catchment is contributing to the runoff at the outlet (Shaw, 1994). This means that the catchment's soil moisture conditions are changing until the peak runoff occurs, after which the rainfall stops and the catchment starts to dry up. This change in the catchment's soil moisture conditions should be reflected in the model. In the present version of the model, this can only be accomplished by a change in the runoff coefficient during the simulation of the storm hydrograph. However, the runoff coefficient in this model represents the fraction of excess rainfall, which can change in conjunction with a change in the catchment's soil moisture conditions. Thus, the model needs an additional coefficient or function, that can possibly describe the change in the runoff coefficient.

8.7.4. Calibration of the partitioning coefficients

A storm hydrograph that contains 80% baseflow will have a flatter recession curve than a storm hydrograph that contains 80% quickflow. Thus, a change in the partitioning of flow among the flow components will result in a change in the recession curve of the storm hydrograph. Any adjustment to the partitioning coefficients must keep the sum of the partitioning coefficients, for each storm type, always equal to 1.

8.8. A summary of the GIS storm hydrograph model

A schematic diagram of the GIS storm hydrograph model is shown in Figure 8.9. It indicates that the information from the DEM (flow directions, slopes, slope lengths, land use and soil types) are utilized in the estimation of each flow component's travel times over individual pixels.

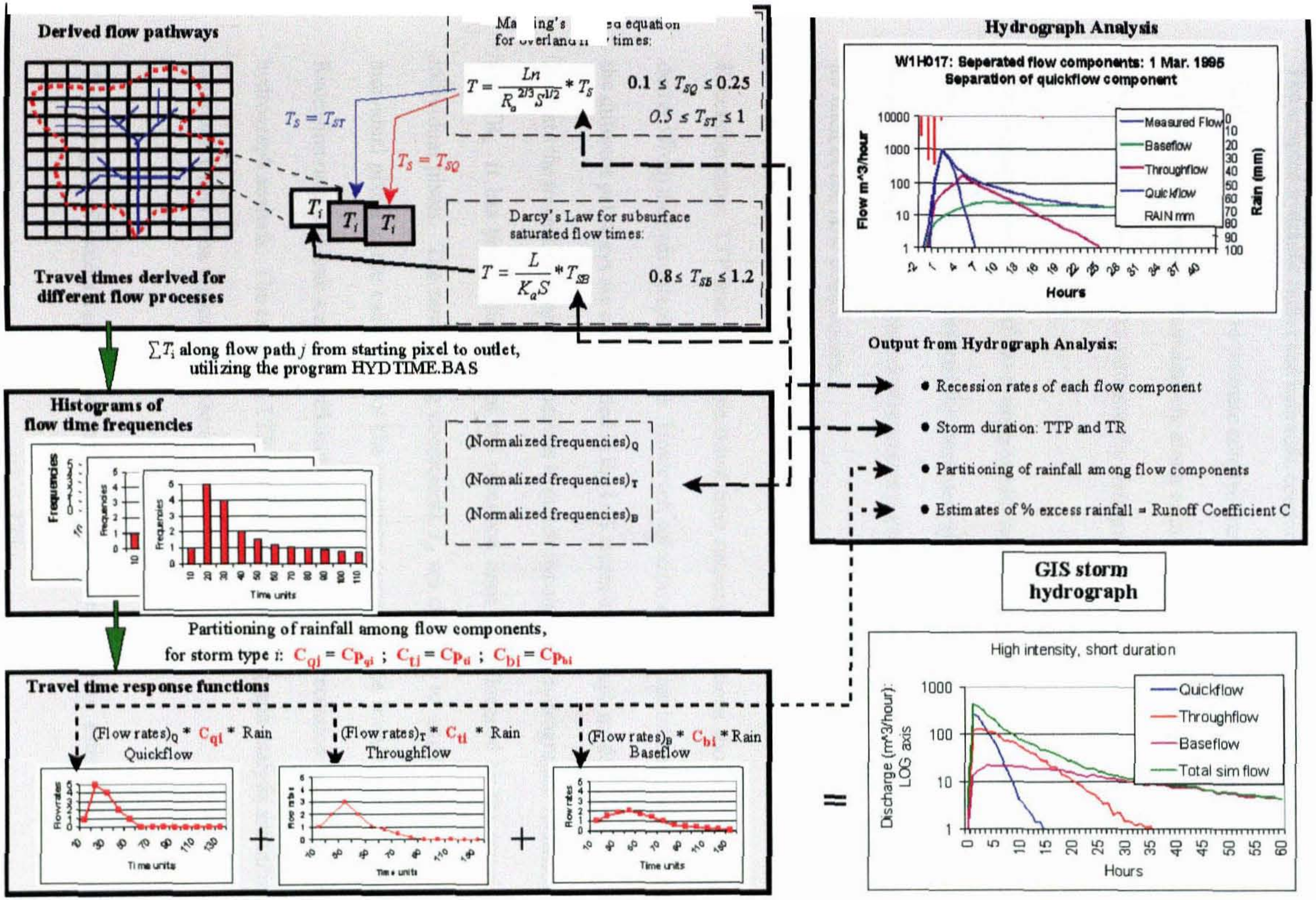

Figure 8.9: Schematic diagram of the GIS storm hydrograph model.

The adapted hydraulic radius and hydraulic conductivities replace R and K respectively in Manning's equation and Darcy's Law to estimate adapted travel times. The travel times are estimated for each pixel, and then summed cumulatively along each of the flow pathways (as indicated by the flow directions from the DEM) to estimate the histogram of the travel time frequencies.

One frequency histogram of travel times is calculated for each flow component and for each storm type. Frequencies are normalized for catchment size and pixel size (equation 8.1). The normalized frequencies of each flow component represent the travel time response function for one unit of rainfall for each of the flow components.

Recession rates, TTP and TR of the travel time response functions should correspond to those derived from the hydrograph analysis. However, some processes that influence the travel times along the different pathways are not included in the GIS storm hydrograph model. This leads to a need to calibrate the travel time response functions to match the observed hydrographs' recession rates, TTP and TR. It has been indicated that the recession rates are influenced by the travel times over individual pixels. The time scaling coefficients T_S are changed to estimated travel times across individual pixels in the calibration of the recession curves of the travel time response functions. Recession rates and time scaling coefficients are compared to the recession rates deducted during the hydrograph analysis. The estimated TTP and TR from the hydrograph analysis are utilized to verify calibrated travel time response functions.

Percentages of excess rainfall (or the runoff coefficients) were estimated for storms in the catchments. The normalized frequencies of each flow component, with calibrated recession rates, are then multiplied by the fraction of rainfall allocated to the flow component, as estimated during the hydrograph analysis. These frequencies are also multiplied by the fraction of excess rainfall for the appropriate storm type. Modelling one unit of excess rainfall on the entire catchment simulates the unit travel time response function for each flow component. The sum of the travel time response functions from the different flow components is the resultant GIS storm hydrograph, for a given rain storm type.

****

9 Evaluation of the GIS storm hydrograph model

The previous chapters described the development and calibration of the GIS storm hydrograph model. This chapter describes the application of the GIS storm hydrograph model in the Ntuze research catchment. The model is applied to a time series of measured rainfall for one rainfall season, over an observation period of five months. Along with the rainfall data, the observed flow data was used for the model calibration, for the same time period.

9.1. Flow components for a consecutive series of storm events, derived from a GIS storm hydrograph

9.1.1. Input to the simulations

The GIS storm hydrograph model utilized the calibrated unit response functions of each storm type, for each flow component, as depicted in Figure 8.2 (for W1H016), Figure 8.3 (for W1H017) and Figure 8.4 (W1H031).

Prior to the simulations, the observed rainfall series were classified into a sequence of storm types according to the rainfall characteristics depicted in Figure 4.3, using the maximum measured hourly rainfall and the total duration (number of hours) of each rain event (Table 9.1).

Table 9.1: Key information of the principle storm types, which occurred in the simulated period, listed with rainfall type.

Date	Rainfall of event	Hours of rainfall	Mean rainfall intensity	Maximum rainfall intensity	Rainfall Type	
	mm	hours	mm/h	mm/h	Rain duration	Rain intensity
Rain storm events:	**W1H016**					
01-Nov-92	37.2	4	9.3	14	Short duration	Low intensity
12-Nov-92	35.6	2	17.8	21	Short duration	High intensity
16-Nov-92	29.4	11	2.7	4.2	Long duration	Low intensity
25-Nov-92	32	18	1.8	9.2	Long duration	Low intensity
13-Dec-92	13.4	7	1.9	4.4	Short duration	Low intensity
21-Dec-92	19.8	11	1.8	6.2	Long duration	Low intensity
10-Jan-93	29.8	4	7.5	12	Short duration	Low intensity
16-Feb-93	18.4	8	2.3	5.6	Short duration	Low intensity
17-Feb-93	10.4	8	1.3	3.2	Short duration	Low intensity
16-Mar-93	26.8	10	2.7	13	Long duration	Low intensity
23-Mar-93	34.4	12	2.9	7.4	Long duration	Low intensity
Rain storm events:	**W1H017**					
1 Nov 1992	35	11	3.2	12.6	Long duration	Low intensity
12 Nov 1992	24.6	2	12.3	20.4	Short duration	High intensity
25 Nov 1992	39.4	16	2.5	10.2	Long duration	Low intensity
13 Dec 1992	33	23	1.4	8.8	Long duration	Low intensity
23 Dec 1993	23.4	11	2.1	7.8	Long duration	Low intensity
10 Jan 1993	31.2	4	7.8	19.4	Short duration	High intensity
24 Jan 1993	55.4	44	1.3	7.6	Long duration	Low intensity
8-Febr-93	36	20	1.8	6	Long duration	Low intensity
15 Mar 1993	38.4	4	9.6	26.8	Short duration	High intensity
Rain storm events:	**W1H031**					
22-Nov-93	49.4	25	2.0	6.4	Long duration	Low intensity
04-Dec-93	50	13	3.8	13.6	Long duration	Low intensity
09-Dec-93	50.6	18	2.8	15.4	Long duration	Low intensity
30-Dec-93	44.8	4	11.2	30	Short duration	High intensity
10-Jan-94	66.6	6	11.1	52	Short duration	High intensity
21-Jan-94	45.6	4	11.4	35.8	Short duration	High intensity
11-Mar-94	19	4	4.8	12.4	Short duration	Low intensity
16-Mar-94	8.4	2	4.2	7.8	Short duration	Low intensity
29-Mar-94	27.4	16	1.7	5.4	Long duration	Low intensity

All events measuring rainfall of less than 1 mm per hour were assumed to have no effect on the catchment outflow, and were ignored. Most rainfall events occur as low intensity and short durations. These rainfall events were not all listed in Table 9.1. Unlisted rain events were classified as events of low intensity and short duration.

9.1.2. Method of simulation

The following method was utilized to simulate the flow at the catchment outlet (the storm hydrographs) for five months of (hourly) rainfall time series data, using the spatial information of the catchment:

1. Scaling of the individual flow components' unit response functions, using the appropriate storm type's response functions and the measured rainfall.

2. Scaling of the response functions by multiplying each response function with the runoff coefficient. A constant runoff coefficient for the entire simulation period was determined by comparing the total simulated and observed flows over the entire simulated period. It was assumed that an optimal calibration of the runoff coefficient was indicated by similar values of simulated and observed total flows.

3. Adjustment of the total amount of baseflow by adding the amount of water to the simulated baseflow which is already present in the river at the start of the flow simulation. This baseflow already present in the river is reduced every hour at a constant rate. This recession rate for baseflow (0.995) was derived through the long term recession analysis.

4. Overlay the different hourly response functions from the different flow components from each rainfall event to calculate the simulated storm hydrograph of the rain event.

5. Calibration of the partitioning coefficients, for each storm type, by adjusting the simulated recession rates to fit the observed recession rates.

A detailed description of the calculations during the simulations are provided in Appendix C. Plots of the simulated consecutive storm sequence are portrayed in Figures 9.1, 9.2 and 9.3 for the catchments of W1H016, W1H017 and W1H031 respectively. The cumulative simulated and observed runoff are plotted in Figures 9.4, 9.5 and 9.6 for the catchments of W1H016, W1H017 and W1H031 respectively.

It must be noted that there are ± two weeks of missing rainfall and flow data in the times series from the catchment of W1H031 (for the dates including 27 Jan., 12H00 until and including 9 Feb. 1994, 24H00). Provision was made for the missing data by assuming that all flows measured on 10 Feb. 1994 at 01H00 (the recommencement of the flow time series) was baseflow, with a recession rate derived from a recession constant of 0.995. The rainfall measurements for the catchment of W1H016 also has a week of missing data (from 20 Jan. 1993 13H00 until and including 27 Jan. 1993 10H00). Simulation after this period of missing rainfall data recommences with measured rainfall on 8 Feb.1993 (DOY 39), 00H00, when very little flow was measured in the river.

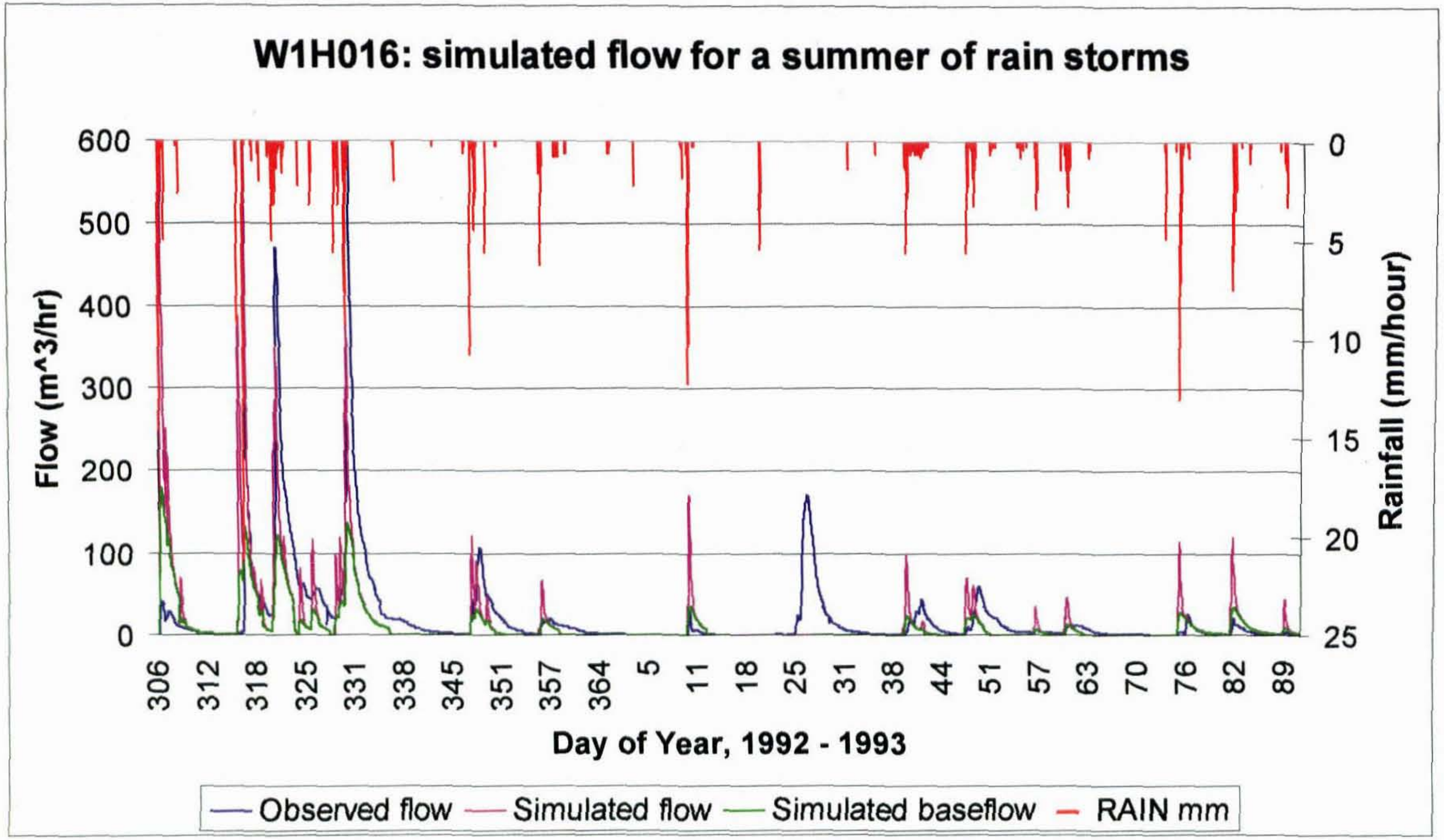

Figure 9.1: Simulated and observed storm hydrographs from the catchment of W1H016, for the time period 1 Nov. 1992 until 31 Mar. 1993.

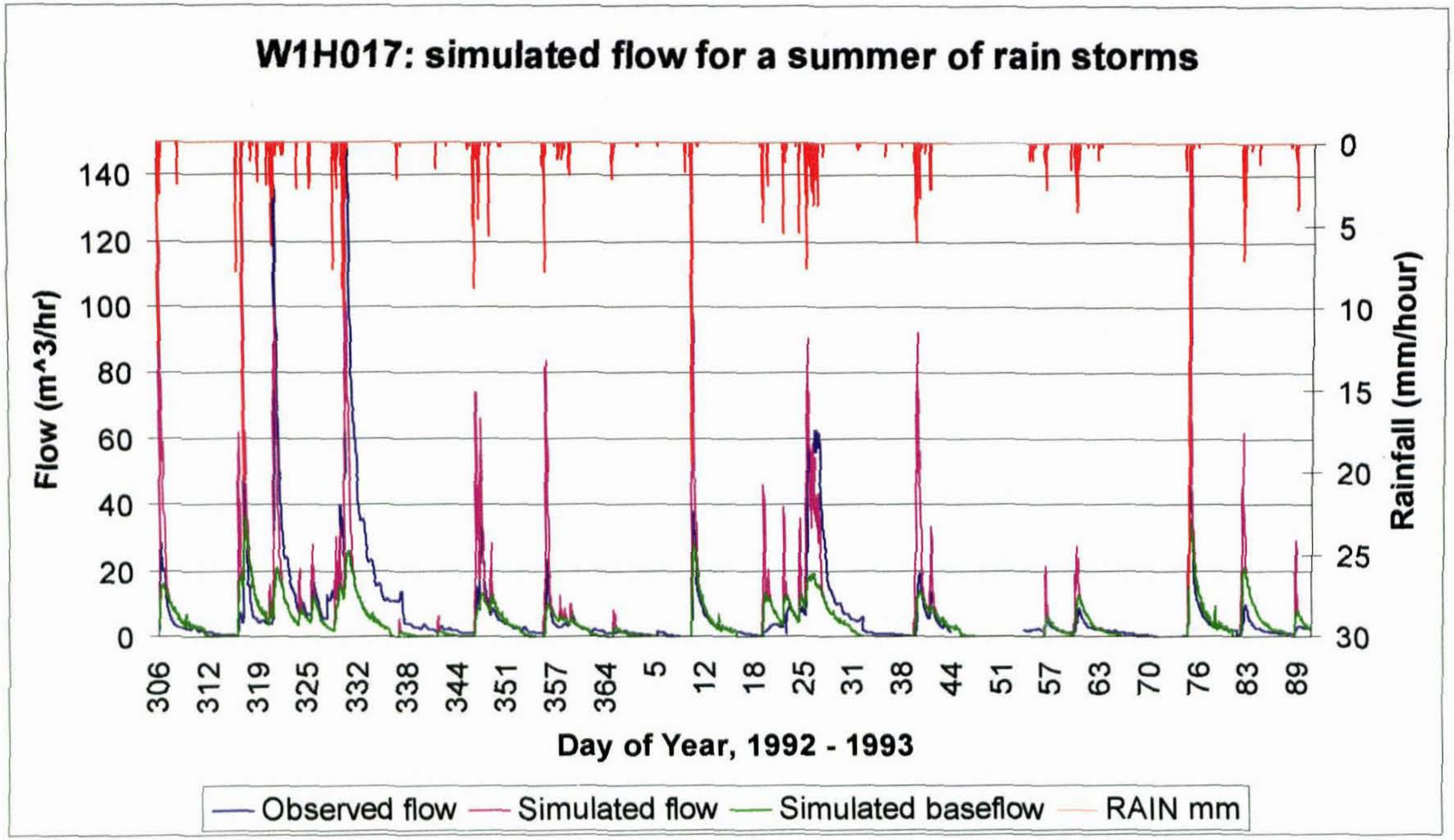

Figure 9.2: Simulated and observed storm hydrographs from the catchment of W1H017, for the time period 1 Nov. 1992 until 31 Mar. 1993.

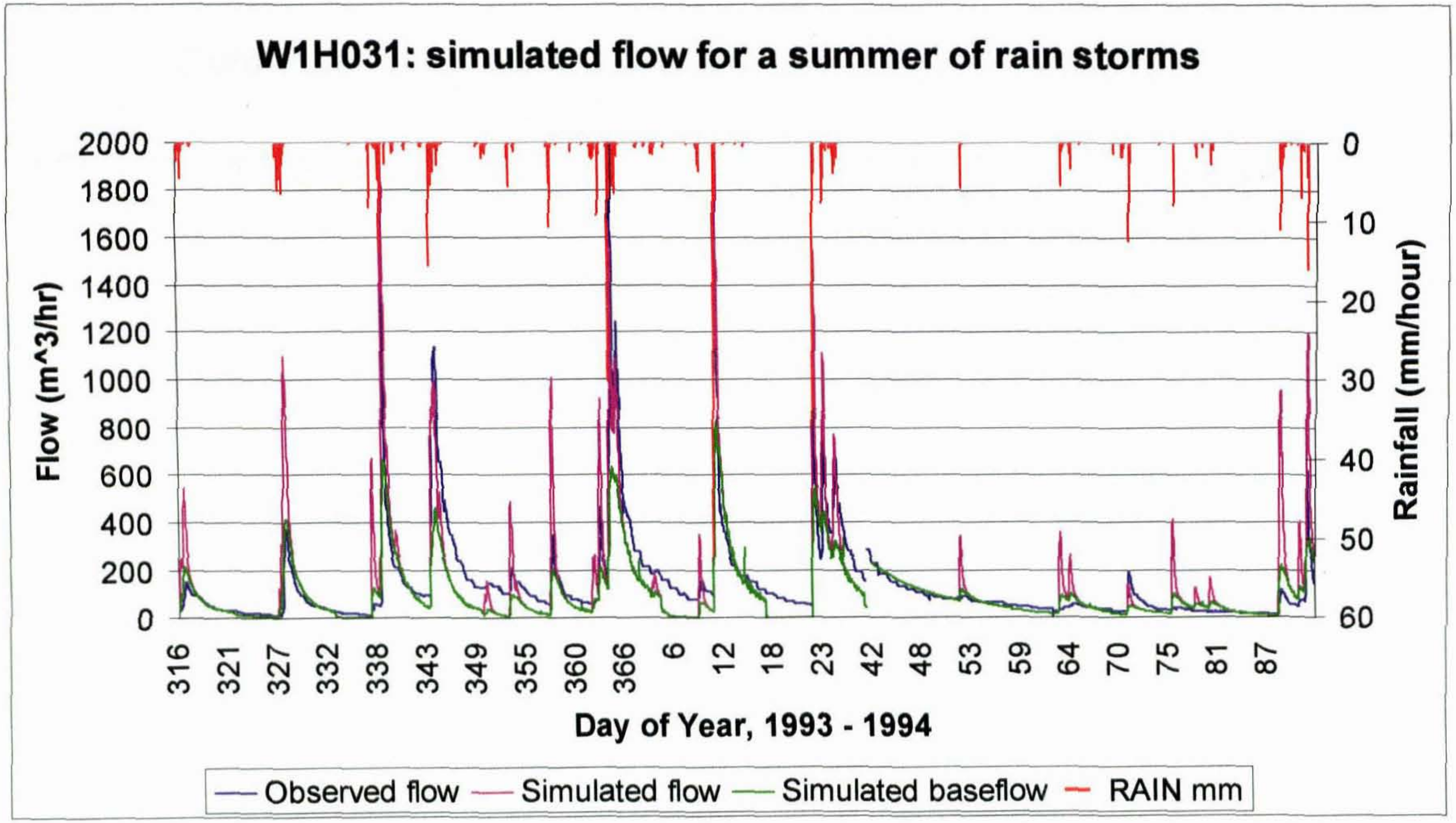

Figure 9.3: Simulated and observed storm hydrographs from the catchment of W1H031, for the time period 10 Nov. 1993 until 31 Mar. 1994.

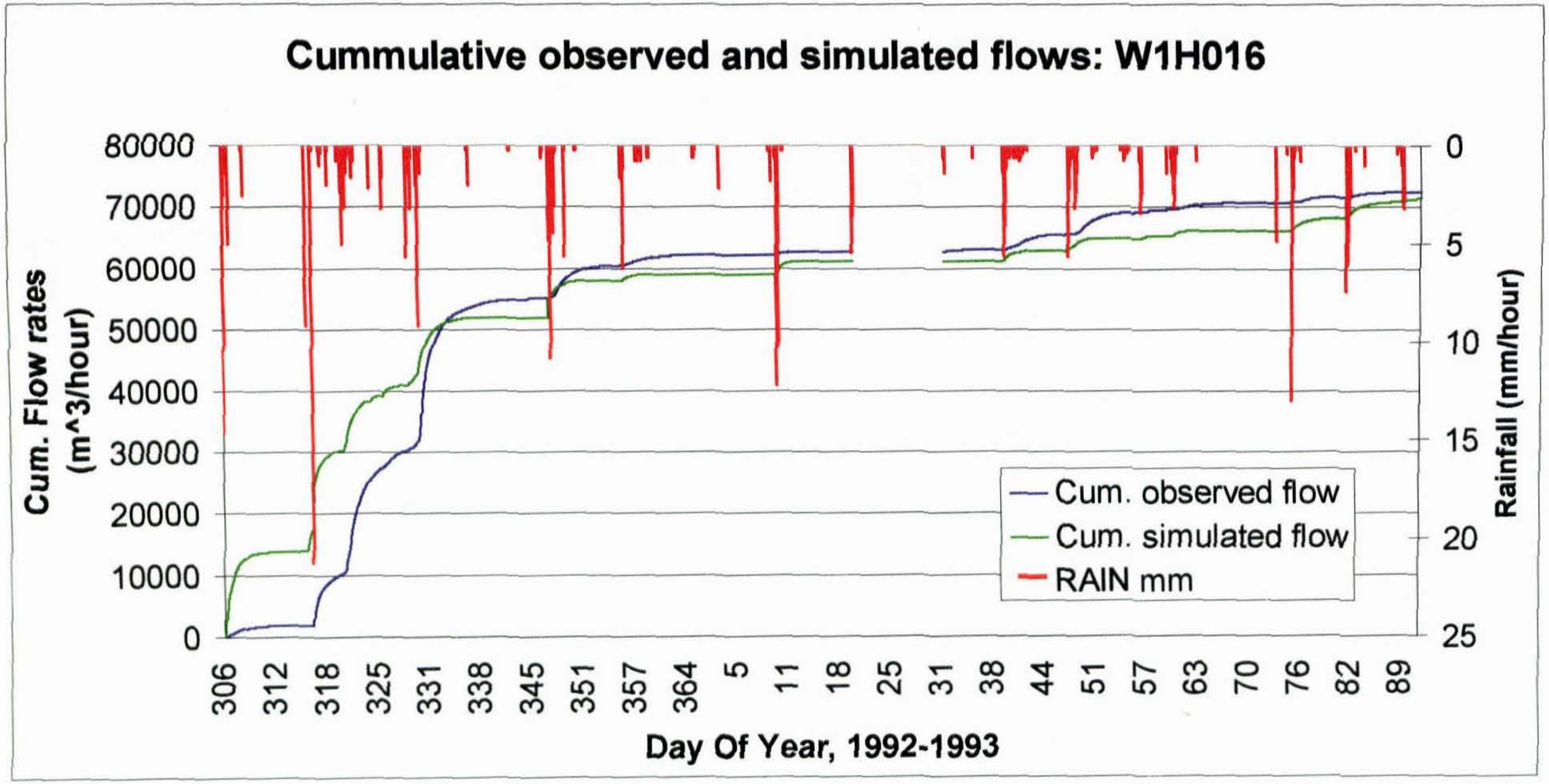

Figure 9.4: Cumulative plots of simulated and observed discharge from the catchment of W1H016, for the period 1 November 1992 until 31 March 1993.

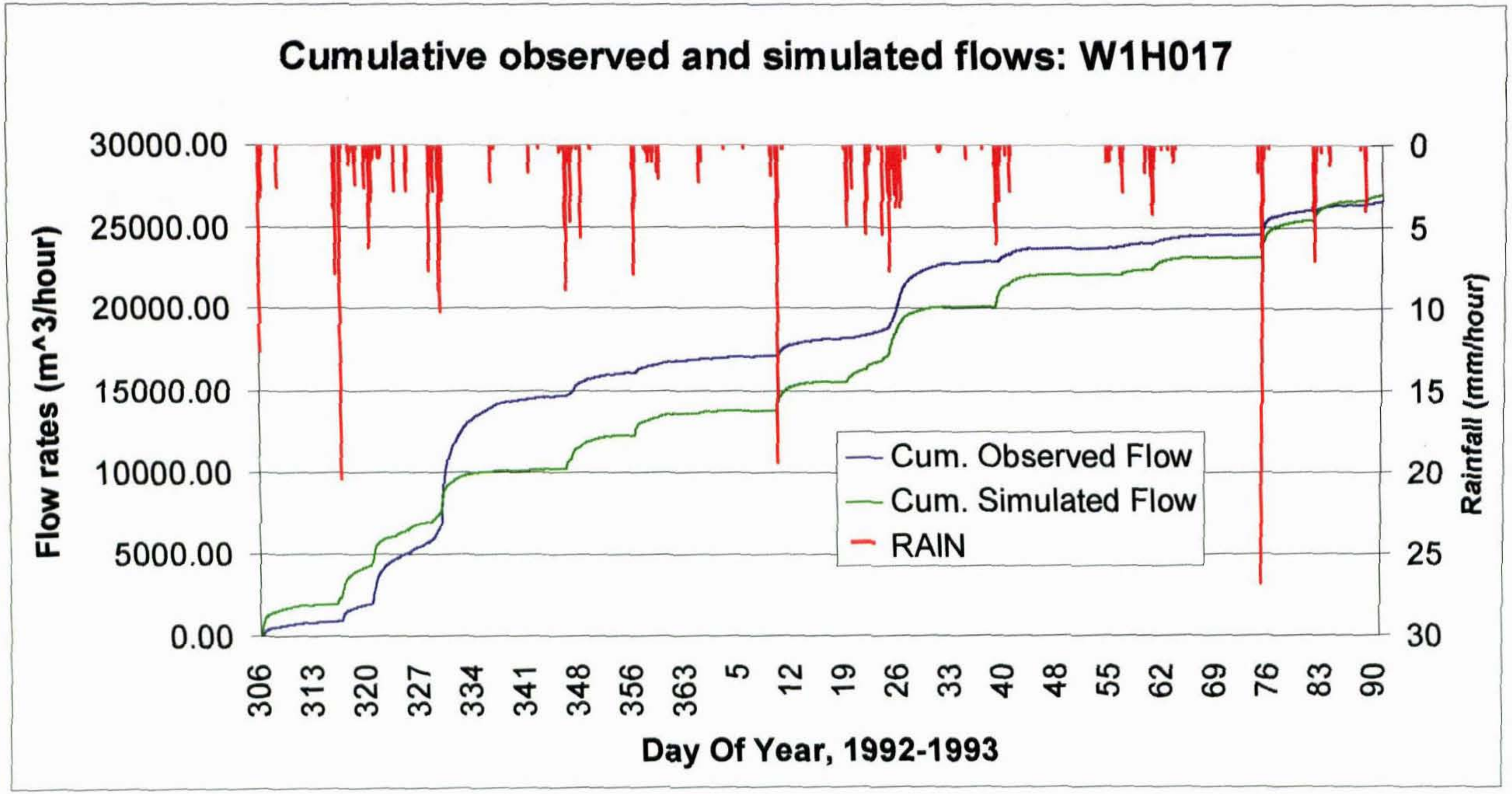

Figure 9.5: Cumulative plots of simulated and observed discharge from the catchment of W1H017, for the period 1 November 1992 until 31 March 1993.

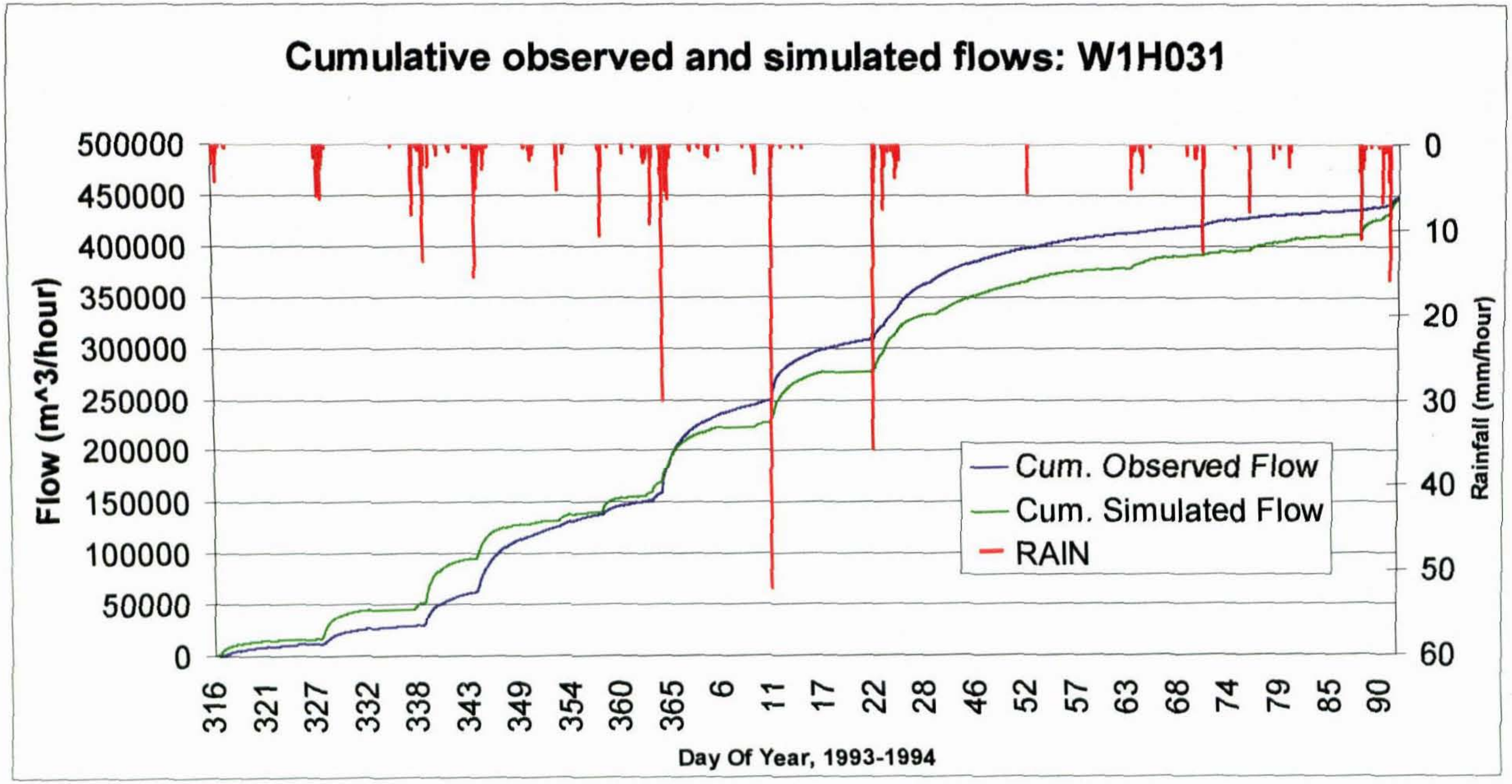

Figure9.6:
1994.

9.2. Calibrated values of the model parameters

Table 9.2 provides the key information of some simulated storms included in the simulation period. The ratio of (Excess rainfall)/(Measured rainfall) was calculated for these storms, as listed in the last column of Table 9.2. For the catchment of W1H016, it was found that the ratio (Excess rainfall)/(Measured rainfall) was dissimilar for the first and second parts of the season. From the beginning of the simulation period until (and including) the storm on 25 November 1992, the ratio (Excess rainfall)/(Measured rainfall) is mostly larger than 0.1. However, storms measured during December, January, February and March mostly indicate a ratio (Excess rainfall)/(Measured rainfall) much smaller than 0.01.

It was suggested that the two different ratios of (Excess rainfall)/(Measured rainfall), mentioned in the previous paragraph, was due to dissimilar antecedent catchment conditions.

The runoff coefficient is estimated by the ratio (Excess rainfall)/(Measured rainfall) (Equation 8.5, Paragraph 8.3). Therefore, the period of the flow simulation from the catchment of W1H016 was divided into two parts, each having its own runoff coefficient, with the second part starting on 12 Dec. 1992, i.e., Day Of Year (DOY) 347 of 1992. Table 9.3 lists the calibrated parameters of each part of the simulation period. It is not clear why the runoff coefficient changes. For the assessment of the model it is assumed that the change is likely to effect the model outcome and needs to be incorporated into the simulation.

Runoff Coefficients: W1H016

Date	Rainfall of event	Excess rain of event	Hours of rainfall	Mean rainfall intensity	Maximum rainfall intensity	Dry period before the storm	Observed flow before storm	Observed peak flow	**Ratio: Excess Rain /Measured Rain**
	mm	mm	hours	mm/h	mm/h	hours	m^3/hour	m^3/hour	No dimension
1 Nov 1992	37.2	0.5	4	9.3	14	60	0	40.8	0.013
12 Nov 1992	35.6	5.3	2	17.8	21	14	3.8	335	0.149
16 Nov 1992	29.4	4.5	11	2.7	4.2	50	25	471	0.153
25 Nov 1992	32	4.2	18	1.8	9.2	14	62	706	0.131
13 Dec 1992	13.4	1.1	7	1.9	4.4	12	1	107	0.082
21 Dec 1992	19.8	0.1	11	1.8	6.2	168	1.4	19.4	0.005
10 Jan 1993	29.8	0.2	4	7.5	12	192	0	29.6	0.007
16 Feb 1993	18.4	0.1	8	2.3	5.6	144	1.3	10	0.005
17 Feb 1993	14.4	0.6	18	0.8	3.2	5	6.1	60	0.042
16 Mar 1993	26.8	0.2	10	2.7	13	23	0.5	4.5	0.007
23 Mar 1993	34.4	0.2	12	2.9	7.4	162	0.5	21.5	0.006

Runoff Coefficients: W1H017

Date	Rainfall of event	Excess rain of event	Hours of rainfall	Mean rainfall intensity	Maximum rainfall intensity	Dry period before the storm	Observed flow before storm	Observed peak flow	**Ratio: Excess Rain /Measured Rain**
	mm	mm	hours	mm/h	mm/h	hours	m^3/hour	m^3/hour	No dimension
1 Nov 1992	35	0.8	11	3.2	12.6	(Missing)	1	28	0.023
12 Nov 1992	24.6	0.5	2	12.3	20.4	24	0.4	7.4	0.02
25 Nov 1992	39.4	8.3	16	2.5	10.2	11	24	404	0.211

Runoff Coefficients:	W1H017								
Date	Rainfall of event	Excess rain of event	Hours of rainfall	Mean rainfall intensity	Maximum rainfall intensity	Dry period before the storm	Observed flow before storm	Observed peak flow	**Ratio: Excess Rain /Measured Rain**
	mm	mm	hours	mm/h	mm/h	hours	m^3/hour	m^3/hour	No dimension
13 Dec 1992	33	0.8	23	1.4	8.8	240	1.3	41	0.024
23 Dec 1993	23.4	0.5	11	2.1	7.8	168	1.2	234	0.021
10 Jan 1993	31.2	1.1	9	7.8	19.4	13	0.01	38	0.034
24 Jan 1993	55.4	4.8	44	1.3	7.6		7	66	0.087
8 Feb 1993	36	1	20	1.8	6	264	0.01	19.2	0.028
15 Mar 1993	38.4	1.7	10	9.6	26.8	360	0.1	98	0.042

Runoff Coefficients:	W1H031								
Date	Rainfall of event	Excess rain of event	Hours of rainfall	Mean rainfall intensity	Maximum rainfall intensity	Dry period before the storm	Observed flow before storm	Observed peak flow	**Ratio: Excess Rain /Measured Rain**
	mm	mm	hours	mm/h	mm/h	hours	m^3/hour	m^3/hour	No dimension
22 Nov 1993	49.4	4.1	25	2.0	6.4	228	12	675	0.083
4 Dec 1993	50	9.8	13	3.8	13.6	22	48	1660	0.196
9 Dec 1993	50.6	13.9	18	2.8	15.4	96	90	1116	0.275
30 Dec 1993	64.2	18	17	3.8	30	24	156	1243	0.280
10 Jan 1994	66.6	11.7	6	11.1	52	40	90	3685	0.176
21 Jan 1994	45.6	3.1	4	11.4	35.8	240	50	1355	0.068
11 Mar 1994	19	1.9	4	4.8	12.4	12	27	195	0.100
16 Mar 1994	8.4	0.6	2	4.2	7.8	120	31	43	0.071
29 Mar 1994	27.4	1.6	16	1.7	5.4	168	13	107	0.058

Table 9.3: Calibrated parameters of GIS storm hydrograph model simulations.

Catchment	Simulation period	Calibrated runoff coefficient	Calibrated partitioning coefficients expressed as percentages									
			High intensity long duration			*High intensity short duration*			*Low intensity Short duration*		*Low intensity long duration*	
			Baseflow	Throughflow	Quickflow	Baseflow	Throughflow	Quickflow	Baseflow	Throughflow	Baseflow	Throughflow
W1H016	1-30 Nov. 92	0.1	10%	30%	60%	30%	20%	50%	60%	40%	80%	20%
	1 Dec. 92 -31 Mar. 93	0.027										
W1H017	1 Nov.92-31Mar.93	0.075	20% Parameters not calibrated*	40%	40%	60%	20%	20%	80%	20%	50%	50%
W1H031	11 Nov. 93-31Mar.94	0.26	20% Parameters not calibrated*	40%	40%	80%	10%	10%	60%	40%	70%	30%

* No rainfall event of high intensity and long duration were measured in the catchments of W1H017 and W1H031 during the simulation period.

The calibrated partitioning coefficients (Table 9.3) were compared to the values listed in Table 5.10. The comparison indicated that the calibrated partitioning coefficients of the baseflow component are mostly larger than the values listed in Table 5.10. This could possibly be due to the drought conditions prevailing during the simulation period, which was finally broken during the rain season of 1995/96. The drought caused most rainfall to be absorbed by the depleting groundwater resources. Thus, a fairly large percentage of water in the observed hydrographs originated from the baseflow component.

9.3. Discussion of simulated flows

Selected storms in the simulated flow time series were plotted on log y axis for the catchment of W1H016 (Figures 9.7 to 9.13). In this manner the recessions of the simulated and observed flow hydrographs were compared. Similar graphs for the catchments of W1H017 and W1H031 are printed in Appendix D.

Times to peak of the simulated hydrographs

Some of the simulated flow peaks did not correspond closely with the observed flow peaks. Some were simulated between five and eight hours, either prematurely or post peak flow. One of the reasons for this may be attributed to the antecedent catchment conditions, which vary with each storm event, and not only for each storm type. Antecedent catchment conditions, which influence travel times of water down the catchments slopes, and therefore also the TTP of the simulated hydrograph, is not currently accommodated in the model.

This problem can also be caused by catchment rainfall data which is recorded at the weir outlet and not close to the centre of the catchment. The storm on 25 Nov. 1992 (Figure 9.7) is an example of this, where there was a difference between the observed and simulated peaks of seven hours.

Catchment rainfall estimation

Small amounts of measured rainfall (in some instances, less than 1 mm or no rainfall at all) have produced some unusually high responses in the observed flow hydrograph. See the examples on 17 March 1993 in Figure 9.8 (on DOY 76), 23 December 1992 in Figure 9.9 (on DOY 357), 2 March 1993 in Figure 9.10 (on DOY 61), and 11 January 1993 in Figure 9.11 (on DOY 11). It is clear that only small amounts of rainfall, or no rainfall at all, were measured at the catchment outlet (and used to estimate the catchment rainfall) but that substantial rainfall must have fallen over the catchment, causing the observed outflow. The model is unable to reproduce the exceeds.

Recessions of the hydrographs

The partitioning coefficients of each storm type were used to adjust the recessions of most individual storms to fit the observed recessions. The rain event on 12 Nov. 1992 (Figure 9.13) is characterized by the highest observed peak flow of the summer, also the highest rainfall intensity and shortest duration (21 mm and 14 mm rainfall in two consecutive hours). The simulated flow hydrograph of the rain event is a perfect match of the observed TTP. However, the peak flow, as well as the recession, of the simulated hydrograph do not compare well with the observed hydrograph. This storm has a second rise in the flow rate shortly after the peak flow. This could indicate that follow-up rainfall in the catchment was not included in the catchment rainfall estimation.

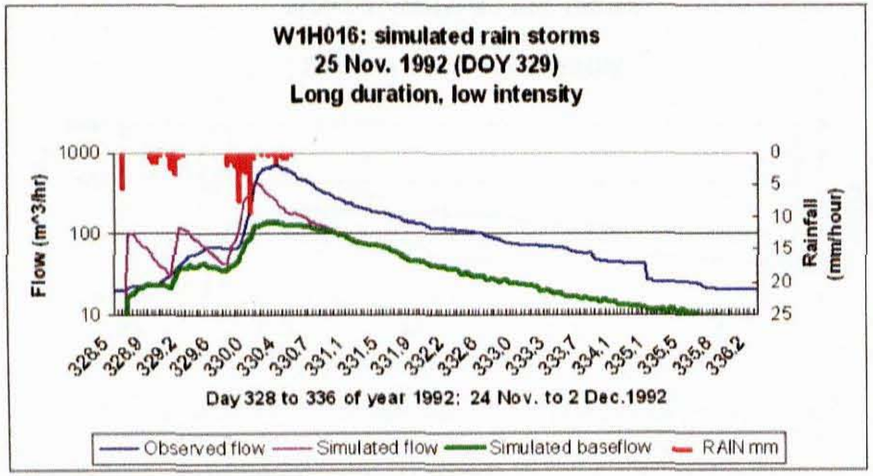

Figure 9.7: A simulated and observed storm hydrograph from the catchment of W1H016: 25 Nov. 1992.

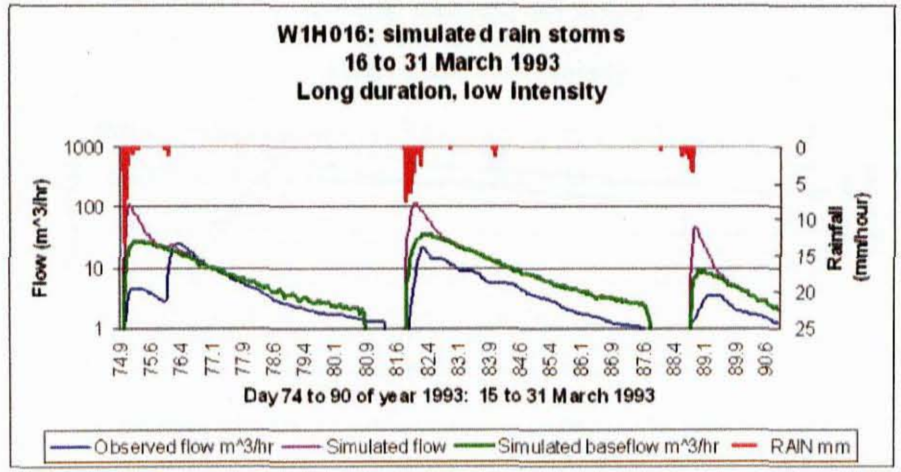

Figure 9.8: A simulated and observed storm hydrograph from the catchment of W1H016: 16 - 31 Mar. 1993.

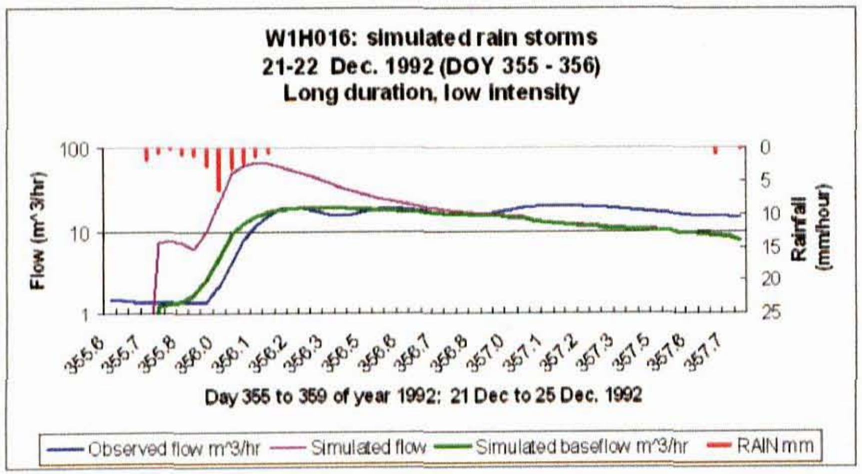

Figure 9.9: A simulated and observed storm hydrograph from the catchment of W1H016: 21-22 Dec. 1992.

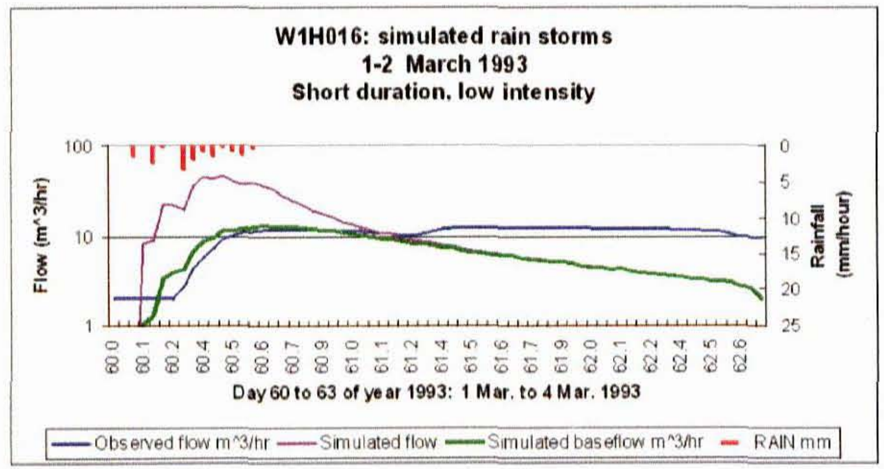

Figure 9.10: A simulated and observed storm hydrograph from the catchment of W1H016: 1-2 Mar. 1993.

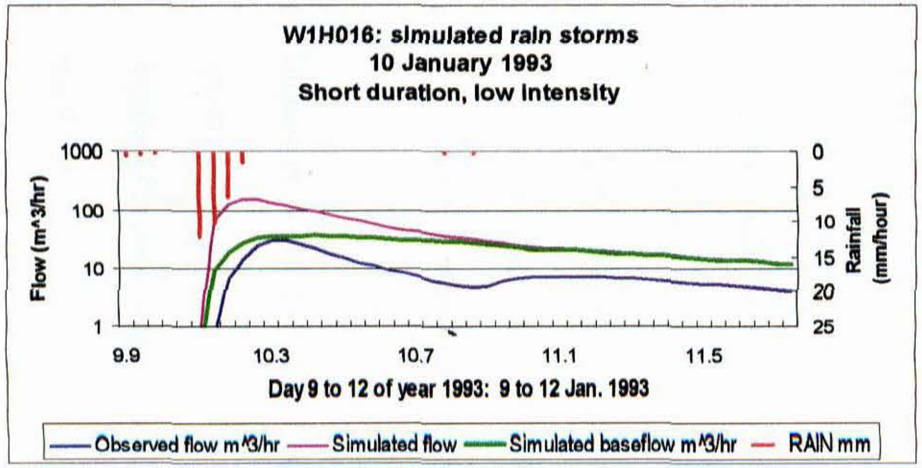

Figure 9.11: A simulated and observed storm hydrograph from the catchment of W1H016: 10 Jan. 1993.

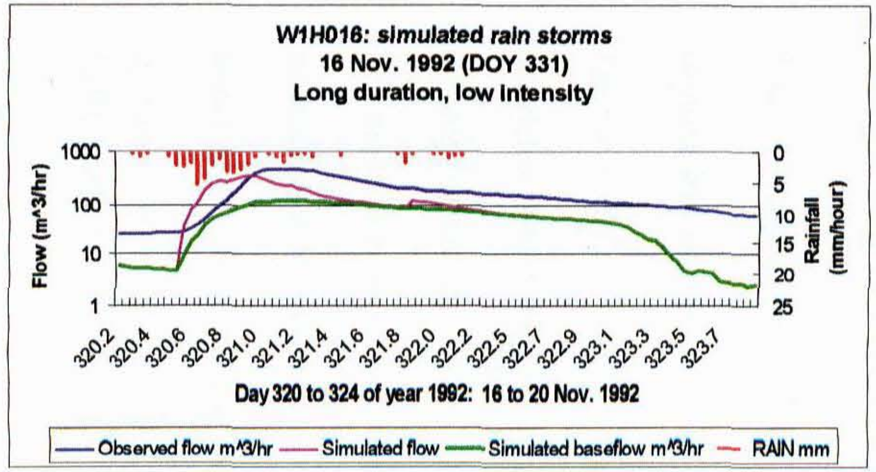

Figure 9.12: A simulated and observed storm hydrograph from the catchment of W1H016: 16 Nov. 1992.

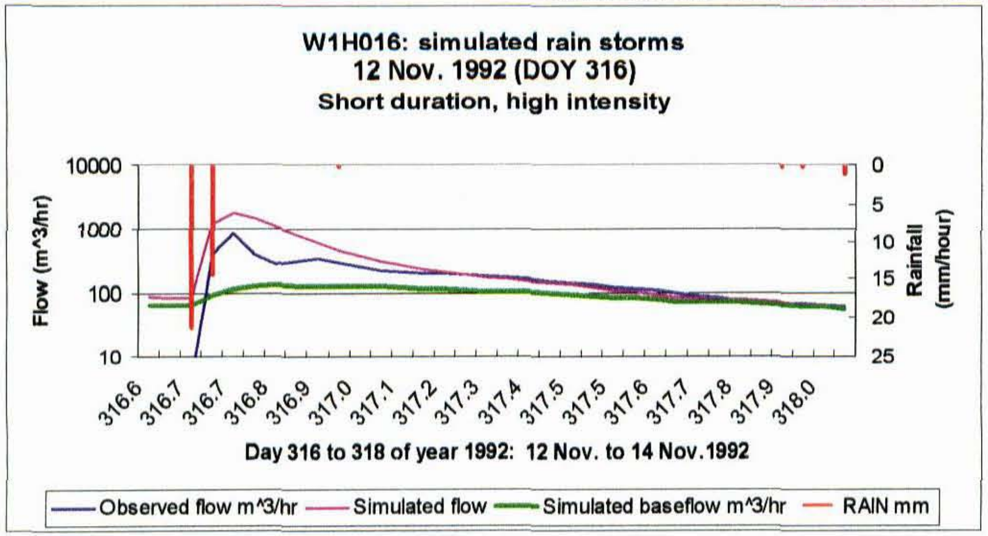

Figure 9.13: A simulated and observed storm hydrograph from the catchment of W1H016: 12 Nov. 1992.

9.4. Comparison of the model results with the results of a baseflow separation model

The observed flow data from storms measured in the research catchment were applied to the model described by Hughes, Hannart and Watkins (2003). It is a continuous baseflow separation method, originally applied by Nathan and McMahon (1990), to estimate low flow characteristics. This model is referred to, in this report, as the Baseflow Separation Model (BSM). It is a statistical method, which uses a simple equation to separate the high and low flows in observed stream data for both daily and monthly time series (Hughes *et al*, 2003):

$$q_i = aq_{i-1} + b(1+a)(Q_i - Q_{i-1})$$
$$(QB)_i = Q_i - q_i$$

where

i = time step index

Q_i = total flow for time step i

q_i = high flow for time step i

$(QB)_i$ = baseflow for time step i

a, b = separation parameters ($0 < a < 1$ and $0 < b \leq 0.5$), using values for $a = 0.995$ and $b = 0.5$, as recommended in Hughes *et al* (2003).

Hughes *et al* (2003) applied the BSM model to both monthly and daily data. The model was applied to the hourly flow data measured in the Ntuze research catchments. Results indicate slightly different simulations of the baseflow component between the models (Figures 9.14, 9.15 and 9.16).

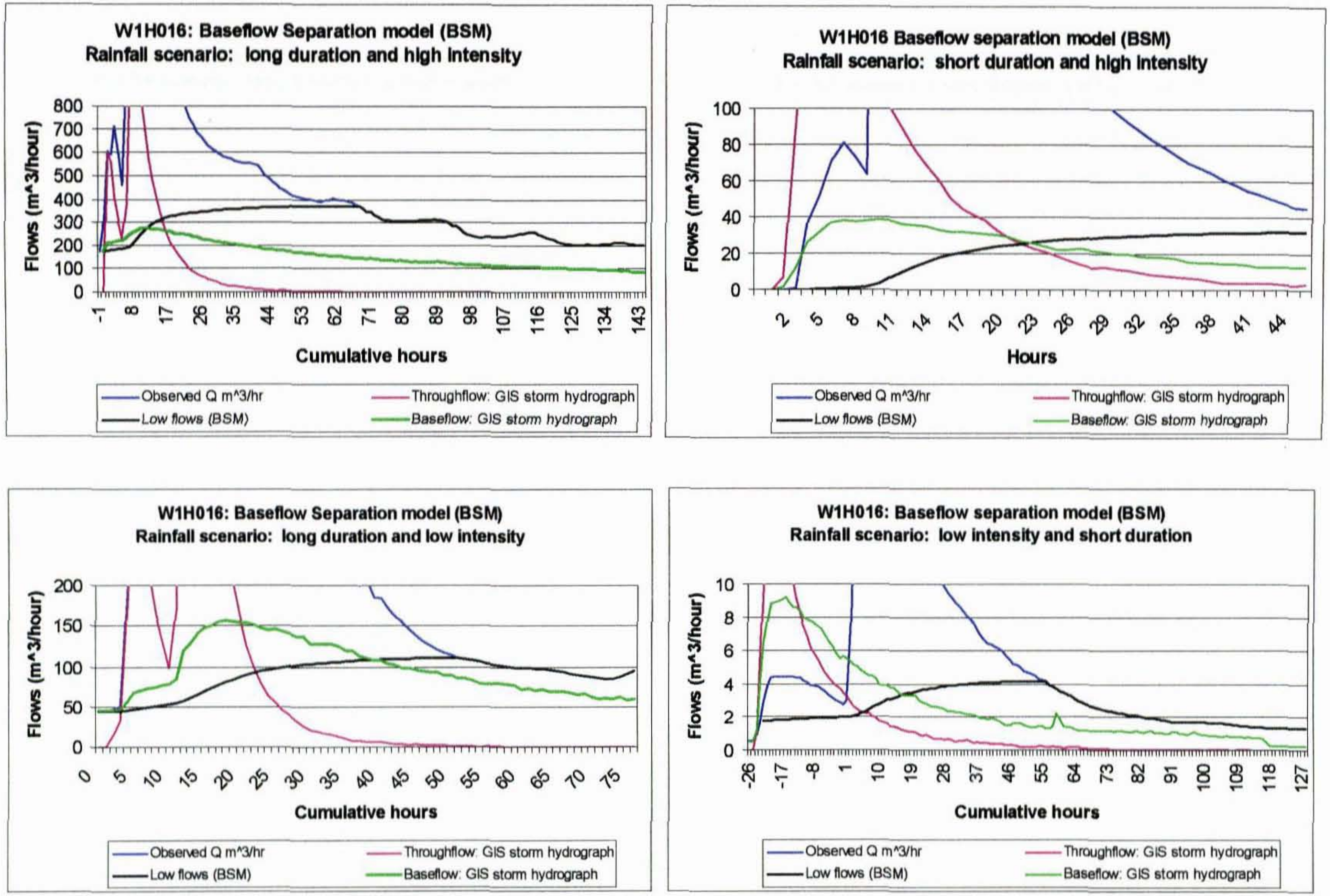

Figure 9.14: Comparison between the Baseflow Separation Model and the GIS storm hydrograph model, in the catchment of W1H016.

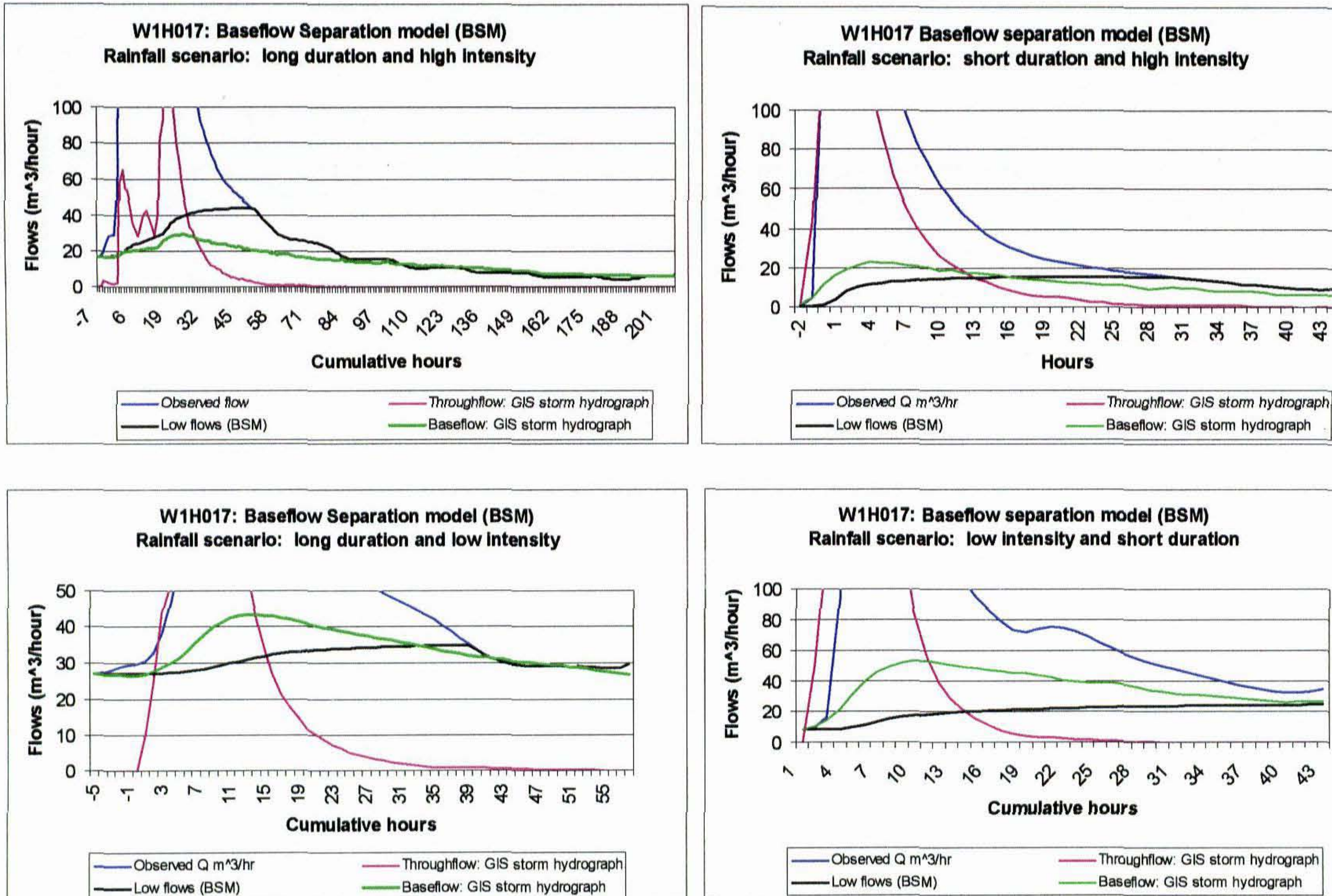

Figure 9.15: Comparison between the Baseflow Separation Model and the GIS storm hydrograph model, in the catchment of W1H017.

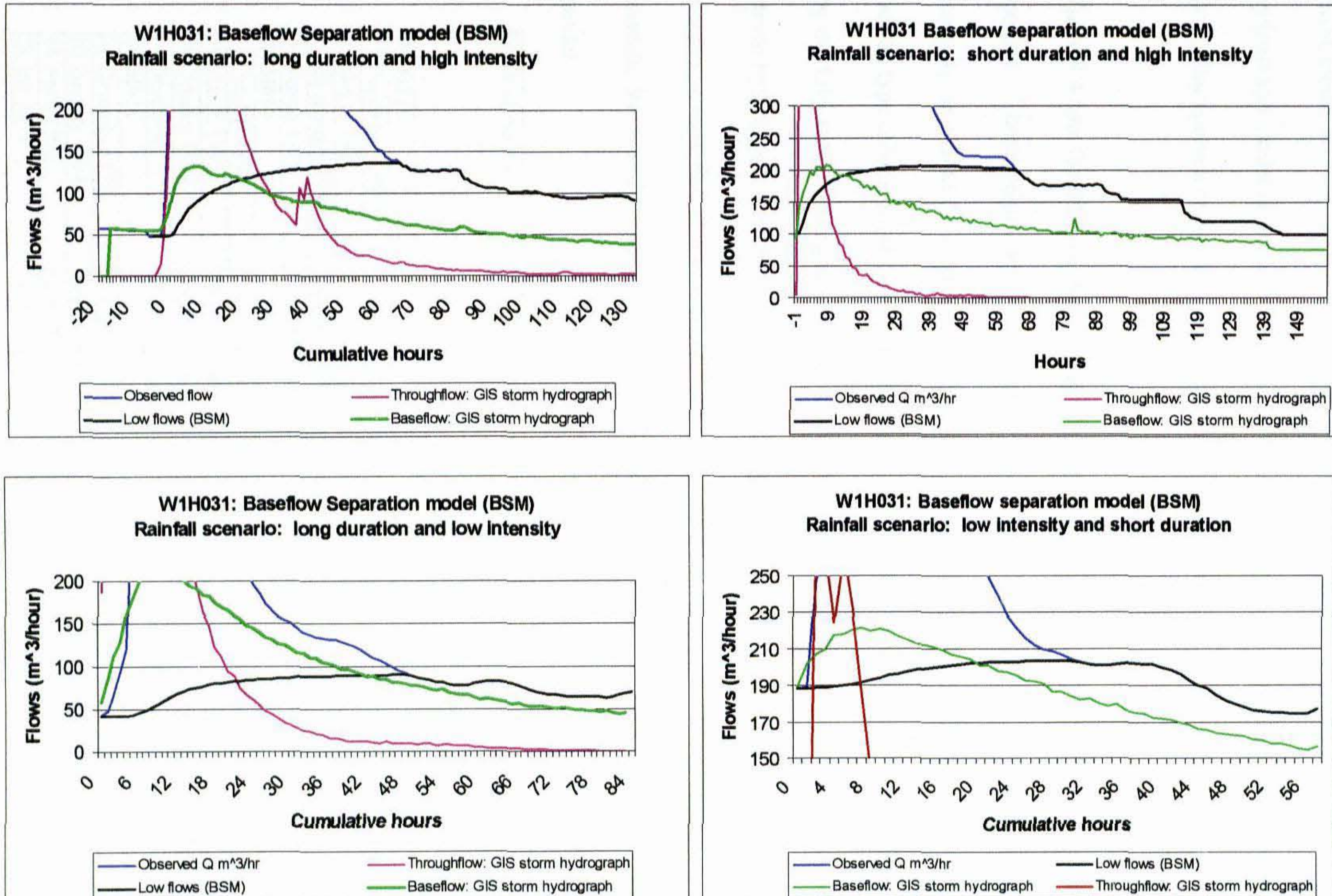

Figure 9.16: Comparison between the Baseflow Separation Model and the GIS storm hydrograph model, in the catchment of W1H031.

The graphs indicate the observed flows, the baseflow separated from the observed flows by the BSM model and the baseflow simulated by the GIS storm hydrograph model. The GIS storm hydrograph model simulates a peak in the baseflow that occurs close to the peak in the observed flow, that is much earlier than indicated by the BSM model.

Table 9.4 lists the different percentage baseflow (of the total observed flow) simulated by both models. These values are comparatively close for rainfall types of short duration and high intensity, as well as the storms of long duration and low intensity for the two catchments. For the rainfall type of long duration and high intensity, there is more baseflow indicated by the BSM than by the GIS storm hydrograph model. The observed baseflow in the river at the start of each storm hydrograph were included in these comparisons.

Table 9.4: Baseflow expressed as a percentage of the total observed flow, indicated by the two models, the baseflow separation model (Hughes et al, 2003) and the GIS storm hydrograph model.

Dates of storms:	Rainfall type:	Model	
		Baseflow Separation Model	GIS storm hydrograph model
W1H016			
15 December 1989	Long duration, High intensity	52%	29%
01 March 1995	Short duration, High intensity	13%	15%
24-25 January 1990	Long duration, Low intensity	34%	37%
16 March 1993	Short duration, Low intensity	44%	47%
W1H017			
13 October 1994	Long duration, High intensity	42%	33%
01 March 1995	Short duration, High intensity	16%	17%
29 October 1994	Long duration, Low intensity	51%	55%
04 December 1993	Short duration, Low intensity	21%	38%
W1H031			
04 December 1993	Long duration, High intensity	52%	45%
10 January 1994	Short duration, High intensity	57%	45%
26 April 1990	Long duration, Low intensity	40%	56%
21 Jan 1991	Short duration, Low intensity	79%	77%

9.5. Conclusions

This chapter has evaluated some of the results from the application of the GIS storm hydrograph model. Some discussion has been presented on the results of individual storms, and problematic characteristics of the model were summarized. More accurate results could possibly be obtained if more storm types are included in the model. Better results can also be obtained if a continuous function, relating excess rainfall (or the runoff coefficient) to the antecedent conditions during the storm simulation, can be incorporated.

****

10 Determination of the GIS storm hydrograph model for the Goedertrouw Dam catchment

This chapter examines the model application to a catchment much larger than the research catchments. The model was used to calculate the storm hydrographs, using the spatial information of the Goedertrouw Dam catchment (Figure 10.1). Some of the parameters describing the hill slope processes, that would not be derived for the Goedertrouw Dam catchment, were extracted from the analysis of observed flow in the Ntuze research catchments. These include the recession rates for the first order streams.

10.1. Spatial scaling in hydrological modelling

The process of transferring parameters from the small research catchment to a large catchment can be guided by certain scaling laws (Becker and Braun, 1999). They provided an outline for distinguishing between the vertical processes and the lateral processes when considering the issue of spatial scaling of a model. Vertical processes include the movement of water in the form of rainfall, evaporation and water in the soils (or infiltration); moving vertical through the atmosphere; moving vertical through the vegetation (by interception) and through the soils (as infiltration and percolation). Lateral processes include the horizontal movement of water along rivers, fractures and through the catchment soils as baseflow or groundwater movement.

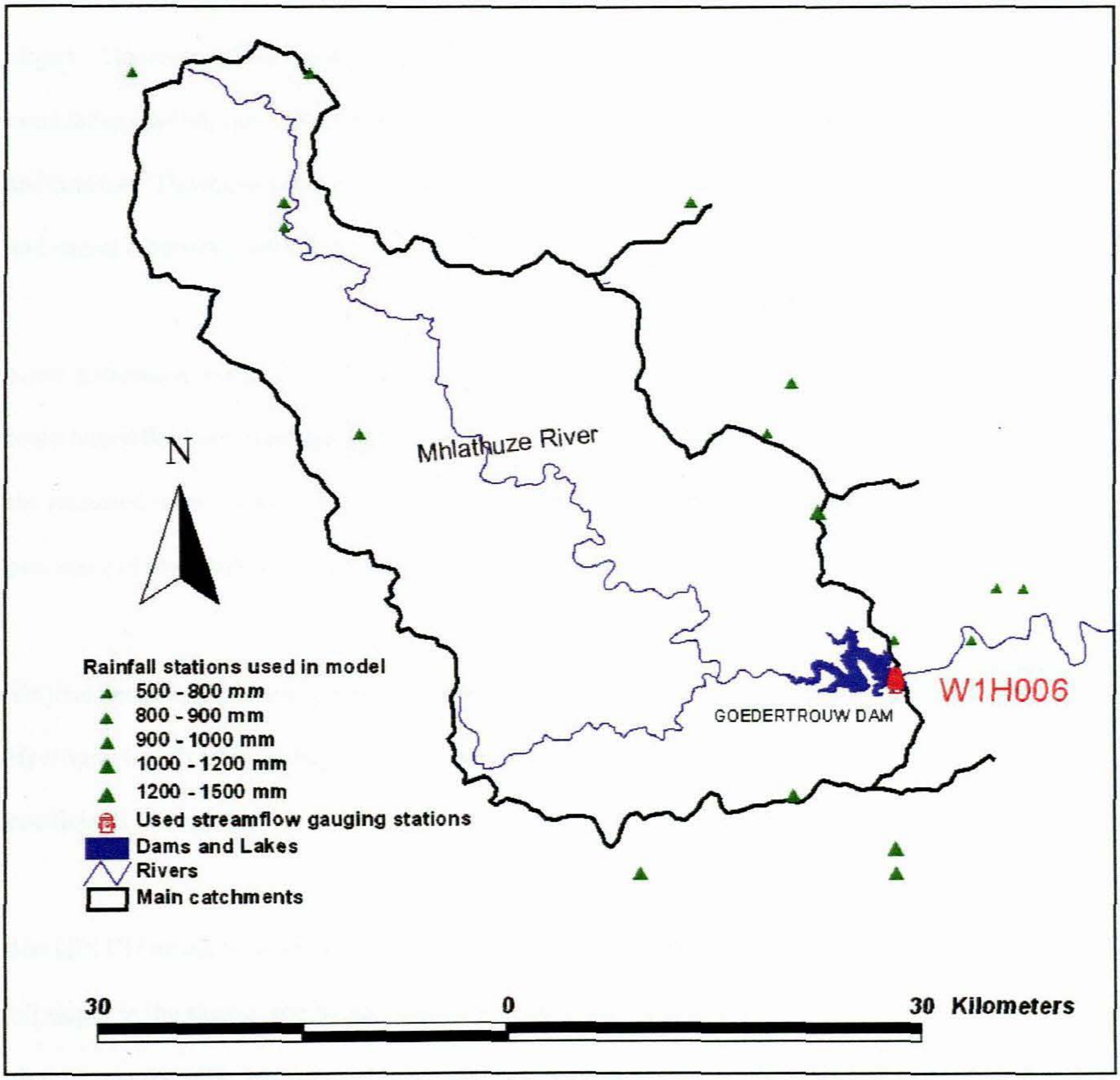

Figure 10.1: Positions of rivers, catchment boundaries and measurement stations (of flow and rainfall) in the catchment of the Goedertrouw Dam.

Becker and Braun (1999) suggested that, when modelling the vertical processes, the land use, topography and soil types are dominant features. Rainfall intensities and the hill side slopes will also play a role, as they determine the routes that the water particles will travel down the hill slopes. However, when modelling lateral processes, the important features are the drainage boundaries (rivers); catchment boundaries and aquifer boundaries; as well as the surface slopes and land use. This implies that different scaling laws will apply to parameter estimation of vertical and lateral modelling processes.

Some parameters extrapolated from the Ntuze catchments in this model application are related to the lateral flow processes along the conceptual pathways of the different flow components; i.e., the recession rates. Other parameters, such as the runoff coefficient, are related to the vertical processes of evaporation; evapotranspiration; infiltration; percolation; etc.

Vertical and lateral processes are interlinked, and this linkage is incorporated in the GIS Unit Hydrograph (GIS UH) model by the relationship between the recession rates and the time scaling coefficients (Paragraph 8.5).

The GIS UH model is based on hill slope processes; so the difference between the lengths of the hill slopes in the smaller and larger catchments will be an important feature in the simulation of all flow components. In the case of the baseflow component, the groundwater is drained from the hill slopes until it reaches a channel (a groundwater drainage boundary). Throughflow and quickflow also move along the hill slopes until both reach the river, or drainage boundary (Figure 2.1). However, if the smaller and larger catchments have similar hill slope characteristics, the modelling of flow along the hill slopes, using the GIS UH model, should also be similar.

One significant difference between a small and a large catchment is the combined lengths of channels in the catchments, that form the drainage boundaries. Channel lengths influence the simulation of all flow components, as mixing of the components happens in the channels. Parameters that are related to the lengths of the channels are the TTP and TR. These parameters will differ with different catchment sizes.

If the catchment contains fractured rocks and faults, these should also be incorporated into the model as a deviation from the preferential pathways through the hill slopes. This could have a significant influence on the hydrograph (TTP, TR, recession rates) of the flow to the drainage boundaries.

Fractured rocks and faults have not been incorporated in the application of the model, as there are no known fractures or faults in the Ntuze research catchments, for verification of the model.

The GIS storm hydrograph model assumes a homogenous rainfall throughout the entire catchment. This hardly ever happens in large catchments. Hydrological simulation models usually assume homogeneous rainfall events on subdivisions of large catchments, where each subdivision (or subcatchment) is assigned its unique homogenous rainfall series. These models then incorporate routing modules which estimate the flow processes between the different subcatchments. The GIS UH model developed for the catchment does not consider spatial modelling of the rainfall pattern.

10.2. Catchment information

The catchment of the Goedertrouw Dam drains towards the coast of northern KwaZulu-Natal, South Africa, and lies in the same geological setting as the Ntuze catchments (Figure 4.1). Table 10.1 lists some of the characteristics of the Goedertrouw Dam catchment.

Table 10.1: Summary information of catchment characteristics

Catchment characteristics	**Goedertrouw Dam catchment**
Catchment size *	1280 km^2
Annual Rainfall (mm/year) *	800 - 1000 mm/year
Annual Evaporation (mm/year) *	1400 - 1500 mm/year
Annual Runoff (mm/year) *	±100 mm/year
Land use **	40% dense trees 20% dense trees or ground cover 25% bush or sparse trees 10% sparse crop <1% bare soil 2% water
Soil types *	Sandy clay-loam to sandy clay
Morphology	Mountainous, deep river valleys
DEM: highest to lowest point (amsl) **	1590m to 200m

* Source: Midgley, Pitman and Middleton (1994).

** Source: Snyman (2000).

10.2.1. Runoff measurements

The upper reaches of the Mhlathuze River catchment drains into the Goedertrouw Dam which was previously monitored by a weir (W1H006), before construction of the dam wall between 1979 and 1982 (Figure 10.1).

Daily and monthly flow measurements were supplied by the Department of Water Affairs and Forestry (DWAF) for the gauge W1H006. This gauge was situated at the site of the present Goedertrouw Dam and measured flow records from 1964 until 1979, when the weir was closed.

A daily rainfall-runoff simulation program, the HYMAS VTI model (Hughes, Forsyth and Watkins, 2000 and Hughes, 1994) was applied to the catchment of W1H006 and extensively described in Snyman (2000). Results from this simulation were used to patch the daily flow measurements taken at weir W1H006. Estimates of the Goedertrouw Dam catchment rainfall were also taken from Snyman (2000).

10.2.2. Rainfall climate and measurements

During the main summer months from September to March, hot and humid conditions characterize the climate of the area. The midpoint of the Goedertrouw Dam catchment is about 50 km from the Ntuze catchments. These catchments experience a similar rainfall regime, as they are situated in relatively close proximity. Information about the general climatic conditions in the Goedertrouw Dam catchment area are listed in Table 10.1.

Rainfall frequently occurs as high intensity, short duration storms during the summer months between September and March. The southern catchment boundary of the Goedertrouw Dam catchment is a mountain range which forms a rainfall shadow inside the catchment of the Goedertrouw Dam. Rain clouds, that approach the catchment from the south, mostly rain on (and south of) the southern catchment boundary. However, most cumulus convection develops in the interior and is driven eastwards by the prevailing upper level western winds. Until recently, large parts of the catchment were generally inaccessible, due to poor road infrastructure. Thus, very little historic rainfall measurements are available inside this catchment for the period of simulation. Estimation of catchment rainfall is based on rainfall measured outside the catchment boundaries (Figure 10.1).

Daily rainfall time series, along with the observed daily runoff response, have been analysed for the time period from December 1970 to September 1973. It was necessary to derive a new rainfall classification scheme using daily rainfall, because hourly rainfall was not available for this catchment. Storm characteristics are illustrated in Figure 10.2, which shows the rainfall durations (in days) in relation to the maximum observed daily rainfall intensity of each event.

This information was used to classify rainfall storms into the four rainfall types used in the GIS storm hydrograph model:

1. Storms with rain intensity higher than 30 mm/day were classified as high intensity rain storms, and storms of rain intensity lower than 30 mm/day as low intensity rain storms.
2. Rain sequences of three days or longer were classified as long duration storm, and rain sequences of one or two days were classified as short duration storms. Most of the storms occurred over one or two days.

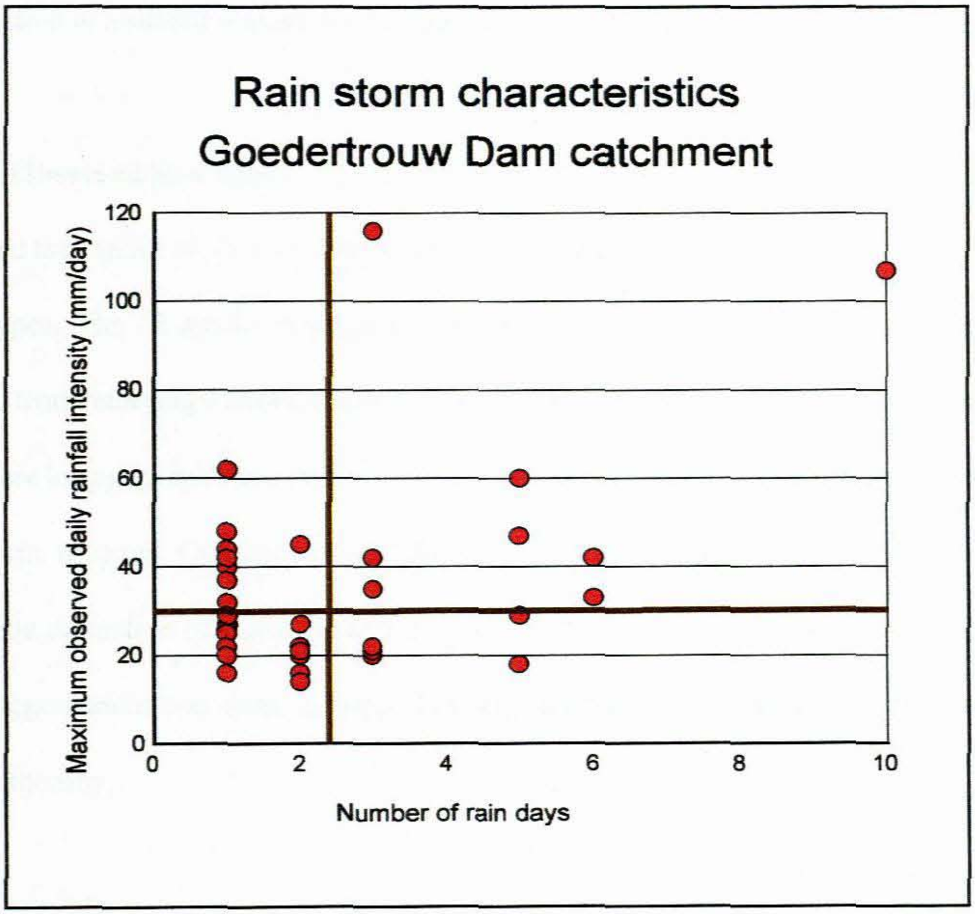

Figure 10.2: Rainfall characteristics of storms in the Goedertrouw Dam catchment.

These daily rainfall classes will differ from the rainfall classes derived form hourly rainfall and used in the runoff simulations of the Ntuze catchments. This rainfall classification scheme does not portray the storm structure that is evident in hourly rain series (Figure 4.3) and this may be a limitation of the model application, with limited rainfall data.

No hourly rain data is available for the Ntuze catchment for the time period used in Figure 10.2, to conduct an investigation of the rain event classification for daily and hourly time steps. The classification of rainfall event types derived from daily rainfall series needs further investigation in the model application. However, it is assumed that the classification of rain events according to hourly rain data (Figure 4.3), and the classification according to daily data series (Figure 10.2) will function in a similar manner for the application of the model.

10.2.3. Observed flow times

Observed time series of flow rates were analysed to estimate mean TTP and TR, for different rain storm types. The TR are not easily identifiable, due to subsequent rainfall events, which restricts the flow from returning to the initial flow rates, before the next rainfall event. On some occasions there were long gaps between storms, so that the flow returned to pre-event flow rates before the next storm occurred. Only storms with rain intensities of more than 10mm/day were considered during the evaluation of storm durations. The selected storms are listed in Table 10.2. Storm type categorization was done as suggested in Paragraph 10.2.2, using the maximum observed rainfall intensity.

The TTP and TR to pre-storm flow conditions are listed in Table 10.2 together with the average for each storm type. Long duration rain storms generally tend towards a longer observed TTP (more than two to three days), while the shorter duration storms tend towards a shorter observed TTP (one or two days). These observed TTP's were utilized to evaluate the GIS storm hydrograph model.

Table 10.2: Details of some observed storms in the catchment of the Goedertrouw Dam, including times to peak (TTP) and times to recede (TR) to pre-storm flows.

Storm type	Date	Rainfall (mm)	Nr of rain days	Max observed rain intensity (mm/day)	TTP (days)	TR (days)
Long duration, high intensity	1969/03/2	111.6	3	65.0	3	14
	1968/12/0	156.0	7	44.8	2	14+
	1967/11/1	79.9	3	43.1	3	10+
	1968/03/0	94.8	8	38.9	4	12
	1965/06/1	71.8	3	36.4	6	20
	1971/10/0	91.5	3	35.7	3	5+
Average TTP for long duration, high intensity storms:					3.5	
Long duration, low intensity	1967/10/2	77.4	4	33.6	4	10
	1978/11/1	77.4	9	29.5	1	14+
	1969/09/2	57.7	3	24.0	3	6
	1978/11/1	76.4	5	20.4	6	9+
Average TTP for long duration, low intensity storms:					3.5	
Short duration, high intensity	1971/05/1	144.0	3	116.3	1	20+
	1970/09/2	78.3	2	66.9	1	8+
	1969/10/1	108.0	2	82.6	2	5+
	1970/09/2	78.3	2	66.9	2	5
	1970/02/0	42.5	1	42.5	1	5
	1966/11/0	41.0	1	41.0	2	6
Average TTP for short duration, high intensity storms:					1.5	
Short duration, low intensity	1971/02/0	27.3	1	27.3	1	2
	1971/02/1	43.4	2	27.3	1	6
	1970/02/1	34.8	2	25.1	1	6
	1971/10/2	24.9	1	24.9	1	4
	1965/07/1	19.5	1	19	1	14
	1969/01/2	15.0	1	15.0	1	5
	1971/03/0	26.4	2	14.3	1	6
Average TTP for short duration, low intensity storms:					1	

10.2.4. Catchment morphology, the DEM and soil profile

The topographical features of the catchment have been captured in a DEM for the entire Mhlathuze River catchment, at a scale of 125m X 125m pixel size, from 100m contours (Figure 10.3).

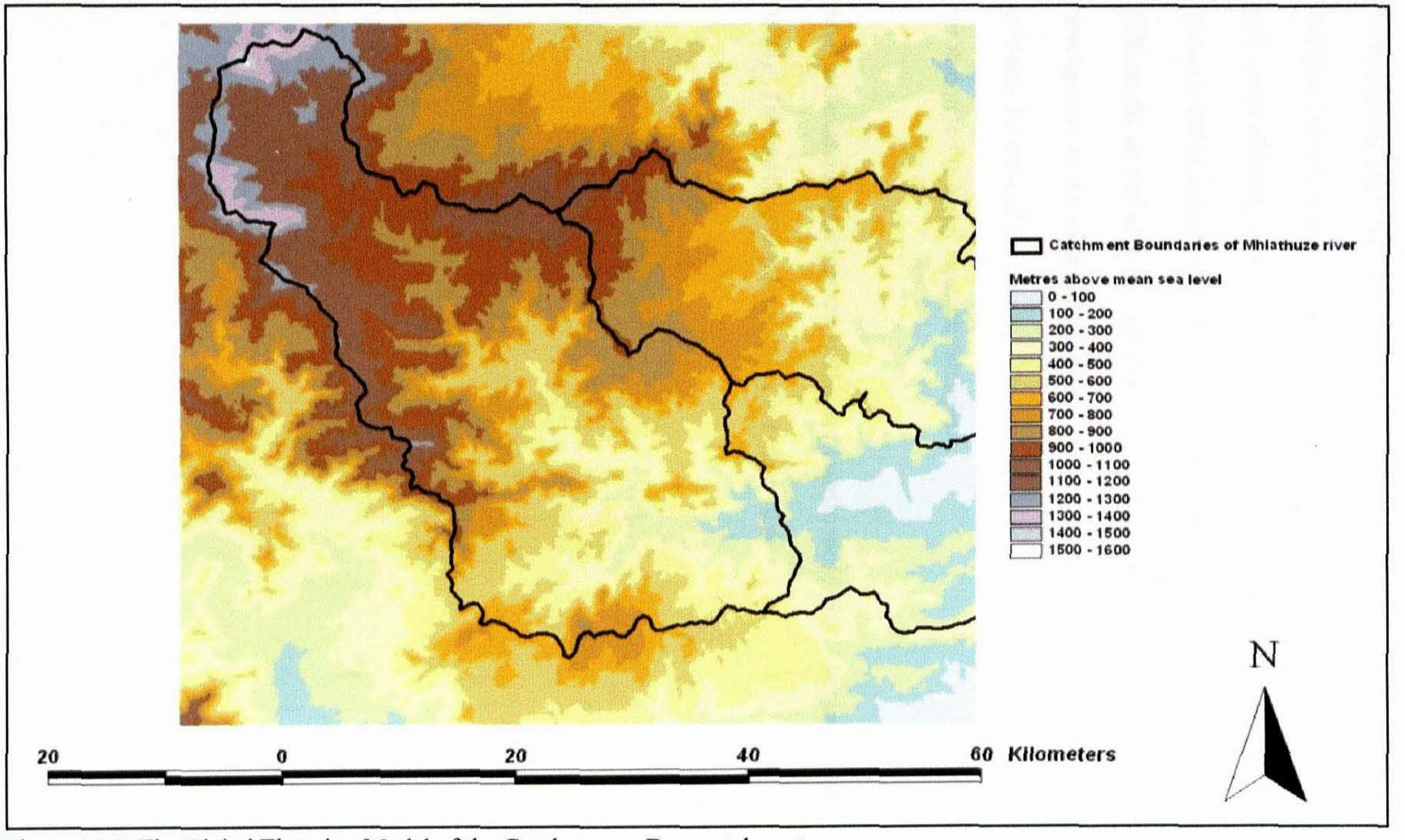

Figure 10.3: The Digital Elevation Model of the Goedertrouw Dam catchment.

Investigations into the effect of grid scale on hydrological modelling was accomplished by Refsgaard (1997), using the distributed SHE (Système Hydrologique Europèen) model. He used grid scales of 500m, 1000m, 2000m and 4000m. He concluded that not much improvement in accuracy will be attained by grid scales finer than 500m. However, his studies were limited to the SHE model; as well as to one research catchment (dominated by groundwater flows). Since the development of the model, the National Department of Survey and Mapping can provide 5m contours for most of the country. This would allow a DEM to be created that was at the same resolution to the Ntuze research catchments.

Soils in the catchment are mostly sandy-clay-loam to sandy-clay (Midgley, Pitman and Middleton, 1994). The soil type map is displayed in Figure 10.4.

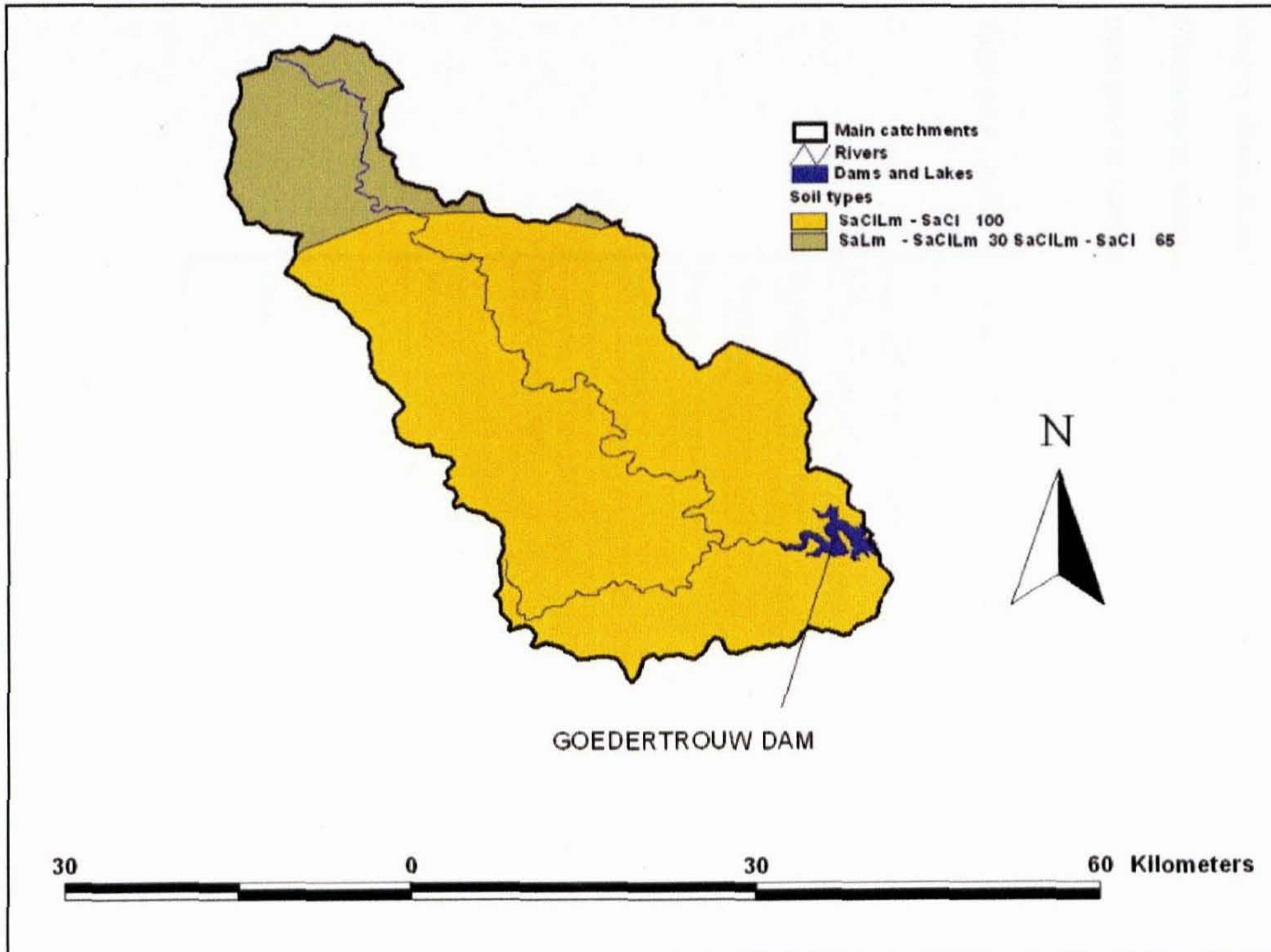

Figure 10.4: Soil types of the Goedertrouw Dam catchment (from Midgley *et al*, 1994).

10.2.5. Land use

Land use for the Goedertrouw Dam catchment was derived from 25m by 25m Landsat Satellite imagery, dated 22 April 1996 (Snyman, 2000). Analysis of this imagery using the Supervised Classification, Maximum Likelihood method by Snyman (2000) indicated 11 different land use types given in Table 10.3 and shown in Figure 10.5.

Table 10.3: Percentage areas of different land uses in the Goedertrouw Dam catchment:

Surface conditions	% Area
Mature sugarcane	1
Recently cut sugarcane	<0.1
Plantations (mature trees)	14
Plantations (recently cut)	11
Natural bush	28
Natural forest	23
Natural grassland	20
Rivers and sand banks	<0.1
Roads	0.5
Tilled farm lands	<0.1
Water	2.5
Total catchment area:	100% ($1280\ km^2$)

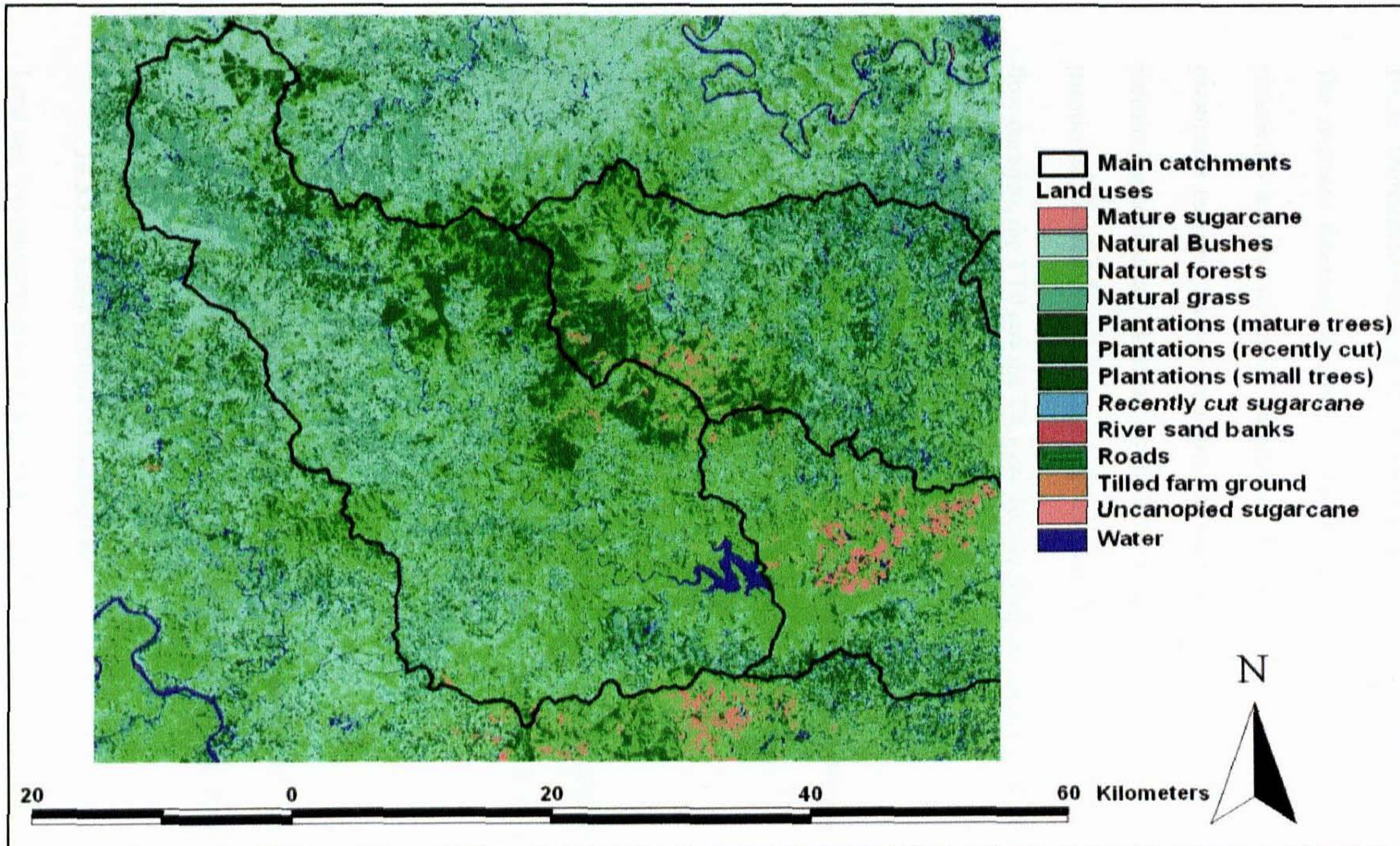

Figure 10.5: Land uses in the catchment of the Goedertrouw Dam (from Snyman, 2000).

10.3. Determination of the GIS storm hydrograph

The response functions for each of the flow components was estimated from the Ntuze parameters and the spatial information of the Goedertrouw Dam catchment. Transferred parameters included the recession rates of each flow component. Calibrated values of the partitioning coefficients from the Ntuze River simulations were used as first estimates of the partitioning coefficients for the Goedertrouw Dam catchment simulations. However, the storm flow duration, the TTP and the TR were derived from observed catchment flow.

10.3.1. Flow times of the quickflow component

The travel time along the quickflow pathways over individual pixels was calculated from equation 7.5. Estimates of the parameters in the equation are discussed below:

10.3.1.1. Slopes

Areas with zero slope occur mostly along the river valleys and on catchment ridges. Areas of zero slopes were given a minimum slope value of 0.01%. The mean slope of the catchment is 5.8 degrees, or 13%, with the mode at 1% slope.

10.3.1.2. Slope lengths

The flow direction of water across pixels in the DEM were derived from pixel dimensions of 125m (for flow parallel to pixel edges) or 177m (for a flow diagonal across the pixel).

10.3.1.3. Land use and Manning's n

Land use was taken from a satellite imagery of the catchment area, as discussed earlier. Table 10.4 lists the eleven different land use classes, with their assumed values of Manning's *n* (Snyman, 2000).

Table 10.4: Values used for Manning's n (Chow et al, 1988; Wilson, 1983):

Surface conditions	n
Mature sugarcane	0.07
Recently cut sugarcane	0.02
Plantations (mature trees)	0.1
Plantations (recently cut)	0.025
Natural bush	0.07
Natural forest	0.1
Natural grassland	0.05
Rivers and sand banks	0.025
Roads	0.018
Tilled farm lands	0.04
Water	0.01

Although the original satellite imagery's resolution is 25m by 25m, it was reduced to the resolution of the DEM (125m by 125m); using a method of pixel thinning (using only every fifth pixel in the X and Y directions).

10.3.1.4. The adapted hydraulic radius

Different classes of rivers were delineated by using the contributing area of each pixel, i.e., *a* from equation 7.4. These river classes are illustrated in Figure 10.6. Approximately 30% of the catchment area contains with no upstream catchment area. These represent the ridges between the drainage boundaries. The dark brown pixels are generally first order streams, while the main river course of the Mhlathuze River is delineated as the blue line.

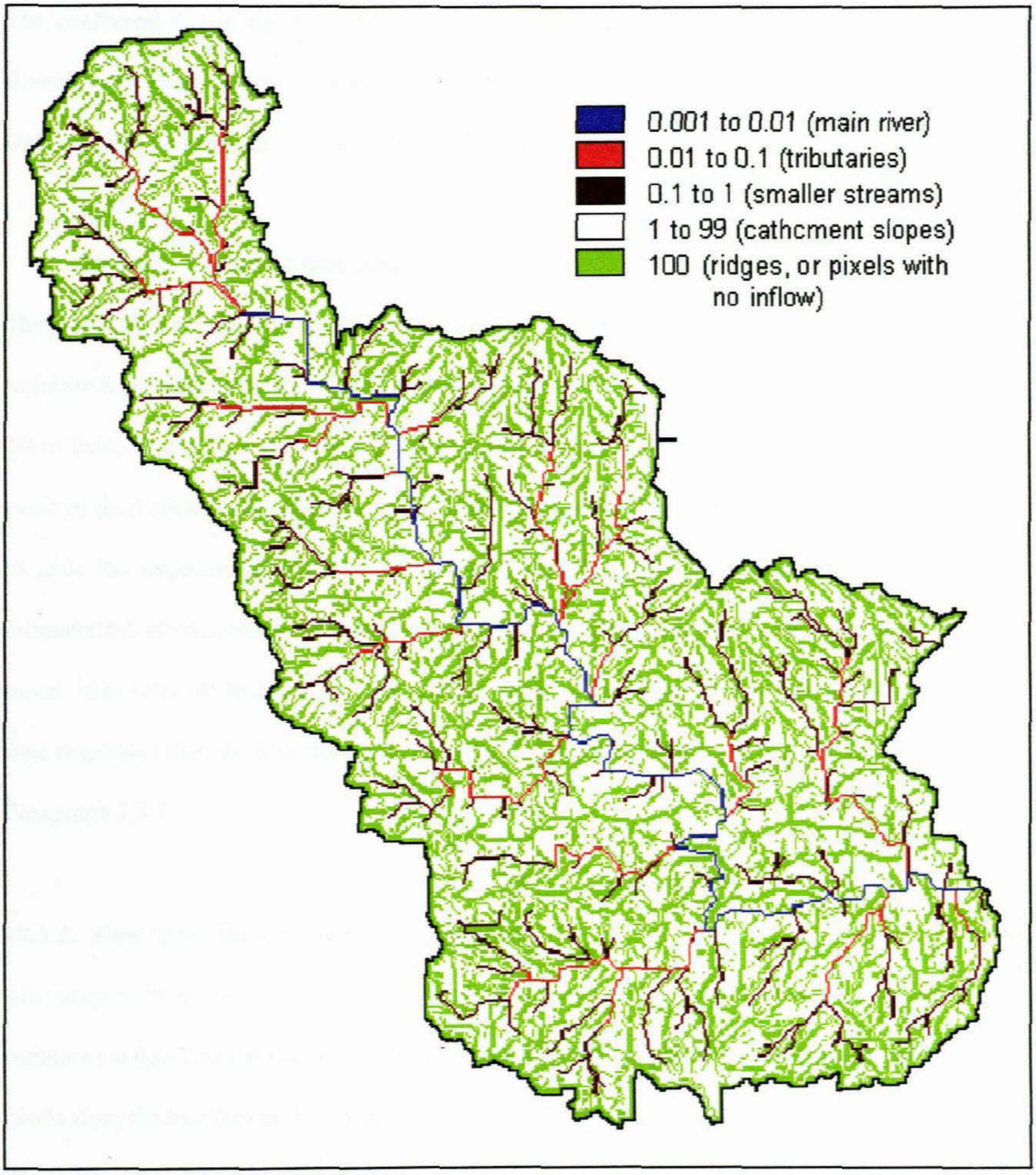

Figure 10.6: A map of the Goedertrouw Dam catchment, indicating the inverse of the percentage contributing areas of each pixel, or (one pixel area)*100/*a*.

The coefficient C_Q in equation 7.4 was estimated to be 5,874,000 m^2 (5.8 km^2) for the Goedertrouw Dam catchment. Values for the adapted hydraulic radius R_a in the Goedertrouw Dam catchment (equation 7.4) vary between 10^{-7} m and a maximum of 3.38 m at the outlet.

10.3.1.5. Estimated flow times

The time scaling coefficient was used to calibrate the estimated total travel times of the travel time response functions against the observed total storm flow durations (i.e., the total of the TTP and TR in Table 10.2). $T_{SQ} = 0.05$ was utilized to scale the quickflow response function for a rainfall event of short duration and high intensity. Generally, T_S values between 0.05 and 0.5, were used to scale the response functions of the quickflow and throughflow components. Pixels that estimated travel velocities faster than 1 m/s were those along the main river in the catchment. The travel times were calculated in minutes and converted to daily time units to calculate the travel time response functions with daily time steps, to overcome the numerical problem described in Paragraph 7.3.2.

10.3.2. Flow times along the baseflow pathways

The adapted flow model using Darcy's Law (equation 7.7) for groundwater was utilized to estimate the flow times along the baseflow pathways for the Goedertrouw Dam catchment. The pixels along the baseflow surface with values of zero slopes were given a minimum value of 0.1%. The mean slope of the baseflow surface was calculated at 12%, with the mode at 1%.

The hydraulic conductivity K was assumed to be 0.1 m/day throughout the catchment, for the sandy-clay-loam to sandy-clay soils of the catchment (Paragraph 10.2.3). In equation 7.6 (the adapted hydraulic conductivity), the value of C_B was calibrated, by comparing the total travel times, estimated from the GIS UH model, to the estimated total travel time of baseflow. After calibration, the mode of the travel times along the baseflow pathways was estimated at 34 hours per pixel. The model limitations (as discussed in Paragraph 7.3.2) prohibited shorter travel time estimations for baseflow simulations.

10.4. Cumulative travel times along the flow pathways

The individual travel times were integrated along the flow pathways of the different flow components to provide a grid of cumulative travel times. The frequency histogram of the cumulative travel times, or the response function, for each flow component and each storm type, was determined.

10.4.1. Model limitations

The cumulative travel times of water down the catchment slopes were calculated from the individual travel times over pixels, using the HYDTIME program. In the description of the HYDTIME program (Paragraph 7.3), the problem of the integer values used during the calculation of cumulative travel times was discussed. These integer values can vary between zero and 32676, a range that is not adequate enough to describe the cumulative travel times of large catchments. This limitation of the HYDTIME program was more evident in the bigger catchment of the Goedertrouw Dam (with longer travel times) than in the smaller Ntuze River catchments. It was partly overcome by using different travel time units for different travel time scenarios.

The travel time of water down a river pixel of 125m length would be approximately two to four minutes (for a travel velocity of 1 to 2 m/s under storm conditions). Thus, the travel times of water over individual pixels was calculated in minutes. Using hourly time units meant that these values would be rounded to zero travel times over river pixels.

By changing the time units (or time steps), the problem of scaling travel times between the minimum and maximum travel times was largely overcome.

10.4.2. Response functions

It has been proposed that the flow times of all flow components are related to the recession rates of the response functions. Time scaling coefficients were used to evaluate different response functions, for different recession rates. Figure 10.7 provides the graphic display of the response functions estimated for the Goedertrouw Dam catchment, for different time scaling coefficients, utilizing both the Manning's equation and Darcy's Law.

The response functions (frequency distributions) were all calculated using daily time steps (which is the same as the observed hydrograph time steps) before being transformed to flow rates. The

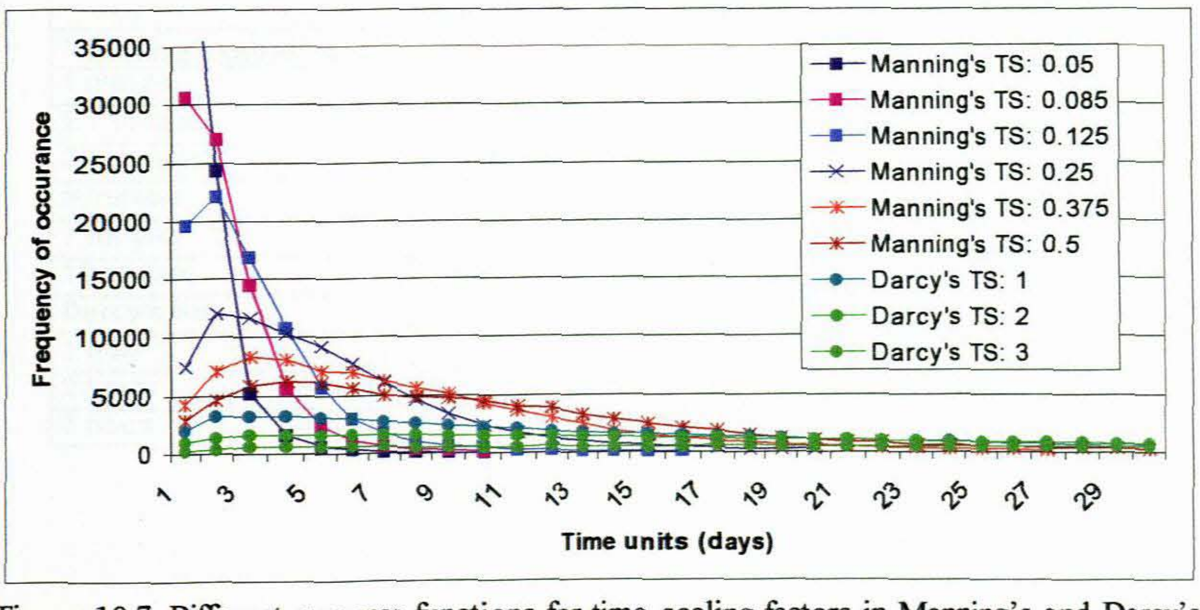

Figure 10.7: Different response functions for time scaling factors in Manning's and Darcy's equations.

relationship between the recession rates and the time scaling coefficients are plotted in Figure 10.8, and listed in Table 10.5.

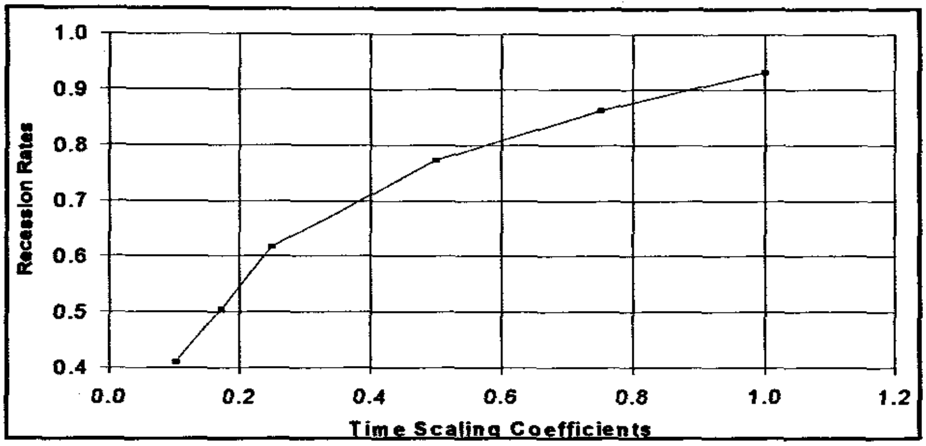

Figure 10.8: Recession rates estimated from response functions, plotted against the time scaling coefficients of each response function, using the Manning's equation to estimate the quicker flow components.

Table 10.5: Mean recession rates for the different time units, each having a different time scaling coefficient T_s:

Time units or time steps	Time scaling coefficients	Recession Rates	Flow component
Manning's equation:			
1 minute	0.05	0.42	Quickflow
1.7 minutes	0.085	0.53	
2.5 minutes	0.125	0.6	
5 minutes	0.25	0.75	
7 minutes	0.375	0.82	Throughflow
10 minutes	0.5	0.91	
Darcy's law:			
1 hour	1	0.95	Baseflow
2 hours	2	0.98	
3 hours	3	0.99	

10.4.3. Recession rates and partitioning coefficients

The different recession constants and the partitioning coefficients for flow components, as determined for the Ntuze River catchment, were transferred to the catchment of the Goedertrouw Dam. Response functions, for the different flow components in the Goedertrouw Dam catchment, were established from the Ntuze parameters by taking the average of the parameters from the three research catchments, for each of the rainfall types (Tables 5.10 and 5.11). The derived parameters for the four rainfall types are summarized in Table 10.6, along with the times scaling coefficients T_s which were derived for these recession rates (from Table 10.5).

Table 10.6: Parameters transferred from the Ntuze research catchment to the Goedertrouw Dam catchment, along with the time scaling coefficients T_s.

Rainfall Type	Flow component	Partitioning coefficients (percentage)	Recession rates	Time scaling coefficient
High intensity, long duration	Quickflow	50%	0.66	0.125
	Throughflow	30%	0.82	0.375
	Baseflow	20%	0.98	2
High intensity, short duration	Quickflow	40%	0.51	0.085
	Throughflow	30%	0.82	0.375
	Baseflow	30%	0.98	2
Low intensity, short duration	*Quickflow not present*			
	Throughflow	50%	0.76	0.25
	Baseflow	50%	0.98	2
Low intensity, long duration	*Quickflow not present*			
	Throughflow	50%	0.79	0.375
	Baseflow	50%	0.99	3

10.5. Derivation of the response functions

The response function for each flow component, for each rainfall type, was normalized for catchment size and pixel resolution (equation 8.1), and converted to flow in cubic metres per second for one unit of excess rainfall (equation 8.4). The different flow components for each rainfall type were combined to estimate the total simulated response functions for each rain type. These unit response functions, for different rain storm types (Figure 10.9), were the input to the storm simulations for the Goedertrouw Dam catchment, using the classified rainfall types. The TTP of the unit travel time response functions are listed in Table 10.7.

Table 10.7: Estimated times to peak (TTP) from the unit travel time response functions for the catchment of the Goedertrouw Dam:

Rainfall type	Estimated TTP (days)
High intensity, long duration,	2
Low intensity, long duration,	3
High intensity, short duration,	1
Low intensity, short duration,	2

These TTP's for the Goedertrouw Dam catchment results from much longer travel path lengths (along the channels) than the Ntuze catchment.

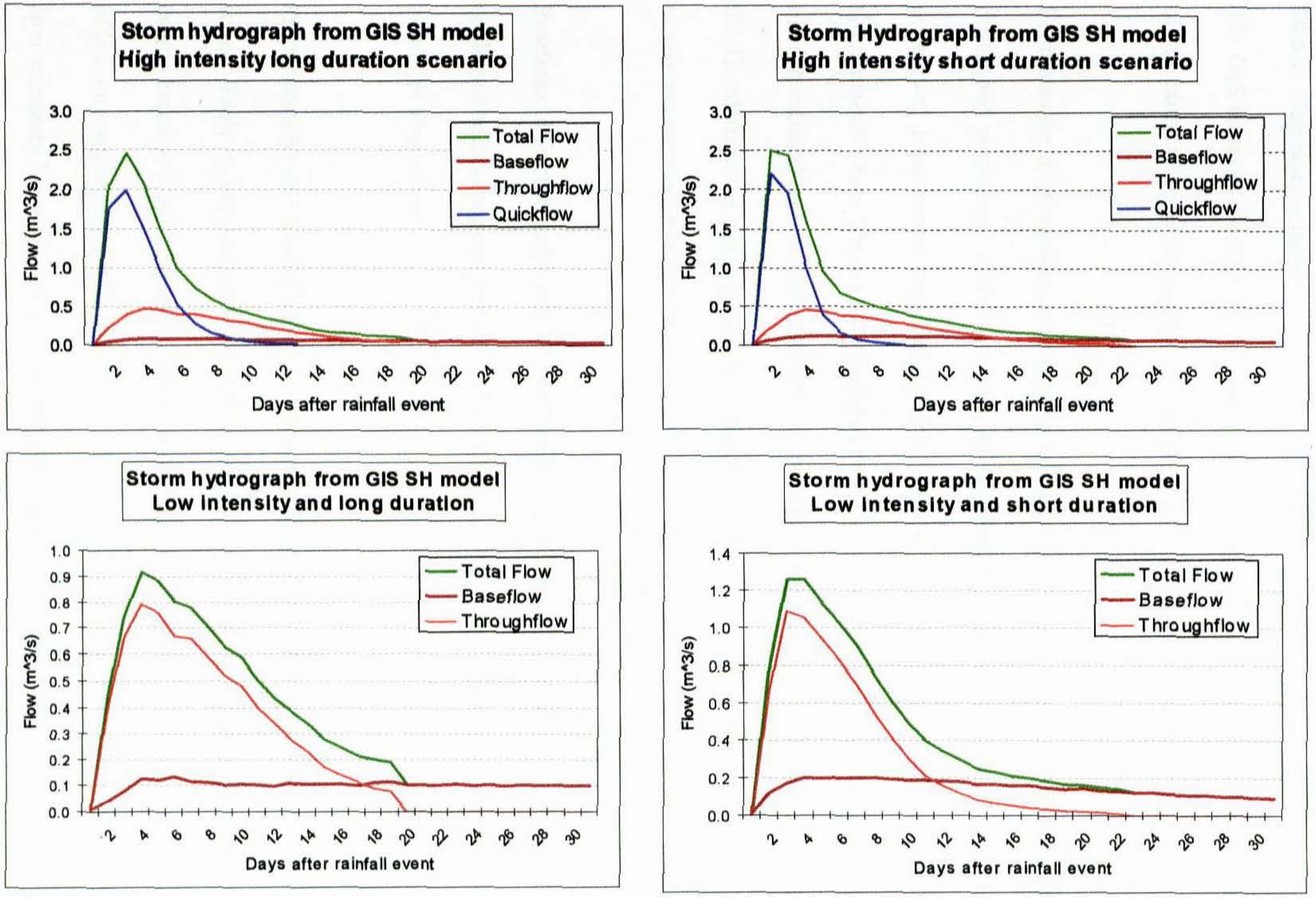

Figure 10.9: Unit storm hydrographs simulated at the outlet of the Goedertrouw Dam catchment, for the different rainfall types.

10.6. Simulation of a series of storms

10.6.1. Simulation input

The GIS storm hydrograph model was applied to the Goedertrouw Dam catchment for a series of rain storms during the summer of 1 Oct. 1971 to 31 March 1972.

Estimates for the Goedertrouw Dam's catchment rainfall were taken from the HYMAS model developed by Snyman (2000) for the greater Mhlathuze River catchment. Snyman (2000) developed a catchment rainfall time series for each of seven subcatchments defined for the Goedertrouw Dam. These seven rainfall records were averaged and weighed according to the size of each subcatchment to calculate the catchment rainfall time series for the whole catchment of the Goedertrouw Dam. In the simulations of the outflow, it was assumed that the entire catchment received this rainfall in a uniform manner.

Positions of fractures and faults in the Goedertrouw Dam catchment were not available so they could not be incorporated in the runoff simulations. This would have significantly influenced the baseflow simulations.

Preparation for the simulations included a classification of the storm events in the rainfall time series. Table 10.8 indicates storms and their classification, along with other information. Rainfall events between 5 and 10 mm/day, which were not listed in Table 10.8, were simulated as storms of low intensity and short duration. The daily water use of trees in the area was estimated to be approximately 5 mm/day on hot summer days during January, February and March (Ettienne Boeke, Natal Irrigation Consultants, personal communications). Therefore, storm events of less than 5 mm/day were ignored.

Simulation of the runoff from the Goedertrouw Dam catchment was obtained by using the same simulation method of the Ntuze River runoff simulations.

Table 10.8: Details of the rainfall events bigger than 10 mm in the simulation period.

Dates	**Rain**	**Nr. of rain days**	**Maximum observed rainfall intensity**	**Rainfall type**	**Ratio: (Excess rain)/ (Measured rain)**
	mm	days	mm/day		
29-Oct-71	11.8	1	11.8	Low intensity, short duration	0.042
01-Dec-71	53.1	3	35.5	High intensity, long duration	0.040
09-Dec-71	51.9	5	14.2	Low intensity, long duration	0.126
10-Jan-72	37.1	3	19.6	Low intensity, long duration	0.113
14-Jan-72	27.1	2	19.0	Low intensity, short duration	0.149
20-Jan-72	65	3	29.9	Low intensity, long duration	0.312
03-Feb-72	27.4	2	16.5	Low intensity, short duration	0.133
16-Feb-72	16	1	16.0	Low intensity, short duration	0.097
21-Feb-72	139.2	5	44.4	High intensity, long duration	0.442
04-Mar-72	15.9	1	15.9	Low intensity, short duration	0.493
18-Mar-72	12.2	2	19.4	Low intensity, short duration	0.469

10.6.2. Calibration and results from the simulations

Figure 10.10 shows the observed and simulated flow series for the Goedertrouw Dam catchment, along with the estimated catchment rain time series. Figure 10.11 shows the cumulative plots of the simulated and observed daily runoff, along with the corresponding daily rainfall. Table 10.9 lists the calibrated parameters of the Goedertrouw Dam simulations.

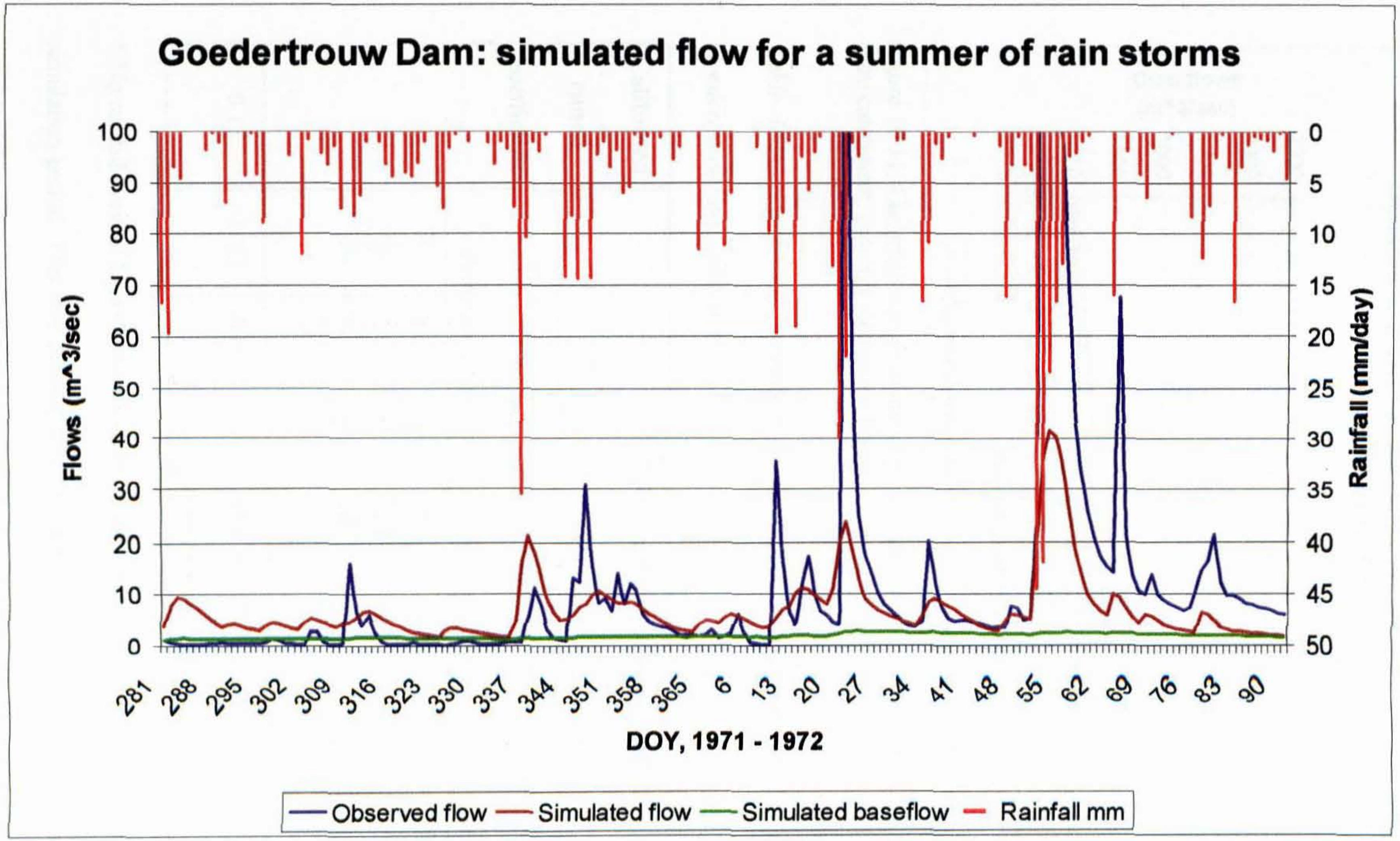

Figure 10.10: Graphic display of the simulated and observed outflow, as well as simulated baseflow, from the Goedertrouw Dam catchment, for the time period 1 Oct. 1971 until 31 Mar. 1972.

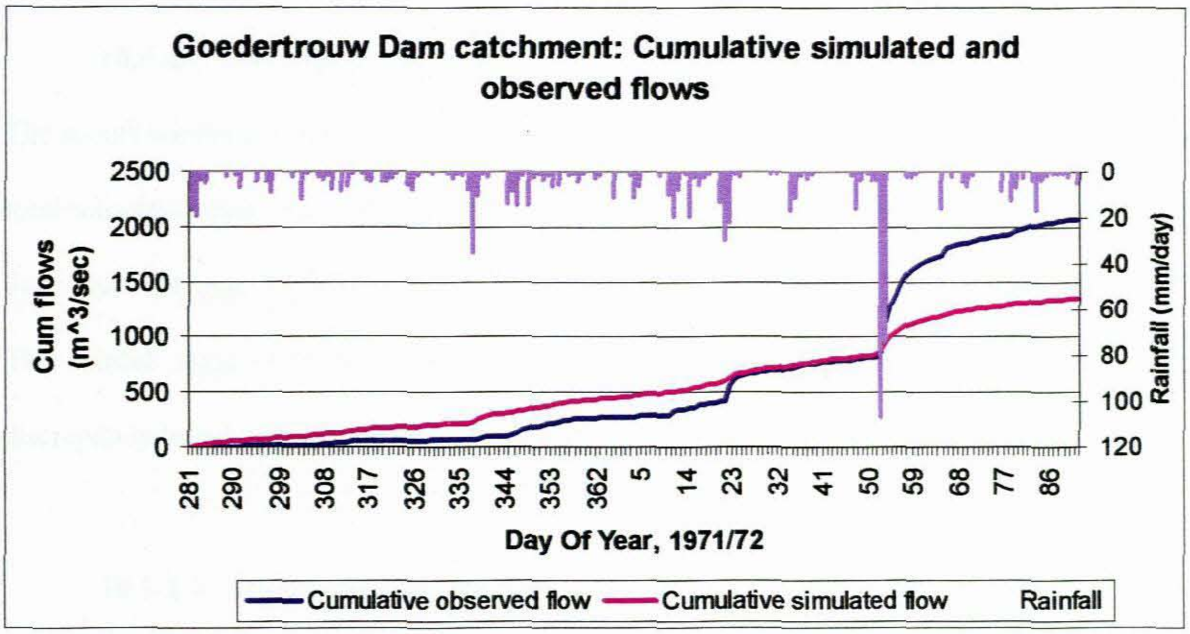

Figure 10.11: Cumulative plots of the simulated and observed flows from the Goedertrouw Dam catchment, over the simulation period.

Table 10.9: Calibrated parameters of GIS storm hydrograph model simulations for the Goedertrouw Dam catchment.

Calibrated runoff coefficient	**Calibrated partitioning coefficients** (expressed as percentages)									
	High intensity Long duration			*High intensity Short duration*			*Low intensity Short duration*		*Low intensit[y] Long dur[ation]*	
	Baseflow	Throughflow	Quickflo	Baseflow	Throughflow	Quickflo	Baseflow	Throughflow	Baseflow	Throughflow
0.13	10%	20%	70%	30%	30%	40%	20%	80%	20%	80'
				Parameters not calibrated *						

* No rainfall event of high intensity and short duration was measured in the catchment during the simulation period. This was possibly due to the rainfall classification scheme built on a daily rainfall series.

10.6.2.1. The runoff coefficient

The runoff coefficient was adjusted to a value of 0.13, to create similar observed and simulated total cumulative flow, over the calibration period from the beginning (DOY 281, 1971) up to the day before the huge rainfall event, starting on DOY 52 (21 Feb.) 1972, shown in Figure 10.11. This rainfall event (140 mm of rainfall over five days, see Figure 10.2) produced a large discrepancy between the observed and simulated time series.

10.6.2.2. Partitioning coefficients

In the simulation of the Goedertrouw Dam catchment, values for the baseflow's partitioning coefficients range between 10% and 30% (Table 10.9). This is in contrast with the findings of Mulder (1988). Mulder measured the amount of quickflow, throughflow and baseflow for a hill slope in the Mhalthuze River catchment with similar characteristics to the hill slopes of the Ntuze catchments. Mulder's results indicated that more than 90% of the storm flow hydrograph originates from baseflow.

However, Mulder's findings raise some questions about the GIS UH model's calibrated values for the partitioning coefficients, both for the catchment of the Ntuze River and the Goedertrouw Dam. Both sets of parameters (Tables 5.10 and 10.9) indicate a lower percentage of simulated baseflow in the channel at the catchment outlet, than estimated by Mulder (1988).

10.6.2.3. Limitations of the model

Figure 10.10 indicates that the estimated catchment rainfall does not correspond with the observed runoff, with the exception of one or two storms. Since the simulated runoff series is built on the catchment rain series, his will induce a poor correlation between simulated and observed runoff.

Generally, the model does not simulate storm hydrographs with sharp rising peaks and quick recessions (Figure 10.10). This could be attributed to simulated travel times over individual pixels that are generally too slow. The limitations of the model (described in Paragraph 7.3.2) did not allow quicker travel times and the rainfall classification excluded the storm type that will most likely generate these conditions. A routing function, allowing quicker routing of flow from subcatchment to subcatchment, down the catchment's channels, will also improve the simulations.

There is recorded rainfall on DOY 281 (7 Oct.) 1971 and DOY 337 (2 Dec.) 1971, but no corresponding flow response (Figure 10.10). The model could not simulate the high peaks in the observed flow which occurred after the high rainfall events of DOY 20 (20 Jan.) 1972 and DOY 52 (21 Feb.) 1972. The cumulative plots (Figure 10.11) indicate less details of changes in the simulated flow than in the observed flow. Details of the catchment and its flow processes, which are not incorporated into the model, include the fractures and faults in the catchment, as well as spatial rainfall variability.

10.6.3. Discussion of individual storm hydrograph simulations

Individual graphs of the storms listed in Table 10.8 are presented in Figures 10.12 and 10.13, in chronological order. All flows in these figures are plotted on log axis.

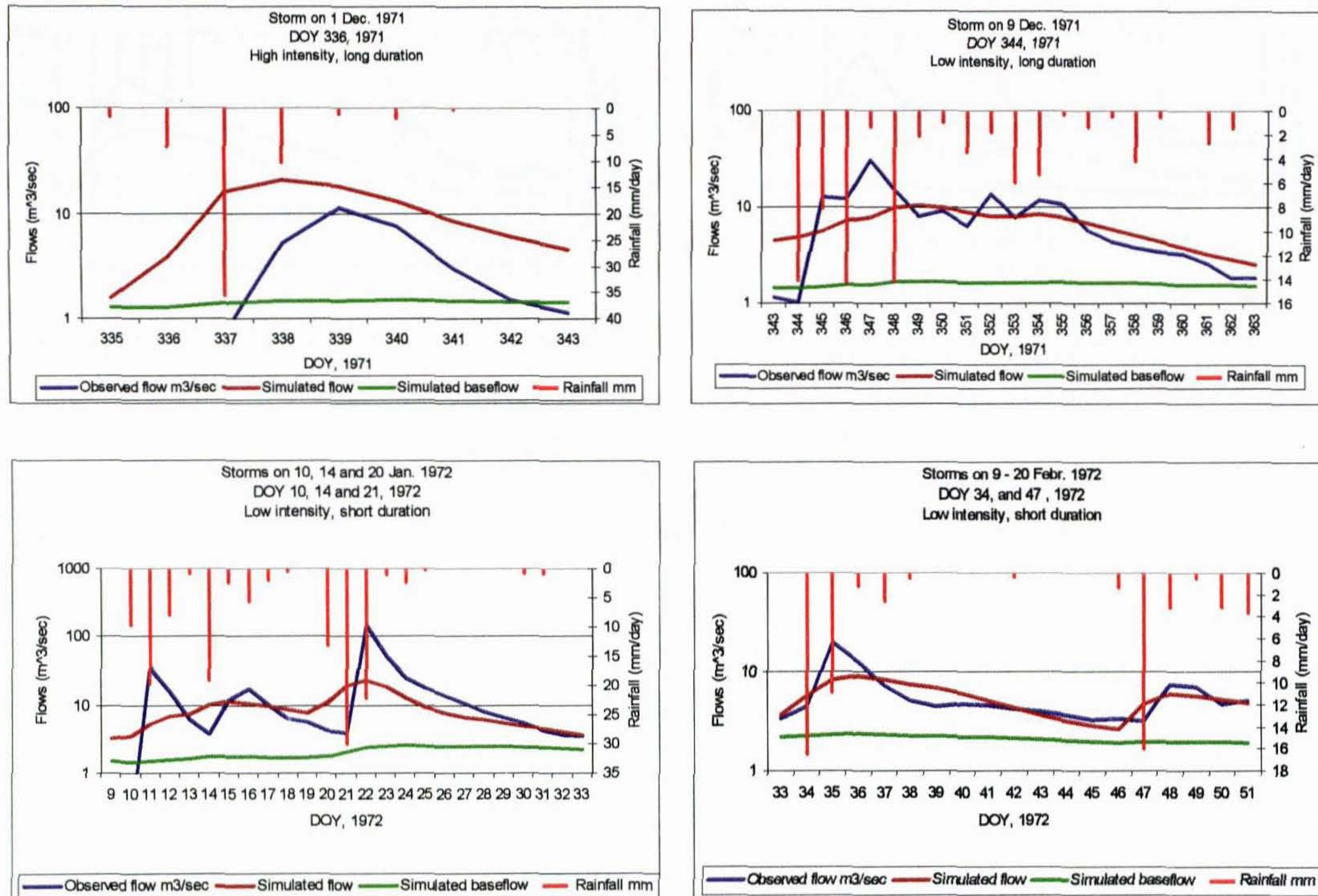

Figure 10.12: Simulated and observed storm hydrographs of individual storms in the catchment of the Goedertrouw Dam.

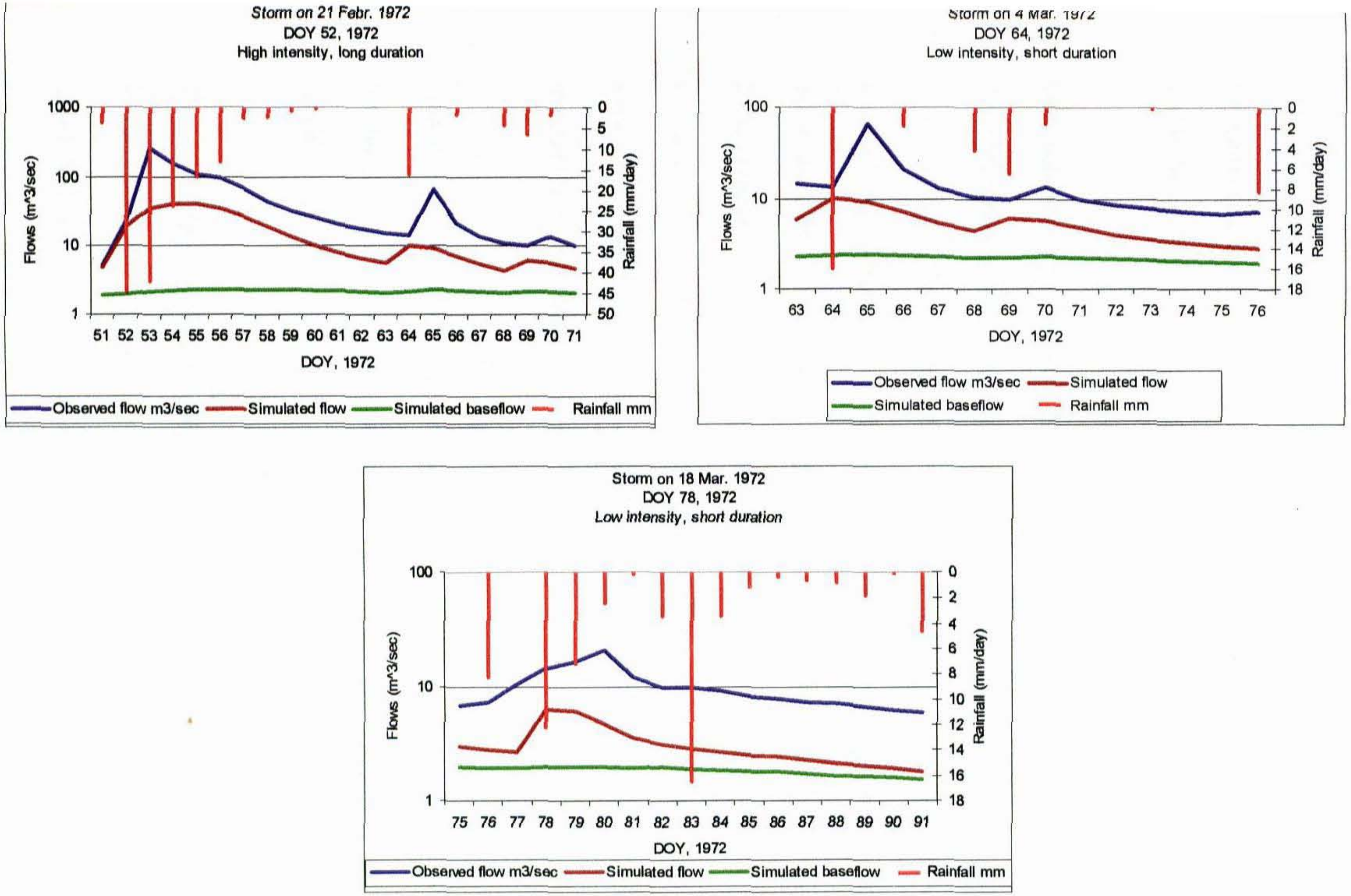

Figure 10.13: Simulated and observed storm hydrographs of individual storms in the catchment of the Goedertrouw Dam.

10.6.3.1. Catchment rainfall unevenly distributed in the catchment

The GIS storm hydrograph model assumes an even spatial distribution of catchment rainfall throughout the entire catchment. This is not the case in a large catchment, where it often happens that it rains on a portion of the catchment.

One method to estimate catchment rainfall is to use the area-weighted averages of rain from different rainfall gauges, where each rain gauge estimates rain on the section of the catchment in its direct vicinity. For example, the simulated outflow can be influenced profoundly if the model assumed that the estimated catchment rainfall (e.g., 20 mm) is uniformly distributed over the entire catchment, when in reality the rainfall was much more (100 mm), on only a fraction, say 20%, of the catchment. The same inherent problem is found in lumped rainfall runoff models. It is suggested that a reason for the difference between the simulated and observed hydrographs for some storms, could be related to the spatially variable rainfall, which is estimated by a spatially invariant rainfall distribution.

Spatially variant catchment rainfall should be incorporated in the GIS storm hydrograph model for application to large catchments. This can be done using a semi-distributed model of the rainfall.

The upper limit of the size of these subcatchments would depend on the size of storms in the area. Kelbe (1984) indicated that the average rain storms in the Mpumalanga area, South Africa, (then called the Eastern Transvaal) covers an area of approximately 600 km^2, with individual storms covering areas that range between 100 km^2 and 1900 km^2. The Mpumalanga area has similar topographic features to the greater Goedertrouw Dam catchment area (Kelbe, 1984). The cumulus clouds studied by Kelbe (1984) causes rain events that can be compared to the rain storms which occur in the Goedertrouw Dam catchment. Therefore, it can be assumed that rain storms in the Goedertrouw Dam area have a similar size distribution. The Goedertrouw Dam catchment size is at the upper extreme of this range and is therefore unlikely to have uniform rainfall over the entire area on any occasion.

Figures 10.14 and 10.15 depicts two graphs with different simulations of the storm on 21 Feb. 1972. This storm has the longest duration and highest intensity in the simulation period. In Figure 10.14, the catchment rainfall was estimated by an area-weighted average from all seven subcatchments. Rainfall is estimated as relatively high quantities that continue for five consecutive days (i.e., 44mm, 42mm, 23mm, 16mm and 12mm of rain). In Figure 10.15 the estimated catchment rainfall was replaced by the catchment rainfall of the subcatchment upstream from the outlet. In this case, the catchment rainfall is two consecutive days of much higher rainfall (107 mm and 74 mm during the first two days), followed by three days of insignificantly low rainfall. In this case a higher peak flow is simulated. This comparison indicates the effect of catchment rainfall estimations on runoff simulation.

10.6.3.2. Rainfall type estimation

The rainfall storm on 18 March 1972 (DOY 78, Figure 10.13), classified as low intensity and of short duration, causes a sharp high peak in the observed runoff, followed by a steep recession limb. This is in contrast to the simulated response functions to rainfall of low intensities and short duration. Simulation of this storm was changed to rainfall of high intensity and short duration, which provided a better simulation of the recession limb. An uneven distribution of rainfall in the catchment could also have caused the discrepancy in the simulation.

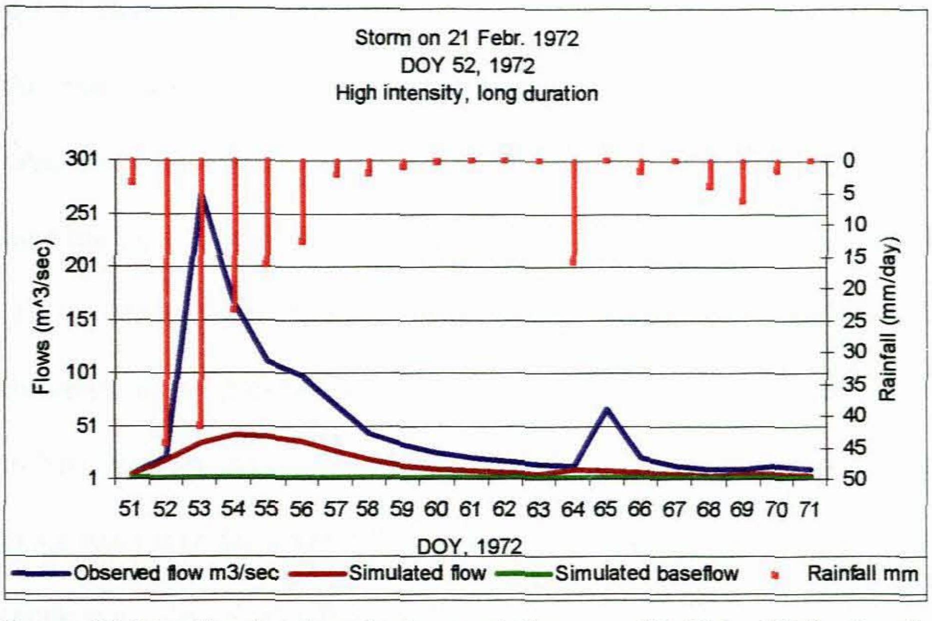

Figure 10.14: Simulated and observed flow on 21 Feb. 1972, for the catchment rainfall estimated by an area-weighted average from al seven subcatchments of the Goedertrouw Dam.

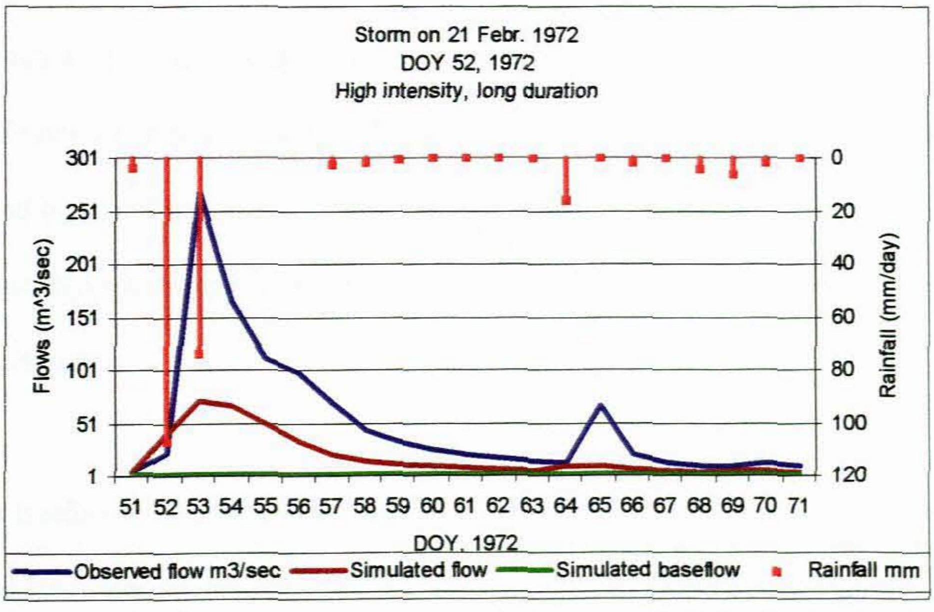

Figure 10.15: Simulated and observed flow on 21 Feb. 1972, for the catchment rainfall estimated by the subcatchment upstream from the outlet of the Goedertrouw Dam.

10.6.3.3. Recessions of the hydrographs

Generally the recessions of most simulated storm hydrographs tend towards slower recessions than those observed. This trend indicates that travel times over individual pixels have generally been estimated too slow (Figure 10.12: 9 Dec. 1971; 10, 14 and 21 Jan. 1972; 9-20 Febr. 1972; and Figure 10.13: 4 Mar. 1972). Simulated catchment flow response to rainfall events should be quicker. However, in the present model simulations, pixels along the main river have been estimated to have zero travel times, as the *catchment flow response* along these main rivers is estimated much faster than the minimum travel times over individual pixels. (This relates to the model limitation that is discussed in Paragraph 7.3.2). If shorter travel times are simulated, more pixels will have zero travel times, thereby extending the length of the river network.

10.6.3.4. Fractures and faults

Recessions rates are related to the travel times along the preferential pathways. If the pathways are diverted by fractures, the travel times can be substantially reduced. The exclusion of the fractures and faults in the baseflow pathways play a significant role in the simulated recessions of the hydrographs.

Suppose a fracture in a rock can be represented by a small channel (with inflow and outflow) which conducts water downward at a slight slant. During dry periods, this fracture may contain no water. The slope, flow direction and the slope length along this fracture will be similar to that of the small channel (Beven, 2001).

Now suppose that this same fracture in the rock is represented by an unlined canal. If this fracture is filled with water, and there is no transmission losses, this fracture will act as a channel.

However, evapotranspiration during dry periods can cause this fracture to become dry. Thus, during a rain event, this fracture must fill up with water before allowing water to flow out of the fracture. This situation will cause delays in the outflow from fractures following dry periods (Beven, 2001).

Thus, faults and fractures can both delay or speed up the movement of water through the catchment slopes, depending on antecedent catchment conditions.

10.7. Conclusions

Storm simulations for the bigger catchment were not as successful as the simulations for the smaller Ntuze River catchments. Poor comparison between observed and simulated runoff can mainly be attributed to the uneven distribution of rainfall through a large catchment area, which is not induced in the model. The omission of the fractured rock network in the catchment could also play a major role in the simulations. The classification of storm types using daily rainfall events is also likely to have problematic effects.

Further development of the model must also include travel times over individual pixels using double precision real values.

****

11 Summary and conclusions

The integrated management of water resources, as required by the South African Water Act No. 36 of 1998, calls for the development of integrated hydrological models. These models need to include all components of the hydrological cycle. Separate management of different water resources under previous water legislation brought about the development of separate hydrological models to simulate and manage different water resources. Integrating the existing hydrological simulation models, to operate parallel to each other, does not address the integrated flow processes. To manage the water resources as an integrated system, management should be supported by integrated models of the water resources, to enhance informed decision making.

The GIS storm hydrograph utilizes the spatial information of a catchment to derive the flow pathways of different flow components. Travel times along these pathways were estimated for each catchment segment. Cumulated travel times along the travel pathways were calculated along the flow pathways for each flow component. The histograms of the flow time frequencies represented the response functions of the catchment along the different flow pathways. Unit response functions of discharge from one unit of excess rainfall were derived. Excess rainfall was partitioned among the flow pathways by calibrating the response functions. The calibration utilized catchment information derived from the observed flow hydrographs. Observed flow hydrographs were analysed to estimate the recession rates of each flow component; the storm durations; the partitioning of flow among the flow components; and the excess rainfall.

In summary, the GIS storm hydrograph model uses spatial information of a catchment, together with information from the observed flow and rainfall, to estimate the storm flow response to a rainfall event on a head water catchment. The model integrates the simulation of surface and subsurface flow processes.

11.1. Data requirements of the model

The current version of the GIS storm hydrograph model is built on readily available spatial data. The estimates of model parameters require catchment specific data that are gathered from historic flow and rain data. Should this data not be available, methods must be developed to replace this catchment information. However, the transferability of parameters and its scaling to larger catchments is still uncertain because the model simulates hill slope processes that have characteristic scales of operation.

11.2. Scenario simulation with the GIS storm hydrograph model

Part of the NWA (1998) implementation was to establish the reserve of water resources (as described in Chapter one). The procedure to determine the reserve can benefit from the GIS storm hydrograph model, if the model can simulate the impacts of changes in the catchment on the flow components. An example will be the extraction of water from the groundwater resources, or the changing of large areas of forestation in the land use of the catchment.

If water is pumped from the groundwater resources, it is perceived as a change in the water table elevation (or surface elevation of the baseflow reservoir). This will create a draw-down in the groundwater table at the abstraction point. This can be simulated by a local sink in the simulated pathways of the baseflow component. Resultant changes in the pathways will create a different unit response function for simulating the baseflow component.

Afforestation (or deforestation) acts as a diffuse abstraction process. Water usage by trees in a catchment can be conceptualized as a network of miniature pumps that extract water from the soils surrounding the root systems, affecting all flow components present. The land use change will also influence the infiltration and percolation rates, leading to a change in the partitioning coefficients. This scenario can be simulated by a change in the partitioning coefficients. The effect of a change in forestation on the quickflow component is simulated by a change in the Manning's coefficient (n). A change in the Manning's n will indicate a different velocity profile, and therefore will derive different unit response functions of the quickflow components.

11.3. Effect of spatial parameters on spatial modelling

The soil structures in the Ntuze River catchments are relatively homogeneous and similar in each catchment (Midgley *et al*, 1994). It was assumed that there was sufficient homogeneity in the soil structure to develop the model on the basis of a uniform soil type. Therefore, the spatial variation in soil structures was ignored during the model development. If the soil distribution is known, then the model should be adjusted by incorporating the spatial variability in the hydraulic properties that impact on the velocity profile that is used to derive the unit response functions.

The spatial diversity of fractured rock and faults can be incorporated in the GIS hydrograph model by means of unit flow responses which indicate the presence of these features (discussed fully in Paragraph 11.6). However, detailed knowledge of flow paths along fractured rocks and faults is difficult to derive.

The GIS storm hydrograph model incorporates the spatial variability of catchment features in the form of a quasi 3D model (i.e., horizontal surface and three subsurface reservoirs). Hence, it is expected to be more realistic than lumped models. The hydrological processes, which cause runoff in a catchment during a rainfall event, are complex, with all variables varying over both space and time. Truly spatial modelling of these processes should allow ALL variables in the model (e.g., rainfall and soil moisture) to change in space and time as it affects the velocity profiles along the flow pathways.

In any hydrological runoff modelling there is a wide range of uncertainties that surround some model parameters and variables, especially spatial variables. Initial estimates of spatial variables are often assumed to be spatially invariant, due to uncertainty about the parameters' values for individual pixels. Calibrations of spatial variable parameters are also difficult, because of the uncertainty that surrounds the values of the parameters. The runoff coefficients; the time scaling coefficients and the partitioning coefficients, as implemented in the current version of the model, are assumed to be spatially invariant model parameters. Future development could attempt to replace these parameters with spatially variant variables, as discussed in following paragraphs.

11.4. Analysis and application of recession rates in model development

In the current version of the model, the travel time of water down each pathway is established for the preferential groups of pathlines. The recession rate of each flow component is utilized to calibrate the time scaling coefficient for each pathway, according to the rainfall type. The concept of different recession rates for different pathways can be extended to the concept of a continually changing recession rate, caused by a gradual change in land use.

Olivera and Maidment (2005) utilized a probability density function to introduce the time spent to flow from pixel to pixel, which is then added to the time spent to flow OVER each pixel, during calculation of the cumulative travel times from pixel to outlet. A statistical function is used to replace the uncertainty regarding the flow of water from pixel to pixel. This benefits the end results, but does not explicitly simulate the physical processes that cause the disturbance in the flow pathways.

11.5. Utilization of rainfall characteristics for runoff partitioning

The four different rainfall types described and analysed in this report provide a simple classification of the broad spectrum of storms that occur in nature. Travel time coefficients and partitioning coefficients have been determined for these four storm types for a given catchment. Procedures need to be developed to interpolate (and possibly extrapolate) these coefficients for other storm types. This could be done if the partitioning coefficients are replaced with some continuous function, which will depend on the rainfall intensity and antecedent soil moisture. If a method of interpolation between the different rainfall types can be developed, it will largely improve the GIS storm hydrograph model.

11.6. Incorporating a fractured rock and fault system in the model

The effects of fractured rocks and faults on river flows have been discussed briefly in the second chapter. It was indicated that a known fault in a catchment will have a significant effect on the catchment outflow at any stage of river flow.

Flow from fractured rocks and faults can be incorporated in the GIS storm hydrograph model by re-routing flow paths during the development of the unit hydrographs of the baseflow component. Flow velocities can be deducted from the individual characteristics of the faults and fractures, i.e., the slopes, the flow directions, the slope lengths and friction against flow.

Antecedent conditions of the catchment will play a major role in the estimation of the characteristics of a fractured rock surface. They may change rapidly when rock fractures fill up during a rain event, and drain out again after the event (Beven, 2001). It is worth-while to incorporate the antecedent catchment conditions in the model along with the flow pathways along fractured rocks.

11.7. Incorporating a spatially variant rainfall and excess rainfall in the model

The possibility for spatially invariant rainfall to occur, varies with the size of the catchment and the rainfall regime of the catchment. The GIS storm hydrograph model must be adapted to simulate runoff for rainfall types where only certain portions or segments of the catchment receive rainfall.

11.7.2. Spatial simulation of the slower flow components

Throughflow is modelled, in the current version of the GIS storm hydrograph, similarly to the flow processes along the quickflow pathways. The model currently assumes slower flows along the throughflow component's pathways than along the quickflow's pathways, using the time scaling coefficient T_{ST}. The movement of water through the upper soil structures is dependent on the soil characteristics, as well as land use. Another spatially distributed parameter, portraying the characteristics of the soil types in the catchment, can be included. However, very little information about the throughflow component is available. The few observations available as criteria to calibrate such a spatial distribution of the throughflow's travel times, is not adequate.

11.7.3. Spatial simulation of the baseflow components

A distributed model of baseflow will accept a spatial variant rainfall, not in the form of excess rainfall, but rather in the form of excess percolation from the top soils. This will influence the groundwater table, which will in turn influence the hydraulic slopes of the flow pathways along the baseflow component. A different groundwater surface will derive a different flow time distribution, which will adjust the response function of baseflow.

In the current version of the model, the coefficient C_B, which is a spatial invariant coefficient, adjusts the travel times in a manner explained by the pressure wave in the baseflow velocities in the catchment (Beven, 2004). The coefficient C_B can be spatially variant, expressed as a function of the effective storage capacity, which is described by Beven (2001). However, uncertainty of baseflow conditions will cause uncertain calibrations of these simulations.

Pathways of baseflow should also incorporate the geological structure of the catchment, e.g., rock fractures and faults. These geological features can lead to pathways along which more rapid travel times occur, or they act as sinks. The effect of these geological structures is incorporated in the present version of the model by a (spatially invariant) time scaling coefficient.

Future development of the model should consider spatial variant wetness (or a similar parameter), as well as a spatial variant parameter that separates the flow components in each pixel. The model could simulate a number of flow components as different layers of pathways that lie horizontally on top of each other (strata), with the top layer parallel to the surface elevation. Water should be able to move between these pathways at any time and space. Outflows from the surface flow component at the outlet will be the final routed outflow from each component.

The model simulates selective features of the hydrograph, but fail to simulate other. The model needs considerable revision, with more accurate distribution of rainfall, and other hydraulic properties.

11.8. Conclusions

11.8.1. Evaluation of the model development for small headwater catchments

The GIS storm hydrograph model can simulate the different flow components as separated parts of the runoff at the catchment outlet. A few storm events show discrepancies between simulated and observed runoff. Possible explanations for these storm events have been presented.

11.8.2. Transferability of the model to other catchments

Mixing of flow components takes place along the channels. The mixing of flow components in a catchment will depend on the catchment characteristics, particularly the channel lengths. The percentage of pixels in the DEM, that represent channels, should increase as the catchment size increase. However, it is assumed that the hill slope lengths for first order streams, in similar geological settings, should be similar. Since the flow separation in the model only occurs on the hill slopes, the model should be transferable between catchments with similar first order stream networks. The mixing of flow components only occurs, in this model, in the channels.

11.8.3. Application of the model concepts and principles

The concepts and principles of the GIS storm hydrograph model have been described and tested in this thesis. The model does not necessarily need to be used as a stand-alone system. The concepts and principles can be applied in other existing runoff modelling systems which simulate the contributions from both the surface water and groundwater resources.

11.8.4. Future model prospects

"...There are theoretical and ... numerical problems that will need to be overcome in the future development of (the spatial) model, but the problem of parameter identification, particularly for the subsurface, will be even greater, and significant progress will undoubtedly depend on the development of improved measurement techniques." (Beven, 2001)

Development of spatial modelling of a catchment has been restricted by the need for large computer resources with heavy data requirements. However, as advanced computer systems become available and affordable, more computer power will enhance model development.

The spatial information of a catchment can be determined from aerial data and satellite coverage. These data sets are becoming more affordable and available.

"The major constraint on the utility of remote sensing (in hydrological modelling) is that ... it can only detect changes on or above the ground surface and the most interesting part of hydrology takes place underground. What is needed, therefore, is revolutionised hydrological thinking; theory development and model development..." (Beven, 2001).

****

12 References

Arnold, J.G. and P.M. Allen (1996). Estimating hydrological budgets for three Illinois catchments, Journal of Hydrology, Volume 176, pp. 57-77.

Becker A. and P. Braun (1999). Disaggregation, aggregation and spatial scaling in hydrological modeling, Journal of Hydrology, Volume 217, pp. 239 - 252.

Bell, R.W, N.J.Schofield, I.C. Loh and M.A. Bari (1990). Groundwater response to reforestation in the Darling range of Western Australia, Journal of Hydrology, Volume 119, pp. 179 - 200.

Berger K.P. and D. Entekhabi (2001). Basin hydrologic response relations to distributed physiographic descriptors and climate, Journal of Hydrology, Volume 247, pp. 169 - 182.

Besbes, M. and G. de Marsily (1984). From infiltration to recharge: use of a parametric transfer function, Journal of Hydrology, Volume 74, pp. 271 - 293.

Beven, K.J. (2001). Rainfall-Runoff Modelling The Primer, John Wiley & Sons Ltd, West Sussex, England.

Beven K.J. (1989). Interflow, Proceedings of the NATO Advanced Research Workshop (June 1988) on Unsaturated flow in hydrological modeling, theory and practice, Ed. H.J. Morel-Seytoux, Kluwer Academic Publishers, Netherlands.

Boeke, Ettienne (2005). Personal Communications, Natal Irrigation Consultants, 17 English Road, Pietermaritzburg, South Africa.

Borg, H., G.L.Stoneman and C.G. Ward (1988). The effect of logging and regeneration on groundwater, streamflow and stream salinity in the southern forest of Western Australia, Journal of Hydrology, Volume 99, pp.253 - 270.

Braune, E. (2000). Towards comprehensive groundwater resource management in South Africa. In: Groundwater: Past achievements and future challenges, Sililo *et al* (eds), 2000, Balkema, Rotterdam ISBN 905809 159 7.

Cannata, M. and M.A. Brovelli (2006) An overview of HydroFOSS, a novel GIS embedded hydrological model, Annual General Meeting of the European Geoscience Union, Vienna, Austria.

Cey, E.E., D.L.Rudolph, G.W.Parkin and R.Aravena (1998). Quantifying groundwater discharge to a small perennial stream in southern Ontario, Canada, Journal of Hydrology, Volume 210, pp. 21-37.

Chiew, F.H.S., T.A McMahon and I.C. O'Neill (1992). Estimating groundwater recharge using an integrated surface and groundwater modeling approach, Journal of Hydrology, Volume 131, pp. 151 - 186.

Chow, V.T., R.D.Maidment and T.W.Mays (1988). Applied Hydrology, McGraw-Hill Book Company, McGraw-Hill series in Water Resources and Environmental Engineering, ISBN 0-07-100174-3.

Criss, R.E. and M.L. Davisson (1996). Isotopic imaging of surface/groundwater interaction, Sacramento Valley, California, Journal of Hydrology, Volume 178, pp. 205 - 222.

De Backer, L.W. (1989). Background concepts and principles, Proceedings of the NATO Advanced Research Workshop (June 1988) on "Unsaturated flow in hydrological modeling, theory and practice," Ed. H.J. Morel-Seytoux, Kluwer Academic Publishers, Netherlands.

Department of Water Affairs and Forestry (2003). Resource Directed Measures, B. Schreiner (Ed) Department of Water Affairs and Forestry, Pretoria, South Africa.

Eagleson, P.S. (1986). The emergence of global scale hydrology, Water Resources Research, Volume 22, No. 1, pp. 6 - 14.

Experiment Station of the South African Sugar Industry (1984). Identification of the soils of the sugar industry, Bulletin No. 19 (Revised), Experiment Station of the South African Sugar Industry, Durban, South Africa.

Fortin, J.-P., R. Moussa, R. Turcotte, A.N. Rousseau and J.-P. Villeneuve (2006). The HYDROTEL distributed hydrological model: a simulation and forecasting model making good use of GIS and RS data, Annual General Meeting of the European Geoscience Union, Vienna, Austria.

Franchini, M. and P.E. O'Connell (1996). An analysis of the dynamic component of the geomorphological instantaneous unit hydrograph, Journal of Hydrology, Volume 175, pp. 407 - 428.

Gordon, N.D., T.A. McMahon and B.L. Finlayson (1992). Stream Hydrology: An introduction for Ecologists, John Wiley and Sons, Chichester, West Sussex, UK.

Gottschalk, L. and R. Weingartner (1998). Distribution of peak flow derived from a distribution of rainfall volume and runoff coefficient, and a unit hydrograph, Journal of Hydrology, Volume 208, pp. 148 - 162.

Guiguer, N. and T. Franz (1996). Visual MODFLOW. The Integrated Modelling Environment for MODFLOW and MODPATH. Version 2.11, Waterloo Hydrogeologic Software, User manual.

Gupta, A.D. and G.N. Paudyal (1988). Estimating aquifer recharge and parameters from water level observation, Journal of Hydrology, Volume 99, pp.103 - 116.

Hebson, C. and E.F. Wood (1982). A derived flood frequency distribution using Horton order ratios, Water Resources Research, Volume 18, No. 5, pp. 1509 - 1518.

Hewlett, J.D and A.R. Hibbert (1976). Factors affecting the response of small watersheds to precipitation in humid areas, in Proceedings of the International Symposium on Forest Hydrology, Ed. W.E. Sopper and H.W. Lull, Pergamon, Oxford, England.

Hope, A.S and G.J.Mulder (1979). Hydrological Investigations of Small Catchments in the Natal Coastal Belt and the Role of Physiography and Land Use in the Rainfall-Runoff Process, Publication Series of the University of Zululand, Kwadlangezwa, South Africa.

Hromadka, T.V. and R.J.Whitley (1999). On formalization of unit-hydrograph and link-node hydrograph-routing systems, Journal of Hydrology, Volume 223, pp. 66 - 84.

Hughes, D.A. (2004). Personal communications. Institute for Hydrological Research, Rhodes University, Rhodes, South Africa.

Hughes, D.A. (1994). HYMAS V1.0 Guide to the system and used manual, Addendum to WRC Report N 235/1/93, WRC, South Africa.

Hughes,D.A., D. Forsyth and D.A.Watkins (2000). An integrated software package for the analysis and display of hydrological or water resources time series data, Water Research Commission of South Africa Report No. 867/1/2000, South Africa.

Hughes, D.A., P.Hannart and D.Watkins (2003). Continuous baseflow separation from time series of daily and monthly streamflow data, Water SA, Volume 29, No.1, pp. 43 - 48.

Hughes, D.A. and F.Munsster (2000). Hydrological Information and Techniques to support the determination of the water quantity components of the ecological reserve for rivers, Water Research Commission of South Africa Report No. 867/3/2000, South Africa.

Jena, S.K. and K.N. Tiwari (2006). Modeling synthetic unit hydrograph parameters with geomorphological parameters of watersheds, Journal of Hydrology, Volume 319, pp. 1 - 14.

Kelbe, B.E. (1984). Cumulus cloud characteristics of the Eastern Transvaal Lowveld, Water SA, Volume 10, No.2, pp. 81 - 90.

Kelbe, B.E. and T. Germishuyse (1999). A study of the relationship between hydrological processes and the water quality characteristics in the Zululand coastal region. Final Report to the Water Research Commission of South Africa Report No. 346/1/99, South Africa.

Kelbe, B.E. *and N.Snyman (1993). Water quality response to land use for short duration, high* intensity storms. Proceedings, 6th National Hydrological Symposium, Pietermaritzburg, South Africa.

Kelbe, B.E., N.Snyman and G.J.Mulder (1996). Modelling Aspects of Hydrological Processes and Water Quality Characteristics in Zululand Coastal Region, Internal HRU report No 364/2/96.

Kelbe, B.E. and B. Rawlins (2004). Groundwater management in South Africa, in Managing Common Pool Groundwater Resources: An International Perspective (pp. 289-310) Ed. M.Brentwood and S.F. Robar. Praoger Publishers, Westport, Cape Town, South Africa.

Ledoux, E., G. Girard and G. de Marsily (1989). Spatially distributed modeling: Conceptual approach, coupling surface water and groundwater, Proceedings of the NATO Advanced Research Workshop (June 1988) on Unsaturated flow in hydrological modeling, theory and practice, Ed. H.J. Morel-Seytoux, Kluwer Academic Publishers, Netherlands.

Ligon, R.K., T.V. Wilson, J.F. Allen and U.P. Singh (1977). Tracing vertical translocation of soil moisture, Journal of Hydraulic Div., American Society of Civil Engineers, Volume 103, pp. 1147 - 1158.

Lin, G.F. and Y.Wang (1996). General stochastic instantaneous unit hydrograph, Journal of Hydrology, Volume 182, pp. 227-238.

Lindsay R.K., M.A. Kholer and J.L.H. Paulhus (1972). Hydrology for Engineers, McGraw-Hill London.

Lorentz, S.K., Bursey and O. Idowu (2006). Definitions and upscaling of key hydrological processes affecting critical perturbations to water resources for application in models, Water Research Commission of South Africa Report No. K5/1320, South Africa.

Lorentz, S.K., S.Thornton-Dibb, C. Pretorius and P. Goba (2003). Hydrological Systems Modelling Research Programme: Hydrological processes; Phase II: Quantification of hillslope, riparian and wetland processes, Water Research Commission of South Africa Report No. K5/1061 and K5/1086, South Africa.

Maidment, D.R., F. Olivera, A.Calver, A. Eatherall, W.Fraczek (1996). Unit hydrograph derived from a spatially distributed velocity field, Hydrological Processes, Volume 10, pp. 831 - 844, John Wiley and Sons, Ltd.

Midgley, D.C., W.V. Pitman and B.J. Middleton (1994). Surface Water Resources of South Africa 1990, Volume VI, Water Research Commission Report of South Africa No. 298/6.1/94, ISBN Set No 1 86845 156 9, South Africa.

Mulder, G.J. (1988). Subsurface stormflow response to rainfall on a hillslope plot within the Zululand coastal zone, Geomorphological studies in Southern Africa, Eds. G.F. Dardis and B.P. Moon, Balkema, Rotterdam, Netherlands.

Mulder, G.J. (1984). *Die invloed van infiltrasie op stormwaterafloop in the opvanggebied van die Ntuzerivier (Zoeloelandse kusstreek).* MSc thesis, Potshefstroomse Universiteit vir Christelike Hoër Onderwys, 132 bl., South Africa.

Mulder, G.J. and B.E. Kelbe (1992). Hydrological response to the drainage morphology of small catchments. Paper presented at the South African Association of Geomorphologists, Biannual conference: Geomorphology and Land Management, Durban, South Africa.

Musy, A., M. Soutter and P. Perrochet (1989). Evaluation of the hydrological response of a drainage network, Proceedings of the NATO Advanced Research Workshop (June 1988) on "Unsaturated flow in hydrological modeling, theory and practice," Ed. H.J. Morel-Seytoux, Kluwer Academic Publishers, Netherlands.

Muzik, I. (1996). A GIS derived distributed unit hydrograph, Application of Geographic Information Systems in Hydrology and Water Resources Management, IAHS Publication No. 235, Edited by K.Kovar and H.P. Nachtnebel, Oxfordshire, United Kingdom.

Nash, J.E. (1957). The form of the instantaneous unit hydrograph, International Association for Hydrological Sciences, Publication No. 45, Volume 3, pp. 114 - 121.

Nathan, R.J. and T.A.McMahon (1990). Estimating low flow characteristics in ungauged catchments, Water Resources Management, Volume 6, pp. 85 - 100.

Newson, M. (1995). Hydrology and the river environment, Oxford University Press, Walton Street, Oxford, UK.

Olivera, F. and D.R.Maidment (2005). Storm Runoff Computation Using Spatially Distributed Terrain Parameters, http://www.ce.utexas.edu/prof/olivera/impr_uh/impr_uh.htm.

Omati, U. and A. Wild (1979). Use of fluorescent dyes to mark the pathways of solute movement through soils under leaching conditions, 2. Field experiments, Soil Science, Volume 128, pp. 98 - 104.

Parsons, P. (2003). Groundwater Resource Directed Measures: GRDM Training Manual. FET Water Groundwater Network, DWAF, Pretoria, South Africa.

Ponce, V.M. and A.V. Shetty (1995). A Conceptual model of catchment water balance: 1. Formulation and calibration, Journal of Hydrology, Volume 173, pp. 27-40.

Refsgaard J.-C. (1997). Parameterisation, calibration and validation of distributed hydrological models, Journal of Hydrology, Volume 198, pp. 69 - 97.

Richards L.A. (1931). Capillary condition of liquids through porous mediums, Physics, Volume 1, pp. 318 - 333.

Rodriguez-Iturbe, I. and J.B.Valdes (1979). The Geomorphological structure of the hydrological response, Water Resources Research, Volume 15, No. 6, pp. 1409 - 1420.

Ross C.N. (1921). The calculation of flood discharge by the use of time contour plan isochrones, Transaction of Institute of Engineers, Australia, Volume 2, pp. 85 - 92.

Schulz, E.F. (1976). Problems in Applied Hydrology, Water Resources Publications, Fort Collins, Colorado, USA.

Seiler, K.-P. and W. Lindler (1995). Near-surface and deep groundwaters, Journal of Hydrology, Volume 165, pp. 33-44.

Shaw, E.M. (1994). Hydrology in Practice, Chapman & Hall, London, UK.

Sherman, L.K. (1932). Streamflow from rainfall by the unit-hydrograph method, Eng. News-Rec, Volume 108, pp. 501 - 505.

Snyder, F.F. (1938). Synthetic unit-graphs, Trans. American Geophysical Union, vol. 19, pp. 447-454, 1938.

Snyman, N. (2000). An information base for a Decision Support System for management of the Mhlathuze River, Thesis submitted towards Masters Degree in Hydrology at the University of Zululand, Kwadlangezwa, South Africa.

Strahler, A.N. (1964). Quantitative geomorphology of drainage basins and channel networks, Section 4-II, in Handbook of Applied Hydrology, ed. by V.T. Chow, pp. 4-76, McGraw-Hill, New York, USA.

Todd, D.K. (1980). Groundwater Hydrology, Second Edition, John Wiley and sons, New York, USA.

United Nations Millennium Declaration (2000). Resolution adopted by the General Assembly, A/RES/55/2, United Nations, USA.

Van Niekerk, L. (2004). Preliminary determination of the ecological reserve on a rapid level for the St Lucia Estuary, Environmentek, CSIR, Stellenbosch, South Africa.

Wang Z.-M., O. Batelaan and F. De Smedt (1996). A distributed model for water and energy transfer between soils, plants and atmosphere (WetSpa), Physics and Chemistry of the Earth, Volume 21, No. 3, pp. 189-193.

Wang, G. and S. Chen (1996). A linear spatially distributed model for a surface rainfall-runoff system, Journal of Hydrology, Volume 185, pp. 183-198l.

Ward R.C. and M. Robinson (2000). Principles of Hydrology, McGraw-Hill Publishing Company, Berkshire, UK, ISBN 0 07 709502 2.

Wilson, E.M. (1983). Engineering Hydrology, The Macmillan Press Ltd, Hong Kong, ISBN 0 333 33338 1.

Wittenberg, H and M. Sivapalan (1999). Watershed groundwater balance estimation using streamflow recession analysis and baseflow separation, Journal of Hydrology, Volume 219, pp. 20-33.

Yue, S and M. Hashino (2000). Unit hydrographs to model quick and slow runoff components of streamflow, Journal of Hydrology, Volume 227, pp. 195-206.

****

Appendix A:

HYDTIME program printout

Part I: File rewriting module

File Rewriting module:

```
10 REM
**********************************************************************
20 REM *  Program to read travel times & flow dir images, & write corresponding
   REM *  pixel's values next to each other in a file called "RANDOM.IMG".
   REM *  This RANDOM.IMG is the input file of HYDTIME.BAS, using random
   REM *  access files to process the data.
30 REM *  Program: RANDIMG.BAS
40 REM
**********************************************************************
60   CLEAR
REM      amount.rows = 390  '110: Cut from matrix:R23, R132 - D1 catchment
REM      amount.columns = 470  '135: Cut from matrix: C153,C287
          amount.rows = 520  '110: Cut from matrix:R23, R132 - D1 catchment
         amount.columns = 960  '135: Cut from matrix: C153,C287

REM Read the two input files, and write them as one file, two corresponding
REM values next two each other.

    TYPE value
     aspect AS INTEGER
     hydtime AS INTEGER
    END TYPE

    OPEN "I", #1, "d:\work\GoedDEM\flowdir8.rst"
    OPEN "I", #2, "d:\work\GoedDEM\ttimes.rst"
    OPEN "d:\work\random.rst" FOR RANDOM AS #3 LEN = LEN(value)

    DIM names AS value

     FOR j = 1 TO amount.rows
      FOR i = 1 TO amount.columns
       INPUT #1, names.aspect
       INPUT #2, names.hydtime
       'PRINT names.aspect; "   "; names.hydtime
       PUT #3, ((amount.columns * (j - 1)) + i), names
      NEXT i
     NEXT j

    CLOSE #1
    CLOSE #2
    CLOSE #3

    END
```

Appendix A:

HYDTIME program printout

Part II: Cumulative travel time calculations

Cumulative travel time calculations:

```
10 REM
*********************************************************************
20 REM *  Program to read hydrological time & aspect images, & calculate
   REM *  the (cumulative)  times it takes for one water drop to travel from
   REM *  pixel to catchment outlet for use in IDRISI program.
   REM *  No allowance
   REM *  is made for circular paths or flat areas.
   REM *  See file preparation module to prepare input to this program.input.
   REM *  Random access input file are used also as output file,
   REM *  and after calculations data is rewritten to travelti.RST IDRISI 32 ASCII file.
   REM *  Specify the column and row of catchment output: outrow amd outcol:
   REM *  Add one to the row and colmumns read in IDRISI image file for
   REM *  catchment outlet.
   REM *  IDRISI ASCII file with integers.
30 REM *  Program: HYDTIME.BAS
40 REM
*********************************************************************
60    CLEAR
     amount.rows = 520  'Mhlathuze catchment
     amount.columns = 960  'Mhlathuze catchment
REM Setting the row and column number of the catchment outlet:
     outrow = 366 + 1
     outcol = 422 + 1

     DIM pathx(2000), pathy(2000), pathd(2000)

     TYPE value
      aspect AS INTEGER
      hydtime AS INTEGER
     END TYPE

     OPEN "d:\work\random.rst" FOR RANDOM AS #1 LEN = LEN(value)
               'Aspect values: 1 <= aspect <= 8
               'Hydtime contain neg. hourly time values for water to
               'travel over one pixel.

     DIM work AS value


     REM *********************************************************************
      SCREEN 9, 1, 1, 1
      LINE (0, 0)-(amount.columns + 1, amount.rows + 1), 14, B
                    'Block around river & catchment boundary map.
```

```
'**************Begin with calculations:******************************************

      FOR n = 1 TO amount.rows 'going along y axis
        FOR m = 1 TO amount.columns  'going along x axis
      i = m
      j = n
      d = 0
      pathx(0) = m
      pathy(0) = n
      count = 0
      GET #1, ((amount.columns * (j - 1)) + i), work

80      DO UNTIL work.hydtime > 0
      GET #1, ((amount.columns * (j - 1)) + i), work
      count = count + 1


'*******Determine the direction of movement; move and calc. distance of
movement:********

620   IF work.aspect = 8 THEN
9       pathd(count) = ABS(work.hydtime): i = i + 1: j = j - 1: GOTO 629
      END IF
      IF work.aspect = 7 THEN
6       pathd(count) = ABS(work.hydtime): i = i + 1: GOTO 629
      END IF
      IF work.aspect = 6 THEN
3       pathd(count) = ABS(work.hydtime): i = i + 1: j = j + 1: GOTO 629
      END IF
      IF work.aspect = 5 THEN
2       pathd(count) = ABS(work.hydtime): j = j + 1: GOTO 629
      END IF
      IF work.aspect = 4 THEN
1       pathd(count) = ABS(work.hydtime): i = i - 1: j = j + 1: GOTO 629
      END IF
      IF work.aspect = 3 THEN
4       pathd(count) = ABS(work.hydtime): i = i - 1: GOTO 629
      END IF
      IF work.aspect = 2 THEN
7       pathd(count) = ABS(work.hydtime): i = i - 1: j = j - 1: GOTO 629
      END IF
      IF work.aspect = 1 THEN
8       pathd(count) = ABS(work.hydtime): j = j - 1: GOTO 629
      END IF

      pathx(count) = i
      pathy(count) = j
```

```
     GET #1, ((amount.columns * (j - 1)) + i), work

'************* TESTING FOR CATCHMENT OUTLET:
***************************
629  IF (i = outcol) AND (j = outrow) THEN
       d = ABS(work.hydtime)
       FOR z = count - 1 TO 0 STEP -1
         GET #1, ((amount.columns * (pathy(z) - 1)) + pathx(z)), work
         work.hydtime = d + pathd(z + 1)
         PUT #1, ((amount.columns * (pathy(z) - 1)) + pathx(z)), work
         PSET ((pathx(z)), pathy(z)), 2 'green line - inside cathment
         d = d + pathd(z + 1)
         pathd(z + 1) = 0
       NEXT z
       GOTO 660
     END IF


'************* TESTING FOR EDGES OF THE MAP:
******************************

     IF ((i >= amount.columns) OR (i <= 1) OR (j >= amount.rows) OR (j <= 1)) THEN

      FOR z = count - 1 TO 0 STEP -1
        GET #1, ((amount.columns * (pathy(z) - 1)) + pathx(z)), work
2004    work.hydtime = 32000
        PUT #1, ((amount.columns * (pathy(z) - 1)) + pathx(z)), work
              '32000 indicates edge of
              'map or a path leading to edge of map.
              '(Max int: 32767)

        PSET ((pathx(z)), pathy(z)), 3  'light blue line
        pathd(z + 1) = 0
       NEXT z
       GOTO 660
     END IF

***********TESTING FOR PATHS ALREADY SUCCESSFULLY CALCULATED:***

400  IF (work.hydtime > 0) THEN
401   IF (work.hydtime < 32000) THEN
      d = work.hydtime
      FOR z = count - 1 TO 0 STEP -1
       GET #1, ((amount.columns * (pathy(z) - 1)) + pathx(z)), work
       work.hydtime = d + pathd(z + 1)
       PUT #1, ((amount.columns * (pathy(z) - 1)) + pathx(z)), work
       PSET ((pathx(z)), pathy(z)), 2 'green line - inside cathment
```

```
        d = d + pathd(z + 1)
        pathd(z + 1) = 0
       NEXT z
      ELSEIF (work.hydtime = 32000) THEN
        FOR z = count - 1 TO 0 STEP -1
         GET #1, ((amount.columns * (pathy(z) - 1)) + pathx(z)), work
2003       work.hydtime = 32000
         PUT #1, ((amount.columns * (pathy(z) - 1)) + pathx(z)), work
         PSET (pathx(z), pathy(z)), 7 'grey line - outside catchment
         pathd(z + 1) = 0
        NEXT z
      ELSEIF (work.hydtime > 32000) THEN
       STOP
      END IF
      GOTO 660
     END IF
'***************************************************************************
*

648  pathx(count) = i
      pathy(count) = j

      GET #1, ((amount.columns * (j - 1)) + i), work

650   LOOP 'UNTIL work.hydtime > 0
'***************************************************************************
**
'Now: HYDTIME.WORK > 0:

655     IF (work.hydtime < 32000) THEN
       d = work.hydtime
       FOR z = count - 1 TO 0 STEP -1
        GET #1, ((amount.columns * (pathy(z) - 1)) + pathx(z)), work
        work.hydtime = d + pathd(z + 1)
        PUT #1, ((amount.columns * (pathy(z) - 1)) + pathx(z)), work
        PSET ((pathx(z)), pathy(z)), 2 'green line
        d = d + pathd(z + 1)
        pathd(z + 1) = 0
       NEXT z
      ELSEIF (work.hydtime = 32000) THEN
        FOR z = count - 1 TO 0 STEP -1
         GET #1, ((amount.columns * (pathy(z) - 1)) + pathx(z)), work
2001       work.hydtime = 32000
         PUT #1, ((amount.columns * (pathy(z) - 1)) + pathx(z)), work
         PSET (pathx(z), pathy(z)), 5 'purple line
         pathd(z + 1) = 0
        NEXT z
```

```
    END IF

660     NEXT m
    NEXT n

'**********************************************************************
***

    PRINT "Writing to output file..."
    OPEN "O", #4, "d:\work\travelti.rst"
    FOR j = 1 TO amount.rows
     FOR i = 1 TO amount.columns
      GET #1, ((amount.columns * (j - 1)) + i), work
      IF work.hydtime = 32000 THEN
2000       PRINT #4, 0
      ELSE PRINT #4, work.hydtime
      END IF

     'Write background values as nills, write to readible ASCII file.
     NEXT i
    NEXT j
    CLOSE

1030 END
```

Appendix B:

Statistical relationship between the recession rates and the time scaling factors

B.1. Calculating the recession rates using the time scaling coefficients in Manning's equation

Free statistical software, CurveExpert 1.3 (a trial version), was downloaded from the internet. It was utilized to determine a curve which can describe the relationship between the recession rates and T_S, in the Manning's equation.

The statistical curve (named the "Rational Model" by the software CurveExpert 1.3) fitted the observations best:

$$y = \frac{a + bx}{1 + cx + dx^2} \qquad \text{(Equation B1)}$$

where y = the recession rate, x = the time scaling coefficient and a, b, c and d are constants. The fitted model for all three catchments is as follows:

$$Rec\,K = \frac{7T_S}{1 + 7T_S} \qquad \text{(Equation B2)}$$

where $Rec\,K$ = the recession rate

T_S = the time scaling coefficient, where $T_S \leq 4$.

$a = d = 0$ and $b = c = 7$

The "observed" recession rates (listed in Table 8.2) and "calculated" recession rates (calculated using the statistical relationship) are plotted for weir W1H016 in Figure B1.

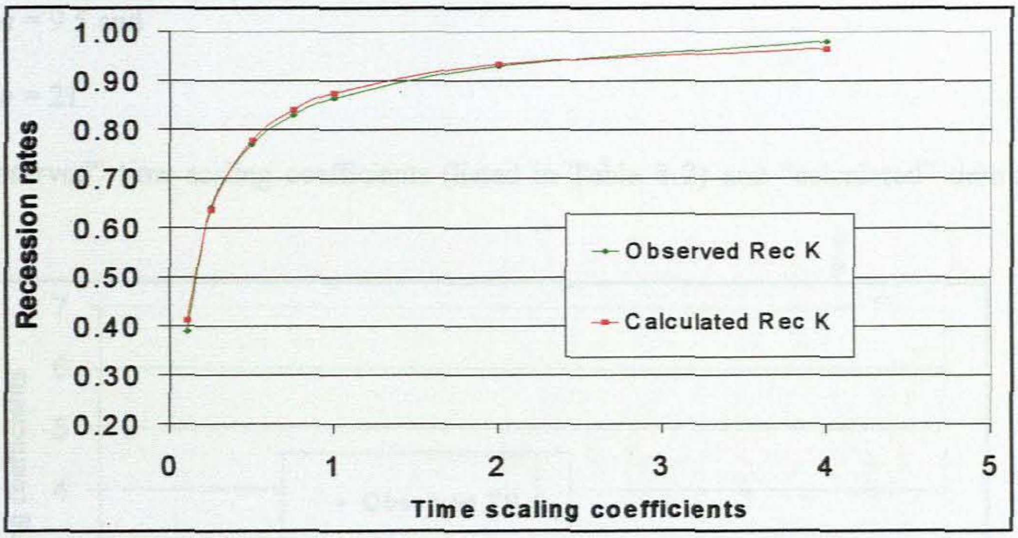

Figure B1: Graphic display of the relationship between the recession rates (calculation from the statistical relationship) and the observed recession rates (as listed in Table 8.2), plotted for different time scaling coefficients in Manning's equation.

B.2. Calculating the time scaling coefficients (T_S) using the recession rates in Manning's equation:

The statistical curve (named the "Geometric Fit" in CurveExpert 3.1) fitted the observations best:

$$y = ax^{bx} \qquad \text{(Equation B3)}$$

where y = time scaling coefficient,

x = the recession rate, and

a and b are constants.

Resultant application of the Geometric fit to the relationship between T_S and the recession rates (*Rec K*) is as follows:

$$T_S = 9.5 * Rec\,K^{(21*RecK)} \qquad \text{(Equation B4)}$$

Where T_S = time scaling coefficient

Rec K = recession rate, where $Rec\,K \leq 0.95$.

$a = 9.5$ and

$b = 21$.

The "observed" time scaling coefficients (listed in Table 8.2) and "calculated" time scaling

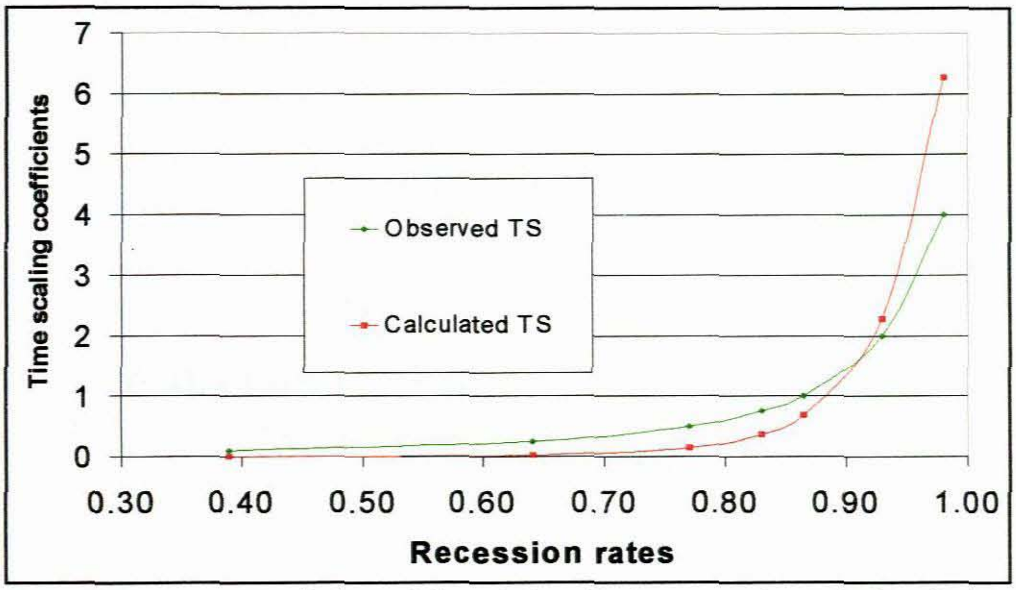

Figure B2: A graphic display of the relationship between the 'calculated' time scaling coefficient TS (calculated from the Geometric Fit) and 'observed' time scaling coefficient (as listed in Table 8.2) in the Manning's equation, plotted for different recession rates.

coefficients (calculated from the recession rate using the Geometric Fit) are plotted for weir W1H016 in Figure B2.

In both the cases of the Rational Model and the Geometric Fit, other models were preferred by the curve fitting software above the author's chosen model. However, these models were not as 'stable' as the chosen models. By 'stability' the author indicates the capability of a model to provide fairly accurate estimations after minor changes in the parameters a, b, c and d of the model.

****

Appendix C:

Calculations in the simulations with the GIS storm hydrograph model

Calculations of the simulation in the GIS storm hydrograph model

Calculations were made in a spreadsheet. Similar calculations can be programmed using linear programming techniques and appropriate software.

Normalization of the frequency histograms:

$(FQ)_{ij}$ = the resultant values of the frequency histogram (after equation 8.1 was applied) for the quickflow component for time step *i*, and storm type *j*

$(FT)_{ij}$ = the resultant values of the frequency histogram values (after equation 8.1 was applied) for the throughflow component for time step *i*, and storm type *j*

$(FB)_{ij}$ = the resultant values of the frequency histogram values (after equation 8.1 was applied) for the baseflow component for time step *i*, and storm type *j*

$i = 1,...,E$

E = the number of time steps in the frequency histograms

j = storm type 1,2,3 or 4.

These values are illustrated in Table C1.

Table C1: Normalized values of the frequencies histograms, of quickflow, throughflow and baseflow, for each storm type.

Normalized frequencies												
	Storm Types											
	High intensity Long duration			Low intensity Long duration			Low intensity Short duration			High intensity Short duration		
Time	Storm type 1			Storm type 2			Storm type 3			Storm type 4		
Steps	Quickflow	Throughflow	Baseflow	Quickfl	Throughfl	Baseflo	Quickflo	Throughflo	Baseflo	Quickflo	Throughflow	Baseflow
1	$(FQ)_{11}$	$(FT)_{11}$	$(FB)_{11}$	$(FQ)_{12}$	$(FT)_{12}$	$(FB)_{12}$	$(FQ)_{13}$	$(FT)_{13}$	$(FB)_{13}$	$(FQ)_{14}$	$(FT)_{14}$	$(FB)_{14}$
2	$(FQ)_{21}$	$(FT)_{21}$	$(FB)_{21}$	$(FQ)_{22}$	$(FT)_{22}$	$(FB)_{22}$	$(FQ)_{23}$	$(FT)_{23}$	$(FB)_{23}$	$(FQ)_{24}$	$(FT)_{24}$	$(FB)_{24}$
3	$(FQ)_{31}$	$(FT)_{31}$	$(FB)_{31}$	$(FQ)_{32}$	$(FT)_{32}$	$(FB)_{32}$	$(FQ)_{33}$	$(FT)_{33}$	$(FB)_{33}$	$(FQ)_{34}$	$(FT)_{34}$	$(FB)_{34}$
4	$(FQ)_{41}$	$(FT)_{41}$	$(FB)_{41}$	$(FQ)_{42}$	$(FT)_{42}$	$(FB)_{42}$	$(FQ)_{43}$	$(FT)_{43}$	$(FB)_{43}$	$(FQ)_{44}$	$(FT)_{44}$	$(FB)_{44}$
...	...	...	...	...	...	...	...	...	...	...	...	...
E	$(FQ)_{E1}$	$(FT)_{E1}$	$(FB)_{E1}$	$(FQ)_{E2}$	$(FT)_{E2}$	$(FB)_{E2}$	$(FQ)_{E3}$	$(FT)_{E3}$	$(FB)_{E3}$	$(FQ)_{E4}$	$(FT)_{E4}$	$(FB)_{E4}$

Division of one unit of rainfall among the flow components in the travel time response functions

$(FQ)_{ij} * (pq)_j = Q_{ij}$
$(FT)_{ij} * (pt)_j = T_{ij}$
$(FB)_{ij} * (pb)_j = B_{ij}$

where pq_i = the fraction of flow allocated to quickflow, or the partitioning coefficient of the quickflow component
pt_i = the fraction of flow allocated to throughflow, or the partitioning coefficient of the throughflow component
pb_i = the fraction of flow allocated to baseflow, or the partitioning coefficient of the baseflow component
$pq_i + pt_i + pb_i = 1$, for storm type $i = 1, 2, 3$ and 4
Q_{ij} = the flow rates in the quickflow component for time step i and storm type j
T_{ij} = the flow rates in the throughflow component for time step i and storm type j
B_{ij} = the flow rates in the baseflow component for time step i and storm type j.

These calculations are illustrated in Table C2.
Table C2: Divisions of one unit of rainfall among the different flow components, for each storm type.

Normalized flow rates: flow rates of unit excess response functions												
Time step	*Storm Types*											
	High intensity Long duration			Low intensity Long duration			Low intensity Short duration			High intensity Short duration		
	Storm type 1			Storm type 2			Storm type 3			Storm type 4		
	Quickflow	Throughfl	Baseflow	Quickflow	Throughfl	Baseflow	Quickflow	Throughfl	Baseflow	Quickflow	Throughfl	Baseflow
1	$(FQ)_{11}*(pq)_1 = Q_{11}$	$(FT)_{11}*(pt)_1 = T_{11}$	$(FB)_{11}*(pb)_1 = B_{11}$	$(FQ)_{12}*(pq)_2 = Q_{12}$	$(FT)_{12}*(pt)_2 = T_{12}$	$(FB)_{12}*(pb)_2 = B_{12}$	$(FQ)_{13}*(pq)_3$ =Q13	$(FT)_{13}*(pt)_3 = T_{13}$	$(FB)_{13}*(pb)_3 = B_{13}$	$(FQ)_{14}*(pq)_4 = Q_{14}$	$(FT)_{14}*(pt)_4 = T_{14}$	$(FB)_{14}*(pb)_4 = B_{14}$
2	$(FQ)_{21}*(pq)_1 = Q_{21}$	$(FT)_{21}*(pt)_1 = T_{21}$	$(FB)_{21}*(pb)_1 = B_{21}$	$(FQ)_{22}*(pq)_2 = Q_{22}$	$(FT)_{22}*(pt)_2$ =T22	$(FB)_{22}*(pb)_2 = B_{22}$	$(FQ)_{23}*(pq)_3 = Q2_3$	$(FT)_{23}*(pt)_3 = T_{23}$	$(FB)_{23}*(pb)_3 = B_{23}$	$(FQ)_{24}*(pq)_4 = Q_{24}$	$(FT)_{24}*(pt)_4 = T_{24}$	$(FB)_{24}*(pb)_4 = B_{24}$
3	$(FQ)_{31}*(pq)_1 = Q_{31}$	$(FT)_{31}*(pt)_1 = T_{31}$	$(FB)_{31}*(pb)_1 = B_{31}$	$(FQ)_{23}*(pq)_2 = Q_{23}$	$(FT)_{32}*(pt)_2 = T_{32}$	$(FB)_{32}*(pb)_2 = B_{32}$	$(FQ)_{33}*(pq)_3 = Q_{33}$	$(FT)_{33}*(pt)_3 = T_{33}$	$(FB)_{33}*(pb)_3 = B_{33}$	$(FQ)_{34}*(pq)_4 = Q_{34}$	$(FT)_{34}*(pt)_4 = T_{34}$	$(FB)_{34}*(pb)_4 = B_{34}$
4	$(FQ)_{41}*(pq)_1 = Q_{41}$	$(FT)_{41}*(pt)_1 = T_{41}$	$(FB)_{41}*(pb)_1 = B_{41}$	$(FQ)_{24}*(pq)_2 = Q_{24}$	$(FT)_{42}*(pt)_2 = T_{42}$	$(FB)_{42}*(pb)_2 = B_{42}$	$(FQ)_{43}*(pq)_3 = Q_{43}$	$(FT)_{43}*(pt)_3 = T_{43}$	$(FB)_{43}*(pb)_3 = B_{43}$	$(FQ)_{44}*(pq)_4 = Q_{44}$	$(FT)_{44}*(pt)_4 = T_{44}$	$(FB)_{44}*(pb)_4 = B_{44}$
...	...	...	...	...	...	...	...	...	...	...	...	...

Observed data

Observed data is the flow rates and rainfall measurements for each time step i, where

$k = 1,....U$

U = the total amount of time steps in the simulation

d_k = the decimal day of year for time step k

q_k = the measured flow rate for time step k

r_k = the measured rainfall for time step k.

Table C3 illustrates the listing of the measured data.

Table C3: Observed flow rates (in m^3/hour) and rain (mm/hour), listed with the time steps of the simulation (decimal days of the year):

Observed data		
Decimal DOY	**Flow** rates	**Rain**
Hours	**m^3/hour**	**mm/hour**
d_1	q_1	r_1
d_2	q_2	r_2
d_3	q_3	r_3
d_4	q_4	r_4
...	...	...
d_U	q_U	r_U

Simulated response functions

Simulated response functions are calculated for each flow component, starting at each time step when positive rainfall is measured:

Quickflow simulations:

$$Q_{ijk} = r_k * C * Q_{ij}$$

where

r_k = the measured rainfall from time step k

C = the runoff coefficient

Q_{ijk} = the flow rate from rainfall that fell on time step k, for the quickflow unit response function on time step i in the response function, flowing pass the outlet on time step $(k+i\text{-}1)$, for storm type j.

Throughflow simulations:

$$T_{ijk} = r_k * C * T_{ij}$$

where

T_{ijk} = the flow rate from rainfall on time step k, for the throughflow unit response function on time step i in the response function, flowing pass the outlet on time step $(k+i\text{-}1)$, for storm type j.

Baseflow simulations:

$$B_{ijk} = r_k * C * B_{ij}$$

where

B_{ijk} = the flow rate from rainfall on time step k, for the baseflow unit response function on time step I, in the response function, flowing pass the outlet on time step $(k+i\text{-}1)$, for storm type j.

Table C4 illustrates these calculations.

Table C4: The calculation of response functions for each flow component, starting at each time step when positive rainfall is measured.

Time steps	Flow due to rain occurrence on time step 1			Flow due to rainfall occurrence on time step 2			Flow due to rainfall occurrence on time step 3			Flow due to rainfall occurrence on time step 4		
	Quick flow	Through flow	Base flow	Quick flow	Through flow	Base flow	Quick flow	Through flow	Base flow	Quick flow	Through flow	Base flow
1	$Q_{1\|1}$	$T_{1\|1}$	$B_{1\|1}$									
2	$Q_{2\|1}$	$T_{2\|1}$	$B_{2\|1}$	$Q_{1\|2}$	$T_{1\|2}$	$B_{1\|2}$						
3	$Q_{3\|1}$	$T_{3\|1}$	$B_{3\|1}$	$Q_{2\|2}$	$T_{2\|2}$	$B_{2\|2}$	$Q_{1\|3}$	$T_{1\|3}$	$B_{1\|3}$			
4	$Q_{4\|1}$	$T_{4\|1}$	$B_{4\|1}$	$Q_{3\|2}$	$T_{3\|2}$	$B_{3\|2}$	$Q_{2\|3}$	$T_{2\|3}$	$B_{2\|3}$	$Q_{1\|4}$	$T_{1\|4}$	$B_{1\|4}$
5	...	...	...	$Q_{2\|2}$	$T_{4\|2}$	$B_{4\|2}$	$Q_{3\|3}$	$T_{3\|3}$	$B_{3\|3}$	$Q_{2\|4}$	$T_{2\|4}$	$B_{2\|4}$
6				...	...	...	$Q_{4\|3}$	$T_{4\|3}$	$B_{4\|3}$	$Q_{3\|4}$	$T_{3\|4}$	$B_{3\|4}$
7							...	...	...	$Q_{4\|4}$	$T_{4\|4}$	$B_{4\|4}$
...										...	...	...

Summation to estimate total flow from each flow component

All flow response from each flow component are summed for each time step, to simulate the total flow response from each flow component for each time step:

> $(TQ)_k$ = the total amount of quickflow response, which occur on time step k, for all types and for all rainfall occurrences,
> $(TT)_k$ = the total amount of throughflow response, which occur on time step k, for all types and for all rainfall occurrences, and
> $(TB)_k$ = the total amount of baseflow response, which occur on time step k, for all types and for all rainfall occurrences.

The baseflow present in the river at the start of the simulations, continuously declines along the entire simulation, or until the declining baseflow time series reaches values close to zero. This baseflow declines at a constant rate of *DeclConst*,
where

> *DeclConst* = 0.995

for the Ntuze simulations, as illustrated in Table D5, column "Declining Baseflow."

$(TotB)_k$ = (Declining baseflow) + $(TB)_k$

Where

> $(TotB)_k$ = the total simulated baseflow for time step k.

Total simulated flow in the river at the outflow of the catchment:

$(Tot)_k = (TQ)_k + (TT)_k + (TotB)_k$

where

> $(Tot)_k$ = the total simulated flow at the outflow of the catchment for time step k.

These calculations are illustrated in Table C5.

Table C5: Calculation of the total flow response (or flow rates) from each flow component for each time step of the simulation.

Total simulated flows	Quickflow	Throughflow	Baseflow	Declining baseflow	Total simulated baseflow
$(Tot)_1$	$(TQ)_1$	$(TT)_1$	$(TB)_1$	q_1	$(TotB)_1$
$(Tot)_2$	$(TQ)_2$	$(TT)_2$	$(TB)_2$	q_1*DeclConst^1	$(TotB)_2$
$(Tot)_3$	$(TQ)_3$	$(TT)_3$	$(TB)_3$	q_1*DeclConst^2	$(TotB)_3$
$(Tot)_4$	$(TQ)_4$	$(TT)_4$	$(TB)_4$	q_1*DeclConst^3	$(TotB)_4$
...	...	...	...	...	...
$(Tot)_U$	$(TQ)_U$	$(TT)_U$	$(TB)_U$	q_1*DeclConst^(U-1)	$(TotB)_U$

Calibration parameters:

Table C6 lists the calibration parameters of the GIS storm hydrograph model.

Table C6: List of the calibration parameters.

<table>
<tr><th>Description</th><th>Acronym</th><th colspan="2">Limits of values</th></tr>
<tr><td>Time scaling coefficient for quickflow</td><td>T_{SQ}</td><td rowspan="3" colspan="2">No model limitations. Limitations on physical meaning of the values.</td></tr>
<tr><td>Time scaling coefficient for throughflow</td><td>T_{ST}</td></tr>
<tr><td>Time scaling coefficient for baseflow</td><td>T_{SB}</td></tr>
<tr><td>Runoff coefficient</td><td>C</td><td colspan="2">$0 < C < 1$</td></tr>
<tr><td>Declining baseflow constant</td><td>*DeclConst*</td><td colspan="2">$0 \le DeclConst \le 1$</td></tr>
<tr><td>Partitioning coefficient of quickflow for storm type *j*</td><td>$(pq)_i$</td><td>$0 \le (pq)_i \le 1$</td><td rowspan="3">$(pq)_i + (pt)_i + (pb)_i = 1$,

for each storm type *i*</td></tr>
<tr><td>Partitioning coefficient of throughflow for storm type *j*</td><td>$(pt)_i$</td><td>$0 \le (pt)_i \le 1$</td></tr>
<tr><td>Partitioning coefficient of baseflow for storm type *j*</td><td>$(pb)_i$</td><td>$0 \le (pb)_i \le 1$</td></tr>
</table>

****

Appendix D:

Graphical simulation results from the GIS storm hydrograph model

Graphs from simulated and observed flows

This section provides some graphic display of the simulated and observed flows, as well as rainfall, from the simulation of a summer of rainfall storms measured in the Ntuze research catchments. The graphs only include the storms listed in Table 10.1, for the catchments of W1H017 and W1H031. Similar graphic display is printed in the main report (Chapter 9) for the catchment of W1H016.

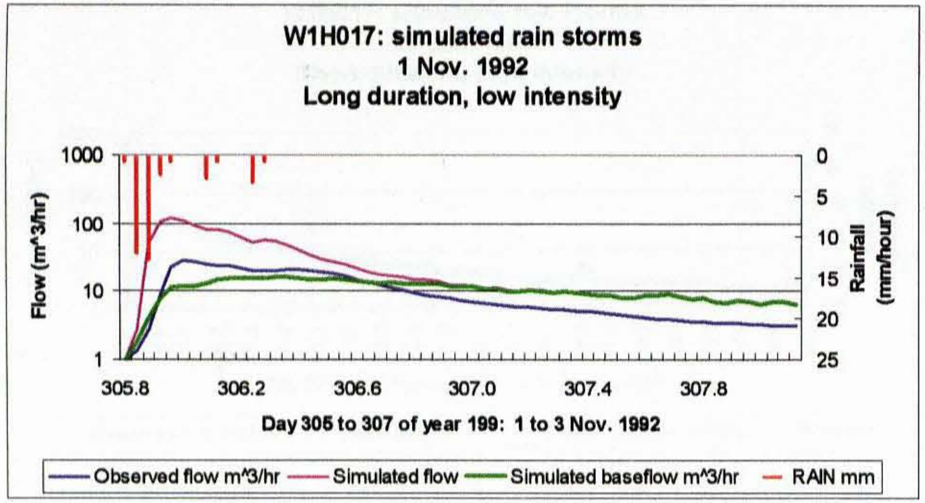

W1H017: simulated rain storms
1 Nov. 1992
Long duration, low intensity
Flow (m^3/hr)
Rainfall (mm/hour)
Day 305 to 307 of year 199: 1 to 3 Nov. 1992
Observed flow m^3/hr
Simulated flow
Simulated baseflow m^3/hr
RAIN mm

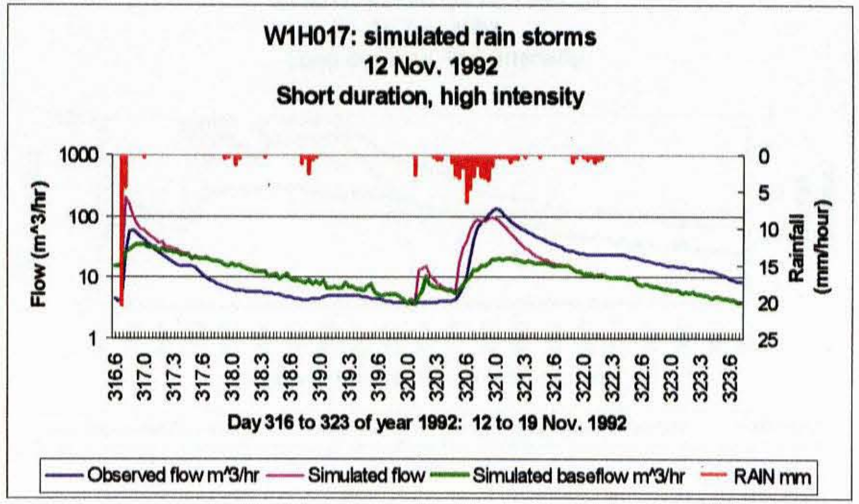

W1H017: simulated rain storms
12 Nov. 1992
Short duration, high intensity
Flow (m^3/hr)
Rainfall (mm/hour)
Day 316 to 323 of year 1992: 12 to 19 Nov. 1992
Observed flow m^3/hr
Simulated flow
Simulated baseflow m^3/hr
RAIN mm

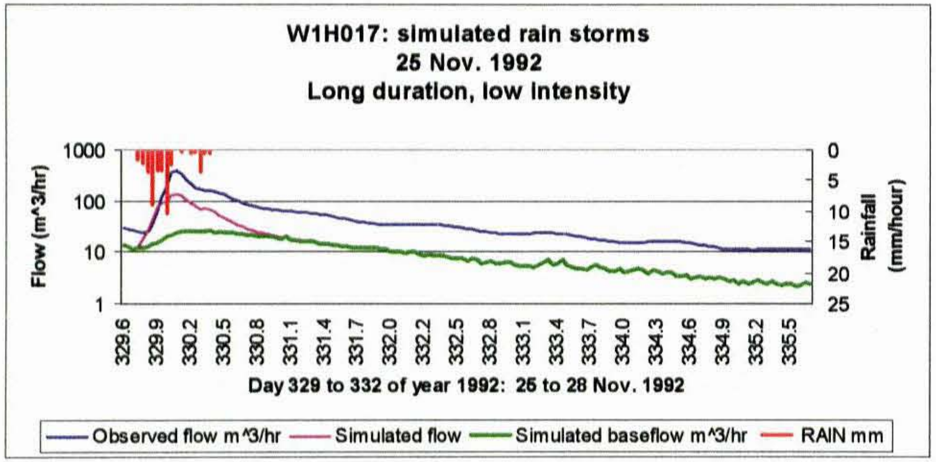

W1H017: simulated rain storms
25 Nov. 1992
Long duration, low intensity
Flow (m^3/hr)
Rainfall (mm/hour)
Day 329 to 332 of year 1992: 25 to 28 Nov. 1992
Observed flow m^3/hr
Simulated flow
Simulated baseflow m^3/hr
RAIN mm

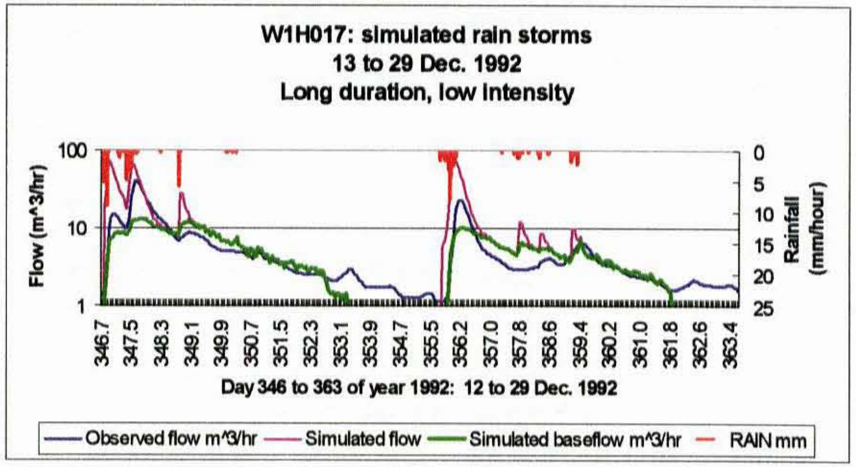

W1H017: simulated rain storms
13 to 29 Dec. 1992
Long duration, low intensity
Flow (m^3/hr)
Rainfall (mm/hour)
Day 346 to 363 of year 1992: 12 to 29 Dec. 1992
Observed flow m^3/hr
Simulated flow
Simulated baseflow m^3/hr
RAIN mm

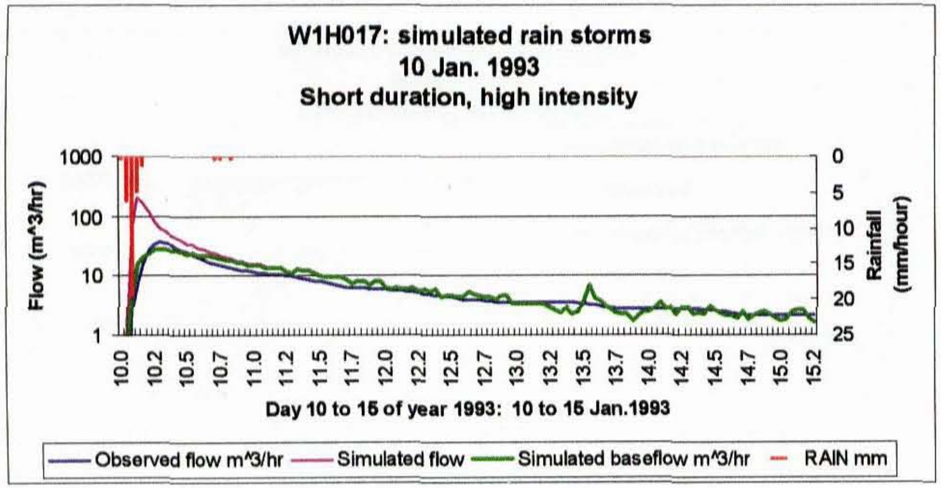
W1H017: simulated rain storms
10 Jan. 1993
Short duration, high intensity
Flow (m^3/hr)
Rainfall (mm/hour)
Day 10 to 15 of year 1993: 10 to 15 Jan.1993
Observed flow m^3/hr
Simulated flow
Simulated baseflow m^3/hr
RAIN mm

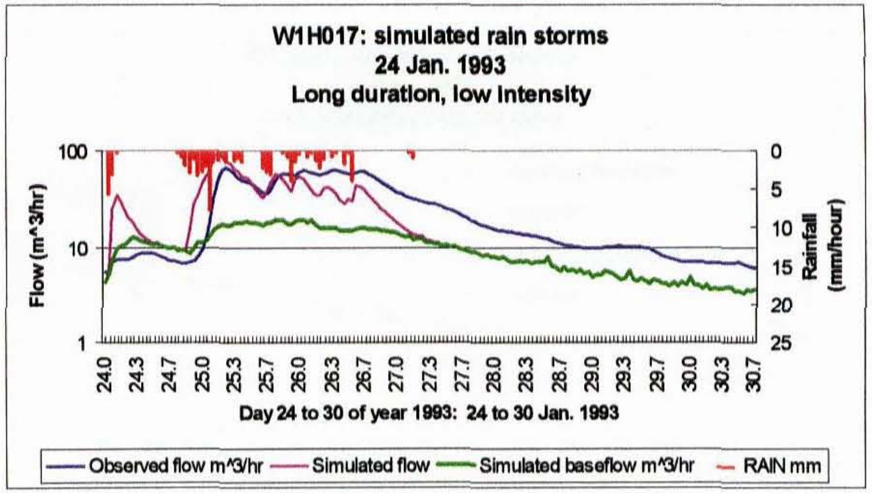
W1H017: simulated rain storms
24 Jan. 1993
Long duration, low intensity
Flow (m^3/hr)
Rainfall (mm/hour)
Day 24 to 30 of year 1993: 24 to 30 Jan. 1993
Observed flow m^3/hr
Simulated flow
Simulated baseflow m^3/hr
RAIN mm

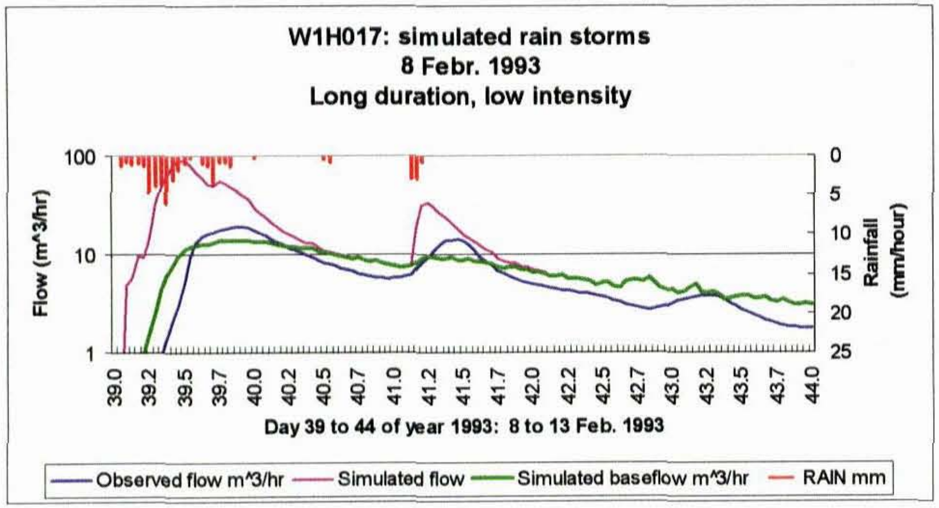
W1H017: simulated rain storms
8 Febr. 1993
Long duration, low intensity
Flow (m^3/hr)
Rainfall (mm/hour)
Day 39 to 44 of year 1993: 8 to 13 Feb. 1993
Observed flow m^3/hr
Simulated flow
Simulated baseflow m^3/hr
RAIN mm

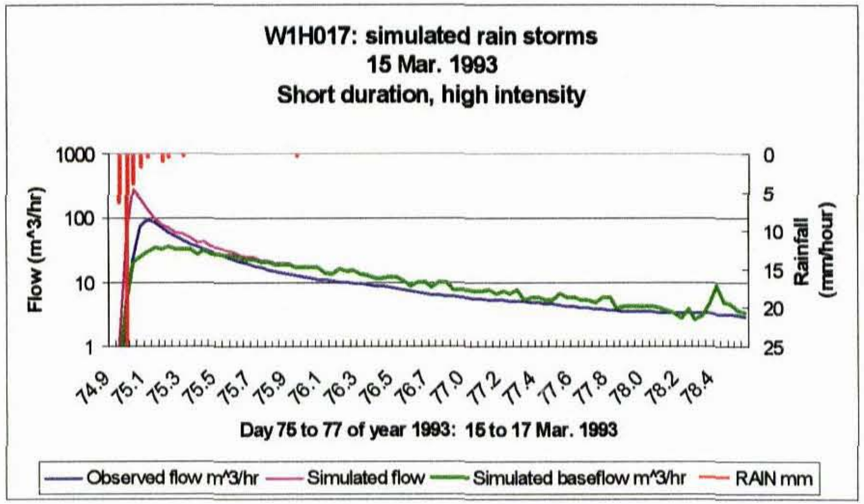
W1H017: simulated rain storms
15 Mar. 1993
Short duration, high intensity
Flow (m^3/hr)
Rainfall (mm/hour)
Day 75 to 77 of year 1993: 15 to 17 Mar. 1993
Observed flow m^3/hr
Simulated flow
Simulated baseflow m^3/hr
RAIN mm

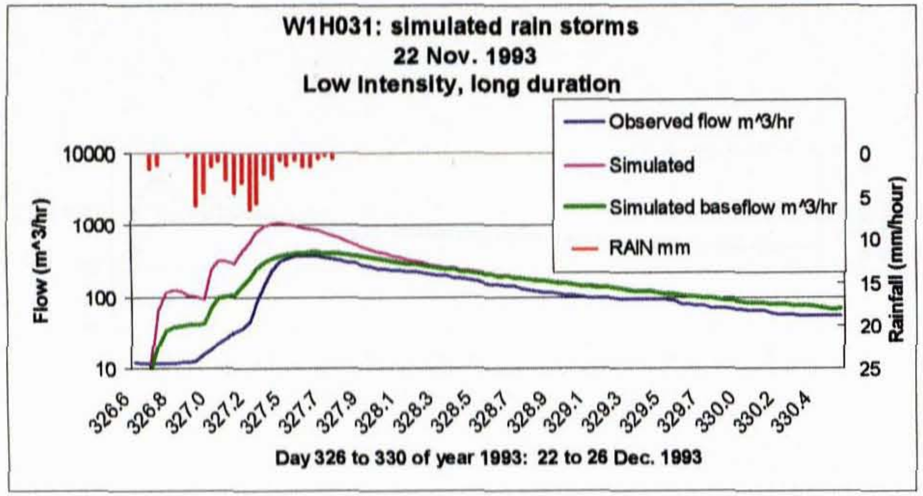
W1H031: simulated rain storms
22 Nov. 1993
Low intensity, long duration
Observed flow m^3/hr
Simulated
Simulated baseflow m^3/hr
RAIN mm
Flow (m^3/hr)
Rainfall (mm/hour)
Day 326 to 330 of year 1993: 22 to 26 Dec. 1993

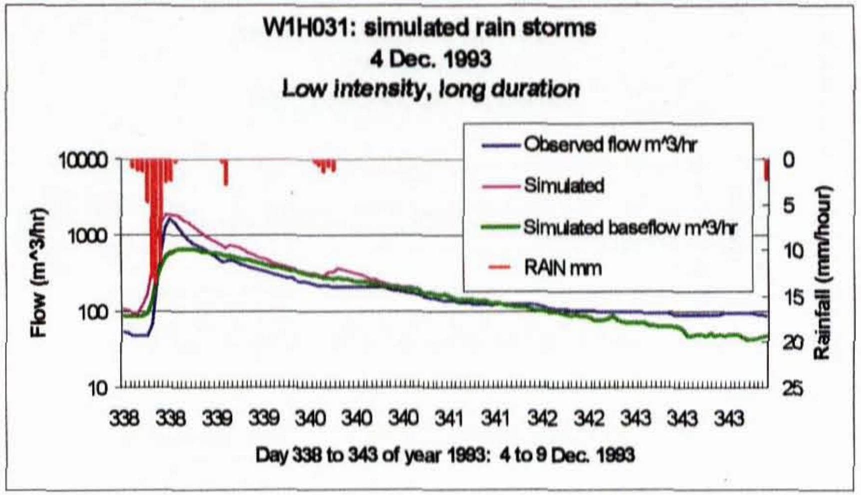
W1H031: simulated rain storms
4 Dec. 1993
Low intensity, long duration
Observed flow m^3/hr
Simulated
Simulated baseflow m^3/hr
RAIN mm
Flow (m^3/hr)
Rainfall (mm/hour)
Day 338 to 343 of year 1993: 4 to 9 Dec. 1993

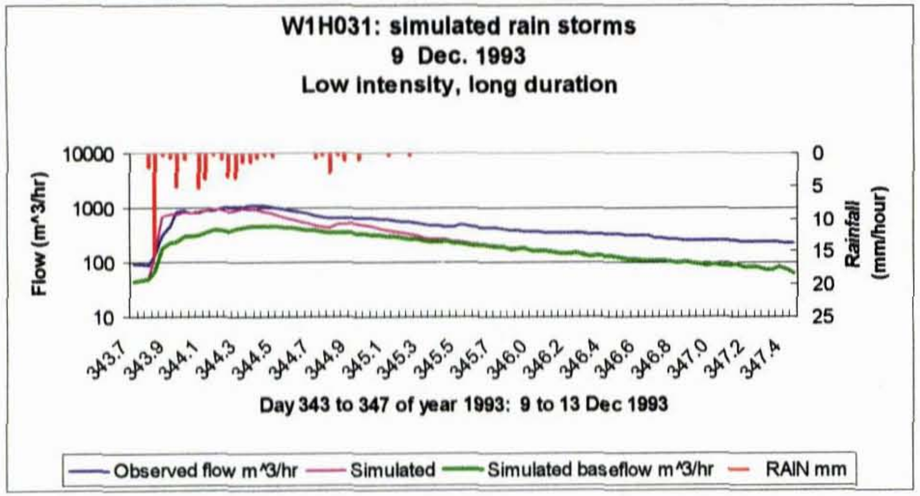
W1H031: simulated rain storms
9 Dec. 1993
Low intensity, long duration
Flow (m^3/hr)
Rainfall (mm/hour)
Day 343 to 347 of year 1993: 9 to 13 Dec 1993
Observed flow m^3/hr
Simulated
Simulated baseflow m^3/hr
RAIN mm

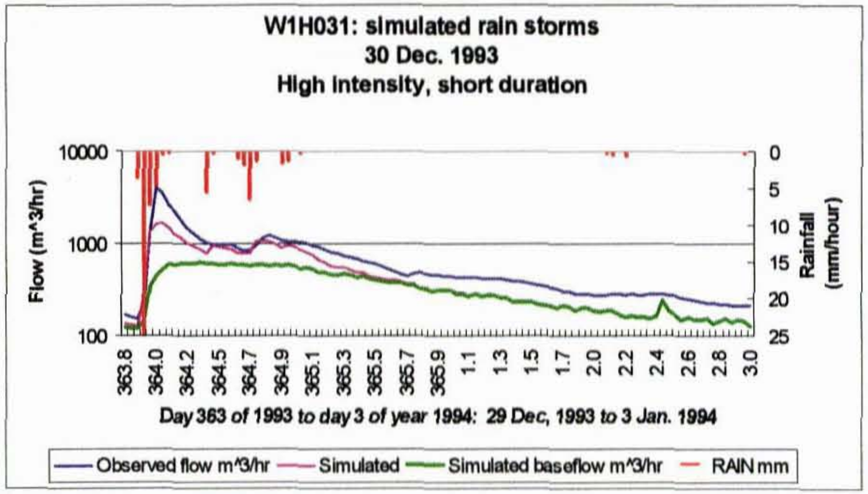
W1H031: simulated rain storms
30 Dec. 1993
High intensity, short duration
Flow (m^3/hr)
Rainfall (mm/hour)
Day 363 of 1993 to day 3 of year 1994: 29 Dec, 1993 to 3 Jan. 1994
Observed flow m^3/hr
Simulated
Simulated baseflow m^3/hr
RAIN mm

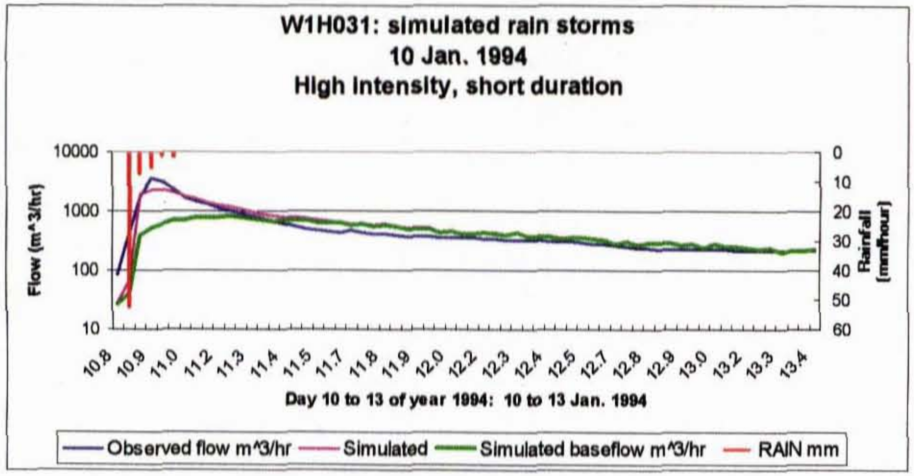
W1H031: simulated rain storms
10 Jan. 1994
High intensity, short duration
Flow (m^3/hr)
Rainfall (mm/hour)
Day 10 to 13 of year 1994: 10 to 13 Jan. 1994
Observed flow m^3/hr
Simulated
Simulated baseflow m^3/hr
RAIN mm

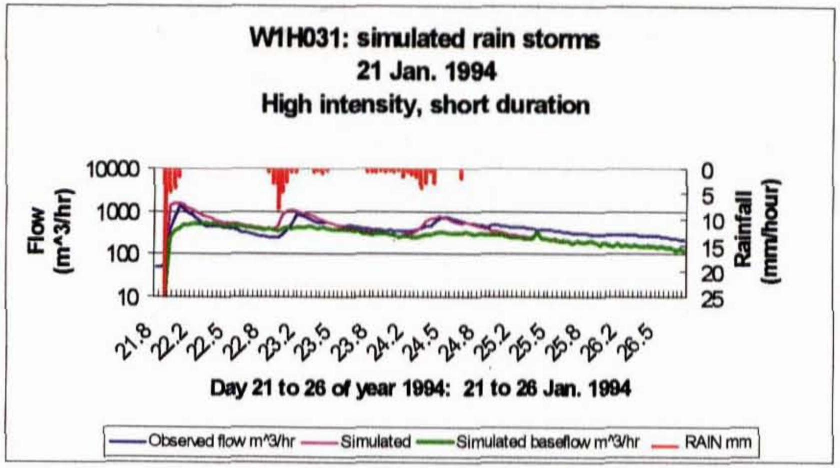
W1H031: simulated rain storms
21 Jan. 1994
High intensity, short duration
Flow (m^3/hr)
Rainfall (mm/hour)
Day 21 to 26 of year 1994: 21 to 26 Jan. 1994
Observed flow m^3/hr
Simulated
Simulated baseflow m^3/hr
RAIN mm

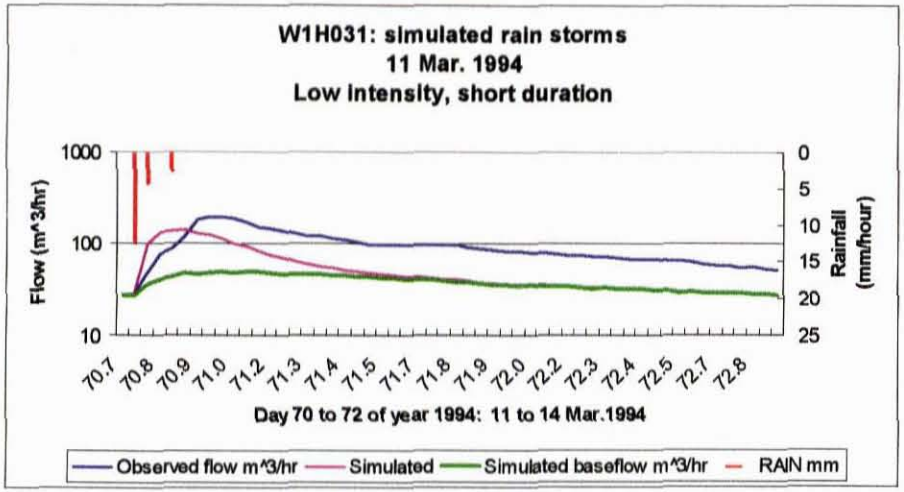
W1H031: simulated rain storms
11 Mar. 1994
Low intensity, short duration
Flow (m^3/hr)
Rainfall (mm/hour)
Day 70 to 72 of year 1994: 11 to 14 Mar.1994
Observed flow m^3/hr
Simulated
Simulated baseflow m^3/hr
RAIN mm

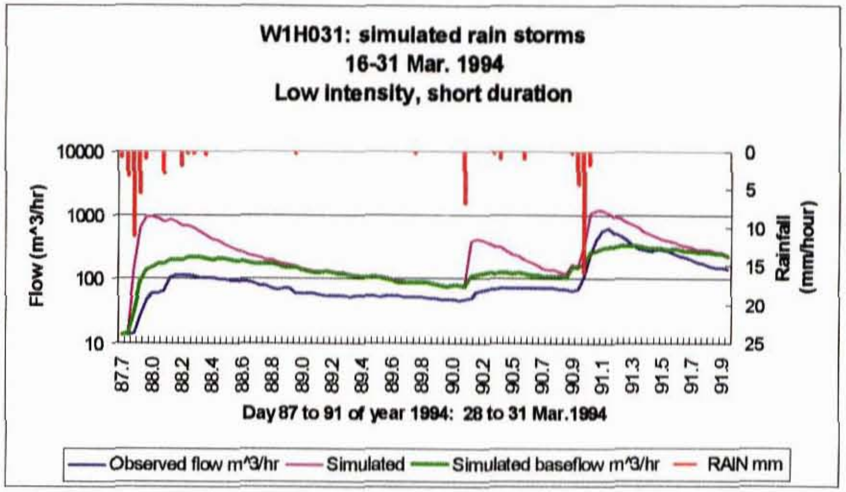
W1H031: simulated rain storms
16-31 Mar. 1994
Low intensity, short duration
Flow (m^3/hr)
Rainfall (mm/hour)
Day 87 to 91 of year 1994: 28 to 31 Mar.1994
Observed flow m^3/hr
Simulated
Simulated baseflow m^3/hr
RAIN mm

****

****